Online structural damage detection using first order eigen perturbation techniques

A

thesis submitted

in partial fulfillment of the requirements

for the degree of

Doctor of Philosophy

by

Basuraj Bhowmik

Department of Civil Engineering

Indian Institute of Technology Guwahati

June, 2018

Certificate

This is to certify that the thesis entitled "**Online structural damage detection using first order eigen perturbation techniques** ", submitted by Basuraj Bhowmik, a research scholar in the *Department of Civil Engineering*, *Indian Institute of Technology Guwahati*, for the award of the degree of Doctor of Philosophy, is a record of an original research work carried out by him under my supervision and guidance. The thesis has fulfilled all requirements as per the regulations of the institute and in my opinion has reached the standard needed for submission. The results embodied in this thesis have not been submitted to any other University or Institute for the award of any degree or diploma.

Signed:

Supervisor: Dr. BUDHADITYA HAZRA
Department of Civil Engineering,
Indian Institute of Technology Guwahati,
Guwahati-781039, Assam, India.

Date:

Abstract

The use of statistical data driven techniques such as principal component analysis (PCA) has shown considerable potential in the area of vibration based structural damage detection. The objective of PCA based methods is to obtain proper orthogonal modes using recorded acceleration data that is subsequently utilized to detect the change in the dynamic behavior of the vibrating system from its pristine state to contiguous linear /non-linear-states, indicating damage. Several PCA based methods utilizing the eigenspace characteristics of a system have been proposed and successfully implemented in the literature. Whereas most of the PCA based techniques process a recorded ensemble of data acquired through batch mode operations, literature involving recursive identification of structural damage as and when the data streams in real time, is missing. Motivated by this challenge, the current research focuses on developing real time damage detection methods to address the problem of identifying fine levels of damage, *online*, even for underdetermined systems, where the number of sensors instrumented are less than the actual number of desired modes. The use of first order eigen perturbation (FOEP) techniques facilitate recursive updates of the eigenspace, which is subsequently used for real time processing of data. This leads to the comprehensive development of real time structural damage detection techniques, such as recursive principal component analysis (RPCA), recursive singular spectrum analysis (RSSA) and recursive canonical correlation analysis (RCCA), along with their possible variations, that pivots around the concepts of FOEP. The transformed response obtained at each time stamp using the algorithms by themselves are insufficient in estimating the spatio-temporal patterns of damage and hence, damage sensitive features (DSFs) premised on the distortion of eigenspace updates are employed as indicators of damage activity. Numerical simulations carried out on linear and nonlinear systems demonstrate the applicability of the algorithms towards real time damage detection. Both experimental and full scale case studies are included to demonstrate the efficacy and robustness of the algorithms ideal candidates for real-time, reference free structural health monitoring.

Acknowledgments

First and foremost, I would like to express my sincere thanks and gratitude to my supervisor, Dr. Budhaditya Hazra, for his inspirational guidance and invaluable support. It has been an honor to be his first PhD student. My PhD has been an amazing experience and I thank Dr. Hazra wholeheartedly, not only for his tremendous academic support but also for his wonderful mentorship and bestowing me with so many amazing opportunities. The joy and enthusiasm he has for his research was contagious and motivational for me, even during tough times in the PhD pursuit, which instilled in me with a right attitude and impetus needed to complete the work on time. My sincere thanks to Dr. Kaustubh Dasgupta, Dr. Santosha K. Dwivedy, and Dr. Amit Shelke, for serving on my thesis committee.

Profound thanks to my collaborator, Dr. Vikram Pakrashi (University College Dublin, Ireland), for providing his insightful comments and valuable suggestions from time-to-time. The jovial conversations with him were instrumental in avoiding pitfalls that helped me immensely in approaching problems with a different perspective. I would also like to thank him for providing experimental data and making it available in a format that could be used in this research.

I am truly grateful to my colleague-turned-friends: Manu Krishnan, Seevani Bali and Tapas Tripura, for their insightful comments, critical appreciation and valuable suggestions during the preparation of the thesis. Their contributions towards my dissertation: be it preparing drafts or assisting me in endless hours of coding and working together in a fun-filled environment, is greatly acknowledged. I have very fond memories of my time here.

There were days that went by with frustrations and disappointments; and all I had to do was make a simple phone call. Thank you Oindrila and Abhishek for sharing my feelings and believing in me. I am grateful for the group of friends back home for the witty conversations and healthy debates over every cricket match that was ever played.

Nothing can beat the love of a mother and the words of advice from a father. I cannot thank my parents enough for their unconditional encouragement, patience, love and support for everything that I have ever attempted to do. Without their unwavering emotional support, this work would have never materialized. I dedicate the entirety of this work to them.

Dedication

To a string of educators with big hearts, nurturing a childish curiosity in all things.

My parents

Bimal Bhowmik

Manasi Bhowmik

For their advice, patience and faith.

Because you always understood.

Table of Contents

List of Tables

List of Figures

Table 1: List of Acronyms

PCA	Principal Component Analysis
POC	Principal Orthogonal Component
POM	Proper Orthogonal Mode
POV	Principal Orthogonal Values
EVD	Eigen Value Decomposition
RPCA	Recursive Principal Component Analysis
RSSA	Recursive Singular Spectrum Analysis
RCCA	Recursive Canonical Correlation Analysis
TVAR	Time Varying Auto Regressive
DSF	Damage Sensitive Features
RRE	Recursive Residual Error
DOF	Degree of Freedom
SHM	Structural Health Monitoring
FOEP	First Order Eigen Perturbation
KPCA	Kernel Principal Component Analysis
KG	Kalman Gain
SDOF	Single Degree of Freedom
MDOF	Multi Degree of Freedom
AR	Auto Regressive
UCLA	University of California Los Angeles
UCLAFB	UCLA Factor Building
SMF	Special Moment Resisting Steel Frame
TMD	Tuned Mass Dampers

Table 2: Nomenclature

X	Displacement vector
$\mathbf{V}$	Mode shape matrix
$\mathbf{Q}$	Modal coordinate matrix
$\mathbf{R}$	Covariance matrix
Ψ	Principal Orthogonal Coordinate Matrix
ε,γ	Error term
R_k	Covariance matrix at k^{th} time instant
Υ	Diagonal matrix of eigenvalues of covariance matrix
W	Matrix of eigenvectors of covariance matrix
$\widetilde{\psi}$	POC estimate vector
$\mathbf{H}_k$	Matrix of eigenvectors of the middle term at k^{th} instant
λ_k	Diagonal matrix of eigenvalues of the middle term at k^{th} instant
α_i	Eigen value corresponding to i^{th} eigen vector
W_k^1	Eigen subspace at k^{th} instant accounting for more than 90% kinetic energy
W_k^2	Eigen subspace at k^{th} instant accounting for remaining kinetic energy
a_1,a_2	Time varying AR coefficients
P_w	Covariance matrix of process noise
b, C, γ	Kalman state variables
μ_{a_i}	Recursive mean of a_i^{th} coefficient
ζ_{a_i}	Recursive sixth moment of a_i^{th} TVAR coefficient
κ	Term controlling level of non-linear force
z, Q, A, β	Bouc-Wen parameters

Chapter 1

Introduction

In the past two decades of accelerated technological development, the reliance on structural and mechanical systems such as aircrafts, buildings, bridges, railways, power generation systems and defense systems is on a steady rise. A significant portion of the built infrastructure could benefit from extensive condition monitoring and data-driven, informed maintenance. However, constraints such as improper planning, negligence in management and unavailability of adequate resources impede their systematic implementation. Operation, within and sometimes beyond the initially designed service life requires assessment of the system in relation to performance metrics considering aging and sustained degradation. This requirement leads to the need of efficient damage detection techniques in order to detect and locate the damage, estimate the severity of the damage and predict the useful remaining life of a structure, often referred to as *structural health monitoring* (SHM) analysis [1–8]. The present work aims to address the identification of damage and locating the occurrence of it simultaneously in real time, through the development of damage detection schemes in a mathematically consistent recursive framework.

Damage is defined as the change in the structural parameters (like stiffness [2,3], damping [1,2,7], mass [1–4], natural frequency [2, 3], damping ratio [7] and mode shapes [9–15]) that may affect its present or future performances. Damages can have significant impacts on the functionality, integrity and serviceability of the system as a whole, which could lead to severe economic losses and adversely affect public safety, if not detected timely. Visual inspections are the basic and most

common maintenance and detection technique used for a long period of time, but this traditional approach can only be applied for simple structures [2, 4]. In the case of complex architecture, visual inspections may not be possible due to restricted accessibility. To alleviate this drawback, a significant number of damage detection algorithms and strategies have been proposed in recent times [1–5]. However, the evolution of real time damage detection schemes capable of conducting baseline-free damage identification, still poses a formidable challenge, primarily, due to the underdevelopment of algorithms that are amenable towards real time implementation. The occurrence of damage is often a sudden event [3] that requires the damage sensitive features (DSFs) to function online, in a recursive fashion, for a continuously streaming data. This can be carried out by extensively by a family of eigen value perturbation techniques called *first order eigen perturbation* (FOEP) methods and tailoring it towards real time SHM. The present work explores the complete family of the FOEP techniques that have been developed in due course of this work such as recursive principal component analysis (RPCA) and recursive singular spectrum analysis (RSSA) and also demonstrates how new hybrid approaches can be proposed catering to application specific problems.

Among the numerous vibration based damage detection methods that have been developed in the recent years [1–10], real time damage detection is a relatively nascent topic that has shown significant promise in dynamic process monitoring and deserves a closer look in the present context. Bulk of the traditional offline damage detection schemes have disadvantages mostly due to their inherent dependence on finite element modeling (FEM) [16–20], windowed analysis through batch data [6, 7] and insensitivity towards initial small damages or imperfections in structures [7]. These damage detection techniques usually exploit changes in the dynamic properties of the acquired response as indicators of change in physical properties due to damage [21–28]. On the contrary, the response based methods mostly rely on the signatures obtained from the recorded vibrations to extract features that indicate a change at the onset of an event [29–46]. These methods overcome the aforementioned limitations by utilizing advanced signal processing techniques over the vibration measurements to monitor the condition of a structure [47–55]. Recent developments in the response based signal processing tools has resulted in a paradigm shift towards application in damage detection [42–44] that includes utilization of various time-frequency analysis methods [51, 53, 56–60] such as wavelet transform [61–67], blind source separation [68–71] and empirical mode decomposition

and Hilbert-Huang transform [77–81]. The offline implementation of these algorithms calls for the development of advanced damage detection strategies that solely function in real time as and when the vibration data streams in.

Figure 1.1: Oakland bridge after San Francisco earthquake

To appreciate the importance of the paradigm of continuous real-time structural health monitoring, let us recollect an event that happened not too long ago. On 17 October, 1989, a shock of magnitude 6.9 centered around the San Andreas fault system, occurred for a span of 15 seconds. The earthquake had adverse affects on human life and incurred socio-economic losses in that region. Figure 1.1 shows the effect of the earthquake on the San Francisco Oakland Bay Bridge that suffered severe damage on the upper deck section. The quake caused the Oakland side of the bridge to shift 7 in (18 cm) to the east, and caused the bolts of one section to shear off, sending the 250-short-ton segment of roadbed crashing down like a trapdoor. The incident sheds light on the importance of damage detection in structures that assess the presence, location, severity of the damage and detect the remaining healthy life of the structure. Detection algorithms aimed at exploring the occurrence and/or initiation of the damage are instrumental in assessing the remaining life of the structure, aiding in retrofitting processes and improving the resistance to earthquake by optimizing the strength

and ductility of the materials used.

The entire work is centered around real time damage detection using recursive eigen decomposition and heavily draws inspiration from first order eigen perturbation techniques (FOEP) [133,135]. FOEP is a mathematical way of expressing the eigen structure of $k+1^{th}$ step in terms of the eigen structure of k^{th} step as $k+1^{th}$ data streams in. This is accomplished by relating the EVD of symmetric positive definite covariance matrix in terms of rank one perturbation of eigenvalue and eigenvector matrices. The four algorithms comprehensively explored in the present work namely: RPCA, RSSA and RPCA-TVAR, RCCA algorithms come under the umbrella of the first order eigen pertubation techniques (FOEP). Although there are a host of other algorithms in the domain of adaptive filtering like Kalman filter [72–74] and recursive least squares [82], that are amenable to online damage detection, FOEP promises to provide a mathematically consistent framework to all the relevant family of algorithms that intend to exploit eigenstructure of the dynamical systems in real-time to detect damage.

1.1 Aims and Objectives

Having introduced the basic ideas of damage and the strategies to identify and detect its real time occurrence, the broad-based objectives of the current research can now be articulated as follows:

1. To develop spatio-temporal damage detection algorithms in a unified framework using FOP techniques and recursive DSFs as indicators of identification.

2. Extend the above methods to improve finer levels of spatio-temporal damage detection in MDOF vibrating systems using full and partial sensor information.

3. To develop algorithms that detect damage using the inputs from a single sensor and to create a unified framework that can consider both single and multi-channel responses of an MDOF system as inputs for real time structural damage detection.

4. To develop a hybrid algorithm based on FOP theory that can be improvised to detect finer levels of damage without compromising on the time complexity and at the same time catering

to application specific problems. Specifically, the performance of the hybrid algorithm in identifying the spatio-temporal patterns of damage will be studied in the context of real time damage detection.

1.2 Organization of the thesis

This thesis contains 7 chapters. First, a detailed description on the state of the art of damage detection techniques is reviewed in chapter 2, followed by the more recent ones which belong to the family of real time structural damage detection methods. During the course of relevant literature review, the basic demerits of the traditional damage detection strategies are highlighted to articulate the objectives of the proposed study.

The third chapter presents the theoretical development of a novel real time damage detection technique, called recursive principal component analysis (RPCA). The theoretical development of this method is premised on the extension of the basic ideas of principal component analysis (PCA) through a first order eigen perturbation (FOEP) technique. The problem statement is first presented wherein the general fabrication of structural dynamics is cast in an RPCA framework. The theoretical derivations are discussed next in detail, followed by the results of numerical simulation on linear and nonlinear systems. Experimental verifications using a cantilever beam setup are presented next. Finally, the results of real time damage detection are presented in detail for a practical case study involving of ambient vibration and earthquake response data obtained from the *UCLA Factor Building* (UCLAFB).

An extension of the RPCA algorithm to perform under nonstationary input excitations is introduced in the fourth chapter. The theoretical development of the method incorporates the use of time varying auto-regressive (TVAR) modeling of the transformed responses obtained from the RPCA algorithm. The real time damage detection scheme, commonly referred to as *RPCA-TVAR* method, extends the concepts of RPCA to improve the detectability of a finer percentage of damage in real time, subjected to both stationary and nonstationary excitations. The chapter provides key detection results for numerically simulated linear and nonlinear systems, using full and partial sensor

information. Validation from experimental setups and applicability of the RPCA-TVAR scheme on practical problems are vividly discussed in the context of online structural damage detection.

A newly developed recursive damage detection method, to identify damage using the inputs obtained from a *single sensor*, is introduced in the fifth chapter. The algorithm, known as recursive singular spectrum analysis (RSSA), is developed to address the cases where the number of instrumented floors of the structure are less than the actual number of desired modes. The method is applied to numerically simulated case studies and validated using experimental setups. An improved hybrid version of the method is presented next that is primarily developed to address finer levels of damage detection in real time without compromising on the time complexity and tailored to cater to a wide range of application specific problems. Key results and discussions are presented in next detail that eventually concludes the chapter.

The sixth chapter considers the theoretical development of a new online algorithm, recursive canonical correlation analysis (RCCA), aimed at identifying damage patterns in real time. Analogous to the RPCA based damage detection scheme, this method is essentially developed to address the deficiencies in detectability of the previously proposed FOEP based methods under certain practical situations. Detection results on numerically simulated systems and comparative studies conducted on experimental test beds provide a central idea to the applicability of the method. Finally, the results of detection on practical case studies are provided and important observations and conclusions are presented.

The main conclusions of this dissertation are summarized in the seventh chapter along with the key accomplishments of the current research work. The recommendations for future research that could be the possible extensions to this work are finally presented which concludes the thesis.

Chapter 2

Background and Literature Review

In this chapter, several popular algorithms are reviewed in the context of damage detection of structural systems. First, an overview of the traditional methods available in the literature is discussed in detail, followed by a detailed review of the more recent ones belonging to the family of output based methods. The central concepts are reviewed and discussed in order to highlight the basic demerits of the conventional methods and enlighten the need for the present study. Some important acronyms relevant to the subsequent discussions are provided in Table 2.1.

Table 2.1: Important acronyms

SHM	Structural Health Monitoring
FOEP	First Order Eigen Perturbation
MBDD	Mode shape based Damage Detection
FBDD	Frequency based Damage Detection
KF	Kalman Filter
EMD	Empirical Mode Decomposition
BSS	Blind Source Separation
PCA	Principal Component Analysis
SSA	Singular Spectrum Analysis

2.1 An overview of the Existing Damage Detection Methods

The advent of the 21^{st} century has witnessed a steady rise in the development of a wide gamut of methods for damage detection of structural and mechanical systems. Initially, these methods were directed at obtaining the damaged state of the systems through a change in the modal parameters. With the advent of sophisticated computational prowess in the context of structural dynamics, updating of finite element (FE) models were also incorporated. This resulted in a profound understanding of the variation of the structural parameters due to damage and the results were successfully reported in the literature [1–4, 6, 7]. Many researchers contributed to this field of study through model-based parameter updates that provided recursive state estimations for identifying damage, utilizing the concepts of Kalman Filter (KF) updates [72–75]. The use of statistical parameters such as Mahalanobis distance for novelty evaluation prompted the implementation of auto-regressive (AR) coefficients [76] for detecting damage in vibrating systems. Most of these methods can be classified as: *model based methods* and *response based methods*. The model based methods involve a comparative analysis with respect to the detailed numerical model of the system, while the response based methods detect damage using the response data acquired from the system (experimentally or otherwise). In this regard, a few noteworthy model based methods of the recent past are reviewed next.

2.1.1 Model based damage detection methods

The model based approaches provide strategies to estimate the location and severity of damage by assuming that a signature of the structure in its pristine (healthy) state is initially available (through experimentation or otherwise), usually identified as a reference or baseline data, possibly recorded under an excitation of known intensity [16–20]. The damage is detected in the structure by comparing this baseline data with the new recorded set of data, through an extensive calibrated FE modeling. These methods also utilize the variations in the modal parameters to ascertain the damage through mathematical formulations directed towards identifying the changes in natural frequencies,

mode shapes and damping, pre and post damage. In this context, some of the most popular methods in structural damage detection literature, are reviewed next.

Damage detection through changes in natural frequency: A brief review

The existence of damage in a structural or mechanical system leads to the modification of vibration modes that are manifested as changes in the modal parameters such as natural frequencies, mode shapes and modal damping. The use of natural frequency as a diagnostic parameter in structural assessment procedures using vibration monitoring has been thoroughly discussed in the literature [26–28], where it is assumed that the natural frequencies are sensitive indicators of structural integrity. A frequency based damage detection (FBDD) scheme aimed at localizing the damage, formulated for MDOF vibrating systems, examines the ratio of the fractional change of the m^{th} eigenvalue to the fractional change of the n^{th} eigenvalue, indicating the presence of possible damage to the system, if any. In this context, the pristine state of the MDOF system is taken into consideration with i^{th} natural frequency ω_i and the i^{th} mode shape ϕ_i. Considering that the structure undergoes damage after a certain time, the resulting characteristic equation of the damaged structure yields, respectively, frequencies and mode shapes ω_i^* and ϕ_i^*, respectively (where the *asterisk denotes the damaged state*). Discretizing the MDOF system into NE number of elements with N modes, the damage inflicted at predefined locations is defined using the sensitivity equation,

$$\sum_{j=1}^{NE} F_{ij}\alpha_j = Z_i \tag{2.1}$$

where α_j describes the damage induced at the j^{th} location which can be corroborated to the fractional reduction in the stiffness of the j^{th} parameter. The fractional change in the i^{th} eigenvalue due to damage, Z_i, is given by:

$$Z_i = \frac{\omega_i^{*^2} - \omega^2}{\omega^2} \tag{2.2}$$

The sensitivity parameter, defined as the fractional modal energy, F_{ij} for the i^{th} mode concentrated in the j^{th} element can be expressed as:

$$F_{ij} = \frac{\phi_i^T \mathbf{C}_j \phi_i}{\phi_i^T \mathbf{C} \phi_i} \tag{2.3}$$

with ϕ_i as the i^{th} mode shape vector, $\mathbf{C}$ is the stiffness matrix and $\mathbf{C}_j$ determines the contribution of the j^{th} element to the system stiffness. The respective quantities Z_i and F_{ij} are determined through experimental trials and numerical iterations. Carrying out proper substitutions to Eqn. 2.1, the location and the size of the damage inflicted to the system can be determined. On considering the same structural system comprising of NE elements ($j = 1, 2, ..., q, ..., NE$) and a measured set of NM vibration modes ($i = 1, ..., m, n, ..., NM$), Eqn. 2.1 can be expressed in terms of any two modes m and n, where $m \neq n$, respectively. On dividing Eqn. 2.1 for mode m by Eqn. 2.1 for mode n, one obtains:

$$\frac{Z_m}{Z_n} = \frac{\sum_{j=1}^{NE} F_{mj}\alpha_j}{\sum_{j=1}^{NE} F_{nj}\alpha_j} \tag{2.4}$$

Assuming that the structure is damaged at a single location q and $\alpha_j \neq 0$ for $j = q$, but $\alpha_j = 0$ for $j \neq q$, Eqn. 2.4 becomes:

$$\frac{Z_m}{Z_n} = \frac{F_{mq}}{F_{nq}} \tag{2.5}$$

From the above equation, $\frac{Z_m}{Z_n}$ provides the ratio of the fractional change in m^{th} eigenvalue to the fractional change in n^{th} eigenvalue. From these discussions, it can be well understood that $\frac{F_{mq}}{F_{nq}}$ provides the ratio of the sensitivity for the m^{th} mode and q^{th} element to that of the n^{th} mode and q^{th} element. Thus the damage inflicted at that location is defined by Eqn. 6.5 which can be extended to compute for all the measured NM modes, given as:

$$\frac{Z_m}{\sum_{k=1}^{NM} Z_k} = \frac{F_{mq}}{\sum_{k=1}^{NM} F_{kq}} \tag{2.6}$$

As the above equation holds true only if element q gets damaged, an error index is introduced

$$e_{ij} = \frac{Z_m}{\sum_{k=1}^{NM} Z_k} - \frac{F_{mq}}{\sum_{k=1}^{NM} F_{kq}} \tag{2.7}$$

where e_{ij} represents localization error for the i^{th} mode and the j^{th} location. In order to account for all the available modes, a single damage indicator (DI) suffices to provide the necessary damage information for the j^{th} memeber as:

$$DI_j = \left[\sum_{i=1}^{NM} e_{ij}^2\right]^{-1/2} \tag{2.8}$$

where $0 \leq DI_j < \infty$ and the damage is located at element j if DI_j approaches the local maximum point.

Damage detection through changes in mode shapes

In the context of structural damage detection, there exists a wealth of literature that deals with identification and localization of damage using changes in the mode shapes, its derivatives, modal curvatures, and so on [9, 10, 12–15]. Detection algorithms premised on the objective of localizing and estimating the severity of the damage through mode shape based damage detection (MBDD) schemes are one of the widely used detection techniques available in the literature. The MBDD method takes into consideration a homogeneous, one dimensional beam of uniform cross section with NE elements with N nodes. The solution of the dynamic eigenvalue problem with i^{th} modal stiffness K_i of the beam is given by:

$$K_i = \int_0^L k(x)[\phi''_i(x)]^2 dx \tag{2.9}$$

where $\phi_i(x)$ is the mode shape of the i^{th} modal vector and $k(x)$ is the bending stiffness of the beam. The contribution of the j^{th} element to the i^{th} modal stiffness can be expressed using:

$$K_{ij} = k_j \int_j [\phi''_i(x)]^2 dx \tag{2.10}$$

where k_j is the stiffness of the j^{th} element. The function is integrated over the entire beam length. The fraction of modal energy of the i^{th} mode concentrated in the j^{th} member, known as sensitivity, is given as:

$$F_{ij} = K_{ij}/K_i \tag{2.11}$$

Considering the corresponding damage parameters obtained from Eqn. 2.9 and 2.11 associated with the damaged state be denoted by asterisks, the sensitivity equation for the damaged state can be expressed as:

$$F^*_{ij} = K^*_{ij}/K^*_i = F_{ij} + \delta F_{ij} \tag{2.12}$$

The corresponding scalars are given by:

$$\left.\begin{aligned} {K_{ij}}^* &= k^*_j \int_j [\phi''^*_i(x)]^2 dx \\ {K_i}^* &= \int_0^L k^*(x)[\phi''^*_i(x)]^2 dx \end{aligned}\right\} \tag{2.13}$$

The fraction of the modal energy at the j^{th} member for the i^{th} mode is represented by the term F_{ij}. On differentiating Eqn. 2.12, one obtains:

$$\delta F_{ij} = \frac{K_{ij}}{K_i}\left[\frac{\delta K_{ij}}{K_{ij}} - \frac{\delta K_i}{K_i}\right] \tag{2.14}$$

Assuming that NE (in the FE discretization sense) is more than unity, $K_i >> K_j$, Eqn. 2.14 can be further simplified as:

$$\delta F_{ij} \cong \frac{\delta K_{ij}}{K_{ij}} \tag{2.15}$$

It is well understood that the quantity δF_{ij} can now be measured directly from the changes in the modal parameters of the system. Assuming that the structure is damaged in ND multiple locations,

$\delta F_{ij} \cong \frac{\delta K_{ij}}{ND}$. The fractional change in the i^{th} eigenvalue due to damage can be thus, represented as:

$$g_i = \frac{\delta K_{ij}}{K_i} \cong \frac{1}{ND}\left(\frac{\delta\omega_i^2}{\omega_i^2}\right) \tag{2.16}$$

in which g_i is a dimensionless factor representing the fractional change in the i^{th} modal parameters. As evident from Eqn. 2.10 and 2.13, the term δK_{ij} represents the variation of the modal stiffness, which can be expressed as:

$$\delta K_{ij} = K_{ij}^* - K_{ij} = \gamma_{ij}^* k_j^* - \gamma_{ij} k_j \tag{2.17}$$

where, $\gamma_{ij} = \int_j [\phi''_i(x)]^2 dx$ and $\gamma_{ij}^* = \int_j [\phi_i''^*(x)]^2 dx$. The detailed steps of derivation fundamentally assume that the Young's modulus and the second moment of area are constant over the entire length of the beam, that loosely translates to $k(x) = k(\hat{x})$ for $0 \leq x \leq L$. Further, on approximating the stress distribution in Eqn. 2.9 by $k_j(x) = k(\hat{x})$ (for $j = 1, ..., NE$), Eqn. 2.15 turns out as:

$$\frac{\delta K_{ij}}{K_i} = \frac{\gamma_{ij}^* k_j^* - \gamma_{ij} k_j}{\gamma_i k_j} \tag{2.18}$$

where the relative change in the j^{th} element stiffness is given by,

$$\gamma_i = \int_0^L [\phi''_i(x)]^2 dx \tag{2.19}$$

It was assumed that the damage was localized only to a single point in the structure. To account for several identifiable modes for the j^{th} location, in the above equation is given by:

$$\beta_j = \frac{k_j}{k_j^*} = \frac{\sum_i \gamma_{ij}^*}{\sum_i (\gamma_i g_i + \gamma_{ij})} \tag{2.20}$$

where the damage is identified as the relative change in the j^{th} element stiffness when the L.H.S of Eqn. 2.20 is greater than unity.

In order to proceed towards estimating the severity of the damage located at the j^{th} element,

Eqns. 2.19 and 2.20 can be referred to evaluate the severity estimation index, α_j, expressed as:

$$\alpha_j = \frac{k_j^* - k_j}{k_j} = \frac{\left(\sum_i \left(\gamma_{ij} - \gamma_{ij}^*\right) + \sum_i \gamma_i g_i\right)}{\sum_i \gamma_{ij}^*} \tag{2.21}$$

where the damage severity is the fractional change in stiffness of the j^{th} element.

Damage detection through the use of Kalman Filter updates

The time-domain analysis of noise-contaminated vibration signals for global structural damage diagnosis can be carried out using the recursive state estimations provided by the Kalman Filter (KF) updates [72–75]. An extension of response-only time-domain auto-regressive -with-eXogenous input (ARX) model [76], the *process* is defined such that the acceleration response at a given DOF is regarded as the *input*, while the accelerations at other DOFs are the *state* with which the *measurements* are associated. Considering the measurements from a reference state (preferably the pristine state) of the structure, a baseline model is created. The relative changes of the structural conditions with respect to this baseline model can be diagnosed by providing the newer set of observations as inputs to the model and analyzing the residual error features. In conjunction with the KF technique, the ARX model provides features for extracting the damage instants and locations even under noisy measurement signals. In order to carry out the damage diagnosis procedure, the ARX model is first expressed in a state-space form in order to introduce the noise terms into the system. The expression of the model in a state-space form facilitates the application of the KF updates.

The KF is an effective tool for stochastic estimation of the state from noisy measurements. Because of its relative simplicity and robust nature, the KF has been widely used to obtain estimates of the state variables in practice [73–75]. The KF updates are basically a set of mathematical equations that aims at minimizing the estimated error covariance in the state estimator. The basic set of equations for a given process and measurement noise are given as:

$$\begin{aligned} x(k+1) &= \mathbf{A}x(k) + \mathbf{B}u(k) + \mathbf{G}\eta(k) \\ y_v(k) &= \mathbf{C}x(k) + v(k) \end{aligned} \tag{2.22}$$

In the above equation, $u(k)$ is the process input of the system, $y_v(k)$ represents the measurement (or the output) with $\eta(k)$ and $v(k)$ being the input and output noise, respectively (also known as *process* noise and *measurement* noise). In most typical cases, the input coefficient for the process noise, $\mathbf{G}$, is introduced into the system together with the input signal, which makes it equal to $\mathbf{B}$. The KF update equations basically belong to a family to predictor-corrector operations. The filter estimates the process state and obtains the feedback from the measurement which is noisy. The first step of the KF updates performs the prediction, known as the "time update", where the *apriori* estimates for the current step is obtained based on the knowledge of the previous state and error covariance. The next step that follows is the correction, known as the "measurement update" that is carried out to obtain an *aposteriori* estimate. Mathematically, these steps are expressed as:

Time update equations:

$$\left.\begin{aligned} \hat{x}(k|k-1) &= \mathbf{A}x(k-1|k-1) + \mathbf{B}u(k-1) \\ \mathbf{P}(k|k-1) &= \mathbf{A}\mathbf{P}(k-1|k-1)\mathbf{A}^T + \mathbf{G}\mathbf{Q}(k-1)\mathbf{G}^T \\ \mathbf{Q}(k) &= E(\eta(k-1)\eta(k-1)^T) \\ \mathbf{R}(k) &= E(v(k-1)v(k-1)^T) \end{aligned}\right\} \tag{2.23}$$

Measurement update equations:

$$\left.\begin{aligned} \hat{x}(k|k) &= \hat{x}(k|k-1) + \mathbf{M}(k)(y_v(k) - \mathbf{C}\hat{x}(k|k-1)) \\ \mathbf{M}(k) &= \mathbf{P}(k|k-1)\mathbf{C}^T(\mathbf{R}(k) + \mathbf{C}\mathbf{P}(k|k-1)\mathbf{C}^T)^{-1} \\ \mathbf{P}(k|k) &= (\mathbf{I} - \mathbf{M}(k)\mathbf{C})\mathbf{P}(k|k-1) \end{aligned}\right\} \tag{2.24}$$

The Kalman gain is obtained from the expression, $\mathbf{K}(k) = \mathbf{A}\mathbf{M}(k)$ On combining the first set of equations from both the time and measurement update modules, one can write:

$$\hat{x}(k|k-1) = \mathbf{A}\hat{x}(k-1|k-2) + \mathbf{K}(k-1)(y_v(k-1) - \mathbf{C}\hat{x}(k-1|k-2)) + \mathbf{B}u(k-1) \tag{2.25}$$

In the above equations, $\hat{x}$ denotes the estimated process state, $\mathbf{P}$ represents the apriori estimate error covariance, $\mathbf{M}$ represents the aposteriori estimate error covariance. Considering the initial conditions $\hat{x}(1|0)$ and $\mathbf{P}(1|0)$, the filtering can be performed by iterating the above sets of equations

at every instant. The filter then produces an optimal estimate of the true response measurements, $\hat{y}_e = \hat{y}(k|k-1)$, by the following expression:

$$\hat{y}(k|k-1) = \mathbf{C}\hat{x}(k|k-1) \tag{2.26}$$

The damage diagnosis procedure can be enumerated in the steps as under:

1. The first step is to obtain the output acceleration response obtained from a newer state of the structure. the baseline model is created by taking the pristine state of the structure into account and kept ready for a future reference.

2. Estimate the model parameters using ARMAX technique on the original set of signals. Ignoring the moving average (MA) portion gives rise to the reference ARX model.

3. Model the newer set of signals using the ARMAX approach. With the raw input $u_v(k)$, the virtual input-output response set is obtained using the stochastic processing of the signals through ARMAX approach.

4. The reference ARX model obtained from step (2) is applied on the virtual input-output response set. The residual error of the ARX results are obtained and the damage is ascertained using an appropriate residual error feature.

5. The steps (2) to (4) are repeated for any other newer state of the system that require diagnosis.

A statistical parameter known as CRE is employed to identify the presence of damage. This parameter is a direct result obtained from the diagnosis of the residual error and is defined as the percentage of the error variation, given by:

$$CRE = \sigma(e)/\sigma(y) * 100\% \tag{2.27}$$

where $\sigma(e)$ is the covariance of the residual error when the reference model is applied on the current-state signals and $\sigma(y)$ is the covariance of the output $y(k)$. The parameter serves as a relative

indicator of the changes in the inherent dynamic system when compared to the CRE obtained from the baseline state of the structure.

2.1.2 Drawbacks of the model based methods

- All the model based methods discussed earlier have a serious problem in *increased computational cost*. FE modeling requires extensive computation causing delay in the functioning of the algorithms, incurring computational penalty and increasing vulnerability towards modeling errors associated with the model.

- In many cases of the model based methods, it has been observed that a single parameter or a group of parameters control the functioning of the algorithm. This makes the method *parametric*, that impedes its possible applications towards versatile problems, leading to erroneous results when the parameter is affected by change of model, increased computation and/or inclusion of embedded environmental variables that might arise during practical case studies.

- Most of the model based methods are *baseline reliant* where the data from a comparatively newer state of the structure is assessed against the data from the structure recorded in its pristine state. This hinders the applicability of the methods towards an online implementation. Literature is replete with instances where the model based methods have failed to show desired damage detection results as compared to online implementations of a similar nature.

- Detection of *lower levels of damage* in a structure remains one of the key challenges of SHM. Engineering practice has shown that very little improvement can be done to tailor these methods towards an effective damage detection scheme, reporting for real life damage scenarios where the order of damage is usually restricted to 30% for a moderate earthquake. This paves the way for developing methods that use only the output of a structure to indicate and localize the damage, which are commonly referred to as response based or vibration based techniques.

2.1.3 Response based damage detection methods

The response based methods, more popularly known as output-based schemes, constitute a separate class of problems that deal only with the vibration data obtained from numerical simulations or recorded in controlled laboratory environments and/or recorded responses from field data [29–46]. This class of methods employ the vibration data to ascertain the changes in the modal parameters of the structure to quantify damage, thereby indirectly administering solutions to inverse structural dynamics problems. The response based methods encompass a wide range of statistical signal processing techniques to quantify the severity of damage and hypothesize its location. Some of the previously established developments in the response based genre of damage detection algorithms utilize the concepts of empirical mode decomposition (EMD) [67, 77–81], blind source separation (BSS) [68–71], Hilbert Huang transform (HHT) [77, 79–81], to capture the key features of damage. A plethora of literature provides instances where physical responses fit using time series models have shown to provide impeccable detection results through the use of certain statistical DSFs [1–3, 5]. This has been achieved by incorporating the analysis of AR, auto-regressive moving average (ARMA) and auto-regressive moving average with exogenous input (ARMAX) model coefficients [82], that determines the occurrence of incipient damage and possibly provide features to identify its location. The use of TVAR coefficients to model a set of responses provides feature vectors for detecting damage in real time. A special case of time invariant coefficients renders the implementation of KF updates on the TVAR modeling, ineffective, thereby reducing the problem to a straightforward application of AR models, which can be easily estimated using basic least squares fit. Interested readers are referred to seminal works [1, 2, 76, 82] on this topic. In the context of structural damage detection, out of the enormous wealth of literature, some of the key algorithms that have consistently provided adequate detection results over the years are presented next in detail [1–3].

Empirical Mode Decomposition (EMD)

The use of empirical mode decomposition (EMD) as a tool for damage detection of structural elements has been well documented in the literature [67, 77–81]. Associated with EMD is the energy damage index (DI) that differentiates the damaged state of the system from its pristine state used

for subsequent health assessment of the system based on its vibration data. EMD is a statistical signal processing transform that decomposes a signal into its intrinsic mode functions (IMFs) that admit a well-behaved Hilbert transform. An IMF is defined as a function that satisfies the following conditions: (i) it is mono-component in nature and (ii) the mean values of the envelopes defined by the local maxima and the local minima are zero. A stalwart in signal decomposition genre, EMD decomposes any given signal into its corresponding IMFs, even under nonstationary environments, in an adaptive manner, without pre-selecting any basis [78, 79]. In modal identification theory, for MDOF systems, the IMFs extracted from the free-vibration responses can be regarded as the modes of vibration.

The procedure of extracting an IMF is called *sifting*, a technique rigorously discussed in supporting literature. Suppose a signal $x(t)$ is to be decomposed. The running mean of the envelope is subtracted which produces the difference $x(t) - m_1 = h_1$ to obtain the first IMF, containing the shortest period component of the signal. The component h_1 is now examined if it satisfies the conditions necessary to be called an IMF. If it does not satisfy these necessary conditions, the sifting process continues in iterations by treating h_1 as the original data until the requirements for an IMF are fulfilled. The original signal is then subtracted from the IMF and the sifting process is repeated to decompose the data into n IMFs, C_i and a residue r_n, which can either be the mean trend or a constant. Mathematically, the procedure can be expressed as:

$$X(t) = \sum_{i=1}^{n} C_i + r_n \tag{2.28}$$

where $X(t)$ is the free acceleration response for any n-DOF system. To obtain the location of damage in the structure, a DI based on the energy of the first IMF of the signal is developed. The vibration response obtained from the pristine state of the system is first acquired and passed through a band-pass filter to ensure the existence of only the first natural frequency within the data. The first IMF is then extracted through EMD to obtain the energy of for each sensor as:

$$E = \int_0^{t_0} (IMF)^2 dt \tag{2.29}$$

The aforementioned procedure is repeated for the system in its damaged state in order to estimate the energy of the first IMF of every signal component. Finally, the application of the EMD DI for each sensor is given by the following expression:

$$DI = \left| \frac{E_{Healthy} - E_{Damaged}}{E_{Healthy}} \right| \times 100 \tag{2.30}$$

In order to determine the exact location of damage to the structure and its severity, the high index values may be associated with the existence of damage close to the respective sensors. However, a key drawback of this approach is the requirement of measured responses at all floor levels. In order to overcome these difficulties, recently developed damage detection algorithms premised on decorrelating the signals using orthogonal transformations are utilized.

Blind source separation (BSS)

The separation of original source waveforms from the sensor signals, without the knowledge of the system characteristics and the sources, is known as blind source separation (BSS) [68–71]. BSS, a non-parametric method, has been extensively used as a powerful signal decomposition tool [68] in the field of acoustic and image processing. BSS can be recast as an inverse problem that is utilized to identify a system in order to estimate the primary source signals. The estimation, mostly carried out on output signals, primarily identifies the mixing system first and then estimates the source signals implicitly by some suitable optimization procedure [68]. In addition to its utility as a system identification tool, BSS can also be used to detect damage in structures by utilizing its second-order statistics such as auto-correlation functions [70] or higher-order statistics like non-Gaussianity [71]. A survey of the previous literature reveals that independent component analysis (ICA), a variant of higher-order BSS, was employed towards structural damage detection [68, 69]. However, it was later observed that ICA suffered from some performance issues such as presence of higher structural damping and measurement noise. The use of auto-correlation functions prompted the utilization of second-order blind identification (SOBI) to undertake damage detection, pivoted around windowing of the vibration datsets, which in turn accounted for increased computational cost and proved insensitive towards lower level of damage in the structure.

Considering the basic dynamics of an MDOF structure as linear, classically damped and lumped-parameter n DOF system subjected to Gaussian broadband excitation, $F(t)$, the equation of motion can be expressed as:

$$\mathbf{M}\ddot{X}(t) + \mathbf{C}\dot{X}(t) + \mathbf{K}X(t) = F(t) \tag{2.31}$$

where $X(t)$ is the vector of displacement coordinates while $\mathbf{M}$, $\mathbf{K}$ and $\mathbf{C}$ are the mass, damping and stiffness matrices of the system, respectively. The solution to Eqn. 2.31 can be written in terms of superposition of vibration modes according to:

$$\mathbf{X}(n) = \mathbf{A}\mathbf{S}(n) \tag{2.32}$$

In the above equation, $\mathbf{X}$ is the measurement matrix composed of the sampled components of X, $\mathbf{S}$ is the matrix of the corresponding modal coordinates and $\mathbf{A}$ is the modal transformation matrix with N number of the total datapoints in the sample space. Furthermore, it has been observed that the columns of the mixing matrix $\mathbf{A}$ are linearly independent that corresponds to the mode shapes of the structure. The main objective of the SOBI is to formulate two covariance matrices $\mathbf{R}_x(0)$ and $\mathbf{R}_x(p)$ evaluated at time lags 0 and p, respectively, form the vibration measurements and perform joint diagonalization in order to evaluate the unknown mixing matrix, $\mathbf{A}$. Mathematically, one can write

$$\left.\begin{aligned} \mathbf{R}_X(0) &= E\left[\mathbf{X}(n)\mathbf{X}(n)^T\right] = \mathbf{A}\mathbf{R}_S(0)\mathbf{A}^T \\ \mathbf{R}_X(p) &= E\left[\mathbf{X}(n)\mathbf{X}(n-p)^T\right] = \mathbf{A}\mathbf{R}_S(p)\mathbf{A}^T \end{aligned}\right\} \tag{2.33}$$

where, $\mathbf{R}_S(p) = E\left[\mathbf{S}(n)\mathbf{S}(n-p)^T\right] = \mathbf{I}$. Typically, SOBI encompasses three key steps that are addressed sequentially: whitening, orthogonalization and unitary transformation. As the data predominantly evolves from a zero mean process, the first step towards whitening is carried out by diagonalizing $\mathbf{R}_X(0)$ as: $\mathbf{R}_X(0) = \mathbf{V}_X\lambda_X\mathbf{V}_X^T$, with $\mathbf{V}_X$ and λ_X being the principal components of eigenspace. The whitened signals are then obtained from the following equation with $\mathbf{Q}$ idealized as the whitening matrix:

$$\bar{\mathbf{X}}(n) = \lambda_X^{-1/2}\mathbf{V}_X^T\mathbf{X}(n) = \mathbf{Q}\mathbf{X}(n) \tag{2.34}$$

The correlation between the measured responses is removed using whitening, given by the relation:

$\mathbf{R}_{\bar{X}}(0) = E\left[\bar{\mathbf{X}}(n)\bar{\mathbf{X}}(n)^T\right] = \mathbf{I}$ due to which the whitening process $\mathbf{R}_X(p)$ transforms to $\mathbf{R}_{\bar{X}}(p)$, according to the following expressions:

$$\mathbf{R}_{\bar{X}}(p) = \frac{1}{N}\left[\sum_{n=1}^{N}\bar{\mathbf{X}}(n)\bar{\mathbf{X}}(n-p)^T\right] = \mathbf{QAR}_S(p)\mathbf{A}^T\mathbf{Q}^T \tag{2.35}$$

From the above equation, it can be understood that as the whitened covariance matrix at a particular time-lag can be diagonalized, the matrix product **QA** is an unitary matrix that can be diagonalized, numerically. The EVD of the matrix $\mathbf{R}_{\bar{\mathbf{X}}}(\mathbf{p})$ can be expressed in the spectral decomposition format, that satisfies the relation, $\mathbf{V}_{\bar{X}}\mathbf{R}_{\bar{X}}(p)\mathbf{V}_{\bar{X}}^T = \lambda_{\bar{X}}$. As the diagonal matrix $\lambda_{\bar{\mathbf{X}}}$ has distinct eigenvalues, the mixing matrix can be readily estimated, according to:

$$\hat{\mathbf{A}} = \mathbf{Q}^{-1}\mathbf{V}_{\bar{X}} = \mathbf{V}_X\lambda_X\mathbf{V}_{\bar{X}}^T \tag{2.36}$$

In order to find the unitary matrix **QA** that diagonalizes the whitened covariance matrix $\mathbf{R}_{\bar{X}}(p)$, at one or several non-zero time lags, the SOBI carries out an approximate joint diagonalization approach based on Givens rotation technique. The problem then transforms to finding a minimum performance index, $\Im$ such that the unitary diagonalization satisfies the relation, $\mathbf{D} = \mathbf{V}^T\tilde{\mathbf{R}}_{\bar{X}}(p)\mathbf{V}$. Therefore,

$$\Im(\mathbf{V}, p) = \sum_{p}\sum_{1\leq i\neq j\leq n_s}\left\|\mathbf{D}_{ij}^{p}\right\|^2 \tag{2.37}$$

where, $\mathbf{V}$ is the the unitary matrix and also the joint approximate diagonalizer for all p-shifted covariance matrices $\tilde{\mathbf{R}}_{\bar{X}}(p)$. Once the mixing matrix is obtained, the estimated sources can now be evaluated, which was the primary objective of carrying out SOBI,

$$\hat{\mathbf{S}}(n) = \hat{\mathbf{A}}^{-1}\mathbf{X}(n) \tag{2.38}$$

The matrix $\hat{\mathbf{S}}(n)$ contains the modal responses from which the modal frequencies and damping ratios can be obtained. It is well understood that the vibration data obtained comprises a damage event which necessitates that each modal response contains sources from both damaged and undamaged states. Once the modal responses are obtained from SOBI, the instant and location of damage need

to be identified. However, it is a well understood fact that the computational efficiency of the entire process is significantly escalated due to the simultaneous algebraic operations that take place in windows and permutation ambiguity [154]. In order to overcome these impediments, comparatively recent trends in structural damage detection are explored that is described in detail in the subsequent sections.

The effects of damage to a structure that entail the alteration of geometry and/or material properties, form the sole basis of implementation of BSS as a damage detection tool. The estimated sources in conjunction with time series analysis are used for the prediction of future measurements to identify the damage. Time series models with pre-selected model orders are used to characterize the sources that are obtained from from the past observations and then the future measurement sources are accordingly predicted [68]. The newer measurements contain the information about the damaged state of the structure and are compared against the baseline data pre-recorded from the pristine state of the system, that enables the estimation of damage, in an adaptive fashion. Although the response based methods open up a new paradigm in the context of vibration based damage detection with certain added advantages, some of the key drawbacks of these strategies are discussed next.

2.1.4 Drawbacks of the response based methods

- In many cases of damage detection, the change in natural frequencies to determine the instant of damage is masked by the varying *operational and environmental conditions*. For this reason, successful damage detection facilities are carried out in a controlled environment and not implemented as field problems. To alleviate this drawback, statistical damage detection model using pattern recognition technique is needed to distinguish damage-induced changes from environment-induced changes. Damage markers should correctly describe the embedding of the environmental variables into the algorithm, which remains a field of development of the response based methods.

- Most of the vibration based methods are currently *offline* in nature, i.e., they require batches of data in order to compare against a recorded set of data obtained from a pristine state of

the structure. In order to track the changes in the structure as and when the vibration data streams in real time, the aforementioned methods need to be implemented in an adaptive fashion that could possibly identify damage at a particular instant of time, without using pre-recorded data.

- A limitation in response based methods is the detection of damage for cases with *progressive damage* because of the time varying nature of the vibrating system. Damage involving changes of stiffness over a period of time, progressively, is captured only through a recursive implementation since the data from a particular instant is taken into consideration and compared against the data obtained from the previous time stamp.

- Almost all the methods discussed in the previous section utilize the data gathered from *all sensors*, i.e., these algorithms do not work well when the number of sensors used is less than the DOF. In practical scenarios, the number of sensors instrumented is mostly less than the total number of active DOF due to cost considerations and accessibility issues. This requires an immediate development of algorithms that detect the exact instant of damage for under-determined cases (where the number of sensors is less than the number of DOF) as well, in a single framework, utilizing the principles of recursion in a perturbation approach.

2.2 Recent trends in damage detection

A class of inverse structural vibration problems involving exploratory analysis of POCs, nonlinearity detection and SHM is carried out using a family of orthogonal transformation based algorithms, popularly known as PCA [83–99]. An extension of the application of EVD (which is the crux of PCA) to elicit principal components (PCs), using the inputs from a single dataset, arranged in a Hankel structure, referred to as singular spectral analysis (SSA), is also gaining popularity in recent times [100–110]. Mathematically, these two approaches are widely different and are discussed in detail in the subsequent sections.

2.2.1 PCA and structural damage detection

In recent years, PCA has been extensively applied to measure structural dynamic response signals with the purpose of dimensionality reduction studies, to account for changes due to environment and structural damage, for sensor validation, and so on [84–90]. In addition to identifying the presence of damage in a system, PCA can also be used to estimate the severity of the damage through the acquired vibration data from numerical simulations and/or experimental trials. PCA builds a baseline model from the output response obtained from the pristine state of the structure and compares it with the newer acquired set of data in order to identify the presence of damage through certain DIs such as T^2, Q, I^2 and ϕ; instances of which, are replete in literature [93].

PCA, can be defined as the orthogonal projection of the data onto a lower dimensional space, known as the *principal subspace*, such that the variance of the projected data is maximized, and can be applied for dimensionality reduction, feature extraction and data visualization. On reducing the complex data set to a lower dimension, PCA reveals some simplified structures relevant to the data set which can be extracted using EVD on the sample covariance matrix. It is closely related to *Karhunen-Loève* transform or proper orthogonal decomposition (POD) [111–122]. The basic idea of KL transform is to decompose a general second-order random process using an orthogonal expansion of uncorrelated random variables. Although classically many authors [93] have attempted to explain the connection using an approach that entails solution of integral equations, it is perhaps more instructive to understand PCA in the light of decorrelation and the pathway to achieving it by dint of eigenvalue decomposition of covariance matrix [121, 122].

Towards that, let a multivariate data $\mathbf{X}$ be defined such that the individual univariate data are correlated. PCA seeks an orthogonal transformation of the form: $\mathbf{T} = \mathbf{PX}$, where $\mathbf{T}$ represents the space of transformed variables that are decorrelated. So, PCA can be thought of as a constrained optimization problem [93] where the objective is to diagonalize $\mathbf{TT}^T$ subject to the constraint $\mathbf{PP}^T = \mathbf{I}$. Mathematically, it translates to defining an objective function $\mathcal{O}$ as under:

$$\begin{aligned} \mathcal{O} &= \mathbf{TT}^T - \Lambda(\mathbf{PP}^T - \mathbf{I}) \\ &= \mathbf{P}^T\mathbf{X}^T\mathbf{XP} - \Lambda(\mathbf{PP}^T - \mathbf{I}) \end{aligned} \tag{2.39}$$

The optimal transformation is obtained by setting the partial derivative of $\mathcal{O}$ to *zero* as follows:

$$\frac{\partial \mathcal{O}}{\partial \mathbf{P}^T} = 0 \implies (\mathbf{X}^T\mathbf{X})\mathbf{P} = \Lambda(\mathbf{P}) \tag{2.40}$$

Thus, from Eqn. 2.40, it is clear that the optimum orthogonal decorrelating transformation is achieved by the eigen-decomposition of the covariance matrix of the correlated data $\mathbf{X}$.

This decomposition produces the eigen value matrices, expressible as time series, known as the *principal orthogonal values* (**POVs**) and eigen vector matrices, also known as *proper orthogonal matrices* (**POMs**) [118,119,122]. Eigen values/POVs describe the relative significance of each POM in the response as a whole. The uncorrelated new set of variables produced by the linear combinations of the original variables are known as the *principal orthogonal components* (**POCs**) [118, 121]. The new set of variables have an improved potential to detect deviations (such as structural damage) in the system as compared to the original set of variables and hence, finds its way in the field of structural damage detection [84, 85].

Damage detection indices based on PCA

The transformed response obtained after PCA does not provide sufficient information regarding the localization of damage and its severity. As these projections are sometimes not enough, it is necessary to use certain statistical parameters that are considered as DIs. In this context, few DIs and their utility are described next.

Q-statistic (SPE index): This damage index is based on analyzing the residual data matrix to represent the variability of the data projection within the residual subspace. Considering the i^{th} row of the matrix $\mathbf{E}$, the *Q-statistic* for each experimental observation is defined as:

$$Q_i = e_i e_i^T = x_i(\mathbf{I} - \mathbf{P}\mathbf{P}^T)x_i^T \tag{2.41}$$

Hotelling's T^2 -statistic (D index): This index is based on the analysis of the score matrix $\mathbf{T}$ to check the variability of the projected data in the new space of the PCs. The concept of Eucledian distance comes into effect by utilizing the covariance matrix $\mathbf{C}_x$ as the normalization factor. For the

i^{th} sample, the DI is expressed according to:

$$\begin{aligned}\mathbf{T}_i^2 &= \sum_{j=1}^{r} \frac{t_{sij}^2}{\lambda_j} = t_{si}\mathbf{\Lambda}^{-1}t_{si}^T \\ &= x_i\mathbf{P}\mathbf{\Lambda}^{-1}\mathbf{P}^T x_i^T\end{aligned} \tag{2.42}$$

In the above equation, t_{si} is the i^{th} row vector of the matrix $\mathbf{T}$, defined as the projection of the experiment x_i onto the new space, related by the expression, $t_si{=}x_iP$

Combined index (ϕ index): This DI is essentially a blend of the Q index and the T^2 index that provided alternatives for merging information into a single value. The mathematical expression defining this DI is given as:

$$\begin{aligned}\phi\ index &= Q\ index + T^2\ index \\ &= x^T M_\phi x \\ &= x^T(\mathbf{I} - \mathbf{P}\mathbf{P}^T + \mathbf{P}\mathbf{\Lambda}^{-1}\mathbf{P}^T)x\end{aligned} \tag{2.43}$$

I index: This DI has its very roots in its utilization for clinical studies and mainly used for meta-analysis, accounting towards a percentage of heterogeneity. The I index provides variation in study outcomes between experimental trials and can be mathematically defined as:

$$\mathbf{M}_I = \begin{cases} \frac{Q-(k-1)}{Q} \times 100\% & for\ Q > (k-1) \\ 0 & otherwise \end{cases} \tag{2.44}$$

where k is the number of experimental trials.

PCA and its relation to structural dynamics

Other than being a purely data driven decorrelating orthogonal transform, PCA can also be interpreted in the framework of structural dynamics. The objective of PCA is to find a orthogonal transformation of the form $\mathbf{T} = \mathbf{P}\mathbf{X}$ (where size of $\mathbf{T}$ is $m \times n$) that completely diagonalizes the covariance matrix of the data set $\mathbf{X}$. $\mathbf{P}$ (also known as POMs) has the orthonormal basis of vectors as rows. Since the structural modes are orthonormal to each other with respect to mass matrix, PCA can be utilized to extract the linear normal modes (LNMs) of vibrating systems which are

closely related to the POMs (i.e. the eigenvectors) of PCA [112–114]. To understand the relationship, consider an undamped MDOF system with mass and stiffness matrices $\mathbf{M}$ and $\mathbf{K}$ undergoing free vibration with $\mathbf{x}$ as the displacement vector. The dynamics of the system can be expressed as:

$$\mathbf{M}\ddot{\mathbf{X}} + \mathbf{K}\mathbf{X} = 0 \tag{2.45}$$

The modal responses are related to the physical responses (as individual functions of t) according to the following expression: $\mathbf{X} = \mathbf{V}\mathbf{Q}$, where $\mathbf{X}$ is a matrix of physical responses arranged column wise, of size $M \times N$, such that $\mathbf{X} = [\mathbf{X}_1, \mathbf{X}_2, \mathbf{X}_3, ..., \mathbf{X}_M]^T$, M being the number of degrees of freedom (DOF) of the structure and N is the number of sampling points. In this context, $\mathbf{V}$ is the eigen vector (mode shape) matrix and the modal ensemble matrix is denoted by $\mathbf{Q}$ which comprises of the numerous vectors of the modal coordinates.

The covariance matrix of the modal responses can be identified as: $\mathbf{R_Q} = \frac{1}{N}\mathbf{Q}\mathbf{Q}^\mathbf{T}$. For undamped free vibration and also for mildly damped system, the covariance matrix of the modal response $\mathbf{R_Q}$ approximate to a diagonal matrix as the samplesize of the responses increase [111,119,121,122]. For forced vibration under broadband excitation, the evolution of the physical response, $\mathbf{x_i}(\mathbf{t})$ and modal response $\mathbf{q_i}(\mathbf{t})$ in time domain can be expressed in terms of the impulse response function $h(t)$ as given by the following expressions: $x_i(t) = \int_0^\infty h(t-\tau)F_i(\tau)d\tau$ and $q_i(t) = \int_0^\infty h(t-\tau)f_i(\tau)d\tau$, where $\mathbf{F}_i(\tau)$, and $\mathbf{f}_i(\tau)$ represent the actual and modal forces, related by the equation $\mathbf{f}_i(\tau) = \varphi_i^T\mathbf{F}_i(\tau)$, where φ is the mode shape corresponding to the mode. The individual elements of the covariance matrix $\mathbf{R_Q}$ can be expressed as:

$$r_{ij}^Q = \frac{1}{N}\sum_{k=1}^{N} q_i(t_k)q_j(t_k) = \int_{\tau=0}^{\infty}\int_{\theta=0}^{\infty} f_i(\tau)f_j(\theta)\left[\frac{1}{N}\sum_{i,j} h_i(t-\tau)h_j(t-\theta)\right]d\tau d\theta \tag{2.46}$$

For finitely large N, $\mathbf{R_Q}$ can be expected to be a diagonal matrix for undamped system and nearly diagonal for light to moderate modal damping. To understand the behavior of r_{ij}^Q in the context of POD, under moderate modal damping and finite sample size, it is instructive to understand the behavior of the term $[\frac{1}{N}\sum_{i,j} h_i(t-\tau)h_j(t-\theta)]$ as $N \to \infty$, which can be achieved by expressing the

POCs (ψ) as a sum of the true linear modal coordinates (q_i) and error terms (ε) according to:

$$\psi_i(t) = q_i(t) + {\varepsilon_i}^T x(t) \tag{2.47}$$

To observe the characteristics of r_{ij}^{Q}, consider the covariance matrix of the POCs as: $\mathbf{R_\Psi} = \frac{1}{N}\mathbf{\Psi}\mathbf{\Psi^T}$. Each individual element of the covariance matrix formed by the POCs can be obtained from the following steps. Substituting from Eqn. 2.47,

$$\begin{aligned} r_{ij}^{\psi} &= \frac{1}{N}\sum_{k=1}^{N}\psi_i(t_k)\psi_j(t_k) \\ &= \frac{1}{N}\sum_{k=1}^{N}[q_i(t_k)q_j(t_k) + \varepsilon_i^T x(t_k)q_j(t_k) + q_i(t_k)\varepsilon_j^T(t_k) + \varepsilon_i^T\varepsilon_j^T x(t_k)^2] \end{aligned} \tag{2.48}$$

Ignoring the second order error terms (i.e., ε^2 terms) Eqn. 4.4 can be written as:

$$\begin{aligned} r_{ij}^{\psi} &= \frac{1}{N}\sum_{k=1}^{N}[q_i(t_k)q_j(t_k) + {\varepsilon_i}^T\varphi_i q_i(t_k)q_j(t_k) + q_i(t_k){\varepsilon_j}^T\varphi_j q_j(t_k)] \\ &= \int_{\tau=0}^{\infty}\int_{\theta=0}^{\infty} f_i(\tau)f_j(\theta)\left[\frac{1}{N}\sum_{i,j}h_i(t-\tau)h_j(t-\theta)\right]d\tau d\theta + \\ &\int_{\tau=0}^{\infty}\int_{\theta=0}^{\infty} {\varepsilon_i}^T\varphi_i f_i(\tau)f_j(\theta)\left[\frac{1}{N}\sum_{i,j}h_i(t-\tau)h_j(t-\theta)\right]d\tau d\theta + \\ &\int_{\tau=0}^{\infty}\int_{\theta=0}^{\infty} {\varepsilon_j}^T\varphi_j f_i(\tau)f_j(\theta)\left[\frac{1}{N}\sum_{i,j}h_i(t-\tau)h_j(t-\theta)\right]d\tau d\theta \end{aligned} \tag{2.49}$$

It is clear from Eqn. 2.49, that for practical systems under moderate modal damping and finite sample size, the POC's provide a good approximation to the true linear modal component which deviate from each other as damping increases. However, the matrix $\mathbf{R_\Psi}$ is still expected to show a diagonally dominant behavior in the limit $N \to \infty$ and when the errors are low (i.e., low to moderate damping) [121, 122]. It can now be well understood that PCA decorrelates the dataset obtained from the inputs of multiple sensors. For practical cases, where the system dimension is large, it is not possible to instrument each DOF. Moreover, PCA does not fare well with the nonlinearities associated with datasets. In this context, the shortcomings of the PCA based methods are discussed

next in detail.

Drawbacks of the PCA based approaches

It has been observed that the the PCA model, once built from the data, is time invariant, while most real life processes are time-varying in nature. When a time invariant PCA model is used to monitor processes with the aforementioned normal changes, false alarms often result, which significantly compromise the reliability of the monitoring system [88]. As PCA is a baseline reliant approach that requires data to be processed in batches or windows, it cannot be implemented towards online detection problems. The aim of the present research is to address the shortcomings of PCA in a systematic manner, by proposing certain essential modifications in its formulations and expand the range of applicability of PCA based approaches towards addressing system-specific problems. The key shortcomings of PCA can be summarized as under:

1. Traditional PCA based methods analyze data in a batch mode, offline. As PCA is a baseline reliant approach, the analyzed data are windowed so as to compare it with reference over certain intervals of time. Practical engineering applications require the choice of window parameters such as window size, shift, overlap, etc. to be discrete and problem specific. This issue is addressed through the modifications proposed in the formulation of basic PCA to tailor it towards an online implementation, utilizing the FOEP techniques to develop a novel real time damage detection algorithm, RPCA.

2. A key shortcoming of PCA appears while dealing with problems involving nonlinearities in the datasets. For applying the concept of PCA for incorporating non-linear dependence between variables, a variation of PCA, known as kernel PCA (KPCA) [89] is sometimes utilized to account for the presence of nonlinearities in the data in the context of damage detection. However, KPCA based approaches relying on the concept of subspace angle is computationally expensive. Moreover, it has been observed that changes in the subspace angle sometimes might appear due to the presence of outliers, which might provide false detections and thereby compromise the reliability of the detection process.

3. The central idea of any PCA based method is to perform EVD on the sample covariance estimate to obtain the eigenvalues and eigenvectors which constitute the *eigenspace* for the dataset. Physically, for a real time framework, performing EVD at each instant is cumbersome. To alleviate this issue, the concepts of RPCA approach provides iterative updates at each instant of time by utilizing the eigenspace and not the covariance estimate as a whole. The details of the RPCA based approach can be found in chapter 3 of this dissertation.

4. The current form of basic PCA is such that it utilizes the streaming vibration data input from multiple sensors. This sometimes become an impediment due to the unavailability of large number of sensors, improper accessibility and cost and other factors. This issue can be addressed by developing a real time damage detection strategy that takes the input from only a single sensor and provides accurate estimation results. Established using the very basics of EVD (as in PCA), the new detection strategy RSSA, towards identifying damage, uses the input from a single sensor only; the details of which are thoroughly discussed in chapter 4.

2.2.2 Singular spectrum analysis (SSA)

SSA is a non-parametric method that works well with arbitrary statistical processes and requires no prior assumptions about the stationarity, linearity or normality of the data set. Somewhat similar to PCA based methods [100, 102, 104], SSA projects the original time series into a smaller dimensional space which is composed of lagged signal components, while retaining most of the variance and the information associated with the particular data set [100–104, 123–126]. The most prominent difference between the methods is that while in PCA, the singular value decomposition (SVD) is carried out predominantly on data gathered from a vibrating system, SSA utilizes the time history data obtained from each sensor and performs SVD on the Hankel matrix formed by the streaming data [100–104]. The superiority of SSA over the basic classical approaches is that the method decomposes a series into its component parts and reconstructs the series by leaving out the random (or noise) component behind. To tailor the traditional SSA method towards online implementation, an extension premised mainly on first order perturbation techniques, known as RSSA, is discussed in detail in the current research, that enables online spatio-temporal damage detection in a single

framework.

2.2.3 Basic SSA

The main objective of SSA is to decompose the original time series into a set of simpler components [100–104] from which three different characteristics can be extracted, namely- *slowly varying trend*, *harmonic* (or *oscillatory*) component and *noise*. The trend components correspond to slow varying additive component of the series in which the oscillations are removed or smoothed [100–102]. The harmonic series are periodic in nature which are either pure or amplitude modulated, while the noise component is any aperiodic series that does not affect the performance and/or functioning of the algorithm since it is omitted during the reconstruction of the time series. The algorithm creates a Hankel matrix out of the time series itself by sliding a window that is shorter than the length of the time series. This process is known as *embedding*. The matrix is then decomposed into a number of elementary matrices of decreasing norm, through the process of *singular value decomposition* (SVD). *Grouping* is done by truncating the summation of the elementary matrices to yield an approximation of the original matrix. This results in an approximated time series which is computed by taking the average of the diagonals, known as *reconstruction* or *diagonal averaging*. The above description is further explained through the following steps [100–102]:

Step 1: *Embedding*

Consider a real valued time series $Y_T = (y_1, ..., y_T)$ [100–102] composed of vectors that indicate measurements from each sensor. Embedding converts the one dimensional time series Y_T into a multi-dimensional series $(X_1, ..., X_K)$ with vectors, $X_i = (y_i, ..., y_{i+L-1})^T$, where L represents the window length and $K = T - L + 1$, where T corresponds to the number of sample points. The result of this step is the trajectory matrix $\mathbf{X} = [X_1, ..., X_K]$, the elements of which are given as :

$$\mathbf{X} = \begin{pmatrix} y_1 & y_2 & y_3 & \cdots & y_K \\ y_2 & y_3 & y_4 & \cdots & y_{K+1} \\ y_3 & y_4 & y_5 & \cdots & y_{K+2} \\ \vdots & \vdots & \vdots & \ddots & \vdots \\ y_L & y_{L+1} & y_{L+2} & \cdots & y_T \end{pmatrix} \tag{2.50}$$

The result of this step is a Hankel matrix. At a snapshot of time, the number of rows of the matrix indicate the number of sensors corresponding to each dof used for measuring the output vibration data, while the number of columns denote the recorded data at each discretized sample point. The one time-dimensional time series is converted to a multi dimensional series using a moving window of constant length. The choice of window parameters depends on the characteristics of data set.

Step 2: *SVD on the Hankel matrix*

The application of SVD on the Hankel matrix formed from the previous step has its roots in basic PCA. In the present context, PCA is carried out by performing an eigen value decomposition (EVD) on the Hankel covariance matrix, $\mathbf{C}_X = \frac{1}{N}\mathbf{X}\mathbf{X}^T$, where the superscript "T" indicates the transpose of the matrix. Let the EVD of the Hankel covariance matrix be written as $\mathbf{C}_X = \mathbf{U}\Upsilon\mathbf{U}^T$, where $\mathbf{U}$ represents the eigen vectors arranged row-wise and $\mathbf{\Upsilon}$ represents the diagonal matrix of eigen values in their descending order of significance.

Step 3: *Eliciting principal components of the Hankel matrix*

Principal components are obtained by projecting the Hankel matrix onto the eigenvectors, thereby transforming the data set onto a new subspace. Let U_i represent the eigenvector corresponding to Υ_i eigen value. Selection of PCs is based on the relative order of significance of eigen values. Principal component corresponding to a particular eigen vector is obtained according to: $\psi_i = (U_i^T)_{1\times L}(\mathbf{X})_{L\times K}$. Once all the PCs are obtained, they can be arranged in a matrix of principal orthogonal components (POCs) as below

$$\mathbf{\Psi} = [\psi_1, \psi_2, ...\psi_L]^T \tag{2.51}$$

Step 4: *Reconstruction of the Hankel matrix and the time series*

The Hankel matrix may be expressed as the summation of d rank one elementary matrices as $\mathbf{X} = \mathbf{R_1} + \mathbf{R_2} + ...\mathbf{R_n}$, where n represents the number of non-zero eigen values in the Υ_i matrix. It should also be noted that the n elementary matrices are selected according to their relative order of significance as given by the decreasing order of their corresponding eigen values. The basic aim of this step is to reconstruct the Hankel matrix and thereby the original time series only using the PCs that explain maximum variance. This ensures elimination of noise and unwanted components

from the time series, which further warrants the usage of a low model order in the succeeding steps. The elementary matrices are obtained by projecting the PCs back into the original eigen space as shown below:

$$\begin{aligned} \mathbf{R}_i &= U_i \times \psi_i \\ \mathbf{X} &= \sum_{i=1}^{n} \mathbf{R}_i \end{aligned} \tag{2.52}$$

The Hankel matrix can now be reconstituted as per the Eqn. 2.52. The reconstituted trajectory matrix is an approximated version of the original matrix and the approximated time series is recovered by taking the average of the diagonals. Let x_{ij} be the elements of the Hankel matrix , where i denotes the row number and j the column number. Considering $L^* = min(L, K)$, $K^* = max(L, K)$ and $T = L + K - 1$, it could be assumed that, x^*_{ij}=x_{ij} if $L < K$ and x^*_{ij}=x_{ji}, otherwise. The individual elements of the time series X_k is obtained using the following equations [100]:

$$x_k = \begin{cases} \frac{1}{k+1} \sum_{m=1}^{k+1} {x^*}_{m,k-m+2} & for \quad 0 \leq k < L^* - 1 \\ \frac{1}{L^*} \sum_{m=1}^{L^*} x^*_{m,k-m+2} & for \quad L^* - 1 \leq k < K^* \\ \frac{1}{T-k} \sum_{m=k-K^*+2}^{T-K^*+1} x^*_{m,k-m+2} & for \quad K^* \leq k \leq T \end{cases} \tag{2.53}$$

From the formulations involved, it is clear that the regular SSA requires a batch of data from a single sensor. These data provide a covariance matrix via the trajectory matrix of the signal in an offline framework. By the subsequent application of SVD on the covariance matrix the PCs of the time series are elicited. This part requires exhaustive matrix operations and makes the SSA unsuitable for online applications.

2.3 First order eigen perturbation technique

Recent developments in vibration based damage detection has seen the advent of numerous statistical signal processing techniques aimed at extracting the key features of damage through the use of certain DSFs. While most of these methods function mostly in batch mode operations, the present research sheds light on to the development of a new class of damage detection strategies that identify the damage in *real time*, using the key principles of *FOEP* technique. Succinctly, FOEP is stated as

the way of expressing the eigenstructure of the $(k+1)^{th}$ step in terms of the eigenstructure at the k^{th} step as the $(k+1)^{th}$ data streams in. This can accomplished by expressing the EVD of the symmetric positive definite covariance matrix in terms of the rank one perturbation of eigenvalue and eigenvector matrices [133, 135, 136]. The scope of this dissertation lies within the application of FOEP techniques in the purview of structural damage detection in real time, towards which, recursive algorithms such as RPCA, RSSA and RCCA, have been proposed. A structured interpretation of the hierarchy of the recursive processes is illustrated in Fig. 2.1.

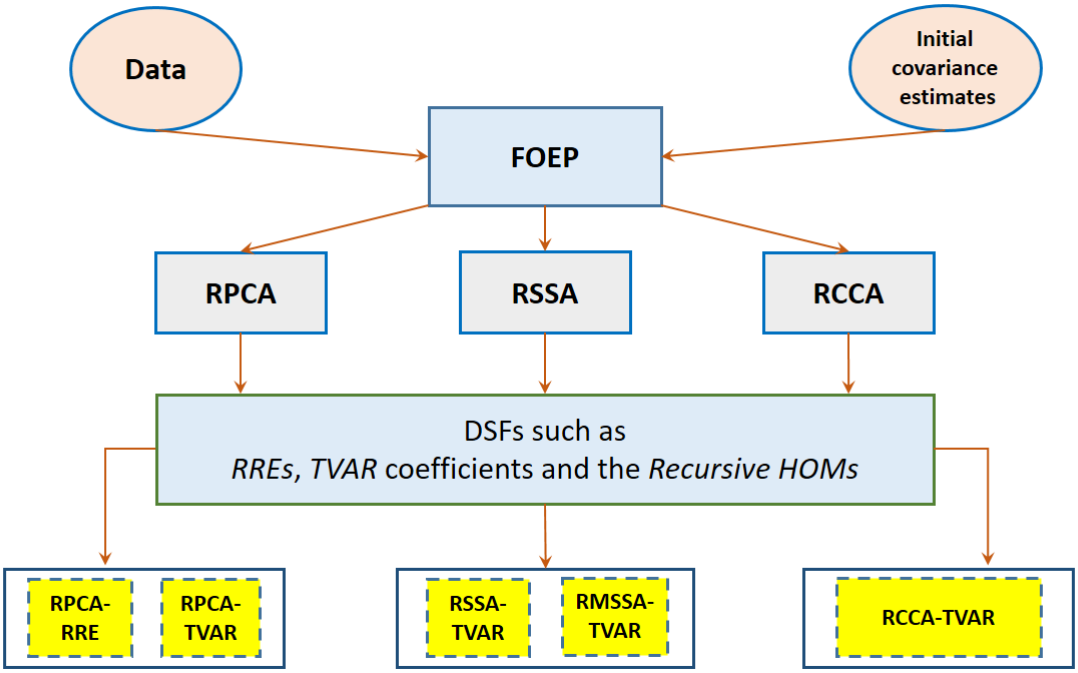

Figure 2.1: Summary of FOEP methods

From the streaming data, the initial covariance estimate for a few samples is carried out. The FOEP technique transforms the batch mode operations into recursive implementations with an added advantage that the covariance estimate at each step can be avoided, simply by providing eigenspace updates evolving at each time stamp. These updates, combined with DSFs, provide indicators of damage in real time. In order to intuitively understand FOEP, consider the eigenvalues of a perturbed matrix $\mathbf{C} + \mathbf{\Delta C}$ to be of the form $\mathbf{\Lambda} + \alpha\alpha^T$, i.e., the *rank-one update* of the matrix

$\mathbf{\Lambda}$. Using the following definitions:

$$\begin{aligned} \mathbf{CV} &= \mathbf{\Lambda V} \\ (\mathbf{C}+\mathbf{\Delta C})(\mathbf{V}+\Delta_{\mathbf{V}}) &= (\mathbf{V}+\Delta_{\mathbf{V}})(\mathbf{\Lambda}+\Delta_{\mathbf{\Lambda}}) \end{aligned} \tag{2.54}$$

where, $\Delta_{\mathbf{V}}$ and $\Delta_{\mathbf{\Lambda}}$ are the perturbation matrices. The EVD of the diagonally dominant term, can be expanded as follows:

$$\mathbf{C}+\mathbf{\Delta C} = \mathbf{V\Lambda V}^T + \mathbf{V\Lambda}{\Delta_{\mathbf{V}}}^T + \mathbf{V}\Delta_{\mathbf{\Lambda}}\mathbf{V}^T + {\Delta_{\mathbf{V}}}^T\mathbf{\Lambda V}^T + O(\epsilon^3) \tag{2.55}$$

Recognizing, that $\mathbf{C} = \mathbf{V\Lambda V}^T$ and invoking the fact that $\mathbf{VV}^T = \mathbf{I}$, the EVD of the perturbed matrix $\mathbf{\Delta C}$ by using Eqn.2.55 and ignoring second order perturbation terms can be written as:

$$\mathbf{\Delta C} = \alpha\alpha^T = \mathbf{V\Lambda}{\Delta_{\mathbf{V}}}^T + \mathbf{V}\Delta_{\mathbf{\Lambda}}\mathbf{V}^T + {\Delta_{\mathbf{V}}}^T\mathbf{\Lambda V}^T + O(\epsilon^3)$$

The above expressions provide a central idea to the data driven nature of the FOEP approach. Based on the above concepts, the proposed FOEP technique has been successfully applied for multivariate datasets. In many practical cases, due to cost and other impeding factors, instrumentation of the structure at every DOF might not be possible; therefore, the recursive updates at each time stamp is carried out using a subset of input channels from the structure, for such cases. For a special case, where there is only a single data channel available as input, recursive update can be carried out by generating a Hankel matrix out of the time series and carrying out the above mentioned formulations. The detailed methodologies and theoretical derivations of the individual FOEP based algorithms are presented in the upcoming chapters.

2.4 Summary

This chapter presents a survey of key methods of structural damage detection, the traditional ones followed by the more recent ones. A plethora of literature on traditional damage detection described the detailed development of the subject and had many limitations associated with it. The major impediments include: (i) *Baseline reliant* approach, which necessitates acquiring the recorded vibration data from the pristine state of the structure (ii) A majority of these methods are associated with *increased computational cost* (iii) Difficulty in estimating *finer levels* of detection for nonlinear systems (iv) Offline processes that make these methods amenable towards detecting *progressive damage*. PCA and SSA based recursive methods addresses these major drawbacks and appears to address the problem of damage detection in real time for nonlinear systems as well. En route, a fine level of damage can be easily detected with the aid of certain damage markers. With the focus of the present work firmly established, the focus now shifts to the formulation of the PCA and SSA based methods in the backdrop of FOEP techniques in order to identify real time structural damage detection using the backdrop of full and sparse sensor economics. The next chapter outlines the comprehensive development of RPCA in conjunction with recursive damage indicators towards real time multivariate structural damage detection.

Chapter 3

Online damage detection using recursive principal component analysis and recursive condition indicators

This chapter presents the theoretical development of a new method called the recursive principal component analysis (RPCA). RPCA method extends the concept of basic PCA to identify the damage instant and locate spatial patterns of damage in a single recursive framework. The chapter is organized as follows. The problem statement is first presented wherein the general problem of structural dynamics is cast in the framework of RPCA. The formulation for RPCA is presented next, followed by the results of numerical simulation on a simple Buoc-Wen model. A separate case study providing identification results for an underdetermined case is also considered. Finally, a comparison between traditional PCA and its recent variation, RPCA, is provided, that highlights the superiority of the RPCA towards exact identification of damage instant. For easy comprehension of the subsequent discussions, some useful acronyms are provided in Table 3.1

Table 3.1: Important acronyms

RPCA	Recursive Principal Component Analysis
EVD	Eigen Value Decomposition
POM	Proper Orthogonal Modes
RRE	Recursive Residual Error
EVC	Eigen Vector Change
MDOF	Empirical Mode Decomposition
CI	Condition Indicator
B-W	Buoc Wen

3.1 Motivation

The use of data driven techniques like PCA have gained significant popularity in SHM literature in recent times [84–87]. PCA, a technique for extracting eigenspace characteristics of a system using response only data, can be used as an indicator of the system's existing state which in turn can be used to detect changes in a structure's health over time. However, PCA frequently requires the use of a baseline data and operates mainly in batches of data which impedes its applicability towards online SHM problems. Moreover, the problem of damage detection through a single sensor input cannot be addressed by PCA based framework and calls on for special modifications in its formulations. The aforementioned practical problems motivates the need for a method that extends the key concepts of PCA to detect damage in real time and also address the problem of detecting damage for nonlinear systems as well. This can be accomplished by recasting the problem of damage detection into a perturbative framework, that provides real time updates of the eigenstructure. This method is termed as recursive principal component analysis (RPCA) [88].

3.2 Problem formulation

The main disadvantage of traditional PCA is that it analyzes the data in batches, offline. PCA in damage detection frequently requires the use of windowing as the analyzed data have to be compared with respect to a reference value (baseline). The choice of parameters (i.e., window size, overlap, shift, etc.) are mostly arbitrary and problem specific. This motivates the need of using a baseline free approach [88] amenable to online damage detection which is addressed by the RPCA based

framework. This algorithm is based on rank-one update of the eigenspace of the covariance matrix applied to the data vector x_k. The covariance matrix can be interpreted as composed of eigenvalues and eigenvectors, and as new sampled data becomes available, the eigenstructure is updated as a whole, instead of updating the covariance matrix directly, thus providing an immediate update of the eigenvalue and eigen vector matrices matrix in a recursive manner.

3.3 Recursive covariance estimation and FOEP

The practice of using PCA for vibration based health monitoring is well documented in the literature [84–87]. In order to tailor basic PCA towards online damage detection, algorithms premised on FOEP are chosen that could update the covariance estimate at each time step, in a recursive fashion [88]. Towards this, it is imperative to understand the basic concepts of FOEP as a data driven method, for recursive covariance update of the sample data matrix. It should be noted that the method is purely data driven and does not make any *apriori* assumptions regarding the nature of the data, thereby finding applications for binary data sets, data evolving from chemical engineering processes [88] and even in structural dynamics problems [85]. The recursive estimation of the covariance matrix is presented next in detail.

FOEP is a way of expressing the eigen structure of $k+1^{th}$ step in terms of the eigen structure of k^{th} step as $k+1^{th}$ data streams in. This is accomplished by expressing the EVD of symmetric positive definite covariance matrix in terms of rank one perturbation of eigenvalue and eigenvector matrices [132–136]. Consider the data matrix $\mathbf{X}^0 \in \Re^{n_1 \times m}$ required to build an initial PCA model for a few datasets, required to stabilize the algorithm. Here n_1 is the number of samples, expressed as rows and m is the number of variables, expressed as columns of the data matrix. The mean of each column is given by the vector: $\mu_1 = \frac{1}{n_1}(\mathbf{X}^0)^T I_{n_1}$, where $I_{n_1} = \begin{bmatrix} 1 & 1 & ... & 1 \end{bmatrix}^T \in \Re^{n_1}$ Under special circumstances, for structural systems, data generally evolve from zero mean processes. However, as the nature of the data is not pre-assumed for the deriving the recursive update expressions, the data is centered to zero by subtracting its mean and scaled to unit variance, according to: $\mathbf{X}_1 = \left(\mathbf{X}^0 - I_{n_1}\mu_1^T\right)\Sigma_1^{-1}$ where, $\mathbf{\Sigma}_1 = diag(\sigma_{1.1}, ..., \sigma_{1.m})$, whose i^{th} element is the standard deviation of the i^{th} measured variable $(i = 1, ..., m)$. The basic covariance matrix can be obtained as: $\mathbf{\Omega}_1 =$

$\frac{1}{n_1-1}\mathbf{X}_1^T\mathbf{X}_1$. It can be expected that the new block of data will augment the data matrix and calculate the covariance matrix recursively, as and when a newer set of data streams in, that forms the basis of the FOEP approach. Considering the k^{th} sample, it is assumed that μ_k, $\mathbf{X_k}$ and $\mathbf{\Omega_k}$ are calculated. The next step of the algorithm is to implement the updates for the $(k+1)^{th}$ sample point, recursively.

Considering, $\mathbf{X}_{k+1}^0 = \begin{bmatrix} \mathbf{X}_k^0 & \mathbf{X}_{n_{k+1}}^0 \end{bmatrix}^T$, for all the $k+1$ sample points, the mean vector μ_{k+1} is related to the mean vector at the k^{th} sample point by the following expression:

$$\mu_{k+1} = \frac{N_k}{N_{k+1}}\mu_k + \frac{I_{n_{k+1}}}{N_{k+1}}\left(\mathbf{X}_{n_{k+1}}^0\right) \tag{3.1}$$

where, the quantity $N_k = \left(\sum_{i=1}^{k} n_i\right)$. The recursive calculation for the data matrix at the $(k+1)^{th}$ sample is given by (skipping detailed steps):

$$\begin{aligned}
\mathbf{X}_{k+1} &= \left(\mathbf{X}_{k+1}^0 - I_{k+1}\mu_{k+1}^T\right)\mathbf{\Sigma}_{k+1}^{-1} \\
&= \begin{pmatrix} \left(\mathbf{X}_k^0 - I_k\mu_k^T\right)\mathbf{\Sigma}_k^{-1}\mathbf{\Sigma}_k\mathbf{\Sigma}_{k+1}^{-1} - I_k\Delta\mu_{k+1}^T\mathbf{\Sigma}_{k+1}^{-1} \\ \left(\mathbf{X}_{n_{k+1}} - I_{n_{k+1}}\mu_{k+1}^T\right)\mathbf{\Sigma}_{k+1}^{-1} \end{pmatrix} \\
&= \begin{pmatrix} \mathbf{X}_k^0\mathbf{\Sigma}_{k+1}^{-1} - I_k\mu_k^T\mathbf{\Sigma}_{k+1}^{-1} - I_k\Delta\mu_{k+1}^T\mathbf{\Sigma}_{k+1}^{-1} \\ \mathbf{X}_{n_{k+1}}\mathbf{\Sigma}_{k+1}^{-1} - I_{n_{k+1}}\mu_{k+1}^T\mathbf{\Sigma}_{k+1}^{-1} \end{pmatrix}
\end{aligned} \tag{3.2}$$

where, $\mathbf{\Sigma}_j = diag(\sigma_{j.1}, ..., \sigma_{j.m}), j = k, k+1$ and $\Delta\mu_{k+1} = \mu_{k+1} - \mu_k$. Following similar lines of development, the it is easy to recognize that the recursive calculation of the covariance matrix has the following form [88]:

$$(N_{k+1}-1)\,\mathbf{\Omega}_{k+1} = \mathbf{X}_{k+1}^T\mathbf{X}_{k+1} - (N_k-1)\,\mathbf{\Sigma}_{k+1}^{-1}\mathbf{\Sigma}_k\mathbf{\Omega}_k\mathbf{\Sigma}_k\mathbf{\Sigma}_{k+1}^{-1} + N_k\mathbf{\Sigma}_{k+1}^{-1}\Delta\mu_{k+1}\Delta\mu_{k+1}^T\mathbf{\Sigma}_{k+1}^{-1} + \mathbf{X}_{n_{k+1}}^T\mathbf{X}_{n_{k+1}} \tag{3.3}$$

For data evolving from structural systems, the recursive update of the sample covariance matrix requires only rank-one modification. In this dissertation, the covariance update is updated at each sample point, instead of updating the entire model, thereby relatively reducing the associated computational effort, for real time monitoring of structures. As previously mentioned, the FOEP technique

transforms the batch mode operations into recursive implementation by providing eigenspace updates of the covariance matrix at each time point, that forms the sole basis of the perturbation associated with rank-one modification. The recursive estimation shown in Eqn. 3.3 can be reduced to:

$$\mathbf{\Omega}_{k+1} = \frac{k}{k+1}\mathbf{\Sigma}_{k+1}^{-1}\mathbf{\Sigma}_k\mathbf{\Omega}_k\mathbf{\Sigma}_k\mathbf{\Sigma}_{k+1}^{-1} + \mathbf{\Sigma}_{k+1}^{-1}\Delta\mu_{k+1}\Delta\mu_{k+1}^T\mathbf{\Sigma}_{k+1}^{-1} + \frac{1}{k+1}\mathbf{X}_{k+1}\mathbf{X}_{k+1}^T \tag{3.4}$$

For structural systems in general, data evolves from zero mean processes. Scaling the data to a unit variance, Eqn. 3.4 can be rewritten as:

$$\mathbf{\Omega}_{k+1} = \frac{k}{k+1}\mathbf{\Omega}_k + \frac{1}{k+1}\mathbf{X}_{k+1}\mathbf{X}_{k+1}^T \tag{3.5}$$

Considering the EVD of the covariance matrix to be of the form $\mathbf{E}_{k+1}\mathbf{\Lambda}_{k+1}\mathbf{E}_{k+1}^T$, where $\mathbf{E}$ and $\mathbf{\Lambda}$ denote the orthonormal eigenvector and diagonal eigenvalue matrices respectively, with $\alpha_{k+1} = \mathbf{E}_k^T\mathbf{X}_{k-1}$, the following recursive formula is obtained, on substitution in Eqn. 3.5:

$$\mathbf{E}_{k+1}(k+1)\mathbf{\Lambda}_{k+1}\mathbf{E}_{k+1}^T = \mathbf{E}_k[k\mathbf{\Lambda}_k + \alpha_{k+1}\alpha_{k+1}^T]\mathbf{E}_k^T \tag{3.6}$$

For finitely large samplesize, the term $[k\mathbf{\Lambda}_k + \alpha_{k+1}\alpha_{k+1}^T]$ is strongly diagonally dominant, which allows the application of Gershgorin's theorem [132], establishing the fact that while its eigenvalues will retain a structure close to the diagonal portion $[k\mathbf{\Lambda}_k]$, the corresponding eigenvectors will be close to identity [88]. Interested readers are also referred to Appendix D for detailed derivation of the theorem and its understanding from a structural dynamics point of view.

3.3.1 RPCA: Theoretical development using POMs

As a combination of detailed theoretical derivation for the basic PCA methodology, let the LNMs be represented as $\mathbf{V}$. Let the POMs be represented by $\mathbf{W}$ that are expressed as a sum of LNMs and error terms. Therefore, the expression $\mathbf{W} = \mathbf{V} + \varepsilon$ holds good. Since the relation $\mathbf{X} = \mathbf{VQ}$ is valid, it can be inferred that $\mathbf{Q} = \mathbf{V^T X}$.

Therefore, the POMs can be expressed as:

$$\mathbf{\Psi} = \mathbf{W^T X} = \mathbf{Q} + \mathbf{\Gamma} \tag{3.7}$$

where $\mathbf{Q}$ is the modal ensemble matrix and Γ is the matrix containing the error terms. Substituting $\mathbf{X} = \mathbf{W\Psi}$, the *covariance matrix of the physical responses* can be obtained as:

$$\mathbf{R} = \frac{1}{N}\mathbf{XX^T} = \frac{1}{N}\mathbf{W}[\mathbf{Q} + \mathbf{\Gamma}][\mathbf{Q} + \mathbf{\Gamma}]^T\mathbf{W^T} \tag{3.8}$$

Equation 3.8 expresses the POCs of the covariance matrix of the acceleration response $\mathbf{X}$ in terms of the LNMs and errors. The basic RPCA equation [88] can be written as:

$$\mathbf{R}_k = \frac{k-1}{k}\mathbf{R}_{k-1} + \frac{1}{k}\mathbf{X}_k\mathbf{X}_k^T \tag{3.9}$$

where $\mathbf{R}_k$ and $\mathbf{X}_k$ are the covariance matrix and the matrix of the data points at the k^{th} instant, respectively; and $\mathbf{R}_{k-1}$ denotes the covariance matrix at the $(k-1)^{th}$ instant. The covariance estimate $\mathbf{R}_k$ can be expressed as an eigen decomposition as shown:

$$\mathbf{R}_k = \mathbf{W}_k\mathbf{\Omega}_k\mathbf{W}_k^T \tag{3.10}$$

Thus for $(k-1)^{th}$ data point the eigenvalue decomposition of $\mathbf{R}_{k-1}$ can be expressed as, $\mathbf{R}_{k-1} = \mathbf{W}_{k-1}\mathbf{\Omega}_{k-1}\mathbf{W}_{k-1}^T$, and the gain depth parameter β_k can be defined as $\beta_k = \mathbf{W}_{k-1}^T\mathbf{X}_k$

On substituting the value of gain depth parameter and the covariance estimate in Eqn. 4.5, the following expressions can be obtained

$$\mathbf{W}_k(k\mathbf{\Omega}_k)\mathbf{W}_k^T = \mathbf{W}_{k-1}\{(k-1)\mathbf{\Omega}_{k-1} + \beta_k\beta_k^T\}\mathbf{W}_{k-1}^T \tag{3.11}$$

For the RPCA algorithm to be stable and robust, it is important that the term $\{(k-1)\mathbf{\Omega}_{k-1} + \beta_k\beta_k^T\}$ is diagonally dominant, which can be demonstrated by expanding $\mathbf{\Omega}_{k-1}$ in terms of LNMs and error

terms as follows:

$$\mathbf{\Omega}_{k-1} = [\mathbf{Q}_{k-1}{}^{\mathbf{T}}\mathbf{Q}_{k-1} + \mathbf{Q}_{k-1}\mathbf{\Gamma}_{k-1}^{T} + \mathbf{Q}_{k-1}{}^{\mathbf{T}}\mathbf{\Gamma}_{k-1} + \mathbf{\Gamma}_{k-1}\mathbf{\Gamma}_{k-1}^{T}] \tag{3.12}$$

From equation 3.12, it is clear that $\mathbf{\Omega}_{k-1}$ can be understood as a sum of $\mathbf{Q^T Q}$ and the first order error terms [88]. As $N \to \infty$, $\mathbf{Q^T Q}$ is approximately diagonal for systems having mild to moderate damping under sufficiently broadband excitations. Eqn. 2.49 forms the basis of establishing diagonal dominance of the $\mathbf{\Omega}_{k-1}$ matrix. Gershgorin's theorem can now be applied on the diagonally dominant matrix which provides recursive eigen space updates using perturbation techniques at each point in time. For dynamical systems of different order (such as chemical systems), [88] the above equations would not hold true and the concept of diagonal dominance has to be enforced upon, for the application of Gershgorin's theorem. Hence for a structural system, the recursive eigen space update is obtained using a first order perturbation (FOEP) approach [133, 135], which provides a less computationally intensive algorithm in a recursive framework for the eigen value decomposition $(\mathbf{T}_k\mathbf{\Lambda}_k\mathbf{T}_k^T)$ of the term $(k-1)\mathbf{\Omega}_{k-1} + \beta_k\beta_k^T$, yielding the following iterative update equations:

$$\left.\begin{aligned} \mathbf{W}_k &= \mathbf{W}_{k-1}\mathrm{T}_k \\ \mathbf{\Omega}_k &= \tfrac{\mathbf{\Lambda}_k}{k} \end{aligned}\right\} \tag{3.13}$$

Eqn. 5.14 provides an iterative relation between eigen spaces at consecutive time instants. On using the FOEP approach, the recursive eigen vectors obtained at each time instant are not ordered in the same sequence as the previous time instant, thus presenting the problem of permutation ambiguity [68]. This can be resolved by arranging the basis vectors according to the decreasing order of the corresponding eigenvalues in $\mathbf{\Omega_k}$.

3.4 Damage detection using real time condition indicators

In the present damage detection framework, RPCA facilitates online processing of data and produces the eigenvalues and eigenvectors recursively. A crucial problem which arises is that the eigen-space by itself is not effective in detecting damage if not processed by a set of damage markers which are

referred to as condition indicators that can detect damage online. Several damage detection and SHM techniques have been proposed in the literature [1–3] that involve use of specific CIs whose changes signify damage to the system. The difficulty in choosing and utilizing condition indicators for the present framework arises from the fact that most of the traditional CIs are not amenable to online implementation. In this research, a set of recursive CIs are developed that are responsive towards online implementation. These indicators are based on the change in the pattern of the eigenspace due to damage which is manifested through alteration of recursively updated eigen-vectors before and after damage. In the following section, temporal recursive residual errors (χ_{RR}), spatial recursive residual errors (ε_{RR}), eigen-vector change (EVC) and scatter plots have been presented.

3.4.1 Recursive residual error (RRE)

The key condition indicator chosen for the present framework is recursive residual error (RRE). It will be shown later that RRE is the most robust and least outlier prone of all the discussed CIs. RRE comes in two flavors: temporal or global RRE (χ_{RR}) and spatial or local RRE (ε_{RR}). The main motivation for this CI is derived from the use of residual error as a criterion in quantification of nonlinear behavior [94] which presents its use as a measure of distortion of subspaces for a nonlinear system with increase in levels of excitation. The RRE as utilized in the present work is derived as follows.

Let $\mathbf{W}_k$ be a matrix of eigenvectors computed at k^{th} time instant and $\mathbf{\Lambda_k}$ be the corresponding diagonal matrix of eigenvalues at that instant. The eigenvalues are structured in descending order of magnitude, and the corresponding eigenvectors are re-arranged. Let, $\mathbf{W_k}$= $[\mathbf{W_k^1 W_k^2}]$ such that, $\mathbf{W_k^1}$ is said to represent the least number of eigenvectors whose corresponding eigen values explain more than 90% of the variance. Considering a damage at the end of $(k-1)^{th}$ instant, the subspace spanned by the updated eigenvector $\mathbf{W_k^1}$ deviates in comparison to the subspace spanned by eigen vectors at the previous time stamp $\mathbf{W_{k-1}^1}$. Apart from the instances of damage, or, the initial few seconds, it can be safely assumed that $\mathbf{W_k^1} \cong \mathbf{W_{k-1}^1}$, as there is no significant deviation in the eigenspace otherwise. Based on this assumption, the RREs due to projection of the response at a

particular time instant k onto $\mathbf{W_{k-1}^1}$ is evaluated as:

$$\mathbf{X}^*(k) = \mathbf{W}_{k-1}^1 * \mathbf{W}_k^{1^T} * \mathbf{X}(k) \tag{3.14}$$

Based on the above concepts, for detecting the instant of damage, the RREs proposed here are χ_{RR-1} and χ_{RR-2} which are expressed by the following equations:

$$\left.\begin{aligned} \chi_{RR-1} &= \left\| \mathbf{X}^*(k) - \mathbf{W}_k^{1^T} * \mathbf{X}(k) \right\|^2 \\ \chi_{RR-2} &= \left\| \mathbf{X}^*(k) - \mathbf{X}(k) \right\|^2 \end{aligned}\right\} \tag{3.15}$$

From the Eqn. 3.15, χ_{RR-1} can be interpreted as the distance metric between the transformed response and its projection on the subspace at the previous time stamp. Similarly, χ_{RR-2} provides a measure of the difference between projections of the transformed response and the original response data.

3.4.2 Recursive eigen vector change

From the precursory discussions, it is certain that there occurs a significant distortion in the eigenspace characteristics at the onset of damage to a system. Hence, tracking the change in the eigenvector updates are expected to show deviations that might correspond to the instant of damage. Pivoted around this key concept, a new CI, eigenvector change (EVC) is proposed in the context of real time damage detection of structures that tracks the eigenspace updates at each instant of time and provides the accurate damage instant when a significant distortion in the eigenspace is encountered. In the due course of rigorous inspection over a varied range of sample numerical simulations and experimental verifications, it was later found that this CI did not provide successful representation of the damage instant for quite a number of instances. Unlike the RREs, EVC is highly susceptible to false detections especially when a change in eigenvector occurs even due to *ambient noise* or some other disturbances from the excitation data, that sometimes become inevitable during experimentation. It was thus kept in consideration for a certain number of cases where it

actually showed some definite results for the damage instant.

$$EVC = \sqrt{diag([\mathbf{W_k^1} - \mathbf{W_{k-1}^1}] * [\mathbf{W_k^1} - \mathbf{W_{k-1}^1}]^T)} \tag{3.16}$$

3.4.3 Outlier detection using correlation coefficient (ρ)

Outliers can be defined as an observation (or subset of observations) which appears to be inconsistent with the remainder set of data. They can arise due to mechanical faults, changes in system behavior, human error or instrument error. In the present context, although RRE is an efficient CI for online damage detection, it is susceptible to mild levels of false detections. This can be resolved by the use of scatter plots in conjunction with the RREs as shown in Fig. 3.13. Scatter plots between two transformed responses and the corresponding correlation coefficients (ρ) are calculated in the neighborhood of damage (small windows before and after the instant of damage). It is observed that there is considerable directional change in the scatter plots (or a change in the sign of ρ) only at the instant of damage, which serves as a viable indicator for removal of false detection in the algorithm. It is essential to note that there is no change in the sign of the correlation coefficient due to the presence of outliers. The change in the sign of ρ takes place at the window where the damage has actually occurred and has been aptly illustrated in the following sections.

3.4.4 Local damage detection

The aspect of addressing damage instant as well as locating the damage in a single framework is more involved, especially if attempted in a recursive construct for online damage detection. In the present research, the proposed RPCA-RRE algorithm provides information on the damage location alongside the instant of damage in the same framework with a reasonable degree of accuracy. The key entitlement incorporated in this work is the simultaneous real time damage detection of structures in a single framework, that has previously not been reported in the contextual literature. To address damage localization, certain formulations in the RRE needs to be modified. First, RREs need to be expressed for each DOF (ε_{RR}) which varies from the temporal RREs (χ_{RR}) that were originally defined for the system as a whole. The key assumption is that when a column of an MDOF structure

is damaged, its effect will be pronounced in the neighboring DOFs, which in turn is manifested as a change in the local RREs for that particular DOF. While finding out the instant of damage (Eqn. 3.15), the concept of spatiality is lost as only global RREs are defined. This motivates the need for a new set of RREs (local or spatial RREs (ε_{RR})) that preserves the individual contribution of the responses, utilized to find the exact location of damage. From Eqn. 3.14 it is clear that the projections of the transformed responses $\mathbf{X}^*(k)$ and the actual responses $\mathbf{X}(k)$ can be expressed as vectors with each individual element corresponding to a degree of freedom (m : total number of DOFs) according to : $\mathbf{X}^*(k) = [x_1^*(k), x_2^*(k), \ldots\ldots, x_m^*(k)]^T$ and $\mathbf{X}(k) = [x_1(k), x_2(k), \ldots\ldots, x_m(k)]^T$ where k represents the time instant at which RRE is estimated. Consider each element of $\mathbf{X}^*(k)$ and $\mathbf{X}(k)$ be represented as $\mathbf{x_i}^*(k)$ and $\mathbf{x_i}(k)$ respectively, where ($\mathbf{i}$) corresponds to a particular DOF. This yields a time series of RRE (labeled as $\varepsilon_{RR} - Y_i$) corresponding to the response for each DOF, which can be expressed as

$$\varepsilon_{RR} - Y_i = \left| \mathbf{x}_i^{*^2}(k) - \mathbf{x}_i^2(k) \right| \tag{3.17}$$

Another useful quantity in this connection is the average RRE for i^{th} response for K data points, which can be estimated according to,

$$\langle \varepsilon_{RR} - Y_i \rangle = \frac{\sum_{k=1}^{K} \left| \mathbf{x}_i^{*^2}(k) - \mathbf{x}_i^2(k) \right|}{K} \tag{3.18}$$

The local RRE averaged over K samples is shown above. This is particularly useful, as shown later, in quantifying the percentage change in RRE (an indirect measure of loss of stiffness) pre and post damage.

3.5 Proposed Algorithm

The overall methodology followed in the context of the RPCA algorithm is shown in Fig. 3.1, that comprises of two key ingredients: *temporal* and *spatial* damage detection modules that occur simultaneously. The first one entails processing of the acceleration data by the RPCA algorithm as it streams in real-time. As previously explained, the RRE is tracked online for any major and

minor changes. Whenever a significant alteration is observed, the outlier detection step operates on the RRE data accumulated till the event instant (i.e. the instant of change) to determine whether the change corresponds to an outlier or a damage. Once the damage instant is detected, the spatial damage detection module further resolves the location of damage.

In a nutshell, the summary of the key steps involved in the RPCA-RRE method are enumerated below:

1. First, the initial estimate of the eigenvector and eigenvalue matrices are computed for a few initial data points.
2. The RPCA algorithm operates on the real time input of the streaming acceleration data.
3. Using the recursive gain depth parameter, the covariance estimate at the present time instant is derived using the covariance estimate at preceding time instant as per Eqn. 4.5 to 3.11. From the recursive updates, the eigen vector and eigen value matrices (eigenspace) are updated using FOEP approach (Eqn. 5.14).
4. The recursive CIs (RRE) employed on the updated eigenspace from the RPCA algorithm are then monitored to observe any sudden changes indicating a possible damage (by setting a tolerance limit of 30% in the change of the RRE before and after damage). Changes in RRE greater than the tolerance limit are then verified using scatter plots. Once the instant of damage is corroborated using scatter plots, the algorithm proceeds to detect the *location of damage* using local RREs in the spatial mode.
5. For the cases of no detections, the present eigenspace is reverted back to the RPCA algorithm which takes it as input along with the new data set obtained at the next time instant, to process the new eigenspace.

A flowchart as shown in Fig. 3.1 outlines the proposed damage detection scheme stepwise. From Fig. 3.1, it is clear that RPCA algorithm can process data as and when it streams in (online) and provides a recursive update of the eigen structure at each data point which are further utilized by the recursive CIs to track the instant of damage. Hence, it can be well established that the algorithm

does not depend on a baseline (reference value), unlike batch PCA, which is solely dependent on a full batch of response data in order to estimate the eigenspace. Cluster plots and RREs are utilized in tandem to detect the time of damage as well as for removal of false detection due to the presence of outliers. It is also clear that there are no parameters controlling the functioning of the algorithm, i.e. it is essentially *parameter free*. It should be noted that cluster plot representation is just a visual aid and it is not mandatory to preselect a specific window size. Any window size that gives an insight on the instances where the RRE shows deviations may be adopted. If there is no change in the orientation of the scatter plots (or, a change in the sign of the correlation coefficient) where RRE shows a deviation, it can be safely assumed to be an outlier, as shown in Fig. 3.13. Since the cluster plots are visualization tools, they consume computational resources, hence, should be used judiciously.

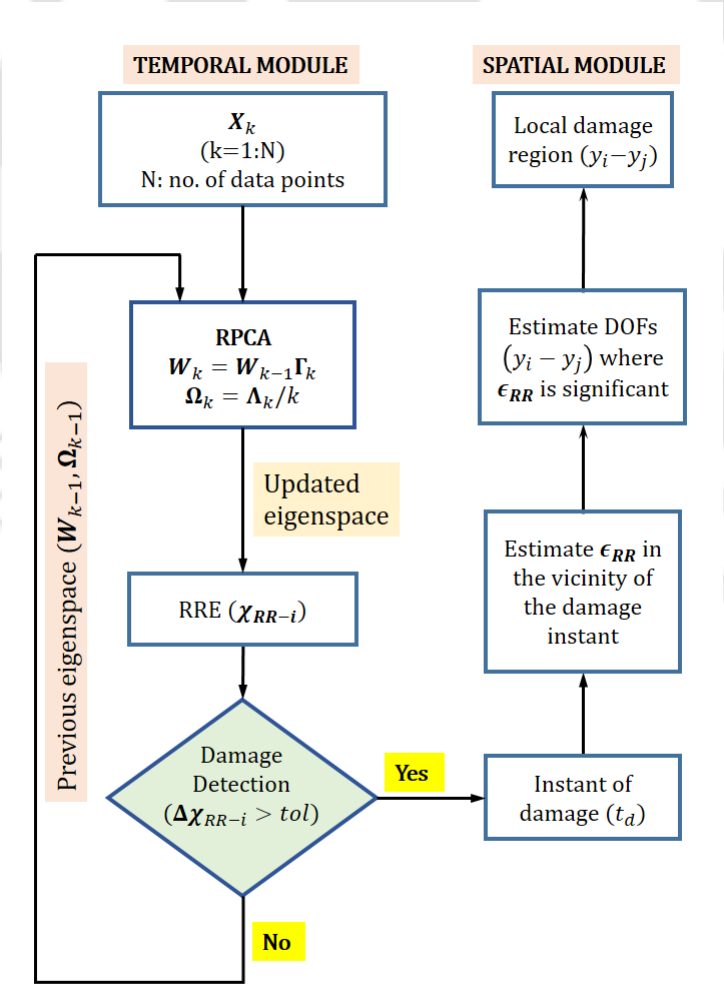

Figure 3.1: Flowchart for the proposed method

3.6 Numerical Example

In order to illustrate an application of the proposed method, numerical simulations are performed on a 5 storey structure modeled with 4 floors and a Buoc-Wen (B-W) base oscillator to simulate nonlinear change of state that is contextually defined as damage. The structure is subjected to white noise excitation of duration $50s$. The level of nonlinearity is controlled by a parameter κ, that is basically used as a multiplicative scale factor with the nonlinear force term. In the later stages of this chapter, a comparative study of the performance of the recently established RPCA-RRE algorithm against the traditional batch PCA applied on the responses obtained from the same model is presented. For the numerical simulations, two kinds of excitations are used: stationary zero mean Gaussian white noise and an earthquake excitation (El Centro ground motion). The input data are sampled at 50 Hz.

3.6.1 Structural model and simulation parameters

The 5 storey structure is modeled with 4 floors and a base. The LRB isolator separates the base from the surrounding ground. The state equations for this system subjected to an external excitation vector $\mathbf{w}$ can be written as:

$$\begin{aligned} \dot{\mathbf{x}} &= \mathbf{A}\mathbf{x} + \mathbf{E}\mathbf{w} \\ \mathbf{y} &= \mathbf{B}\mathbf{x} \end{aligned} \tag{3.19}$$

Here, the vector $\mathbf{x}$ is the vector of states and the vector $\mathbf{y}$ represents the output vector, which is governed by the $\mathbf{B}$ matrix. The system matrix, $\mathbf{A}$, and the excitation matrix $\mathbf{E}$ are given by

$$\begin{aligned} \mathbf{A} &= \begin{bmatrix} [\mathbf{O}]_{\mathbf{5\times5}} & [\mathbf{I}]_{\mathbf{5\times5}} \\ -\mathbf{M^{-1}K} & -\mathbf{M^{-1}C} \end{bmatrix} \\ \mathbf{E} &= \begin{bmatrix} 0 & 0 & 0 & 0 & 0 & -\frac{1}{m} & -\frac{1}{m} & -\frac{1}{m} & -\frac{1}{m} & -\frac{1}{m} \end{bmatrix}^T \end{aligned} \tag{3.20}$$

The equation of motion for the system can be summarized as:

$$\mathbf{M}\ddot{u} + \mathbf{C}\dot{u} + \mathbf{K}u = \mathbf{\Lambda}f - \mathbf{M}\mathbf{I}\ddot{\mathbf{u}}_{\mathbf{g}} \tag{3.21}$$

Here, **M**, **C**, and **K** are the assembled mass, damping, and stiffness matrices, respectively. A simple shear building representation is assumed to arrive at the expressions for **M**, **C**, and **K** which are skipped here for brevity. Numerical simulations are carried out on a simple 5 DOF mass, spring, and dashpot system. The mass at each of the four floor levels from the top is 7461 kg and at the base is 6800 kg. The damping coefficients for each floor level above the base is 23.71 kNs/m and 3.74 kNs/m for the base. The stiffness coefficients for each of the floors above the base is 11912 kN/m and that for the base is 232 kN/m.

In Eqn. 3.21, $\mathbf{\Lambda}$ represents the location of the base at the point of application of the force due to the LRB base isolator and $\ddot{\mathbf{u}}_\mathbf{g}$ represents the ground acceleration. The vector $\mathbf{x}$ represents the displacement of each floor including the base and f represents the nonlinear force exerted by the LRB. It should be noted that the forces due to base damping and stiffness terms (k_b and c_b) have been included in the force f due to the LRB base isolator, which can be expressed as:

$$f = \kappa z Q_{pb} + k_b x_b + c_b \dot{x}_b \tag{3.22}$$

where, $Q_{pb} = \left(1 - \frac{k_{yield}}{k_{initial}}\right) Q_y$ and k_b and c_b are the stiffness and the viscous damping respectively, in the horizontal direction. $k_{initial}$ is the initial shear stiffness and k_{yield} is the post yield shear stiffness of the LRB. The nonlinear force exerted by the LRB is expressed using the B-W system. The evolutionary variable z is used to provide the hysteretic component of the horizontal force, $Q_{hyst} = zQ_{pb}$. The variable z can be obtained by solving the following nonlinear differential equation:

$$\dot{z} = -\gamma z \left|\dot{x}_b\right| \left|z^{n-1}\right| - \beta \dot{x}_b \left|z^n\right| + A\dot{x}_b \tag{3.23}$$

where γ, β, A and n are the shape parameters of the hysteresis loop. For the current model, $A = \left(\frac{k_{yield}}{k_{initial}}\right)$, $\gamma = \beta$ and n=1. The yield force Q_y is selected as 5% of the total weight of the building which gives Q_y = 17800 kg and pre-yield to post-yield stiffness ratio $\left(\frac{k_{yield}}{k_{initial}}\right) = \frac{1}{6}$. For the present study of the model, γ=β=39.1. The constant κ controls the nonlinearity introduced into the equation of motion of the system (through the nonlinear force term). For instance, a change in κ from 1 to 0.3 is conveniently assumed as a 70% change in nonlinear characteristics of the system.

For all subsequent discussions, this model will henceforth be referred to as *5-DOF B-W system*.

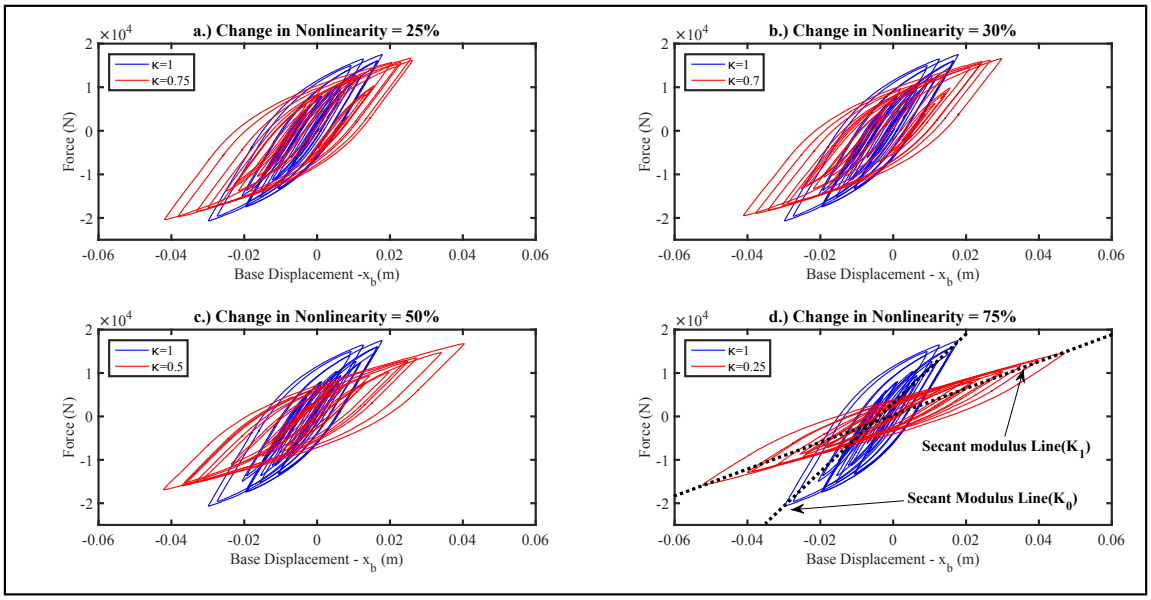

Figure 3.2: Force-displacement curves for various levels of nonlinearity

Simulation of damage

As previously explained, the constant κ introduced in Eqn. 3.22 controls the nonlinearity associated with the model under study. The change in the value of κ is considered as damage in the present context as it contributes to a change in the nonlinearity associated with the system. This change is treated as a global damage, affecting the entire structure as a whole, which does not wear out with the progression of time. Cases involving changes in nonlinearity of 25%, 30%, 50% and 75% have been studied in the following section, which corresponds to change in κ from 1 to 0.75, 0.70, 0.50 and 0.25, respectively. This change in the value of κ takes place at a particular time instant, emulating a temporal damage to the system. Fig. 3.2 shows the effect of change in the value of κ on the nonlinear force-displacement relationship of the B-W system. In order to quantitatively represent this damage, an empirical damage index (DI) [159], is used in this study. The empirical DI is expressed as follows:

$$DI = 1 - \left(\frac{K_1}{K_0}\right) \tag{3.24}$$

where $\left(\frac{K_1}{K_0}\right)$ is defined as the ratio between the secant modulus (K_1) associated with a changed level of nonlinearity (damaged state) to the initial secant modulus(K_0) of the pristine (undamaged) state. For cases of no damage, the ratio $\left(\frac{K_1}{K_0}\right)$ becomes *unity*, thereby making the damage index zero. The values of the DI corresponding to various levels of change in nonlinearity along with the corresponding κ values are shown in Table 3.2. From the results in Table 3.2, it is clear that the change in the nonlinear force parameter has a direct correspondence and follows a linear relationship with the DI.

Table 3.2: Damage index for varying levels of nonlinearity

Change in nonlinearity (%)	κ	Damage index (DI)
25.00	0.75	0.32
30.00	0.70	0.38
50.00	0.50	0.51
75.00	0.25	0.66

3.6.2 Results for White Noise

Temporal damage detection cases are studied first by sequentially changing the κ corresponding to 25%, 30%, 50% and 75% changes in nonlinear characteristics respectively. Subsequently, the examples of outlier detection are described next followed by simultaneous temporal and spatial damage detection. The results of damage detection for an underdetermined case clearly portray the potential of the proposed algorithm to identify instant of damage online even when the number of sensors used are less than the number of actual DOF.

Temporal damage detection results

The response of the top floor of the B-W system under different nonlinear states is shown in Fig. 3.3. The damage is induced through change of nonlinearity by 25%, 30%, 50% and 75% at a particular time instant of 31s. As evident from the figure, changes due to 25%, 30% and 50% shift of nonlinearity cannot be directly discerned from the response data visually. The damage is detected using two iterative condition indicators- EVC and RREs (χ_{RR-1} and χ_{RR-2}). Besides these, a scatter

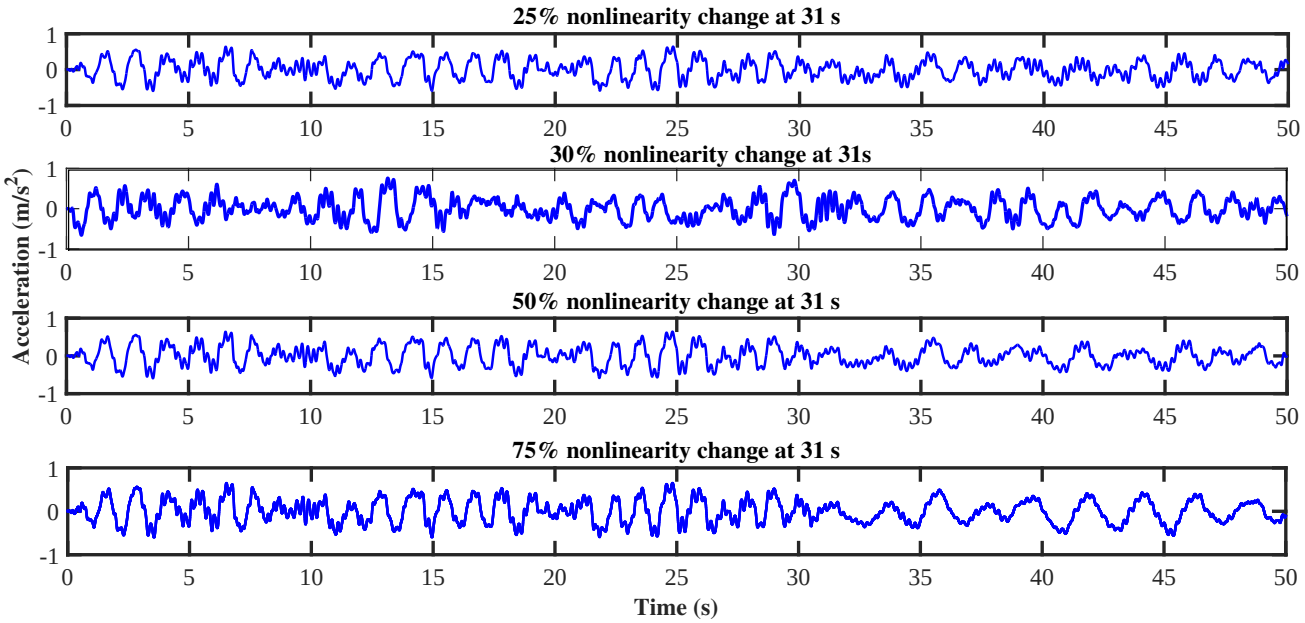

Figure 3.3: Acceleration plots for white noise excitation for different cases of non linearity

plot of the transformed responses of the system at pre and post time instants of 30s and 32s is also provided. It can be observed from Fig. 3.4 that EVC is capable of detecting sudden damages. While the RREs show damage by a significant change at that instant and then hitting a plateau region for the rest of the duration of the excitation, the scatter plot between the transformed response show a definite change in orientation which can be depicted easily from the plot (Fig. 3.4(d)). By looking at Fig. 3.4(b) and 3.4(c), it can be seen that there is a significant rise in the estimate of the residual errors χ_{RR-1} and χ_{RR-2}. It can also be observed from Fig. 3.4(a), that EVC could capture the essence of fault detection which shows up as a significant peak at the damage instant. The EVC however, shows a period of activity around the 0-8s mark and also shows a false detection at 37s. This shows that although EVC is useful in certain cases, its utility diminishes corresponding to lower percentage of damage cases (results not reported for brevity). Fig. 3.5 shows the performance of χ_{RR-1} and χ_{RR-2} for various cases of damage. It is worth noting from the figure that the efficacy of the RREs for less than 25% damage detection is slightly questionable which indicates that the current online framework is less reliable when the extent of damage suffered is low (i.e. less than 25%).

The scatter plot between the recursive transformed responses ($Y_t r^i$ vs $Y_t r^j$) can also serve as a

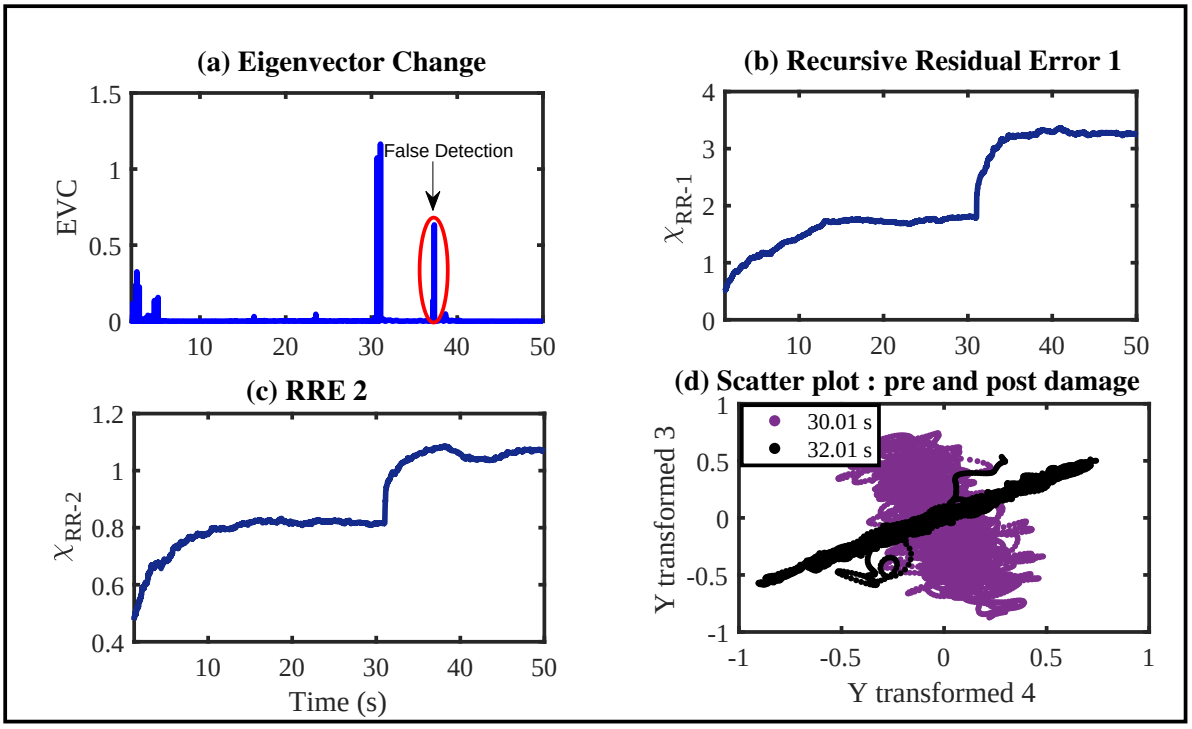

Figure 3.4: Damage detection using condition indicators for 50% non linearity change

robust visual CI for detecting damage. Since the transformed responses update recursively, showing point-wise scatter plots is time and memory consuming. To demonstrate the efficacy of scatter plots, data are considered in growing windows with initial window size of 10s and at increments of 10s before damage and a slightly smaller increment in the vicinity of damage (31s). It can be clearly observed from Fig. 3.6 that there is a significant change in orientation of the scatter, also reflected by the change in the signs of the correlation coefficients, between the successive windows immediately before and after damage. Considering the time of damage as 31s (as obtained from RRE plot), the 4^{th} window clearly indicates the damage instant for the specified level of non linearity.

Fig. 3.7 shows the robustness of the RREs for various instants of damage for 30%, 40%, 50% and 75% percent damage cases. As seen from Fig. 3.7, the RRE shows distinct change for higher percentage change in non linearity. For lower percentages of damage, the changes is slightly less distinct. However, this is not an impediment so far as current online damage detection framework is considered, since any event of change can always be verified using the scatter plot to finally decide on the occurrence of damage. The relative change in global RREs corresponding to different levels of damage is shown in Table 3.3. It is clear from the results in Table 3.3 that the percentage change

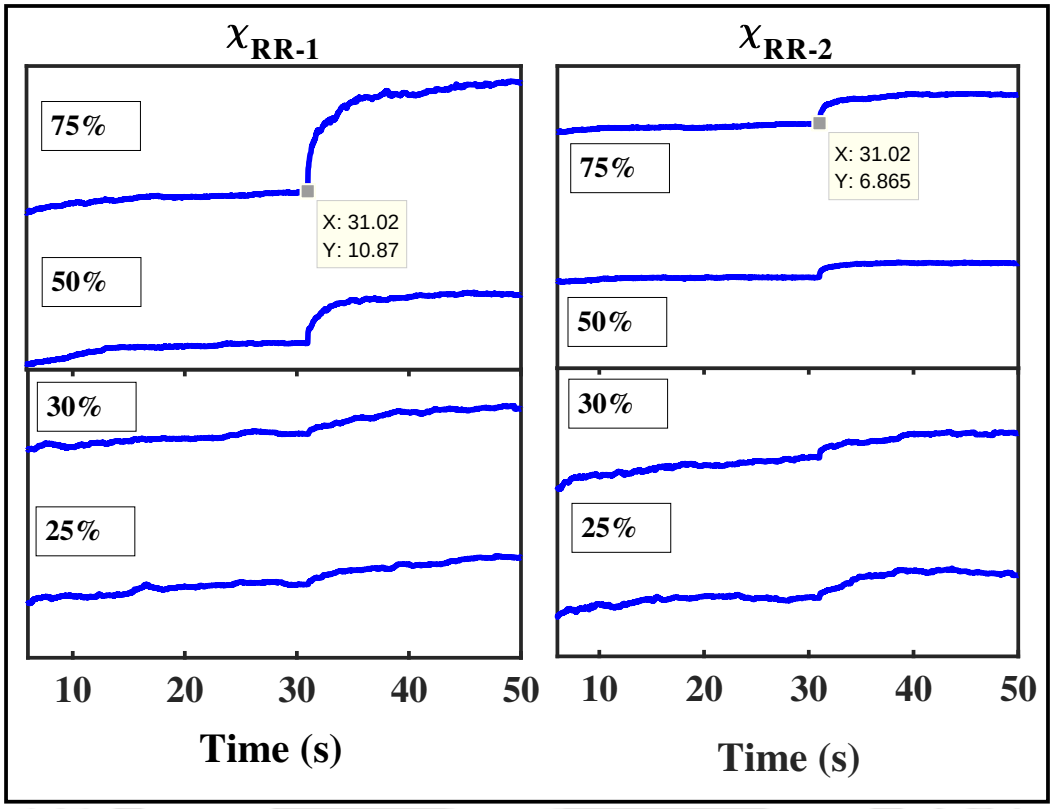

Figure 3.5: Damage detection using residual errors for varying cases of non linearity change in RRE increases with the level of damage.

Table 3.3: Global RREs for numerical modeling (using white noise)

Change in nonlinearity (%)	Pre-damage RRE	Post-damage RRE	% change
25.00	0.74	0.98	32.43
30.00	0.71	0.97	36.62
35.00	0.77	1.06	37.17
40.00	0.68	1.02	50.15
50.00	0.69	1.27	84.06

Spatial damage detection results

Damage, in the present context is simulated by a change in linear stiffness of an individual storey at a particular time instant. The streaming data is processed by the algorithm online in order to find out the exact time and location of damage through a change in local RRE. For the simultaneous temporal and spatial damage case (online spatio-temporal damage), 50% and 35% changes in linear stiffness of 3rd storey are considered. The nonlinearity level κ is kept at 1 (fully nonlinear). From

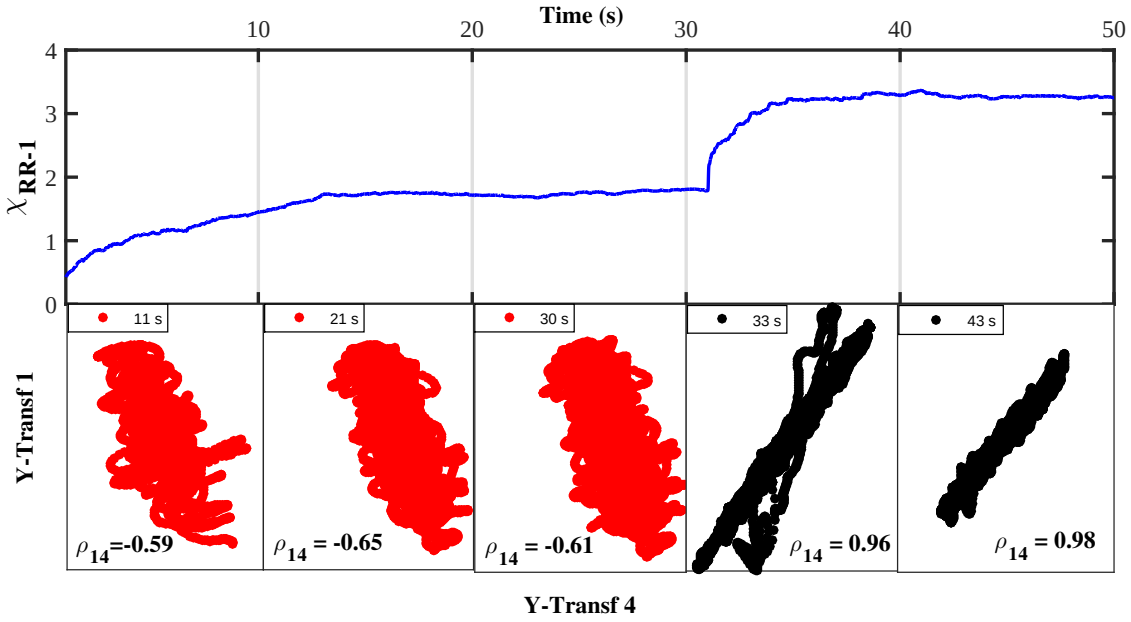

Figure 3.6: Damage detection using RE and scatter plots for 50% non linearity

Fig. 3.8, it can be shown that using the CI χ_{RR-2} a clear damage instant is found at 31s. Once the damage instant is detected, attention is turned to the spatial RRE $\varepsilon_{RR} - Y_i$ in a small neighborhood in the vicinity of damage (29 to 33s). It can be clearly observed from Fig. 3.8 that $\varepsilon_{RR} - Y_3$ shows a significant change at 31s compared to the other responses which indicates that damage has occurred in the third storey. It should be understood at this stage that both the RREs are tracked online recursively and $\varepsilon_{RR} - Y_i$ is shown separately represented in the neighborhood of the damage instant to capture the spatial effect of the damage visually. From Fig. 3.9, it is evident that the spatial RRE for 35% damage indicates a visible change at t=31s. However, as the extent of stiffness degradation reduces, detecting spatial damage detection gets increasingly difficult compared to the detection of the temporal damage alone.

3.6.3 Results for Underdetermined case-White Noise Excitation

In this section, the possibility of applying the proposed algorithm to handle an underdetermined case of structural damage detection is explored. An underdetermined case can be defined as the instance in which the number of sensors is less than the number of actual DOF. Such a system might arise in

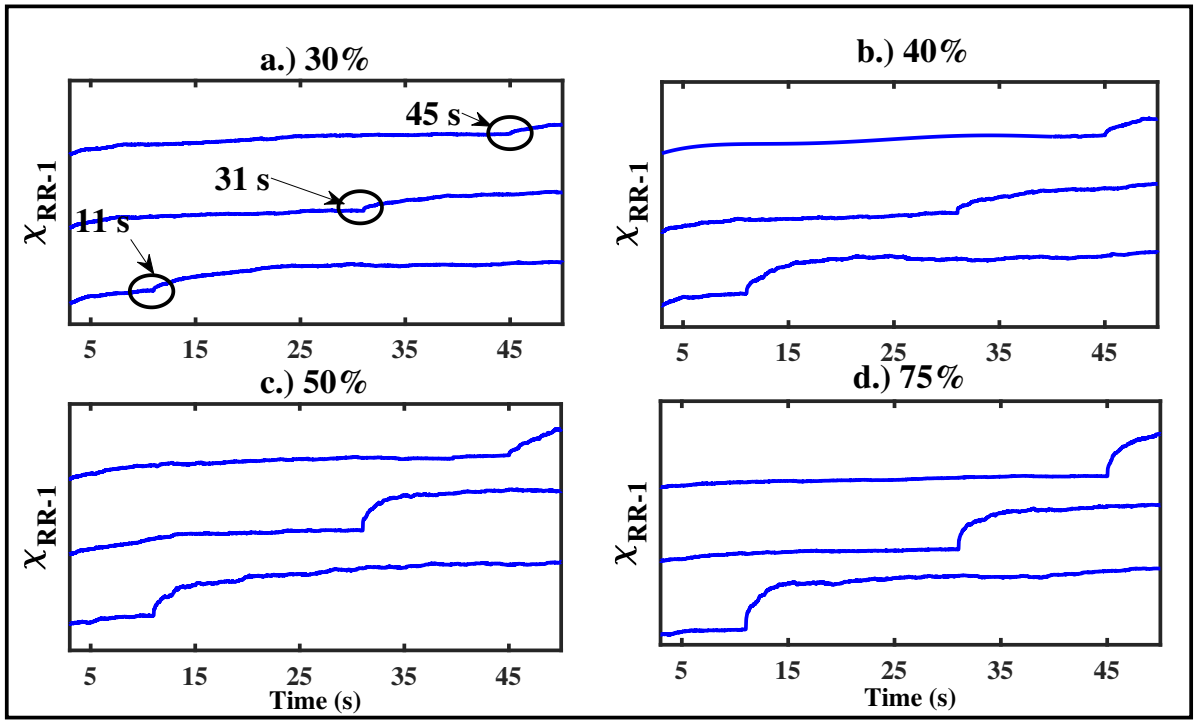

Figure 3.7: Damage detection using RRE1 for various non linearity change at different time instances

flexible systems that are instrumented with a relatively smaller number of sensors because of cost, unavailability of good quality sensors, improper accessibility, and other factors. So far the discussion has been limited to cases where full measurements are available, which is a restrictive assumption, especially while dealing with practical problems in engineering. The proposed algorithm tries to address this issue by assuming that only a subset of the sensor measurements are available for online damage detection. In this context, the damage detection capabilities of recursive CIs are explored to cast the problem of underdetermined mixtures within the framework of the RPCA method, as explained subsequently.

In order to conduct the damage identification study, the proposed algorithm addresses this issue by assuming the number of DOF in the structure to be equal to number of available measurements. Theoretically, to satisfy the rank condition of the eigenvector matrix, the number of instrumented DOF should be at least equal to number of actively participating modes. Hence for a 5-DOF structure, if only 3 degrees of freedom are instrumented with sensors, the proposed algorithm assumes the system to be a 3-DOF structure, producing corresponding eigenvectors (POMs) and eigenvalues (POVs), thereby, the eigenspace as a whole. The RPCA algorithm is applied on the streaming

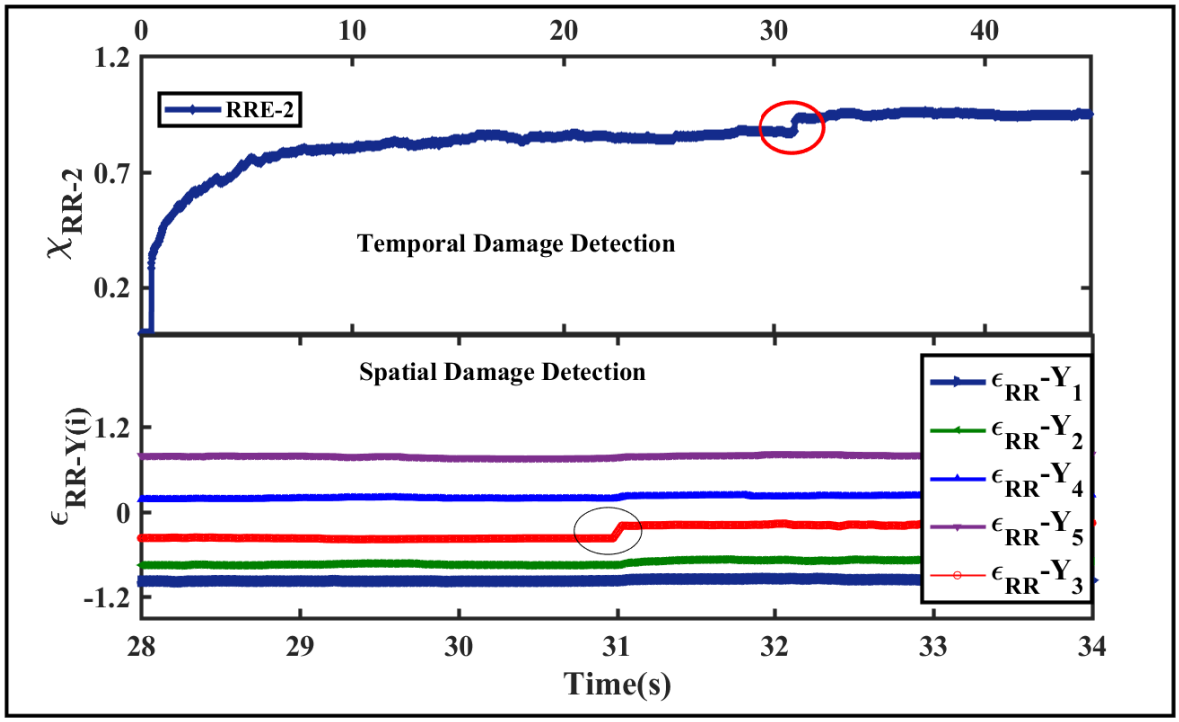

Figure 3.8: Comparison between spatial and temporal damage for 50% change

data which produces an eigenspace corresponding to the reduced DOF. Recursive CIs applied on the reduced eigenspace provides *visual aids* of damage manifestation in the system, as shown in Fig. 3.11. Fig. 3.10 shows the cumulative contribution in percentage of the principal components which indicates that for the present model, 3 principal components are sufficient to capture the dynamics of the structure, thus facilitating utilization of lesser number of responses (3 out of 5 in this case). To illustrate the applicability of the algorithm towards an underdetermined system, the model proposed in Section 3.6.1 with acceleration response data missing from 2^{nd} floor and 4^{th} floor are taken for analysis. Global damage was induced by a 25% change in nonlinearity at 31s. Real time data streaming from all the sensors was made available to the RPCA algorithm as input for online damage detection and the results providing a case study of the RRE plot is shown in Fig. 3.11.

Fig. 3.11 shows that the proposed algorithm is able to ascertain the instant of damage through RRE even without access to the complete set of response. As observed from the RRE plot, it is worth noting the fact that there is a period of activity before the actual instant of damage is reached, which can be solely attributed to the instabilities arising from the underdetermined nature

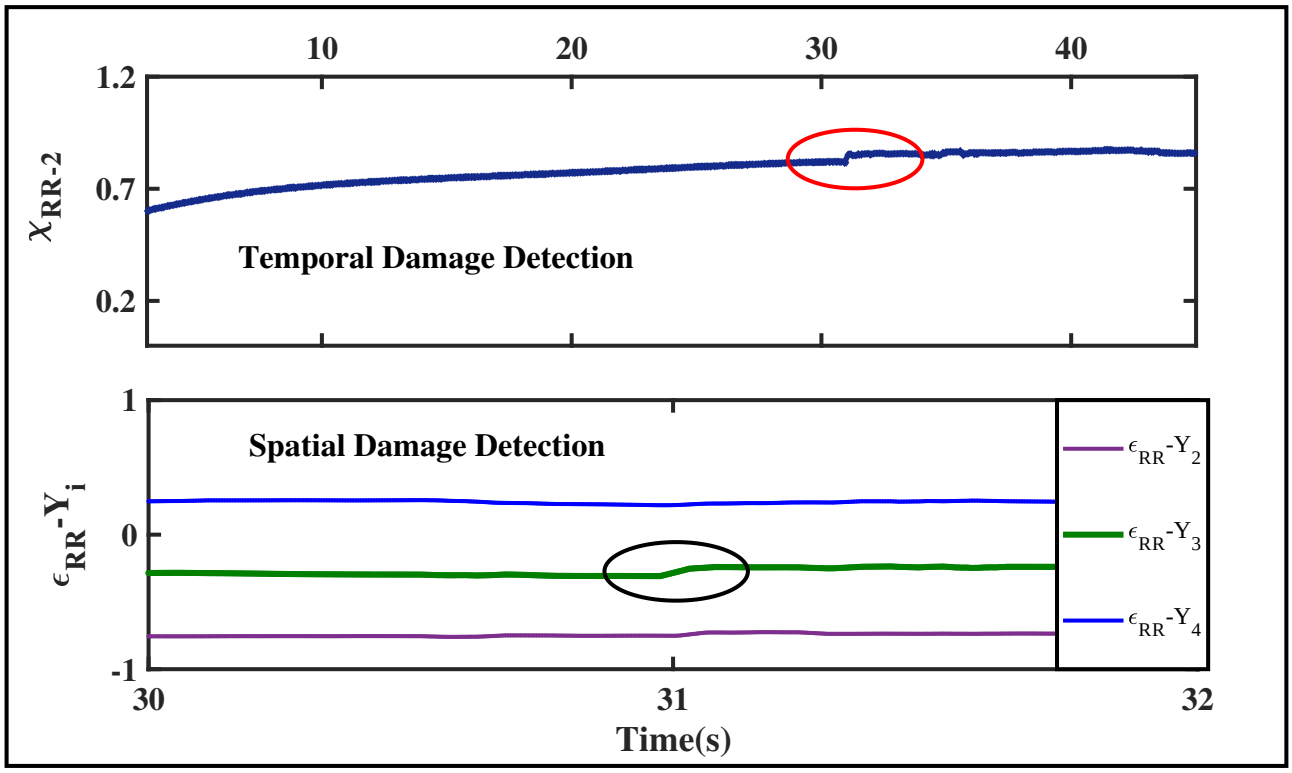

Figure 3.9: Comparison between spatial and temporal damage for 35% change

of the response. However, the proposed RPCA-RRE approach indicates the exact instant of damage through a change in the mean level of the plot. This substantiates the fact that the algorithm is fully equipped to tackle such type of situation which closely emulates to a real-life scenario where the number of sensors instrumented in the structure are lesser than the DOF of the structure.

3.6.4 Comparative study with batch PCA

In this section, the performance of the proposed method using RPCA is compared with traditional PCA. The study is conducted on the B-W system under a white noise excitation of 50s duration. The damage is induced by changing the nonlinearity level of the system by 50% at 31 s. χ_{RR-1} is employed as a recursive CI for the proposed algorithm, and an *analogous CI* for operation in batch mode $\chi_{RR-1}^{b_i}$ is defined to justify the comparison with batch PCA. At each time stamp, the proposed algorithm using RPCA evaluates the χ_{RR-1} values online. On the contrary, batch PCA accumulates the data gathered over a definite period of time and calculates $\chi_{RR-1}^{b_i}$ using windowed data. The implementation of batch PCA over the data provides a single value of RRE for each 10s window

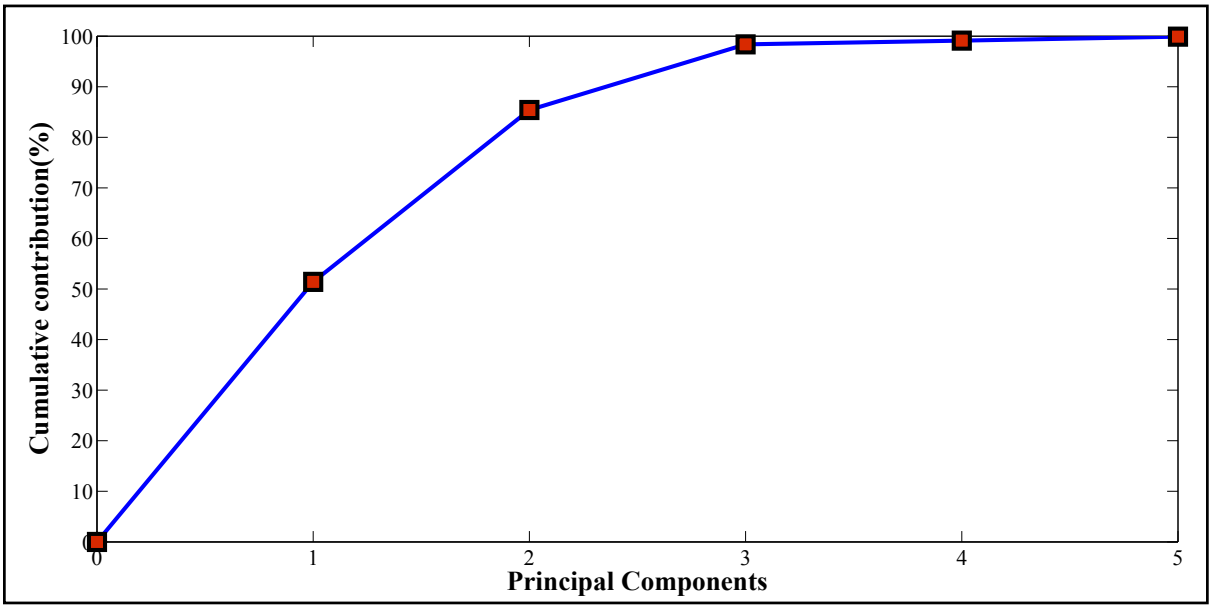

Figure 3.10: Cumulative contribution of principal components

span. The analogous batch RRE is calculated for any i^{th} window using traditional PCA through the following expression:

$$\chi_{RR-1}^{b_i} = \left\| \mathbf{X}^{b_i *} - \mathbf{W}^{b_i} \mathbf{X}^{b_i} \right\|^2 \tag{3.25}$$

In the above expression, $\mathbf{X}^{b_i}$ represents the response matrix containing the i^{th} window of data. $\mathbf{W}^{b_i}$ is the orthogonal eigenvector matrix derived from the EVD of the covariance matrix $\frac{1}{N}\mathbf{X}^{b_i}\mathbf{X}^{b_i T}$ for the corresponding i^{th} window data matrix having N time instants. Subsequently, the recursive CI (χ_{RR-1}) values are plotted against time to demonstrate the detection results of the RPCA based algorithm. On the same plot, the batch PCA detection results are plotted for comparison.

From Fig. 3.12, it is observed that the proposed algorithm using RPCA almost instantaneously detects the exact damage instant, through a significant change in the variation of χ_{RR-1} at $31s$. The batch PCA results using the CI $\chi_{RR-1}^{b_i}$ show almost constant values for the first three windows which lie before the instant of damage, which is also established through RPCA. A significant change in the value of $\chi_{RR-1}^{b_i}$ indicates that the damage instant lies in the 4^{th} *window*, within the time interval between $30s$ to $40s$. However, the batch PCA based CI is unable to identify the exact instant of damage, as it shows a range of time interval where the probable damage instant might have occurred. Therefore, it becomes clear that windowing of the data is necessary for executing batch PCA based

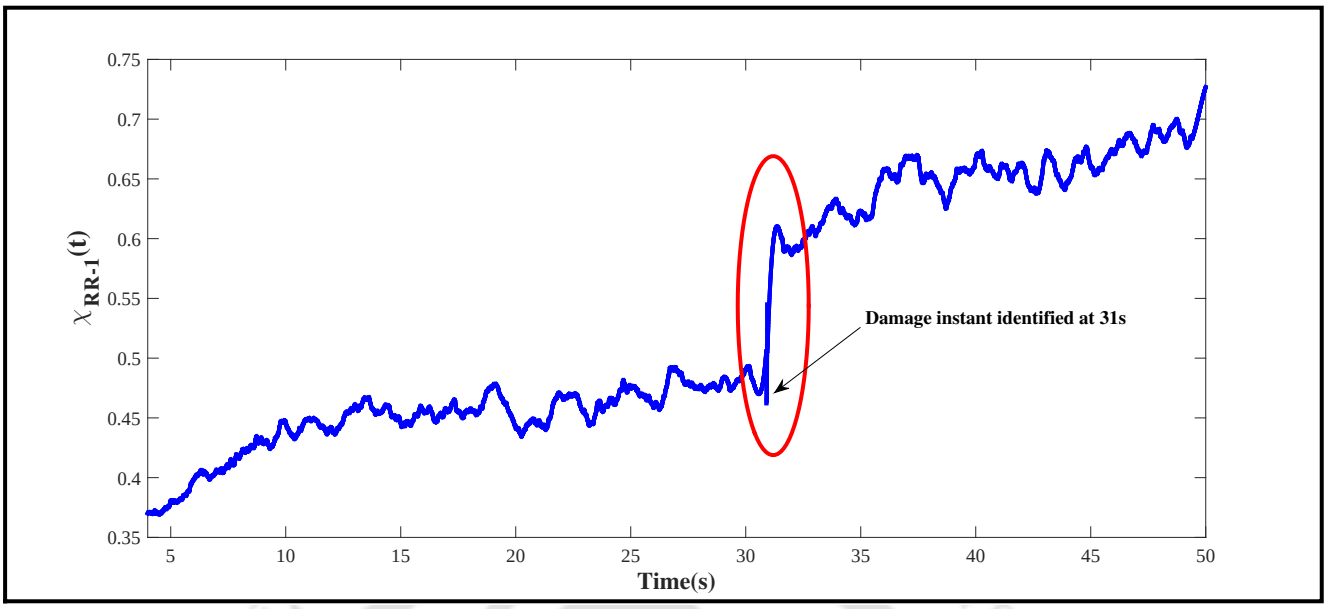

Figure 3.11: CIs for Underdetermined case- Global Damage, 25% change in nonlinearity

damage detection which prevents any possibility of online implementation of the method. Thus, it can be inferred from the above results the proposed algorithm based on RPCA is advantageous over batch PCA based method in terms of exact identification of damage time instant and easy applicability online without the need of *ad-hoc windowing* of the response data.

3.6.5 Results for El Centro ground excitation

Numerical simulation is performed on the B-W system excited using El Centro vibration data. The damage is simulated by changing the value of κ from 1 to 0.6 which corresponds to a 40% change in nonlinearity at 29s. Using the proposed method, the transformed response obtained is processed by the set of previously developed CIs, displayed in Fig. 3.13. It is clear that χ_{RR-2} clearly shows significant change at 29 s. As observed from Fig. 3.13, the ground and the top floor accelerations do not show any indication of the damage. To remove the possibility of false detection corresponding to events in the vicinity of 10 s, scatter plots are utilized in conjunction with ρ, which clearly proves that the events indeed correspond to an outlier (ρ doesn't change in sign). A change in the value of ρ from a high positive value $\rho = 0.99$ to a high negative one $\rho = -0.84$ at $t = 29s$, clearly indicates that damage has indeed occurred at $t = 29s$. It should however be noted that simultaneous spatial and temporal damage detection is difficult in this case owing to amplitude non-stationarity of the

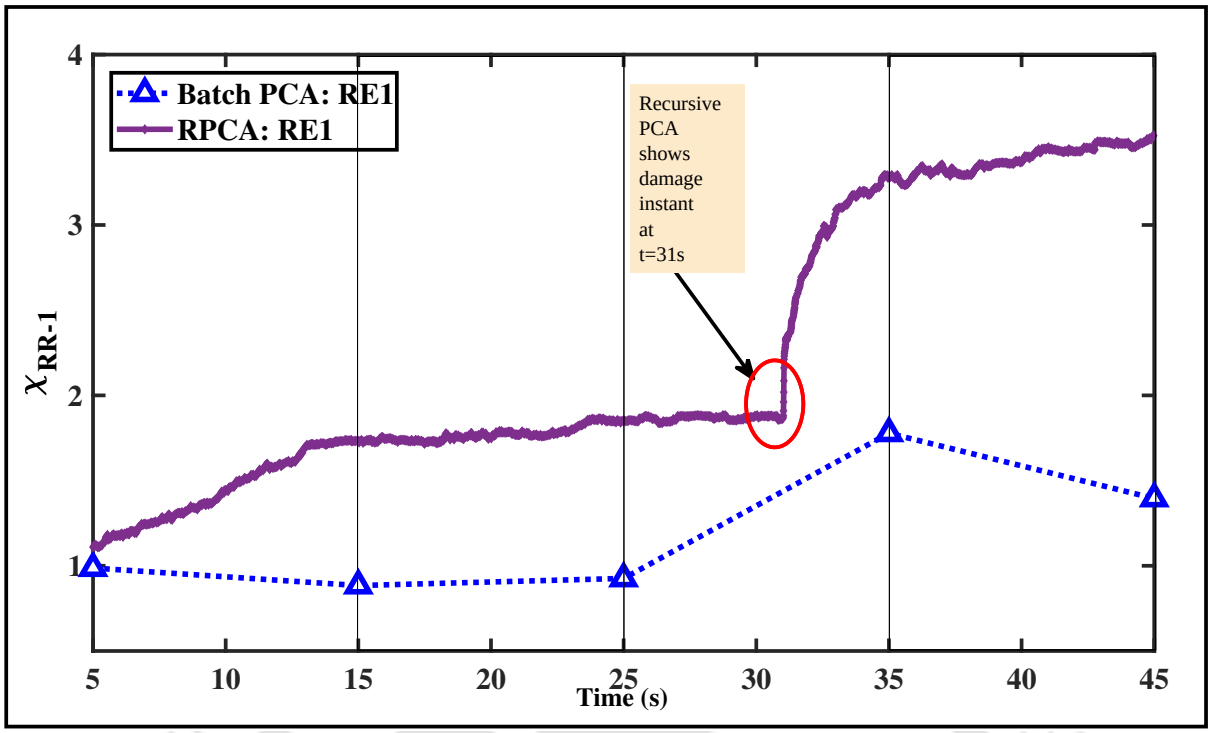

Figure 3.12: Comparison between batch PCA and RPCA

ground motion and thus the results are not shown.

3.7 Practical implementation studies

To substantiate the efficacy of the algorithm implemented online, two case studies have been presented:

1. An experimental model setup in a laboratory environment comprising of an aluminum beam excited by a ground motion, having a rubber strip attached to its free end.

2. A full-scale study using recorded ambient and earthquake-excited responses obtained from UCLA factor building.

3.7.1 Experimental study

An experimental setup has been devised to emulate an online damage and the current algorithm has been utilized to identify the instant of damage in real time (Fig. 3.14). The setup consists of an

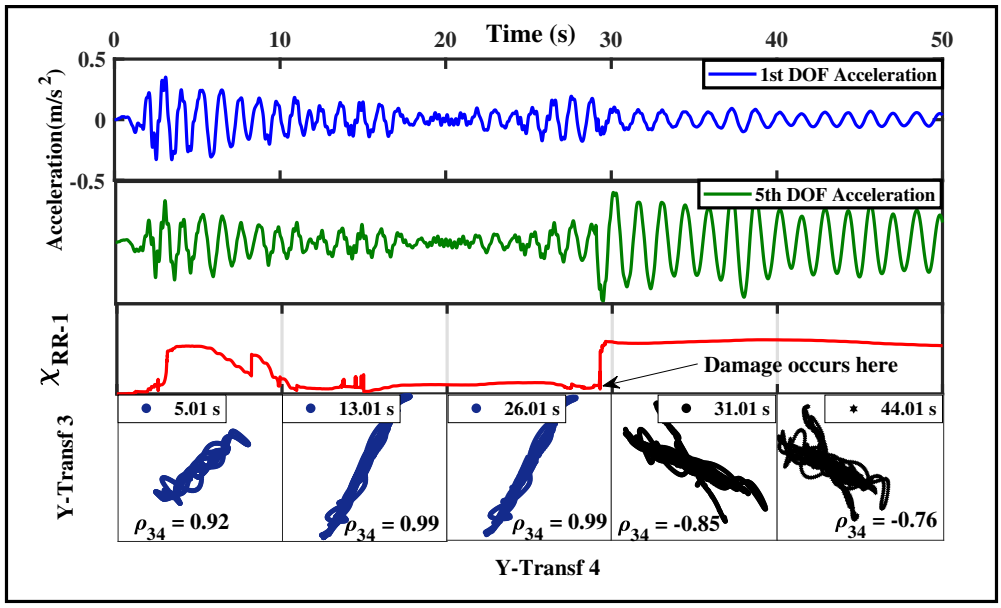

Figure 3.13: Residual error and scatter plots for El Centro excitation

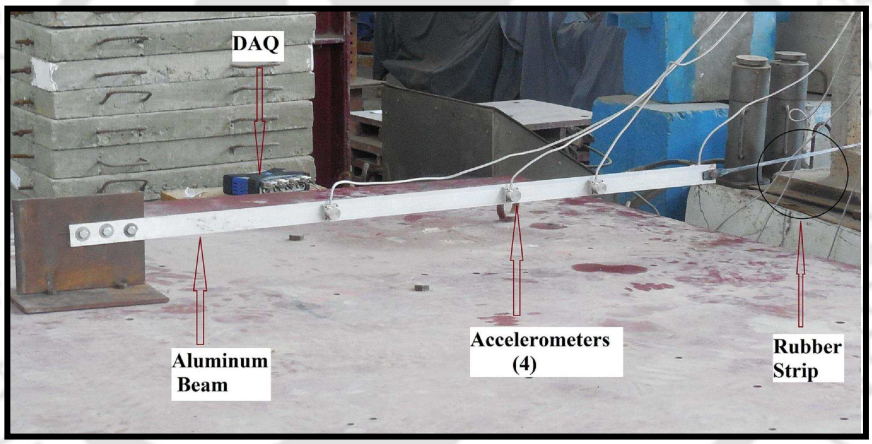

Figure 3.14: Details of the experimental setup, courtesy [157]

aluminium beam of dimension $120cm \times 3.5cm \times 0.5cm$ fixed on a base plate which is drilled on top of a shake table (model no. Bi-00-300). The base plate is a welded structure of two plates at right angle butt weld having dimensions $23cm \times 15cm \times 1cm$ each. The shake table specifications include: (i) table dimensions- $150cm \times 150cm$. (ii) payload capacity- $5tons$. (iii) peak velocity- $153cm/sec$. (iv) peak acceleration- ± 2.0 g. (v) frequency range- $0 - 20$ Hz. The model is subjected to an earthquake excitation and the acceleration data are collected using QuantumX MX410 HBM^{TM} Data Acquisition System (DAQ) at a sampling frequency of 75 Hz. The aluminium beam model is instrumented using Honeywell accelerometers $TEDS$ by HBM^{TM} at four positions. The positions of the four accelerometers from the free end are $1cm$, $30cm$, $47cm$ and $81cm$ respectively. The output

acceleration plot obtained from the sensors is shown in Fig. 3.15. The free end of the cantilever beam is attached with a thin rubber strip (Fig. 3.14) which has a taut length of 70 cm and the other end of which is clamped rigidly on a heavy steel platform. This rubber strip induces a nonlinearity to the experimental setup. This model can be readily used to validate the accuracy of the proposed method as explained in the following segment.

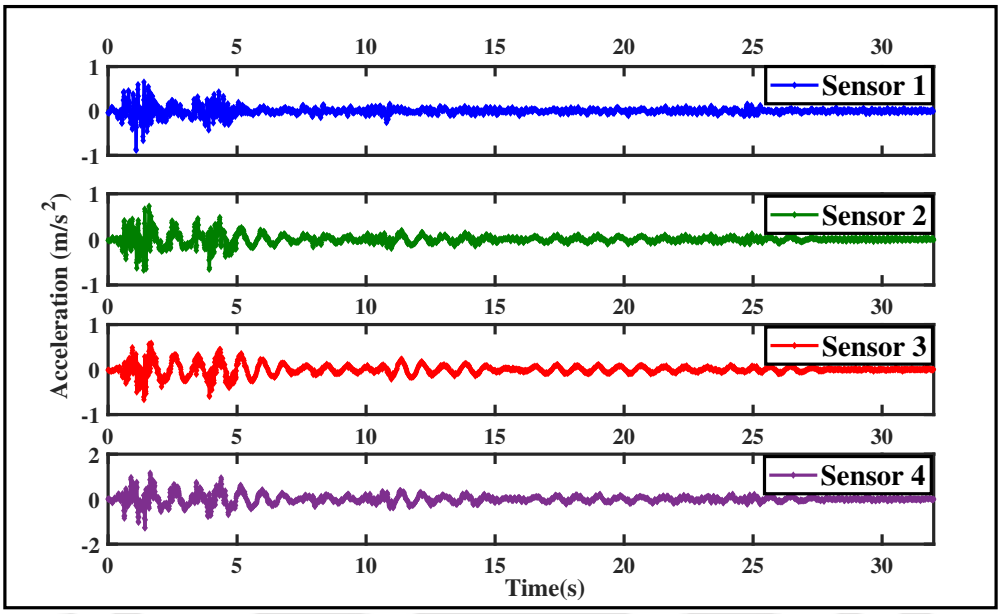

Figure 3.15: Output acceleration plot obtained from experiment

In order to simulate earthquake response of the structure, scaled ChiChi ground motion is used. A realistic case of damage employed in this study involves a change in the nonlinear state of the system, induced by snapping the rubber strip suddenly at a particular time instant. The snapping of the rubber strip accounts for an overall reduction in the stiffness of the model and is interpreted as damage to the system. The measurement of the instant of the snap is accurately done using a stop watch. To ensure that the time instant of damage is recorded accurately, the entire experiment is recorded in the form of videos. The recorded time of damage is exactly 33s. However, caution should be exercised in interpreting the event itself. Damage ideally should be an instantaneous phenomenon, the action of snapping action as observed after repeated trials of experimentation takes at least 0.5 to 1s. This small lag should be considered while calculating the damage instant. Hence, it is safe to assume that there is an error of 0.5 to 1s in recording the time of damage. The real time streaming of data is acquired by the DAQ and then the RPCA algorithm is applied.

Interpretation of the damage

To investigate the effect of the rubber strip on the response of the structure, the cantilever beam model with the rubber strip attached at its free end was excited using ChiChi earthquake scaled to different intensities (1.0 and 1.1 respectively). Fig. 3.16 shows the fourier spectra of the measured responses which clearly indicates a shift in the dominant frequency of the response obtained from the higher intensity excitation. The increase in the first modal frequency (of the order 12%) with the increase in the amplitude of the excitation reveals that a stiffening type of nonlinearity is induced in the aluminium beam by the rubber strip. As previously mentioned, damage in this case is inflicted by a sudden cut of the rubber strip at a particular instant of time, thereby reducing the stiffness of the structure in real time. To further validate this reduction, the Fourier spectra of responses of pre and post damage conditions are shown in Fig. 3.17. It can be clearly observed from the figure that there is a significant reduction (of the order of about 30%) in the first modal frequency of the damaged system as compared to the undamaged one.

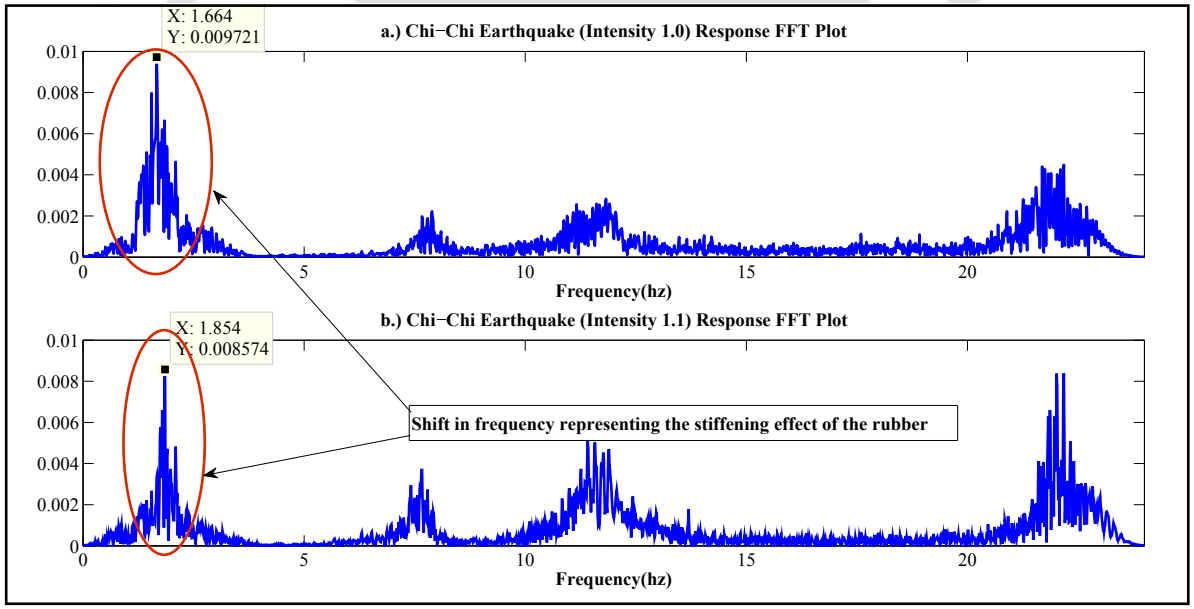

Figure 3.16: FFT plots for response obtained from scaled versions of ChiChi earthquake

Experimental Results

The real time streaming data from the sensors are processed by the online algorithm to identify the instant of damage by utilizing a set of recursive CIs. The proposed algorithm is tested to

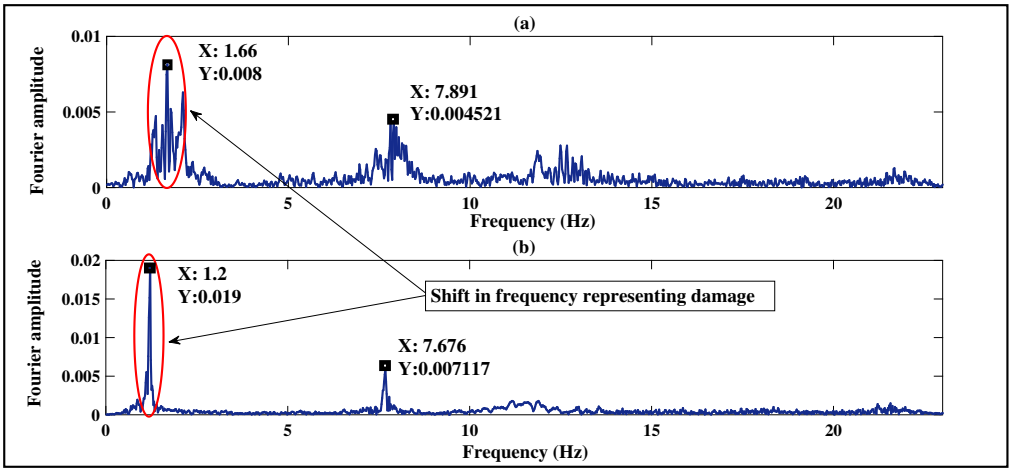

Figure 3.17: (a) and (b) Respective FFT plots of damaged state and undamaged states

detect damage for an underdetermined case study as well. As previously discussed in section 3.6.3, an underdetermined case assumes a subset of sensor measurements available for online damage detection. Studies are carried out for the following cases:

1. Case 1: All the sensors available
2. Case 2: 3 sensors are available (this case considers the output from the sensors 1, 3 and 4)
3. Case 3: 2 sensors are available (sensors 1 and 4)

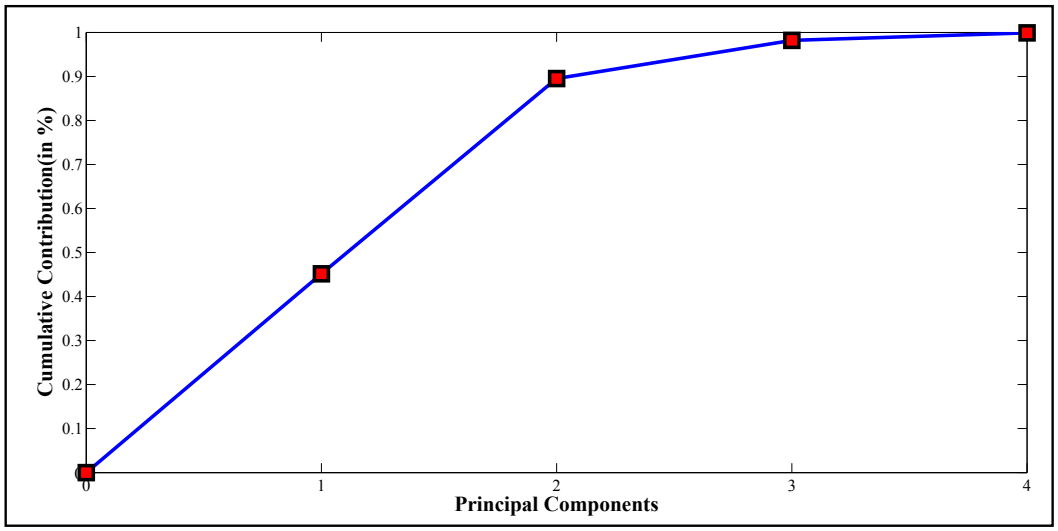

Figure 3.18: Contribution factor for PCs

For the first case, real time streaming data from all the sensors are made available to the RPCA algorithm. However, for the subsequent cases, the proposed algorithm assumes a reduced order

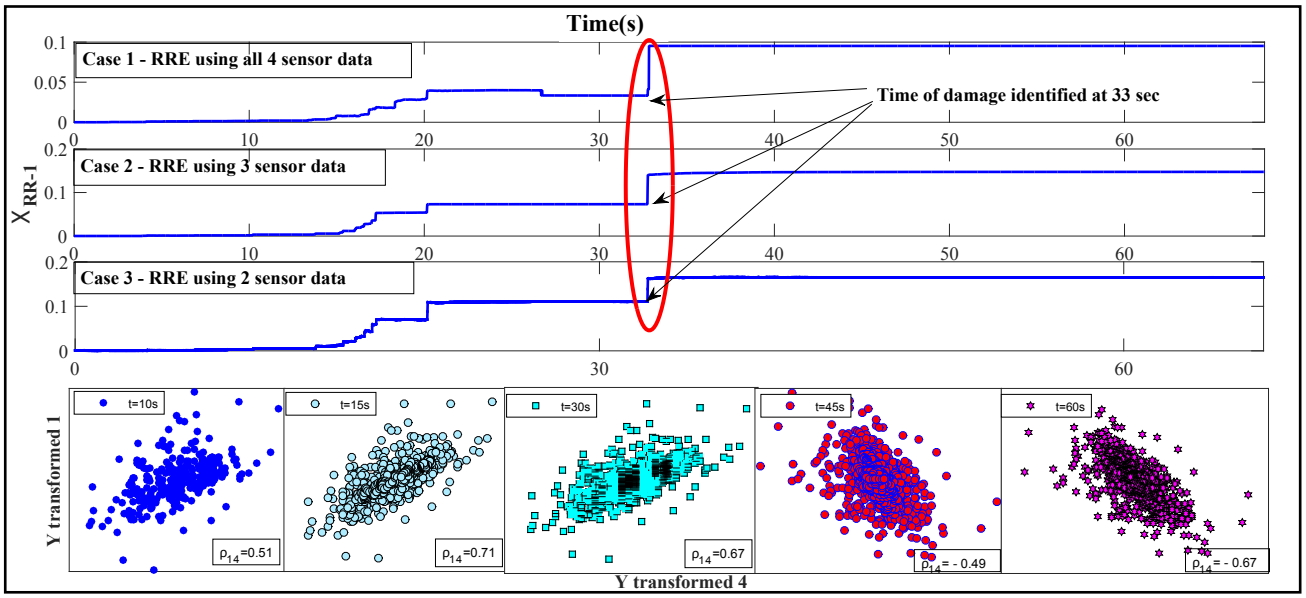

Figure 3.19: Recursive CIs for experimental trial

system, corresponding to the streaming data available from the number of sensors taken under consideration. Hence, RPCA algorithm produces eigen spaces corresponding to the reduced DOF. Fig. 3.18 shows the cumulative percentage contribution of the PCs, clearly indicating that 2 PCs are sufficient to capture the dynamics of the present experimental setup, thus facilitating utilization of lesser number of responses (2 out of 4 in this case). Recursive CIs applied on the reduced eigen space provide indications of damage in the system, as shown in Fig. 4.13, for all the aforementioned cases. It can be seen from the figure that plots of χ_{RR-1} ascertain the instant of damage at $33s$ for all cases which indicates the efficacy of the proposed algorithm to detect damage for a practical case where the number of sensors instrumented are less than the number of dof. The plots in Fig. 4.13 clearly indicate the instant of damage by showing a change in the level of RRE at $33s$ and then hitting a plateau region which is continued for the rest of the duration.

Scatter plots are considered for the final case where data from 2 sensors are made available as inputs to the algorithm. The scatter plots corroborate with the damage instant, showing a change in orientation at $33s$, with justifies the ground truth. Although plots of RRE reveal some fair amount of activity before the instant of damage is reached, these are primarily due to the nonstationary nature of the input excitation and the proposed algorithm further substantiates the instant of damage with a change in orientation of scatter plots only at $33s$, as clearly seen from Fig. 4.13. The percentage

change in global RREs for the experimental trial are shown in Table 3.4. It is worth noting from the table that the percentage change in RRE decreases (from 57.39% to 33.33%) with the decrease in the number of sensor data available as input to the algorithm. However, it should be noted that the algorithm is able to detect global damage in real time with a reasonable degree of accuracy even when the number of sensors is reduced down to 2 (which corresponds to a 33.33% change, as reported in Table 3.4) from the original set of sensor data input. The case studies validate that the proposed algorithm is well equipped to handle an underdetermined practical scenario where the number of sensors instrumented in the system are less than the actual number of DOF of the structure.

Table 3.4: Global RREs for experimental case

Damage cases	Pre-damage RRE	Post-damage RRE	% change
Case 1	0.04	0.09	57.39
Case 2	0.07	0.13	46.71
Case 3	0.11	0.17	33.33

It is important to note that a lot of experimental setups have been devised in recent times to demonstrate damage detection strategies. In the present work, an effort has been made to create damage as a manifestation of nonlinear change in state that happens in real time amenable towards demonstration of online damage detection strategies.

3.7.2 Case study of the UCLA Factor building

The proposed algorithm is now applied to full scale field data of recorded responses obtained from UCLA factor building (UCLAFB) as a part of extensive ambient vibration monitoring program. Designed and constructed in the late 1970s, the 17 story 216.5 ft high UCLAFB is a $G + 15$ story structure (with basement and sub basement levels) that consists of special moment resisting steel frames (SMFs) supported by concrete bell caissons and spread footings. After the 1994 Northridge earthquake, the building was instrumented with a network of 72 Kinemetrics FB-11 uniaxial accelerometers at all the floor levels. Each level has two pairs of orthogonal sensors parallel to the NS and EW directions. The array of sensors are converted to an equivalent array of NS, EW and θ directional sensors lumped at the center of rigidity of each of the floors [63]. The data is sampled at 100 Hz. UCLAFB has been studied extensively in recent times mostly in the context of output only

modal identification and the results are reported in some published works [63]. To test the efficiency and damage detection capability of the proposed algorithm, a combination of floor accelerations due to ambient data and data recorded during the event that occurred on September 28, 2004, 10:15 AM PDT, due to ground shaking originating (with M= 6.0 on the moment magnitude scale) from Parkfield, CA, are considered.

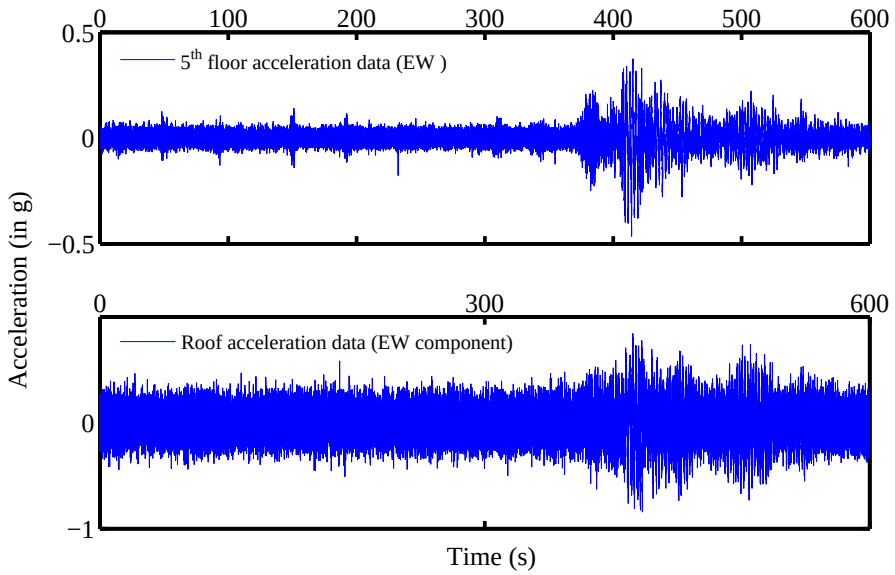

Figure 3.20: Roof and 5^{th} floor acceleration responses for UCLAFB in EW direction

The acceleration data at roof and fifth floor in EW direction is shown in Fig. 3.20. As seen from the figure, there is a considerable incidence of nonstationary activity in the vicinity of t=380s which indicates the onset of the Parkfield earthquake (magnitude of Mw=6.0). The data prior to the occurrence of the earthquake corresponds to ambient vibration regime which is evident from Fig. 3.20. The instant of shaking as well as the instant of maximal structural change can be estimated from the temporal RRE ($\chi_{RR} - 2$) plots for the $N - S$ and $E - W$ components responses. Upon a close analysis of the data, it could be easily inferred that the system response deviates from the ambient level at around t=380s, while the pronounced damage occurs at around t=410s. It is normal to expect these two instants to be different from each other because it takes a finite time for the structure to undergo significant changes (i.e. alteration of stiffness).

Previous modal identification studies on UCLAFB [63] show 14.31%, 13.95%, 15.61%, 8.49%,

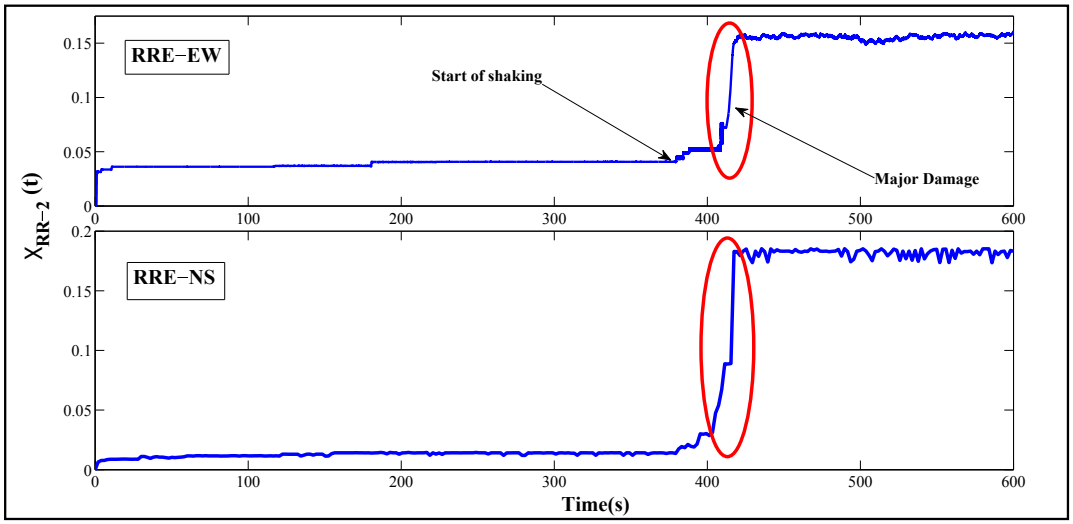

Figure 3.21: Residual error plots for UCLA in EW and NS directions

7.24%, 4.95%, 4.95%,30%, 6.5%, 4.75% percentage reduction in the values of identified frequencies between ambient vibration and earthquake data, which indicates significant global reduction in stiffness values. In the present context, global damage is expressed through percentage change in the average spatial RRE values (i.e. $\Delta\langle\varepsilon_{RR} - Y_i\rangle$ using Eqn. 3.18) between the ambient and earthquake regimes corresponding to pre and post damage scenarios. Fig. 4.15 shows the plot $\varepsilon_{RR} - Y_i$ for a few representative floors. It can be observed from the figure that $\varepsilon_{RR} - Y_i$ deviates from the ambient regime at around t=380s and significantly in the vicinity of t=410s indicating the occurrence of damage. The percentage change in post damage RRE and pre damage RRE (i.e. $\Delta\langle\varepsilon_{RR} - Y_i\rangle$) for each floor as shown in Table 3.5 which indicates the appearance of damage not only at a single floor but the system as a whole which corroborates to the previously mentioned results on modal identification [63].

As mentioned in the previous sections, the proposed algorithm is well equipped to solve an underdetermined system which illustrates its ability to handle practical scenarios as well. In this context, responses from only the odd numbered dof are made available as input to the algorithm, closely emulating a practical underdetermined system where it is not feasible to instrument all the dof. Fig. 3.23 shows that χ_{RR-2} clearly indicates the instant of damage even without processing the data from all the DOF, compared to Fig. 4.15 where the response from all the dof were made available to the algorithm.

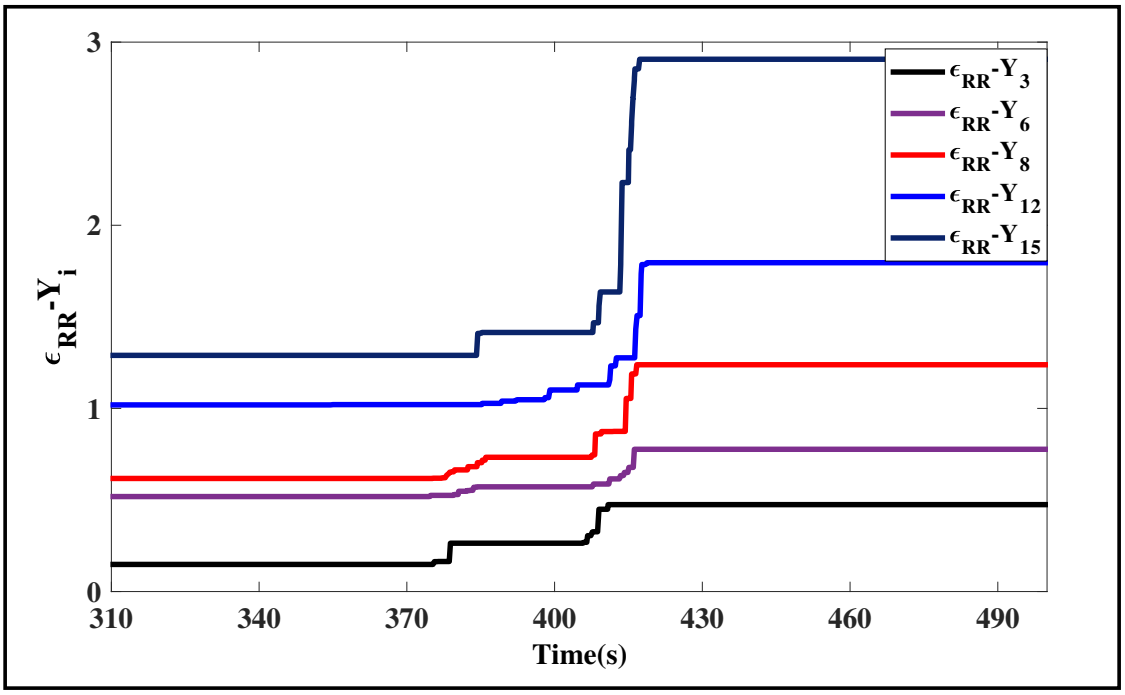

Figure 3.22: Residual error plots for floors of UCLA

Based on the results of application of the proposed RPCA based online damage detection method to practical scenarios, it can be safely concluded that the proposed framework is quite robust in detecting the instant of damage online. However, on the downside, the method still requires improvement as far as simultaneous spatio-temporal damage detection is concerned especially for practical nonstationary excitations. Although the present algorithm achieved significant success in detecting spatial and temporal damage simultaneously in simulation scenarios, the combined presence of amplitude and frequency domain nonstationarities in excitation still poses challenges in simultaneous spatial and temporal detection of damage especially in field implementations, which is kept as a future work to be addressed by the author.

3.8 Summary

In this chapter, a new online damage detection algorithm for vibrating structural systems using a combination of RPCA and online CIs is presented. Clearly, RPCA and its residual error, is one of the potential candidates to capture damage in real time. Spatial and temporal RREs allowed simultaneous detection of damage instance and location under the same online framework. Application of

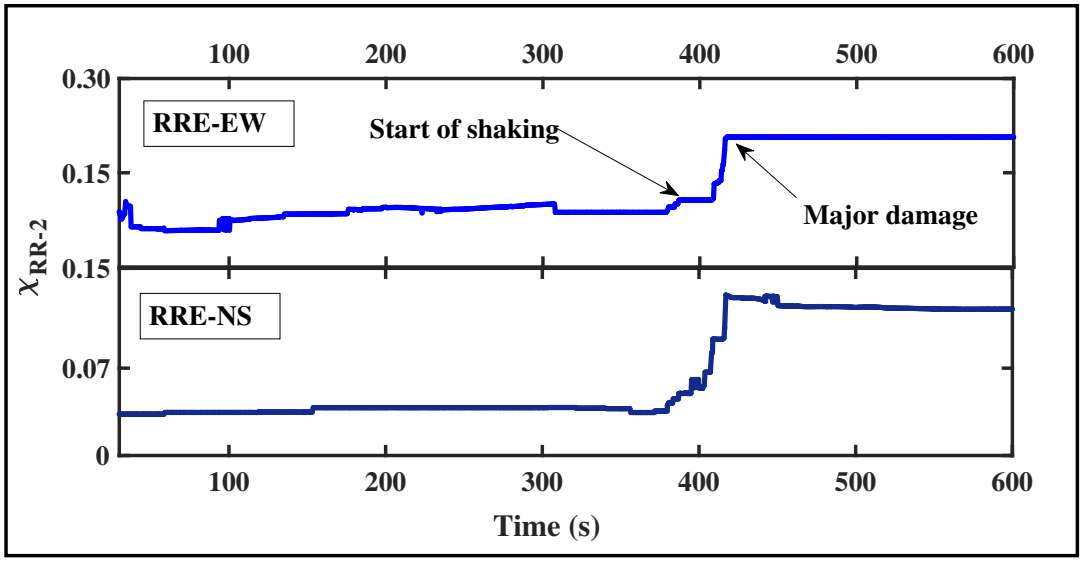

Figure 3.23: Residual error plots for UCLA underdetermined case

cluster plots further eliminated the presence of outliers, by observing the change in correlation coefficient between the transformed responses. The proposed methodology provided successful results for numerical simulations both for white noise and earthquake excitations. Case studies have shown that the proposed algorithm is well equipped to detect damage when the number of sensors used to acquire data is reduced (i.e., for underdetermined systems), which is clearly an advantage while dealing with practical economics of health monitoring of real full-scale structures. The results show efficacy of the current framework to detect damage for underdetermined cases up to 25% change in the level of nonlinearity. The RPCA based damage detection framework was shown to be more effective than the use of traditional counterpart, the windowed PCA. Presented case studies reveal that the proposed approach results in successful damage detection and works well when used with both experimentally acquired data as well as large scale field data closely emulating practical scenarios. It has been observed that due to the presence of nonstationary input excitation, the exact instant of damage gets masked, where RRE fails to recognize the event. To tackle these type of situations, the transformed response obtained from the RPCA based approach needs to be modeled accurately to elicit sufficient information regarding the damage patterns evolving in time. This issue is addressed in detail in the forthcoming chapter.

Table 3.5: Spatial RREs for the UCLA factor building

	Y-EW			Y-NS		
Response No	Pre-damage	Post-damage	$\Delta\varepsilon_{RRE}(\%)$	Pre-damage	Post-damage	$\Delta\varepsilon_{RRE}(\%)$
1	2.03	14.76	86.25	3.86	17.84	78.34
2	3.70	40.90	90.95	6.34	28.09	77.42
3	4.93	37.46	86.84	3.45	34.43	89.98
4	4.43	28.26	84.32	4.54	13.05	65.24
5	2.22	21.45	89.63	1.19	10.77	88.97
6	1.93	27.68	93.04	2.12	26.04	91.85
7	1.84	19.12	90.37	2.01	12.34	83.74
8	1.79	63.84	97.20	1.74	15.21	88.55
9	1.52	41.65	96.34	1.55	24.29	93.63
10	3.08	21.08	85.39	6.96	50.89	86.33
11	2.14	49.98	95.72	1.39	40.71	96.58
12	2.01	79.54	97.47	3.60	31.07	88.42
13	2.01	52.56	96.17	1.59	28.09	94.36
14	3.14	86.25	96.36	2.70	21.94	87.70
15	50.10	240.64	79.18	6.18	61.10	89.88
16	31.00	69.27	55.24	11.75	104.82	88.79

Chapter 4

Real time damage detection using RPCA and TVAR modeling

This chapter presents the theoretical development of RPCA in conjunction with time varying auto-regressive modeling (TVAR). The RPCA-TVAR method is a direct extension of the RPCA-RRE approach, discussed in detail in the previous chapter. This method extends the concepts of the RPCA based approach to determine the spatio-temporal damage patterns under nonstationary input excitations in real time. The fundamental concepts of the RPCA-TVAR approach, central to the development of the proposed methodology, are reviewed first. The formulation of the method in conjunction with TVAR modeling is presented next, followed by case studies on numerical simulations on the B-W system under finer levels of nonlinearity changes. To examine the efficacy of the proposed methodology, experimental setups devised under controlled laboratory environments are then employed to identify the exact instant of damage. Finally, the results of damage detection are presented for the UCLAFB, using recorded ambient vibration data and the recorded responses from the Parkfield earthquake, followed by the key findings and the main summary of this study. To facilitate easy understanding of the material in the subsequent discussions a list of acronyms is provided in Table 4.1.

Table 4.1: Important acronyms

AR	Auto regressive
TVAR	Time Varying Auto Regressive
POC	Principal Orthogonal Components
DSF	Damage Sensitive Feature
HOM	Higher Order Moment
UCLAFB	University of California, Los Angeles, Factor Building

4.1 Motivation

In the previous chapter, the concepts of basic PCA were extended to develop RPCA method that clearly showed improved and exact detection results for numerically simulated case studies, experimental verifications and even for practical problems. In case of nonstationary excitation as input, it has been observed that the previously described RPCA-RRE algorithm does not provide significant outcomes at the instant of damage. The exact instant of damage obtained from the RRE plots gets masked due to the nonstationary nature of the input, compounded with the nonlinearities inherently present in the system. Achieving exact detection results in real time for underdetermined systems with nonstationary input excitation data is an uphill task that necessitates certain modifications in the formulation of the FOEP based RPCA approach. Motivated by these practical performance issues, the basic RPCA based methodology can be extended in order to improve the quality of real time detection. Towards this, TVAR modeling in conjunction with the existing RPCA approach is presented in this chapter. The basic idea is that the transformed response obtained from the RPCA algorithm are modeled using TVAR approach, using a model order for the signal. The resulting signal so obtained contains information related to the spatial and temporal patterns of damage, which are then examined to obtain the location and instant of damage occurred to the system. This is the first FOEP based approach appended with a TVAR methodology that is explored in this thesis.

4.2 Background

The utilization of the concepts of RPCA necessitates that the recursive eigenspace updates obtained at each time stamp should be tracked globally, online, in a recursive framework [135]. Once the eigen space updates are obtained, the proposed framework utilizes TVAR modeling in conjunction with

DSFs for identifying the instant of damage. An autoregressive (AR) process may be used to model activity that is generated by one or more superimposed responses, operating under the premise that past values obtained from a time series affects the current values, based on some statistical calculations [1–3]. The implementation of AR algorithm towards structural damage detection is beyond the scope of this work and the readers are referred to seminal works [1, 2, 107] on the topic for details. The primary advantage of the AR model is that the underlying process that produces the observed data can be inferred directly from the AR parameters without resorting to spectral representation. Time series models work extremely well in capturing the key features of any data series. Literature utilizing time series modeling for damage detection is quite extensive [51, 53] but with the disadvantage that basic AR modeling is not amenable for online implementation. To tailor AR modeling towards recursive implementation and to better capture the non-stationarity involved with any data or due to the damage induced, TVAR modeling has been proposed. However, a major concern for using the TVAR models is pre-selection of the model order. In the proposed method, TVAR modeling is applied on the transformed responses obtained from the RPCA algorithm rather than the raw vibration responses. Therefore, relatively low model order of time-series model [51, 53] is sufficient to capture the dynamics of the structure in the transformed domain. The online damage detection framework, exclusive of baseline data, is used to identify the damage instant in the monitored system through the time varying coefficients of the TVAR models. In the proposed framework, damages in structures can be detected both spatially and temporally in real time.

4.3 RPCA and structural dynamics: A POC based formulation

In order to understand the application of RPCA in the purview of structural dynamics, consider a linear, classically damped, and lumped parameter system with mass, stiffness and damping matrices $\mathbf{M}$, $\mathbf{C}$ and $\mathbf{K}$ subjected to an external force, with $\mathbf{x}$ as the displacement vector.

$$[\mathbf{M}]\{\ddot{x}(t)\} + [\mathbf{C}]\{\dot{x}(t)\} + [\mathbf{K}]\{x(t)\} = \{\mathbf{F}(t)\} \tag{4.1}$$

where $\mathbf{F}(t)$ is the input excitation which is assumed to be Gaussian and broadband. The symbols have their usual meanings as denoted in the previous chapter. The solution of the equation can be written as $\{\mathbf{x}\}_m = [\mathbf{V}]_{m\times s}\{\mathbf{q}\}_s$, where $\mathbf{x}$ is the measurement matrix of size $m \times N$, $\mathbf{q}$ is the matrix of corresponding modal coordinates of size $s \times N$. Here m represents the number of DOF and s corresponds to the number of modes considered with N sampling points. $[\mathbf{V}]_{m\times s}$ is the mode shape matrix which transforms the data from modal coordinates to the physical space. An important characteristics of the mode shape matrix is that each columns of the mode shape matrix are orthogonal to each other with respect to the matrix $\mathbf{M}$. The covariance matrix of $\mathbf{X}$ ($\mathbf{R} = \frac{1}{N}\mathbf{X}\mathbf{X}^T$) can be expressed as $\mathbf{R} = \frac{1}{N}\mathbf{V}\mathbf{Q}\mathbf{Q}^\mathbf{T}\mathbf{V}^\mathbf{T}$.

From the above expression, $\mathbf{R_Q} = \frac{1}{N}\mathbf{Q}\mathbf{Q}^\mathbf{T}$ can be identified as the covariance matrix of the modal responses. For undamped free vibration (i.e., $\mathbf{C} = 0$ and $\mathbf{F} = 0$ in Eqn. 4.1), $\mathbf{R_Q}$ is exactly a *diagonal matrix*, while under mildly damped forcing conditions (i.e., $\mathbf{C} \neq 0$ and $\mathbf{F} \neq 0$ in Eqn. 4.1), the matrix $\mathbf{R_Q}$ is an *approximately diagonal* matrix for finitely large samplesize [88]. Under broadband excitations, the evolution of the physical response, $\mathbf{x_i(t)}$ and modal response $\mathbf{q_i(t)}$, in time domain can be expressed in terms of the impulse response function as $q_i(t) = \int_0^\infty h(t-\tau) f_i(\tau)\, d\tau$, where $\mathbf{f}_i(\tau)$ represent the modal forces, related by the equation $\mathbf{f}_i(\tau) = v_i^T\mathbf{F}_i(\tau)$, where v_i represents the mode shape corresponding to the mode and $\mathbf{F}_i(\tau)$ represent the actual forces. The individual elements of the covariance matrix $\mathbf{R_Q}$ can be expressed as:

$$r_{ij}^Q = \int_{\tau=0}^{\infty}\int_{\theta=0}^{\infty} f_i(\tau)f_j(\theta)\left[\frac{1}{N}\sum_{i,j} h_i(t-\tau)h_j(t-\theta)\right]d\tau d\theta \tag{4.2}$$

Eqn. 4.2 shows that for finitely large N, $\mathbf{R_Q}$ can be expected to be a diagonal matrix for undamped system and nearly diagonal for light to moderate modal damping. The POCs (ψ) or orthogonal transformation of the data can be written as product of POMs ($\mathbf{W}$) and the data vector ($\mathbf{x}$) as:

$$\begin{aligned}\psi_i(t) &= \mathbf{W}^\mathbf{T}x_i(t)\\ &= q_i(t) + \gamma\end{aligned} \tag{4.3}$$

Hence POCs (ψ) can be expressed as a sum of true linear normal coordinates (q) and an error term (γ). To understand the behavior of covariance matrix of POC, $\mathbf{R_\Psi} = \frac{1}{N}\mathbf{\Psi}\mathbf{\Psi^T}$ its essential to realize the individual elements of the $\mathbf{R_\Psi}$ matrix. Substituting from Eqn. 4.3,

$$\begin{aligned} r_{ij}^{\psi} &= \frac{1}{N}\sum_{k=1}^{N}\psi_i(t_k)\psi_j(t_k) \\ &= \frac{1}{N}\sum_{k=1}^{N}[q_i(t_k)q_j(t_k) + \gamma q_j(t_k) + q_i(t_k)\gamma + \gamma^2] \end{aligned} \tag{4.4}$$

For practical systems having low to moderate damping and finite sample size, it can be understood from Eqn. 4.4 that POC provides a good approximation to the true linear modal component which deviates from each other as damping increases [121, 122]. Hence the POC covariance matrix $\mathbf{R_\Psi}$ is still expected to show a diagonally dominant behavior in the limit as $N \to \infty$ and when the errors are low (i.e., low to moderate damping) [121].

The main objective of RPCA is to provide a recursive estimate of $\mathbf{W}$ as well as ψ_k at each time instant as and when the data streams in real time. For structural systems with low to moderate damping, obtaining the POCs at each time instant is equivalent to obtaining the normal coordinates at each instant. Since the normal coordinates are independent, they are likely to be mono-component in nature, thereby a lower order time series model would be sufficient to capture the dynamics of the same. The response covariance matrix $\mathbf{R_k}$ at any instant k can be written as a function of the covariance matrix of the previous time instant $\mathbf{R}_{k-1}$ and response vector $\mathbf{x_k}$ at the k^{th} time instant as shown:

$$\mathbf{R}_k = \frac{k-1}{k}\mathbf{R}_{k-1} + \frac{1}{k}\mathbf{x}_k\mathbf{x}_k^T \tag{4.5}$$

The covariance estimate R_k can we written in terms of its EVD as $[\mathbf{R}_k] = [\mathbf{W}_k]\,[\mathbf{\Upsilon}_k]\,[\mathbf{W}_k]^T$. On substituting in Eqn. 4.5, the expression for the covariance matrix is rewritten as:

$$\mathbf{W}_k\mathbf{\Upsilon}_k\mathbf{W}_k^T = \frac{k-1}{k}\mathbf{W}_{k-1}\mathbf{\Upsilon}_{k-1}\mathbf{W}_{k-1}^T + \frac{1}{k}\mathbf{x}_k\mathbf{x}_k^T \tag{4.6}$$

The estimate POC vector at k^{th} time instant can be written as $\left\{\tilde{\psi}_k\right\} = [\mathbf{W}_{k-1}]^T\{\mathbf{x}_k\}$. On

substituting in Eqn. 4.6, the following expression can be obtained

$$[\mathbf{W}_k]\,[k\boldsymbol{\Upsilon}_k]\,[\mathbf{W}_k]^T = \mathbf{W}_{k-1}\left[(k-1)\,\boldsymbol{\Upsilon}_{k-1} + \tilde{\psi}_k\tilde{\psi}_k^T\right]\mathbf{W}_{k-1}^T \tag{4.7}$$

For the RPCA algorithm to be stable and robust, it is important that the term $[(k-1)\,\boldsymbol{\Upsilon}_{k-1} + \tilde{\psi}_k\tilde{\psi}_k^T]$ is *diagonally dominant*, in order to evaluate the EVD by dint of Gershgorin's theorem [121, 122]. The term $\tilde{\psi}_k\tilde{\psi}_k^T$ represents the correlation between the POC estimates at a particular instant. Substituting from Eqn. 4.3, the covariance between POC estimates can be written as (to an arbitrary scale factor):

$$\begin{aligned}\tilde{\psi}_k\tilde{\psi}_k^T &= \mathbf{W}_{k-1}^T x_k {x_k}^T \mathbf{W}_{k-1} \\ &= q_{k-1}{q_{k-1}}^T + \gamma {q_{k-1}}^T + \gamma^T q_{k-1} + \gamma\gamma^T\end{aligned} \tag{4.8}$$

As far as the dynamics of structural systems are considered, the error term in the Eqn. 6.13 can be neglected as the number of sampling points increases and under moderate to low damping. The first term in Eqn. 6.13 resembles the covariance of the normal coordinates at the instant $(k-1)$, which are in turn mono-component in nature. Thus the term $q_{k-1}{q_{k-1}}^T$ represents a matrix whose diagonal terms dominate its off-diagonal terms; hence, the term $\tilde{\psi}_k\tilde{\psi}_k^T$ can be safely assumed to be diagonally dominant. This in turn, ensures the diagonal dominance of the matrix $\left[(k-1)\Upsilon_{k-1} + \tilde{\psi}_k\tilde{\psi}_k^T\right]$, facilitating straightforward application of Gershgorin's theorem. Hence for a structural system, the recursive eigen space update is obtained using a first order perturbation (FOEP) approach which provides a less computationally intensive algorithm in a recursive framework. The EVD of the matrix $\left[(k-1)\Upsilon_{k-1} + \tilde{\psi}_k\tilde{\psi}_k^T\right]$ can be substituted as $\mathrm{H_k}\boldsymbol{\Lambda}_k\mathbf{H}_k^T$ into Eqn. 5.12 as,

$$[\mathbf{W}_k][k\Upsilon_k][\mathbf{W}_k]^T = [\mathbf{W}_{k-1}\mathbf{H}_k][\boldsymbol{\Lambda}_k][\mathbf{W}_{k-1}\mathbf{H}_k]^T \tag{4.9}$$

which yields the following iterative update equations:

$$\left.\begin{aligned}\mathbf{W}_k &= \mathbf{W}_{k-1}\mathrm{H}_k \\ \boldsymbol{\Upsilon}_k &= \tfrac{\boldsymbol{\Lambda}_k}{k}\end{aligned}\right\} \tag{4.10}$$

The recursive algorithm of Eqn. 4.5 is transformed to obtain the values of H_k and Λ_k. Since the term $(k-1)\,\boldsymbol{\Upsilon}_{k-1} + \tilde{\psi}_k \tilde{\psi}_k^T$ is diagonally dominant, the eigen values can be assumed to be the diagonal entries of the matrix. Hence the i^{th} diagonal entry of the term Λ_k can be represented as $(k-1)\,\lambda_i + \tilde{\psi}_i^2$, where λ_i is the (i,i) element of $\boldsymbol{\Upsilon}_{k-1}$ and ψ_i is the i^{th} entry of the POC estimate. Once the eigen values are known, the corresponding eigen vectors can be found out, leading to H_k.

One of the key problems faced while applying FOEP approach is that the recursive eigen vectors obtained at each time instant are not ordered, which poses the problem of *permutation ambiguity* [68]. This can be addressed by arranging the basis vectors according to decreasing order of the corresponding eigenvalues in Υ_k. At each time instant, the eigenvalues indicate the contribution of the particular eigenvectors. The contribution factor can for a particular i^{th} eigen vector w_i at each time instant can be written as $\frac{\alpha_i^2}{\sum_{i=1}^{n} \alpha_i^2}$, where α_i^2 is the eigenvalue corresponding to w_i. Let $\mathbf{W}_k = [\mathbf{W}_k^1 \mathbf{W}_k^2]$, where $\mathbf{W}_k^1$ is the subspace at k^{th} time instant consisting of eigenvectors, that account for more than 90% of the energy in the participating modes of the system and $\mathbf{W}_k^1$ is the subspace at k^{th} time instant accounting for the remaining kinetic energy. These recursively estimated subspaces, are the subsequently utilized to find the true POC at each instant of time as per the expression $\psi_k = \mathbf{W}_k^T \mathbf{x}_k$. The first element of the ψ_k vector represents the major principal component. TVAR modeling is now performed on the first major principal component.

4.4 TVAR modeling

The implementation of RPCA algorithm provides the POC updates recursively at each instant of time. Once the modal responses are obtained using the proposed algorithm, the next step is to find out the instant of damage. In order to characterize the behavior of the POC updates (which can be approximated to normal coordinates), TVAR modeling is adopted here. The use of TVAR modeling for detecting structural damages has been attempted in the recent times with fair amount of success [51]. TVAR coefficients of the modeled transformed response are tracked in real time in order to identify the damage instant. The sudden changes in AR coefficients indicate the alterations in the dynamical properties of the system, such as shifts in natural frequencies, changes in the mode

shapes of the system, etc., induced due to the damage occurred in the system. In the proposed work, the transformed response (i.e.,the first POC) extracted from the RPCA algorithm is modeled using a TVAR model. However, the main drawback associated with using TVAR models is the selection of model order a priori such that the resulting TVAR model correctly characterizes the data during the times of interest. The use of POCs instead of the raw vibration data, whose near resemblance to normal coordinates enables the use of a low model order, resolves the issue of model order selection.

Let $\psi^1(k)$ represent the POC at any instant which captures the maximum kinetic energy of the system and let $v(k)$ denote the zero mean Gaussian white noise with variance σ_v^2. Then the AR model of order p can be represented as:

$$\psi^1(k) = \sum_{i=1}^{p} a_i \psi^1(k-i) + v(k) \tag{4.11}$$

The nonstationary nature of the POC, necessitates recursive updates of the AR coefficients in which a_i becomes $a_i(t)$, to capture the dynamics of the normal coordinate effectively. For this purpose, the Kalman filter is utilized to estimate these time-varying coefficients, knowing the observations of data [72–74]. The following equation is the discrete representation of the $a_i(t)$ coefficients and $w(k)$ is the process noise with variance σ_w^2 and covariance, $\mathbf{P_w} = \mathbf{I_{p\times p}}\boldsymbol{\sigma}_{\mathbf{w}}^{\mathbf{2}}$. Both noise measurements $v(k)$ and $w(k)$ are mutually independent and uncorrelated. Consider the following set of equations, where the unknown state vector $b(k)$ is expressed as shown:

$$\begin{aligned} \mathbf{b(k)} &= \mathbf{\Gamma(k-1)b(k-1)} + \mathbf{w(k)} \\ \psi^1(k) &= \mathbf{C(k)b(k)} + \mathbf{v(k)} \end{aligned} \tag{4.12}$$

The state vector $b(k)$ is given by: $\mathbf{b}(k) = [a_1(k), a_2(k), \ldots\ldots a_p(k)]^T$. The matrix $\mathbf{\Gamma}(k-1)$ is an identity matrix ($\mathbf{I}_{p\times p}$). The matrix C_k is the observation data with discrete k steps given as: $\mathbf{C}(k) = [\psi^1(k-1), \psi^1(k-2) \ldots\ldots \psi^1(k-p)]$. The Kalman filter has mainly two processes: one is the stepwise time update (prediction) and the other one is measurement update (correction) of

the predicted data. At each step, the set of the Kalman filter equations can be written as [72–74]:

$$\begin{aligned}
&\mathbf{b}\left(k|k-1\right)=\mathbf{b}\left(k-1|k-1\right)\\
&\mathbf{P}_b\left(k|k-1\right)=\mathbf{P}_b\left(k-1|k-1\right)+\mathbf{I}\sigma_w^2\\
&\psi^1\left(k|k-1\right)=\mathbf{C}\left(k\right)\mathbf{b}\left(k|k-1\right)\\
&\sigma_{\psi^1}^2\left(k|k-1\right)=\mathbf{C}\left(k\right)\mathbf{P}_b\left(k|k-1\right)\mathbf{C}(k)^T+\sigma_v^2
\end{aligned} \tag{4.13}$$

And,

$$\begin{aligned}
&\mathbf{KG}\left(k\right)=\mathbf{P}_b\left(k|k-1\right)\mathbf{C}(k)^T\sigma_{\psi^1}^2(k|k-1)^{-1}\\
&\mathbf{b}\left(k|k\right)=\mathbf{b}\left(k|k-1\right)-\mathbf{KG}\left(k\right)\left[\psi^1\left(k\right)-\psi^1\left(k|k-1\right)\right]\\
&\mathbf{P}_b(k|k)=[\mathbf{I}-\mathbf{KG}(k)\mathbf{C}(k)]\mathbf{P}_b(k|k-1)]
\end{aligned} \tag{4.14}$$

where $\mathbf{b}\left(k|k-1\right)$ represents apriori estimate and its linear combination would result in $\mathbf{b}\left(k|k\right)$, which is a posteriori. The Kalman gain $KG(k)$ gives a weightage to the prediction error $\psi^1\left(k\right)-\psi^1\left(k|k-1\right)$, to minimize the state estimation error $\mathbf{b}\left(k|k\right)$. this means that the apriori and the posteriori covariance estimates are given by $\mathbf{P}_b\left(k|k-1\right)$ and $\mathbf{P}_b\left(k|k-1\right)$, respectively. Although the TVAR model facilitates adequate representation of the non stationary transformed response, but in order to use it for damage detection, only TVAR model is not enough; hence, DSF are applied on the TVAR coefficients to detect damage as described next. Alongside TVAR coefficients, these statistical indicators (or the DSF) are applied to detect damage which run in real time. These DSF have a real time fervor and hence, these are amenable towards online implementation and has been explored in the present context.

4.5 Damage sensitive features

In the present framework, RPCA facilitates online processing of data producing recursive updates of eigen vectors and eigen values, referred to as eigen subspace. The eigen subspace by themselves cannot detect the change in system properties inflicted due to damage, if not processed by a set of damage markers commonly referred to as damage sensitive features (DSF) [1–3]. The key features of good DSFs are their ability to detect the presence of damage, effectively distinguish between

the damaged and undamaged states of the structure, followed by their capacity to possibly locate and quantify the extent of damage. Additionally, to detect damages in real time, the proposed DSFs should be amenable for online implementation and should accurately identify the presence of damage as and when the response data streams in continuously. Several damage detection and SHM techniques have been proposed in the literature [1, 2] that involve use of specific DSFs whose changes signify damage to the system. The disadvantages associated with the traditional DSFs includes requirement of (**i**) baseline or reference data from a healthy structure; (**ii**) windowing of response data etc., which impedes their application in an online framework. In this section, a brief background on the formulation of *online DSFs* is proposed utilizing the concepts of TVAR coefficients and recursive signal statistics. These features are based on the *reorientation of eigenspace* due to damage which is manifested in the form of change in the pattern of TVAR modeling before and after damage. In the following sections, TVAR coefficients (a_i), signal statistics on TVAR coefficients (μ_{a_i},ζ_{a_i}), spatial recursive residual errors (ε_{RR}) are presented.

4.5.1 Time varying auto-regressive coefficients

In the context of the current study, the TVAR coefficients are treated as the key DSFs. The motivation for this DSF is derived from the use of AR coefficients as a criterion for novelty evaluation [51], which presents the use of a statistical parameter known as Mahalanobis distance applied on AR coefficients to distinguish between a damaged state and an undamaged state. However, estimation of AR coefficients frequently requires the use of windowing and baseline data to detect damage, making online implementation difficult. Motivated by these key shortcomings, a TVAR modeling based framework [51] is implemented which does not require any baseline data to detect damage in real time, enabling it to capture the non stationary nature associated the data due to damage. The proposed method tracks the TVAR coefficients online, which are used to ascertain the damage induced in the structure by a change in the peak of the plot, at the exact instant of damage. The near mono-component nature of the transformed response ensures that low model order is sufficient to capture its dynamics; therefore, in the proposed framework, a model order of 2 (two) is pre-selected

for all the cases. The basic Eqn. 4.11 becomes:

$$\psi^1(k) = a_1(k)\psi^1(k-1) + a_2(k)\psi^1(k-2) + v(k) \tag{4.15}$$

where the symbols carry the same meaning as that of Eqn. 4.11. Although a_1 and a_2 are expected to alter mildly at each time instants, the damage instant is characterized by sudden changes in the overall behavior of TVAR coefficients post damage. Tracking this change in a_1 and a_2 serve as an indicator of damage.

4.5.2 Recursive statistics on TVAR coefficients

The transformed response obtained after implementation of the RPCA algorithm sometimes show modulatory/wavy behaviors, which can mask the accurate determination of damage instant. This is attributed to the non stationary and near mono-component nature of the transformed response ($\psi(t)$). As explained in Section 4.3, the POC tends to normal coordinates only under certain assumptions which may not be realized in practice always. Hence, even though TVAR coefficients reflect the damage in a system, the change may not be always obvious. To address the aforementioned issue, recursive versions of the commonly used signal statistics are employed on TVAR coefficients [51]. The damage in a structural system is corroborated by the change in the behavior of TVAR coefficients which is manifested in the form of : (**i**) sharp peak in a_1 and/or a_2 in the vicinity of damage; (**ii**) drift of post damage a_1 and/or a_2 from the pre-damage values. This prompted the use of recursive mean (μ_{a_i}), and higher moments (ζ_{a_i}) of AR coefficients which can capture the essence of damage in a better reflective way.

$$\begin{aligned}
\mu_{a_i}(k) &= \frac{k-1}{k}\mu_{a_i}(k-1) + \frac{1}{k}a_i(k) \\
{\sigma^2}_{a_i}(k) &= \frac{k-1}{k}{\sigma^2}_{a_i}(k-1) + \frac{1}{k}a_i(k)a_i(k) \\
\zeta_{a_i}(k) &= \frac{(k-1)\zeta_{a_i}(k)/k + a_i(k)a_i(k)a_i(k)a_i(k)a_i(k)a_i(k)/k}{\left((k-1)\sigma^2_{a_i}(k-1)/k + a_i(k)a_i(k)/k\right)^3}
\end{aligned} \tag{4.16}$$

where ζ_{a_i} refers to the sixth order moment and $\sigma^2_{a_i}$ represents the second moment or variance.

4.6 Proposed Algorithm

The overall methodology followed in this section entails the amalgamation of separate modules which detect two key ingredients: *temporal* and *spatial* damage detection, simultaneously. The first module deals with the global damage detection, wherein the raw acceleration data is processed by the RPCA algorithm as the data streams in real time. This accounts for an online damage detection framework as no batches of data are utilized in order to form a baseline. TVAR modeling is carried out on the updated first principal component which yields TVAR coefficients at each instant of time. As previously explained, TVAR coefficients are tracked online for any major and minor changes. DSFs (like higher moments) are utilized to corroborate the instant of damage, that provides a validation to the plots obtained from the TVAR coefficients. Once the damage instant is detected, the spatial damage detection module further resolves the location of damage.

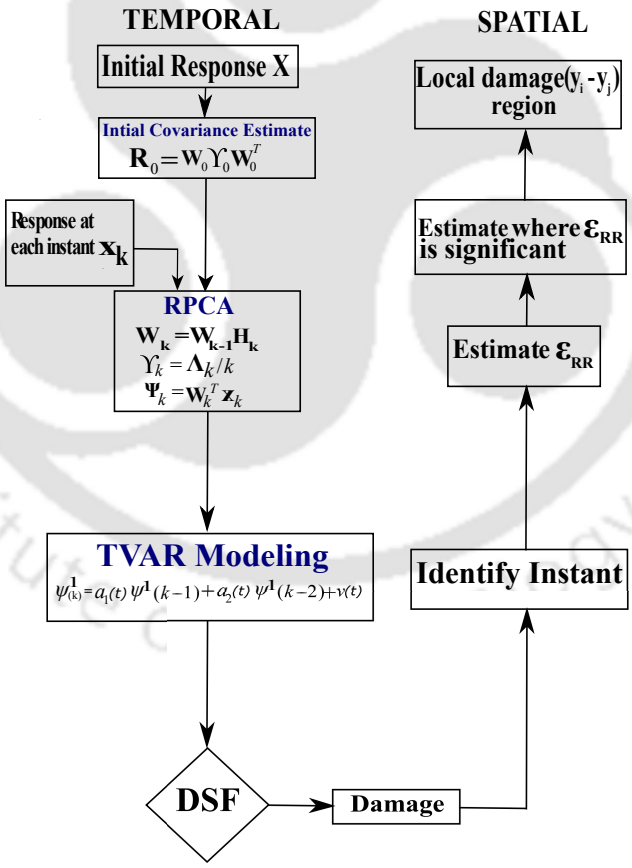

Figure 4.1: Flow chart of the proposed RPCA-TVAR algorithm

For easy comprehension of the flowchart, the basic steps of the algorithm are enumerated as

follows:

1. First, batch PCA is employed on some initial data points in order to estimate the initial eigen vector and eigen value matrices, i.e., the initial eigenspace.

2. The RPCA algorithm then operates online on the real time input of the streaming data.

3. Using the recursive gain depth parameter, the covariance estimate at the present time instant is derived using the covariance estimate at preceding time instant. From the recursive updates, the eigen vector and eigen value matrices are updated using FOEP approach and the transformed responses (principal components) are obtained using the RPCA algorithm.

4. Suitable time series models are generated based on the responses to fit a TVAR model. The DSFs are tracked in real time in order to extract the changes in the model coefficients, thereby revealing the faults in the system.

5. Once the instant of damage is determined, the algorithm shifts on to the next module where the spatial detection of damage takes place. The local RREs are tracked online recursively to capture the spatial effect of the damage, visually.

A flowchart as shown in Fig. 5.1 outlines the proposed damage detection scheme, step-wise. Vibration responses are processed by the RPCA algorithm to obtain the transformed responses, then the TVAR modeling is utilized to extract the time-varying coefficients through which damage instant is detected. It is to be noted that the aforementioned proposed algorithm has the following few characteristics: (**i**) the data is processed at each time instant, as and when it becomes available, i.e the algorithm works *online*. (**ii**) to locate the instant of damage a reference value (baseline) is not required, i.e. it is *baseline free*. (**iii**) there are no parameters controlling the working of the algorithm, hence its *parameter free*. The above mentioned characteristics of the proposed algorithm makes it an ideal choice for a real time damage detection framework.

4.7 Numerical example

The B-W model described in the previous chapter (Sec. 3.6.1) is taken into consideration for damage detection studies. The reason for choosing the same model for numerical case studies is to identify the improvement in the detection prowess of the newly proposed RPCA-TVAR algorithm. The parameters of the model remain same as previously discussed, and assumes a linear dependence of DI with the change in then nonlinear force term. The B-W system is chosen for an intuitive understanding of the behavior of RPCA-TVAR algorithm towards validating the spatio-temporal aspect of damage in real time. The current study considers global damage through a change in the nonlinear force term κ, while the concept of spatial damage is emulated through a reduction in the linear storey stiffness. The detection studies are presented for the system subjected to white noise excitation followed by certain key results and observations.

4.8 Temporal damage detection results

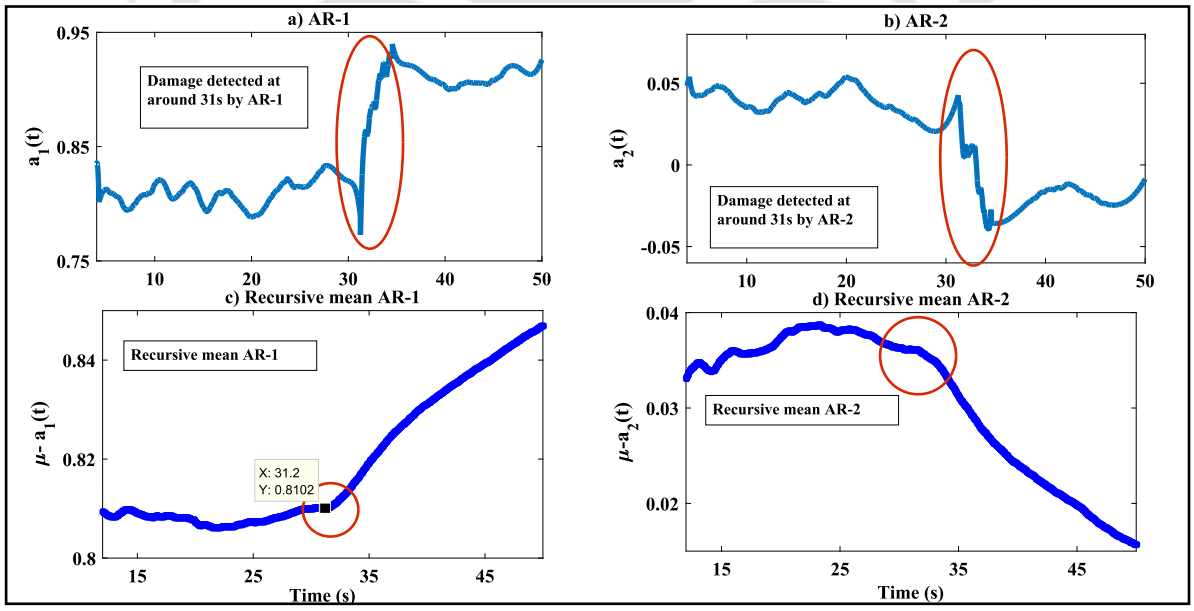

Figure 4.2: Damage detection using damage sensitive features for 30% non linearity change

Typical recorded accelerations at the roof of the structure subjected to various levels of nonlinearity have already been presented in Fig. 3.3. It can be observed from the figure that the presence

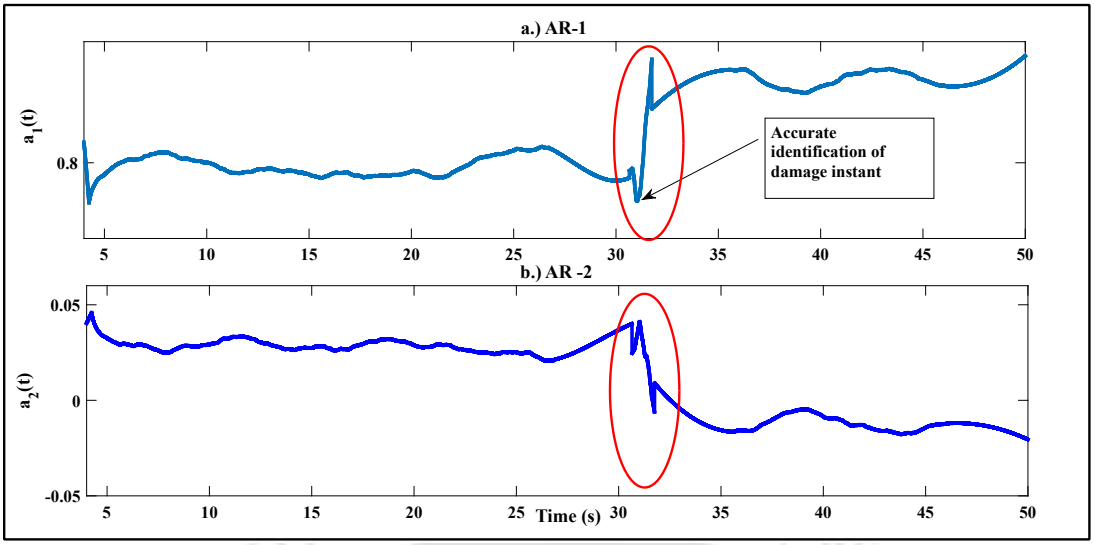

Figure 4.3: Damage detection using TVAR coefficients for 15% non linearity change

of damage due to the change in the nonlinear force parameter is not quite discernible from the acceleration plots. In order to identify the damage occurred, the raw vibration responses need to be processed with the newly proposed RPCA-TVAR algorithm. The damage is induced through change of nonlinearity by 15%, 20% and 40% at a particular time instant of 31s. In order to detect the temporal damage, two DSFs are used: TVAR coefficients and their higher order moments (HOMs). It can be clearly observed from Fig. 4.2 that the damage instant can be easily detected using the TVAR coefficients by exploiting their sudden changes in the mean level at the damage instant. Thus, it confirms that TVAR modeling is amenable to online damage detection in a recursive framework. Since the transformed responses obtained using the RPCA algorithm are mono-component in nature, a relatively low model order (say,2) can be used, which is shown in Fig. 4.2. It can also be observed from Fig. 4.2(b) that recursive mean could capture the essence of fault detection where it shows a significant deviation in its original trajectory at $31s$. However, it will be shown in the following sections that the plots for HOMs provide much accurate results than recursive mean as observed for experimental case.

The efficacy of recursive DSF is less effective for lower percentage change in nonlinearity. As evident from literature, damages of the order of 25% have been often reported as a lower limit for vibration based damage detection [51]. However, in the present study the use of TVAR coefficients successfully detects damage corresponding to 15% change in nonlinearity. As seen from Fig. 4.3,

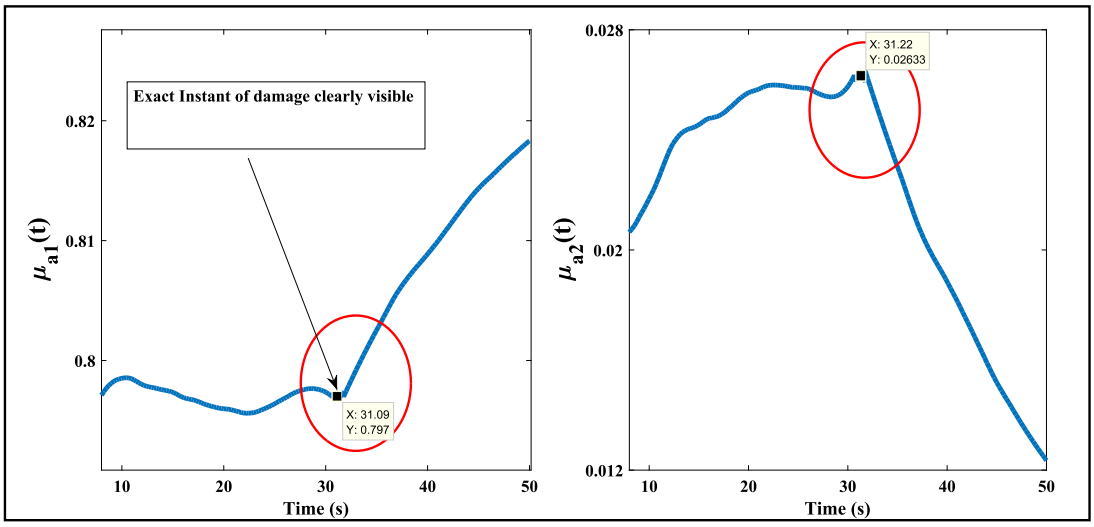

Figure 4.4: Damage detection using recursive mean for 15% non linearity change

the TVAR plots serve as a robust DSF for detecting damage. The damage instant can be clearly identified from the figure as $31s$ using the proposed method.

It can be observed from the figure that there is a small peak within 5 seconds after start both in Fig. 4.3(a) and 4.3(b). This can be attributed to the fact that as the proposed method is purely an online implementation, the algorithm requires certain number of data points to stabilize till the TVAR coefficients start to show consistent evolution in time that could be utilized for damage detection. The exact instant of damage is identified at $31s$ for even a 15% change in nonlinearity, which now establishes a finer level of detection as compared to existing literature [51]. The fact that these peaks are not associated with any damage can be further substantiated by the use of scatter plots. The scatter plots between the POCs serve as a robust visual DSF for detecting damage, which show a change in orientation (change in the sign of the correlation coefficient) only at the instant of damage. Thus, the spurious peaks around the 5 second mark in the plots displayed in Fig. 4.3 do not correspond to a damage event which is clear from Fig. 4.5(no change in the sign of ρ). The use of scatter plots is purely an offline process requiring windows of data and serving as visual markers for detection of false alarm. Scatter plots are computationally expensive and must be used judiciously only for ruling out certain spurious peaks related to non-damage events. The current framework keeps the scatter plots as an optional tool that could be used only when needed.

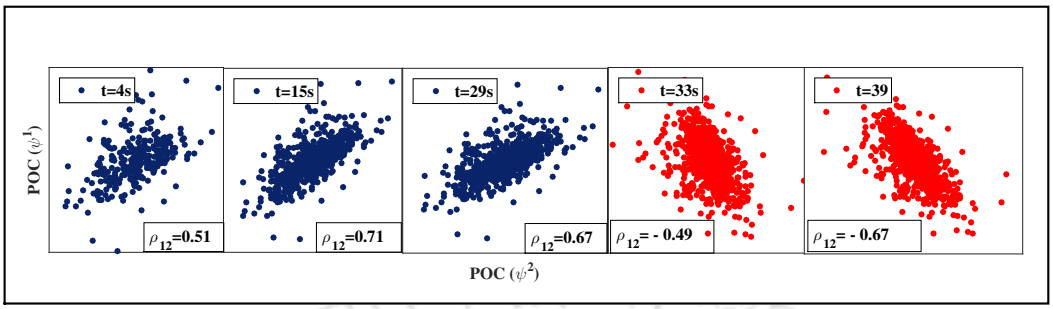

Figure 4.5: Scatter plots for visual confirmation of damage instant

In order to further validate the damage instant obtained from the TVAR plots, the use of recursive mean on the TVAR coefficients are tracked to show any significant changes, online. By looking at Fig. 4.4(a) and 4.4(b), it can be clearly seen that there is a significant change in the estimate of the recursive mean. It can also be observed from the figures that the DSF utilized for tracking the changes shows distinct peaks indicating the exact instant of damage occurred in the system. It becomes imperative to review and report the computational efficiency of the proposed method. As previously established, damage being a real time event necessitates that the algorithm assigned to track it in real time must function online, with less computational exhaustion and provide detection results as and when the vibration data streams in. In this context, the time taken for a single iteration of the algorithm is found to be 4.59 milli seconds, which closely emulates a real time process. The arrangement of basis vectors in the decreasing order of the corresponding eigenvalues consumes 79.2 micro seconds, which is 1.7% of the total time consumed for a complete single iteration. However, the time consumed depends upon the computational power of the system used and is more efficient for systems with superior processing power, higher gigabytes of RAM, multiple cores, etc

4.8.1 Spatial Damage Detection Results

In the previous sections, the notion of global damage had been discussed through variation in the nonlinear force term κ in the equation of motion of the system. In the present section, the local damage to the structure is perceived to be an alteration in the linear storey stiffness for a particular

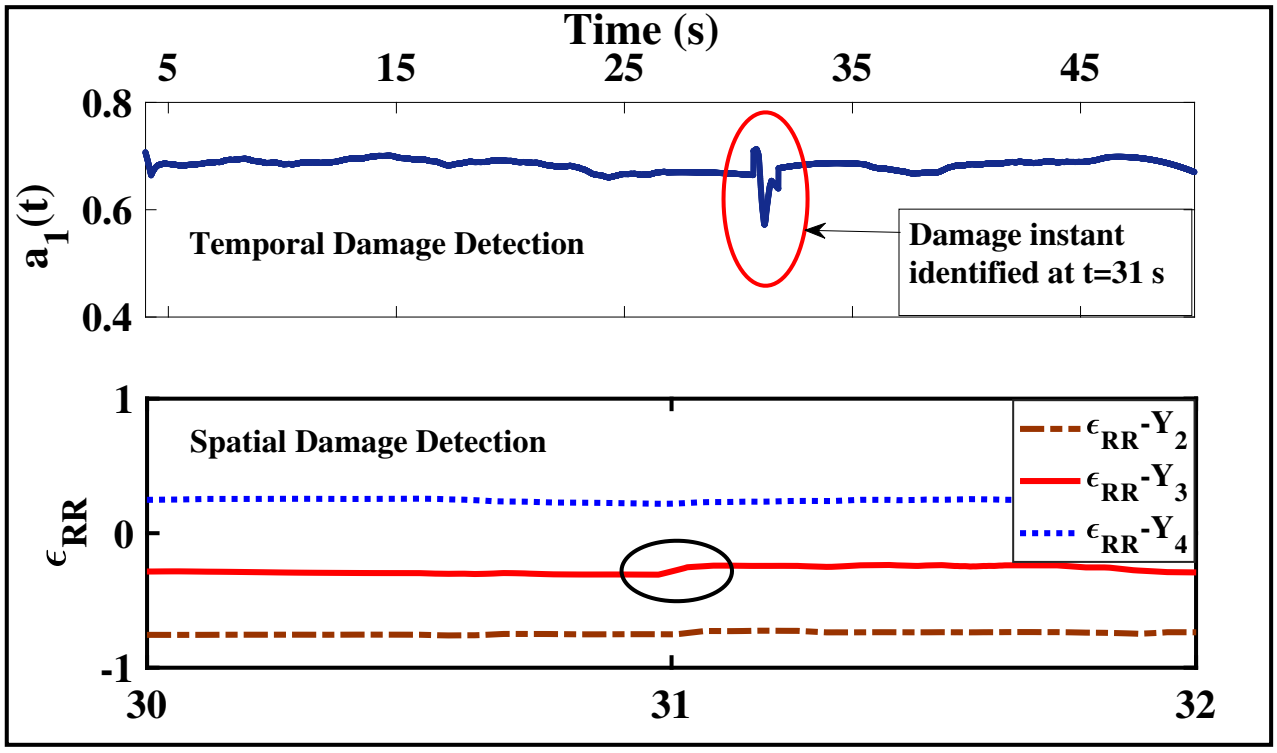

Figure 4.6: Comparison between spatial and temporal damage for 35% change

floor that subsequently correspond to the concept of *online spatio-temporal* damage detection. As already mentioned, only when the instant of damage in ascertained, the algorithm shifts on to spatial damage detection module in order to identify the location of the damage. The simultaneous temporal and spatial case deals with 35% and 25% changes in linear stiffness in the 3^{rd} storey of the structure. The system is assumed to be fully nonlinear by scaling the value κ to 1. Once the damage instant is detected by tracking the change in the mean of the TVAR coefficients, the spatial module starts functioning online in order to localize the position of damage occurred in the system. From Fig. 4.6, it can be shown that clear damage instant is identified at 31s for a 35% damage. Once the damage instant is detected, the spatial RRE in the neighborhood of the vicinity of damage (say, 29s to 33s) is examined. From the same figure, it is clearly observed that the spatial RRE for third degree of freedom shows a significant change at 31s compared to the other set of responses, thereby indicating that the damage has occurred in the third storey. From Fig. 4.7, it is evident that the the spatial RRE for 25% damage indicates a visible change at t=31s. As outlined before, the temporal and spatial detection module should run simultaneously. The changes in the TVAR coefficients and the local RRE are tracked online recursively in order to capture the essence of temporal and spatial

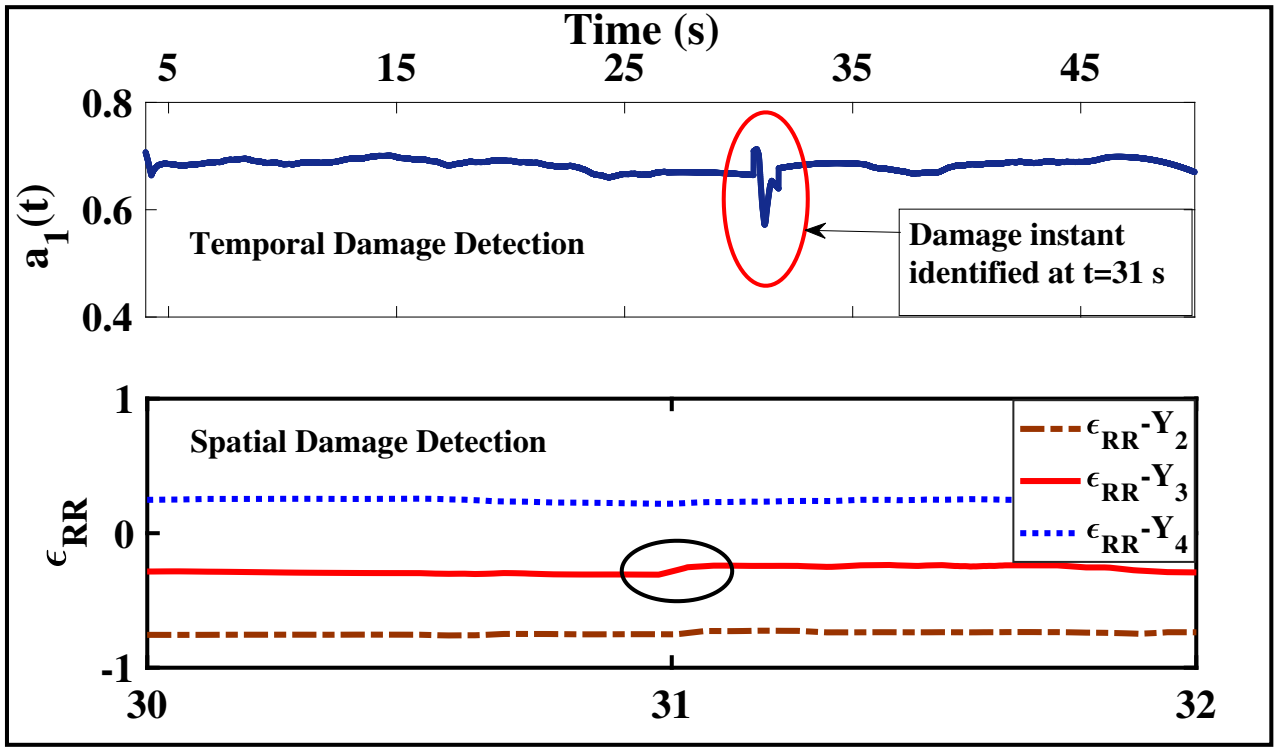

Figure 4.7: Comparison between spatial and temporal damage for 25% change

damage detection, respectively. As seen from Fig. 4.6 and 4.7, damage detection can be interpreted from the change in local RRE corresponding to the third DOF which substantiates the localization of the damage. However, it is worth mentioning the fact that as the extent of stiffness degradation decreases, detecting spatial damage becomes increasingly difficult as compared to detecting temporal damage *alone*, evident from Fig. 4.7.

For the case of local damage, the nonlinear force term is kept constant at unity, which indicates that the value of the damage index (DI) is zero, in this case. As far as the system dynamics is concerned, the damage is manifested in the form of a linear stiffness change, identified as local damage, which is captured by the temporal damage detection module and is reflected by a peak in the TVAR plot, shown in Fig. 4.6. The phenomenon of local damage, unlike the change in nonlinearity at the base of the model, is confined only to a particular DOF and does not affect the structure as a whole, which is clearly observed from the plot of spatial RREs in Fig. 4.6(b). The plot of the TVAR coefficients retains its original trajectory even after the algorithm indicates the damage instant not because the system is repaired but rather the strength of frequency burst ceases

to maintain its localization and intensity after a certain point of time.

The use of RREs as an effective damage localization tool emanates from the idea that spatial RREs show significant distortions in the trajectory only in the DOF that has undergone damage in the structure. It is further assumed that the presence of nonlinear force at the base is unlikely to propagate significantly to the individual DOFs, which is quite valid, considering the weakly nonlinear nature of the system. To substantiate the point, a simple case is implemented to demonstrate that the nonlinearity associated at the base doesn't have significant effect in reducing the efficacy of RRE. The damage is simulated at local level by reducing 3^{rd} storey linear stiffness by 25% and 35%, respectively, at a particular time instant of $t = 31$ s for the case of κ=0.02 (nonlinear force nearly equal to zero) and compared with the aforementioned κ=1 (hysteretic nonlinear force is fully present) case. In both the two cases,$\varepsilon_{RR} - Y_3$ is able to detect local damage quite clearly as evident from the Fig. 4.8 and Fig. 4.6. This clearly shows that the presence of hysteretic nonlinearity at the base doesn't affect the real time detection of damage significantly at least for the above case. However, the proposed methodology might not be suitable if the individual DOFs are modeled as nonlinear oscillators.

4.8.2 Results for El Centro ground excitation

To illustrate the potential application of the proposed method, numerical simulation is performed on the B-W system excited using El Centro recorded vibration data. The damage is simulated for a 30% change at 25s. The proposed algorithm processes the data and the simultaneous tracking of the DSFs are done online, recursively, in order to accurately identify the damage instant. From Fig. 4.9, it can be seen that the plots of TVAR coefficients do not indicate a clear instant of damage due to the highly nonstationary behavior of the input excitation. In order to mask the nonstationary behavior of the input data, HOMs of the TVAR coefficients are employed to clearly indicate the instant of damage. The effect of structural damage on the plots of the HOMs is much more significant than the effect of local non-stationarity associated with the input excitation, thereby making the HOMs (ζ_{a_i}) better equipped to capture the essence of damage. In the present damage scenario, the sixth moment of the TVAR coefficients($\zeta_{a_1}(t)$,$\zeta_{a_2}(t)$) is effectively used to indicate the exact instant of

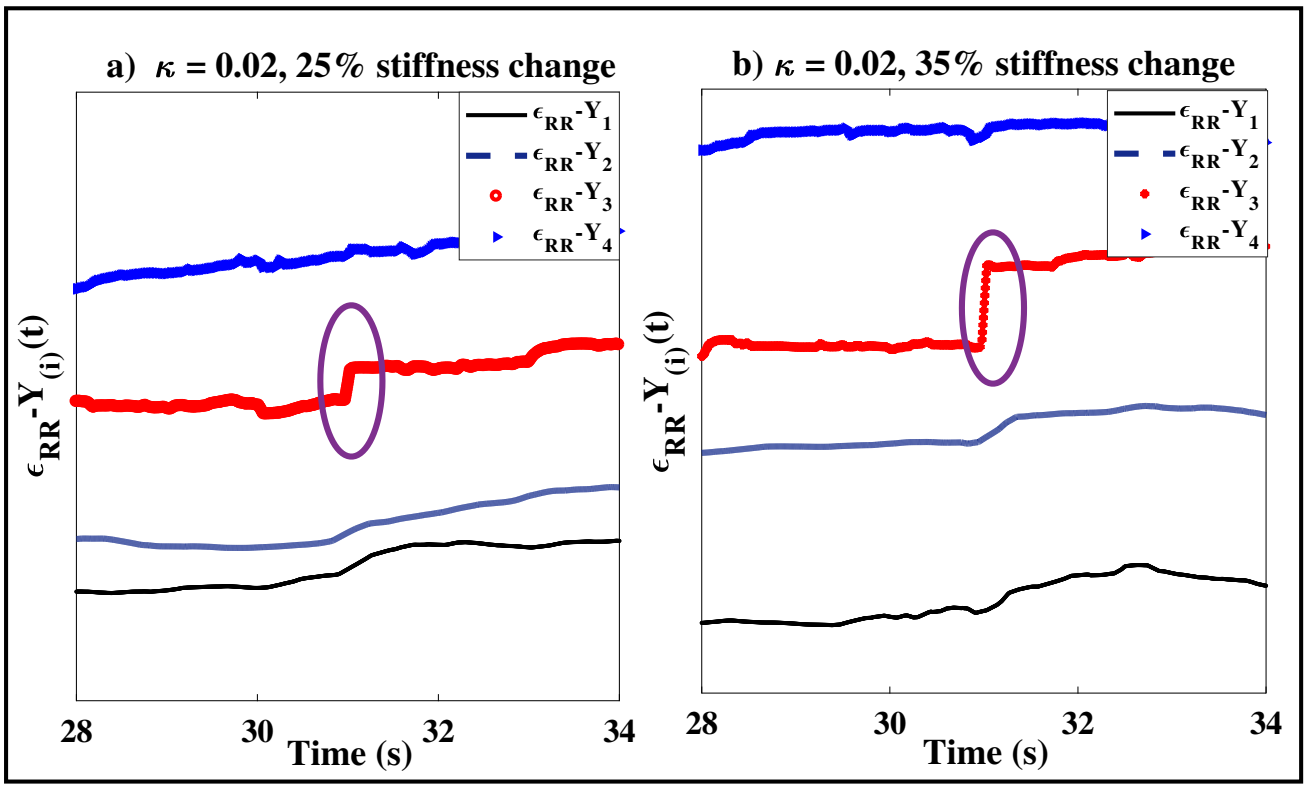

Figure 4.8: Spatial damage detection for negligible non-linearity

damage by observing a change in the mean level of the plots. As observed from Fig. 4.9, plots for sixth order cumulant for $a_1(t)$ and $a_2(t)$ show sudden change in the mean level. While approaching the damage instant, the plots show a significant change in the mean level which validates that the damage has indeed occurred at t=25s. It should however be noted that simultaneous spatial and temporal damage detection is difficult in this case owing to amplitude non-stationarity of the ground motion.

4.8.3 Results for time-diluted damage

This section mainly deals with the effect of time diluted nonlinearity change due to progressive degradation of the base isolator. The progression of degradation is considered at a rate of 2% nonlinearity change (κ) every 2 seconds. This phenomena is closely related to real life cases where a structure deteriorates due to the aftermath of earthquake and at each passing second, the system undergoes a transitory state of collapse. This phenomena can be directly attributed to the loss of stiffness, a numerical study of which is carried out in this section and the results are reported

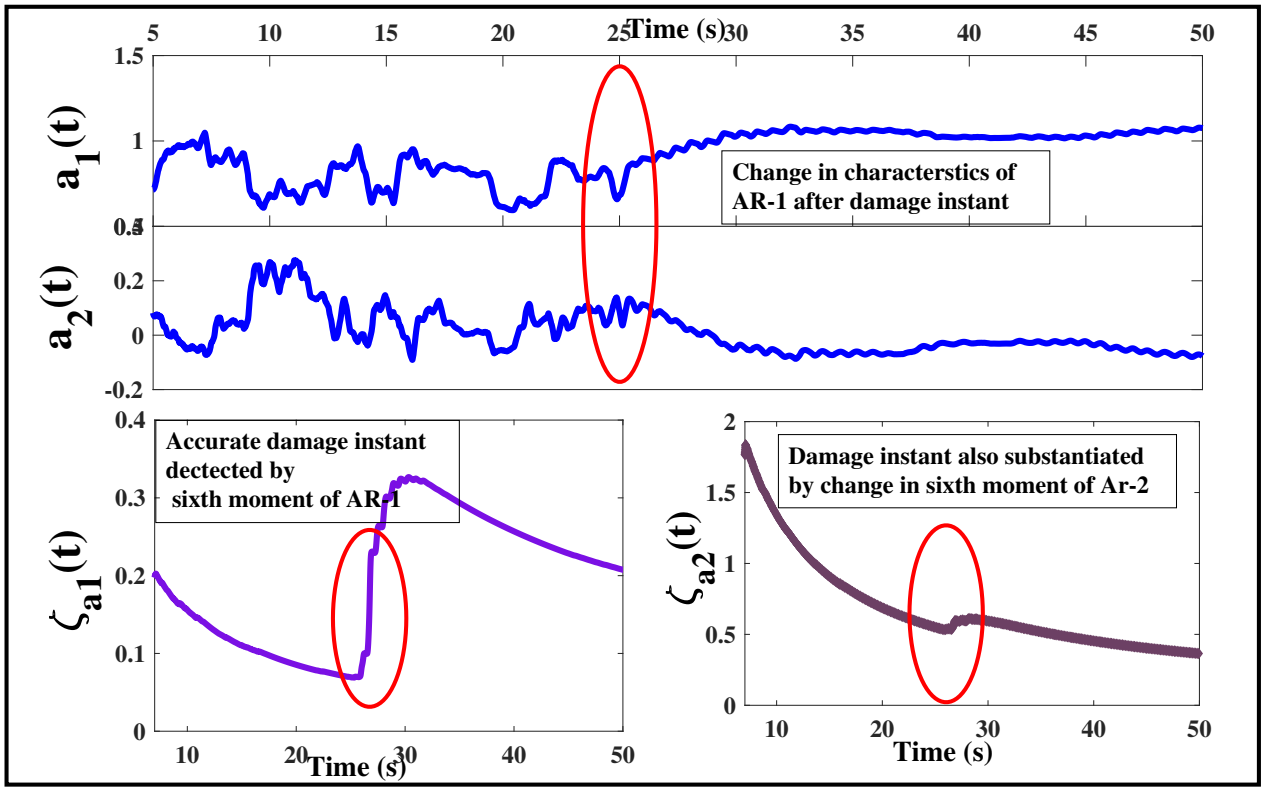

Figure 4.9: DSF for El Centro excitation for 30% change

for inference. In this context, simulation studies are performed where the value of κ changes at a steady rate for a period of 50 seconds. It can be clearly observed from Fig. 4.10(a) and Fig. 4.10(b) that the AR coefficients continuously show a change in the mean level from 20 seconds (which indicates the commencement of damage) until 70 seconds, when the time-diluted damage has ended over a period of 50 seconds. This results a change in the value of the nonlinear force term κ from 1 to 0.5, which indicate the period of slow time-diluted degradation induced in the system that is successfully detected by the RPCA algorithm by tracking the TVAR coefficients over the timespan of 50 seconds. The above results (i.e. from Fig. 4.10) clearly indicate the efficacy and the robustness of the algorithm to capture a *time-diluted progressive damage*. It can be clearly observed from Fig. 4.10(a) and Fig. 4.10(b) that the TVAR coefficients continuously show a change in the mean level from 20 seconds (which indicates the commencement of damage) until 70 seconds, when the time-diluted damage has spanned over a period of 50 seconds. This results in an alteration in the value of the nonlinear force term κ from 1 to 0.5, which indicate the period of slow time-diluted damage induced in the system. This phenomenon is successfully detected by the RPCA algorithm

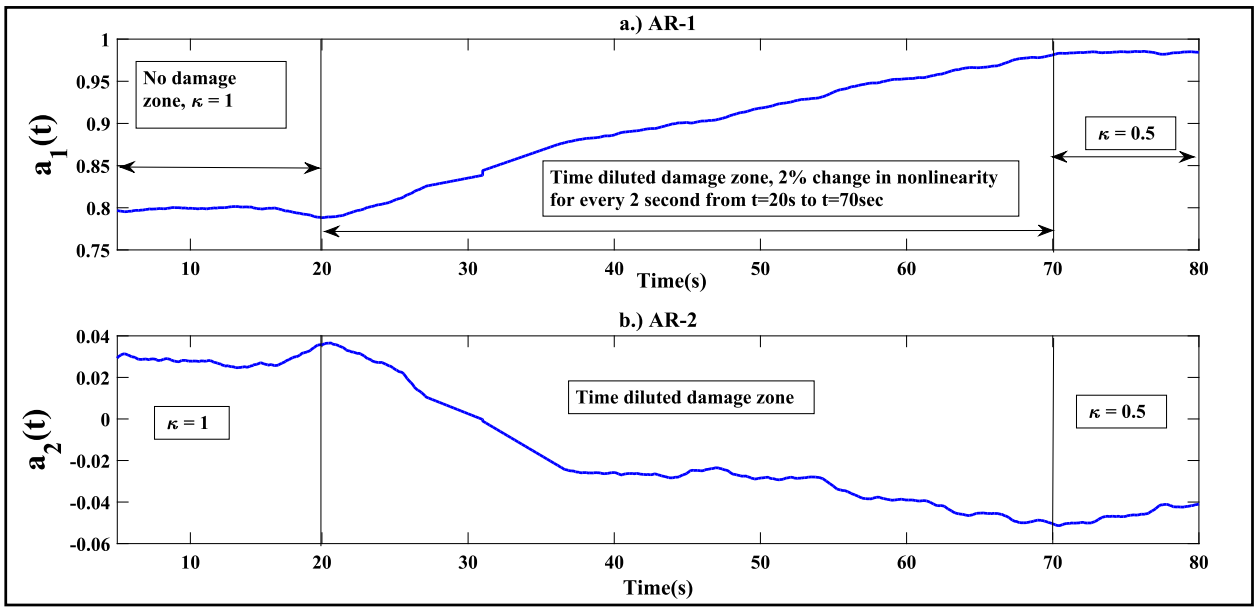

Figure 4.10: Damage detection using AR coefficients for a time-diluted damage

by tracking the TVAR coefficients over the timespan of 50 seconds.

4.8.4 Results for underdetermined case-White Noise Excitation

To assess the applicability of the proposed method for a more practical situation, consider again an underdetermined system, similar to the one described in the previous chapter. Physically, such a system arises in flexible structures that are instrumented with a relatively smaller number of sensors because of cost and other factors. The proposed algorithm tries to address this issue by assuming the number of DOF in the structure to be equal to number of available measurements. Since in the proposed algorithm, TVAR modeling is carried out on the first transformed response, the detection finesse is not compromised for an underdetermined system. Theoretically, the number of DOFs instrumented should be at least equal to number of actively participating modes. The vibration response data from the top few DOFs is of foremost importance as it has the maximum effect on the first modal response and retains the major information on the occurrence of damage. As previously discussed for the RPCA-RRE approach, the same B-W system with the recorded acceleration response data missing from second floor and fourth floor are taken for analysis. Damage was induced for the following two cases i) Sudden change in nonlinear base isolator force at 31 s ii) Local damage induced in 3^{rd} storey at 31s. Considering the first case, the damage is induced

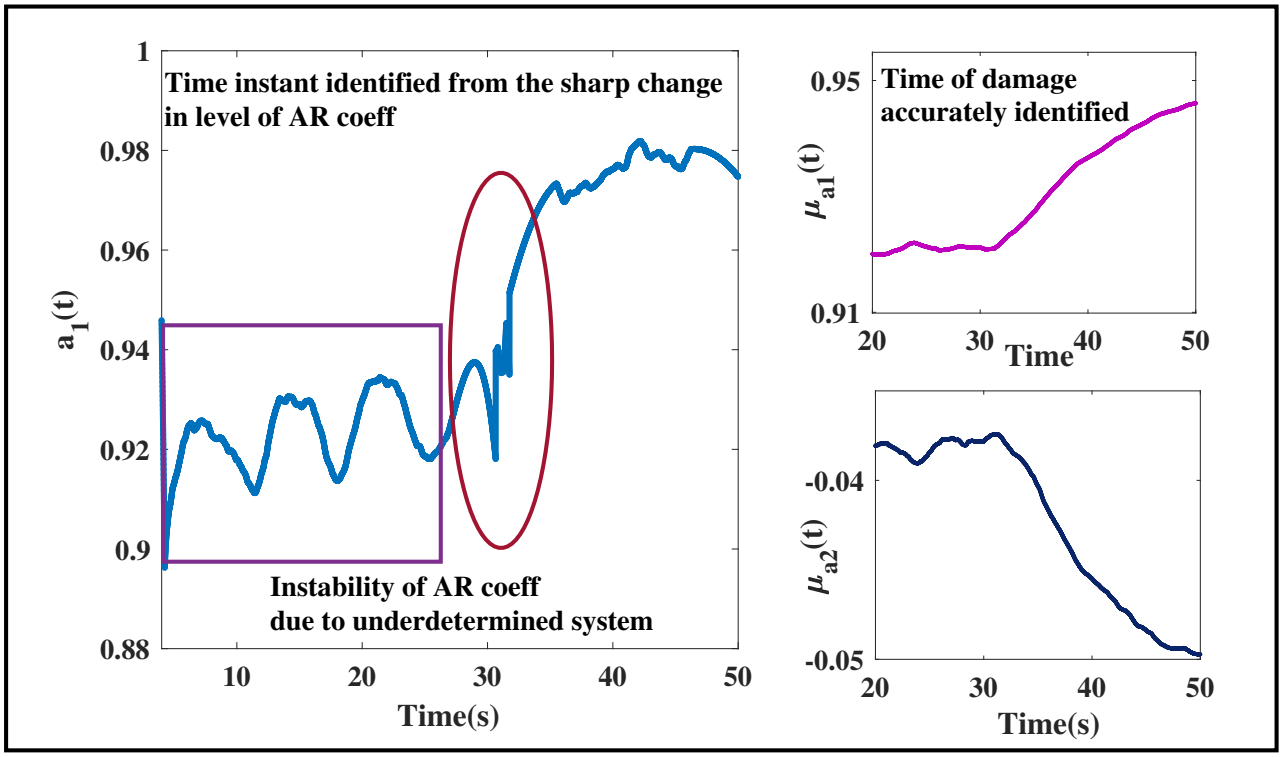

Figure 4.11: DSF for Underdetermined case 1- Global Damage, 20% change in nonlinearity

through a 20% change in nonlinearity at a particular instant. From Fig. 4.11, it is clear that the algorithm is able to perceive damage through the DSF even without the availability of the complete set of response. It is worth noting the fact that the number of DOF selected will have an impact on the detectibility limit. For the above case, the algorithm was able to detect changes in nonlinearity up to 20%. For the second case, 30% reduction in stiffness was induced in the fourth storey column at 31s and vibration responses from all the floors except the second and fourth were made available as input to the algorithm. The results are as shown in Fig. 4.12 From the figures it can be seen that there is a lot of activity present before the instant of damage is attained. Albeit these instabilities, it can be safely concluded that the algorithm is well equipped to estimate spatio-temporal damage even for underdetermined systems, which is a key entitlement of this thesis. From the results obtained, it can be clearly understood that the applicability of the proposed method towards dealing with nonstationary excitations for nonlinear systems surpasses the detection potential of the recently established RPCA-RRE based scheme.

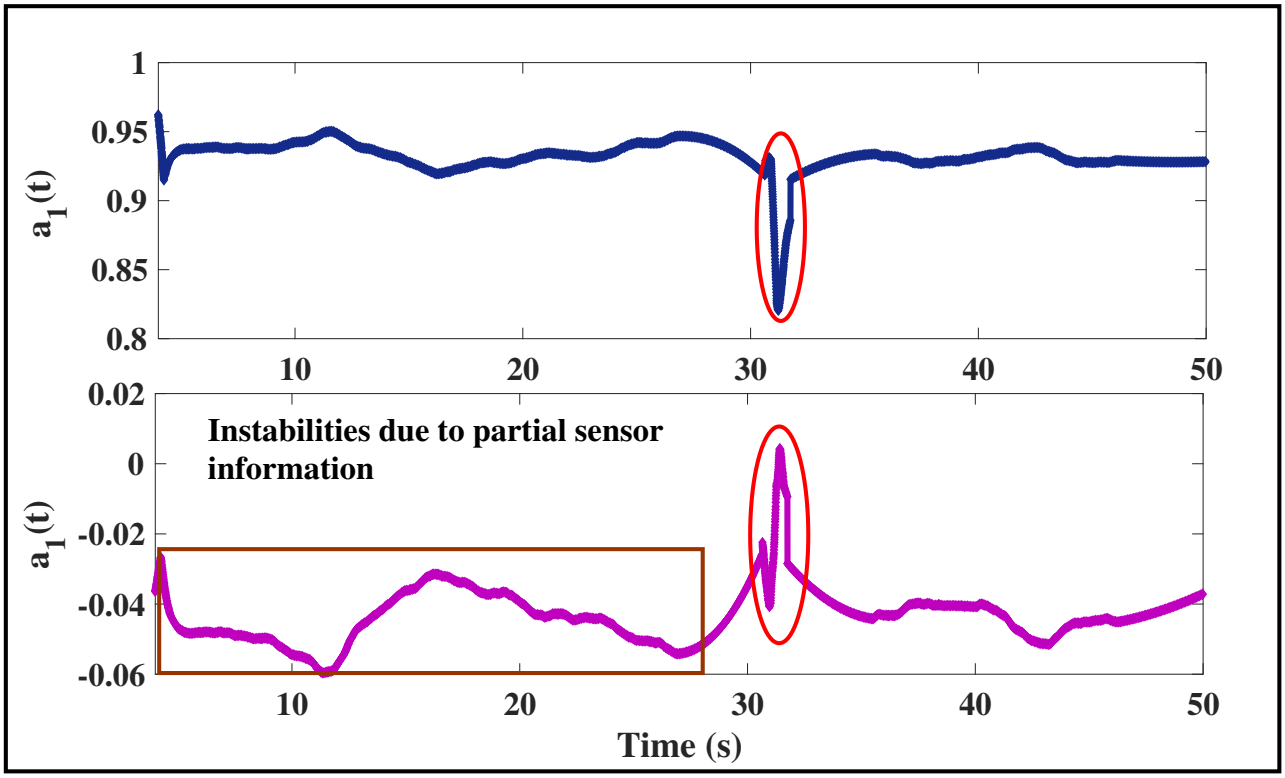

Figure 4.12: DSF for Underdetermined case 2- Local Damage, 30% change in stiffness

4.9 Experimental study

4.9.1 Detection results for the experimental case

The aluminum beam experimental setup described in the previous chapter is taken under consideration for carrying out damage detection studies using the proposed FOEP based approach. The use of the same setup is justified from an utility perspective, primarily due to the fact that the proposed methodology provides a better set of detection results as compared to the ones obtained from the RPCA-RRE scheme, for nonstationary nature of the input excitation. Abiding by the prior experimental scheme, the trials are carried out by subjecting the aluminum beam to a scaled ground motion (1999 Chi-Chi ground motion, scaled to peak $0.3g$). In order to simulate a real time damage scenario, the rubber strip attached to the free end of the cantilever beam is snapped accurately at a fixed time instant, during the shaking motion of the beam. The recorded output acceleration plots obtained from the sensors are shown in fig. 3.15.

The instant of damage is well reflected by the plot of the DSF, which cannot be directly perceived

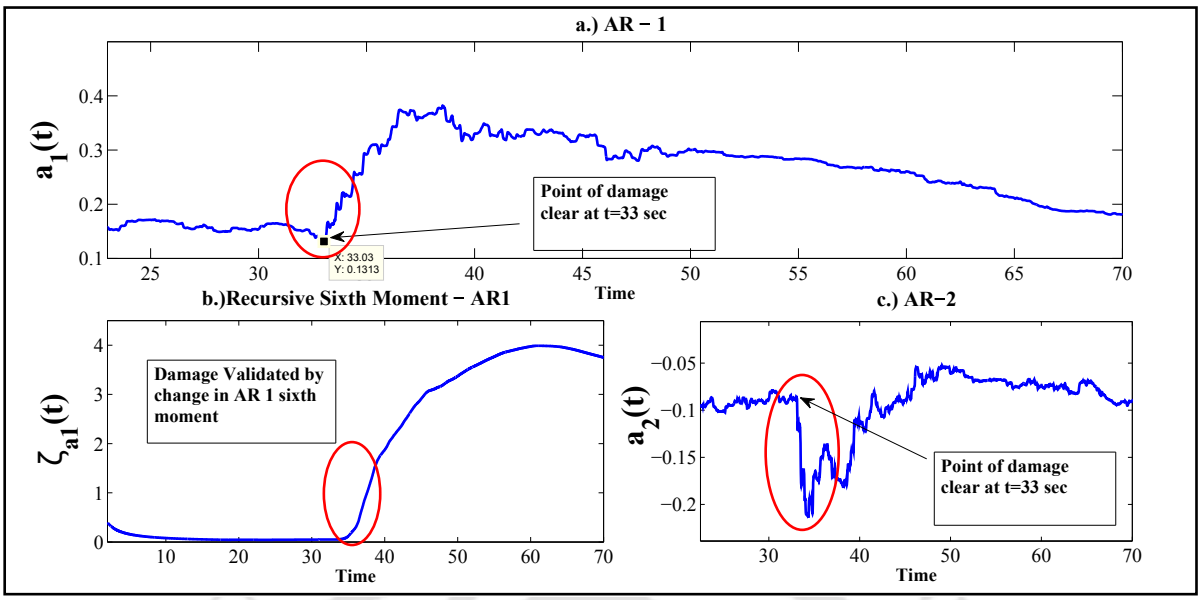

Figure 4.13: DSFs used for an experimental trial

from the raw acceleration data recorded from the sensors. It is duly noted from Fig. 4.13 that the TVAR coefficient $a_1(t)$ shows a significant change in mean at 33s, that corresponds to the exact instant of damage for the experimental trial. Accompanying this figure, is the plot of the other TVAR coefficient $(a_2(t))$ that clearly delineates the accurate damage instant at 33s, indicating the occurrence of damage. To validate these findings, the HOM $(\zeta_{a_i}(t))$ plot shows a clear change in the mean level, thereby substantiating the accurate instant of the rubber-snap, an event that closely corresponds to a real life damage. Hence, it can be concluded that the proposed method provides quality detection results even when the nature of the excitation is predominantly, nonstationary.

4.9.2 Case study for the UCLA factor building

An important aspect to be ventured while dealing with damage detection strategies is its applicability in identifying events that evolve from real life scenarios. In the previous chapter, a nifty illustration for the same was proposed using the ambient and recorded earthquake vibration data collected from the heavily instrumented UCLAFB. In the present context, the same exemplar is revisited, primarily to perceive the key differences and understand the subtle nuances that arise due to the implementation of the newer proposed methodology based on the RPCA-TVAR approach. In the later stages of this dissertation, a comparative study of all the FOEP based techniques would be

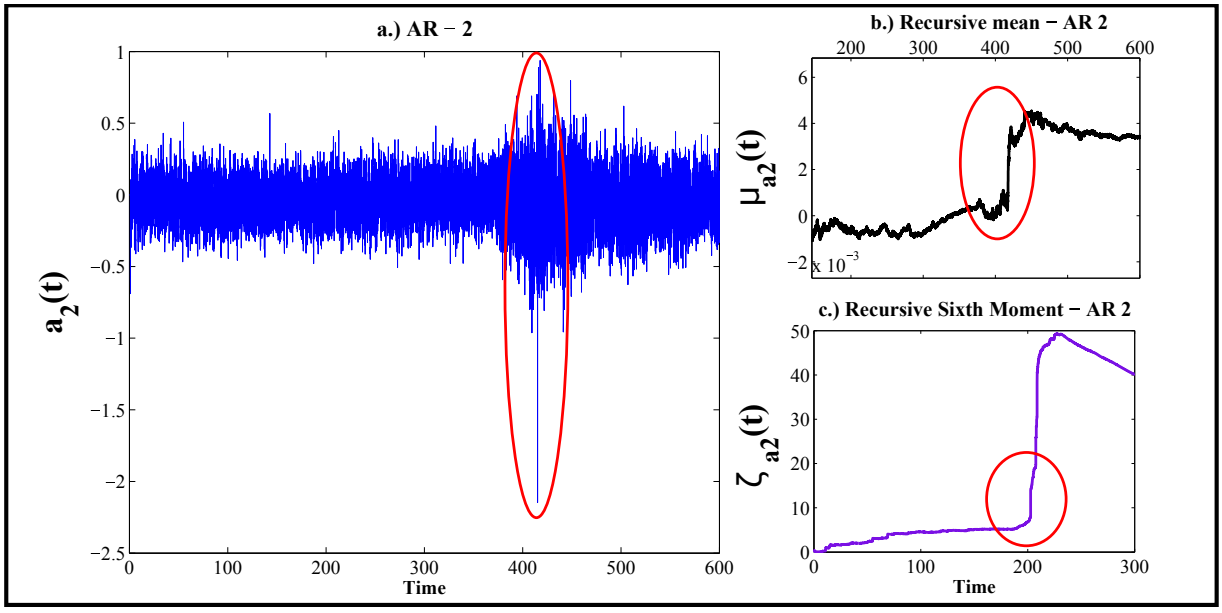

Figure 4.14: DSF for the UCLAFB

portrayed, reviewing the featured detection results based on the input vibration data of the same model. Towards this, the build up of the comparative study using the detection results of various algorithms on the UCLAFB recorded vibration data is an important aspect that needs to be reviewed. On applying the proposed method on the recorded vibration data obtained from the sensors oriented in the translational directions, it was observed that the transformed response by itself could not identify the accurate instant of damage. The temporal RRE plots illustrated in the previous chapter (Fig.....), failed to portray significant deviations at the onset of the earthquake at 380s but could clearly capture the prominent damage instant at around the 410s mark. On the contrary, the plots of the HOM applied on the TVAR coefficient shown in Fig. 4.14b) and c), clearly depict the onset of the earthquake, as well as the start of the significant damage around the vicinity of the 410s mark. It is normal to expect these two instants to be different from each other because it takes a finite time for the structure to undergo significant changes (i.e. alteration of stiffness). In the present context, local damage is expressed through percentage change in the average spatial RRE values (i.e. $\Delta\langle\varepsilon_{RR} - Y_i\rangle$ using Eqn. 3.18 between the ambient and earthquake regimes corresponding to pre and post damage scenarios. Fig. 4.15 shows the plot $\varepsilon_{RR} - Y_i$ for a few representative floors. It can be observed from the figure that $\varepsilon_{RR} - Y_i$ deviates from the ambient regime at around t=380s and significantly in the vicinity of t=410s indicating the occurrence of damage. The percentage change

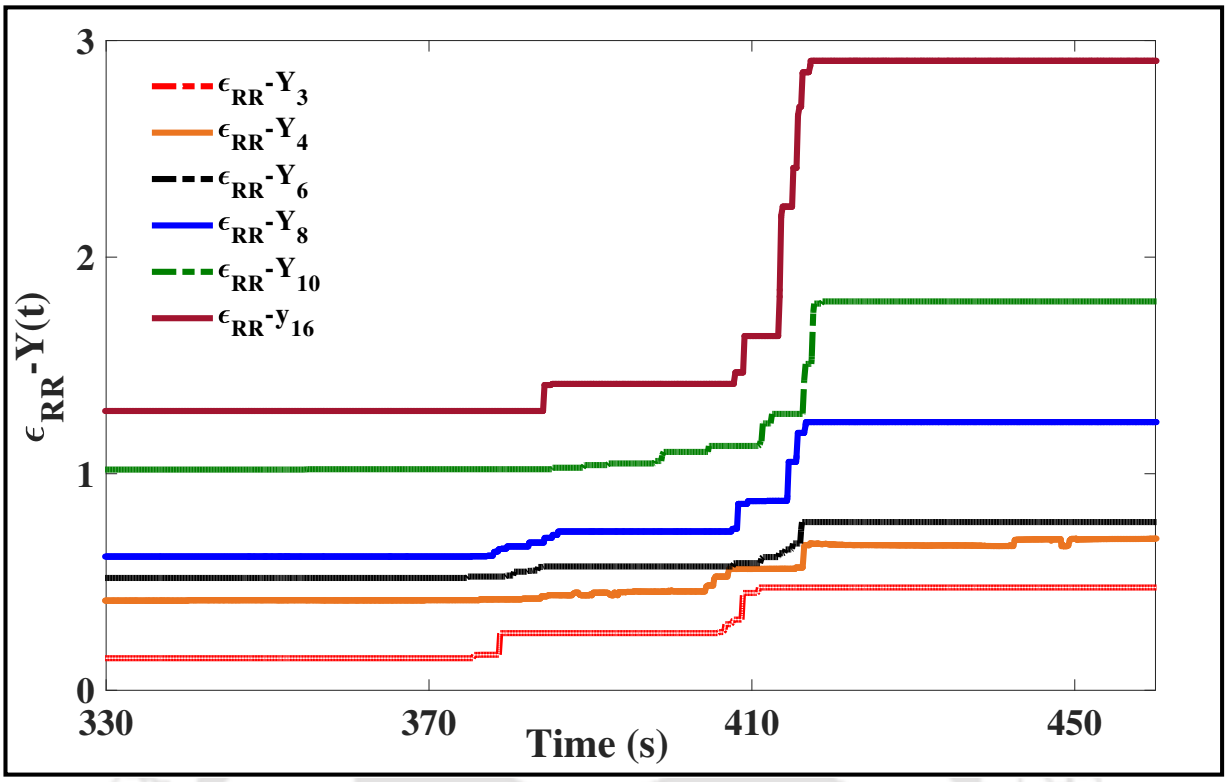

Figure 4.15: Local RRE plots for floors of UCLA building

in post damage RRE and pre damage RRE (i.e. $\Delta\langle\varepsilon_{RR} - Y_i\rangle$) for each floor as shown in bardiagram (Fig. 4.16) which indicates the appearance of damage not only at a single floor but the system as a whole which corroborates to the previously mentioned results on modal identification [63].

4.10 Summary

A real time damage detection algorithm for vibrating systems based on recursive principal components in conjunction with TVAR model is presented. Recursive updates of the eigen subspace using rank one perturbation facilitated real time evolution of the principal components. Subsequent modeling of principal component explaining maximum variance makes the transformed response amenable to a low order TVAR model which is a key step of the proposed framework. The use of temporal RRE in conjunction with TVAR coefficients facilitated real time spatio-temporal damage detection. The proposed framework provided successful detection results for damages even up to 15% for the white noise excitation and up to 30% for the El Centro excitation case. Case studies have shown

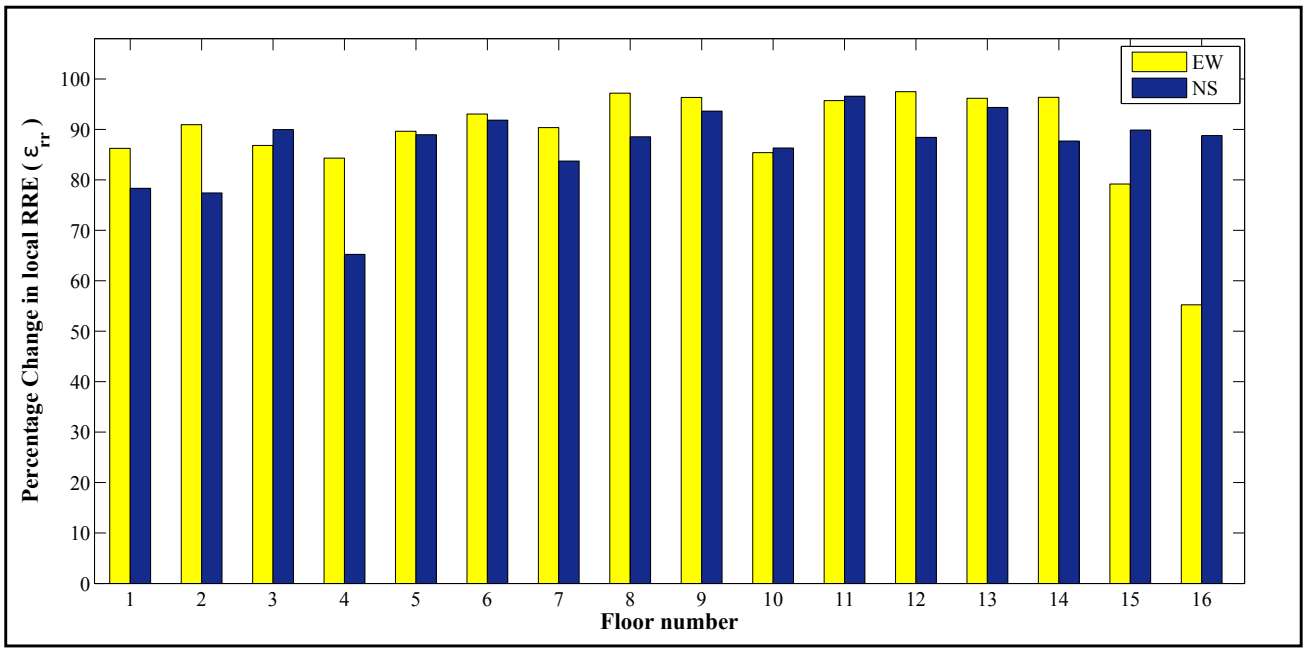

Figure 4.16: Bar diagram indicating percentage change in local RRE for EW and NS direction

that the proposed algorithm is well equipped to detect damage when the number of sensors used to acquire data is reduced (i.e., for underdetermined systems), which is clearly an advantage while dealing with practical economics of health monitoring of real full-scale structures. The results show efficacy of the current framework to detect damage for underdetermined cases up to 20% change in the level of nonlinearity. The superiority of the RPCA based damage detection framework is clearly evident through the comparison with the traditional windowed batch PCA based framework, which is promising from a real time damage detection standpoint. Presented case studies show that the proposed approach results in successful damage detection and works well even when used with both experimentally acquired data as well as large scale field data closely emulating practical scenarios.

Although the proposed methodology provides successful detection results even for underdetermined systems, it is expected that the method will not function if the input is provided only from a *single sensor*. An essential prerequisite of the RPCA based processes is the requirement of *multi-channel* input data, a luxury that sometimes cannot be afforded due to cost, unavailability of good quality sensors and other factors. This issue is addressed in detail in the next chapter where the theoretical development of a newer real time damage detection strategy is discussed in detail that functions using a single-channel input data.

Chapter 5

Online damage detection using recursive singular spectrum analysis and its hybrid extension

One of the main limitations of the RPCA based methods reviewed in the previous chapter is their inability to operate in situations where the input to the algorithm is obtained from a *single sensor*. Such instances occur, for example, in tall structures where instrumentation in each DOF is practically not feasible, embedding a dense array of sensors is economically not viable and positioning of these sensors into strategic locations for continuous monitoring is inaccessible. For such instances, algorithms solely premised on detecting spatio-temporal real time damage from single sensor input is clearly advantageous over the traditional identification schemes as well as some recent trends in the associated area. Towards this, a new algorithm known as recursive singular spectrum analysis (RSSA) is newly proposed in this chapter that takes into consideration the input from a single sensor in order to determine the spatio-temporal patterns of damage to the structure. To the best of the knowledge of the author, concepts utilizing RSSA in the purview of real time structural damage detection has so far not been explored in the literature.

In this chapter, a novel framework has been introduced using RSSA as a structural damage detection tool that works in real time as the data streams in. The motivation to identifying dam-

age patterns using single sensor vibration data as input is provided first, followed by the detailed description of the methodology. The key DSFs used to address the detection problem is presented next. Subsequently, the applications of the proposed method on numerically simulated systems, experimental verification and practical case studies are also presented. En route, a novel framework has been proposed using an improvised variation of the FOEP approach through the association of **RPCA-RSSA methods** as online damage detection tool that works in real time. The key idea is to *detect finer levels damage in real time*, an attempt that has not been established in the literature so far. In this context, a new hybrid approach is proposed where the output vibration response is first transformed utilizing the RPCA algorithm to be subsequently utilized by the RSSA algorithm for providing eigenspace updates in real time. In order to provide an easy understanding of the terminologies used in this chapter, the important acronyms are provided in Table 5.1.

Table 5.1: Important acronyms

RSSA	Recursive Singular Spectrum Analysis
PC	Principal Components
ERD	Eigen Ratio Difference
RMSSA	Recursive Multi-channel Singular Spectrum Analysis

5.1 Motivation

The development of online damage detection techniques based on processing of response streaming in real time, still remains a challenge. The primary motivation behind the present work is to develop a *unified damage detection framework using single and multiple sensors* that can process data online and detect damage in a structure in real time. Applications involving aging and wearing out of components, processes dealing with seismic signals, are generally time-varying where the signals evolve in real time and the process becomes too complex to be analyzed via a simple offline method [1, 2]. In practical SHM scenarios, data streams continuously in real time, which further necessitates that the algorithm should be amenable towards online implementation, independent of any baseline (reference) data. Traditional SSA requires a batch of data to elicit principal components (PCs) of the original time series, via eigen decomposition of the covariance matrix, that solely works offline. In this chapter, a baseline free approach has been proposed which facilitates the monitoring of

structural systems directly using acceleration data, based on RSSA, as a tool for real time processing of data using single channel input data. The proposed method utilizes the FOEP approach for the *Hankel* covariance matrix estimate with every new sample obtained in real time. While the traditional SSA approach processes chunks of data acquired in batch mode, RSSA provides online processing of data based on rank one eigenvector updates in a recursive framework, as and when the data streams in real time. Once the eigen-space updates are obtained, an approximation of the original time series is carried out by reconstruction, where the framework then utilizes TVAR modeling in conjunction with DSFs for identifying the instant of damage [51].

Largely premised on the idea that damage is manifested through an alteration in the structural dynamical properties such as natural frequencies, mode shapes and damping, a significant number of damage detection algorithms and strategies have been proposed in recent times [1–5]. However, the evolution of real time damage detection schemes capable of conducting baseline-free damage identification, still poses a challenge, primarily, due to the underdevelopment of algorithms that are amenable towards real time implementation. The occurrence of damage is often a real time event [3] that requires the DSFs to function online, in a recursive fashion, for a continuously streaming data. As the majority of the established damage detection algorithms function offline in batch mode process, the development of online algorithms becomes imperative in the context of real time structural damage identification [75, 96]. This can be carried out by extensively by a family of eigen value perturbation techniques known as the FOEP based implementations [133, 134] and tailoring it towards real time SHM. This chapter explores the family of the FOEP techniques that have been developed in the recent years (includes RPCA and RSSA based algorithms) and also demonstrates how new hybrid approaches can be proposed based on the requirement of a particular type of SHM problem. The key entitlement of any new proposed algorithm within the family of FOEP techniques is that it should exhibit finer levels of detectability compared to the other members of the FOEP family, in the backdrop of sparse and dense sensor economics and different types of nonlinearities inherently present or induced by the damage event.

There are two major issues that are overcome using the methods proposed here. The first one is the difficulty introduced in the damage detection process due to the requirement of multi-channel sensor data. The second difficulty is in the finer level of real time damage detection that

is successfully addressed by the hybrid FOEP based RPCA-RSSA approach, which remains one of the major entitlements of this dissertation. Despite the amalgamation of the recursive approaches in the hybrid algorithm, the time complexity for providing eigenspace updates in real time is still a bare minimum, which is reported in the later stages of this chapter. The scope of the present work assesses the detection prowess of the proposed FOEP based real time SHM methods in general and a hybrid method in particular, to address simultaneous temporal and spatial damage of both linear and nonlinear systems in real time. Case studies aimed at detecting real time damage for weakly to strongly nonlinear family of structural systems have been explored in detail. The present work deals with damage detection on numerically simulated systems, complemented with experimental test beds involving the previously described setups and newer trials using vibro-impact systems, from which important conclusions are drawn. Both the methods are successfully applied on real life cases on the vibration data obtained from UCLAFB that concludes the chapter with an extensive comparison of the performance of the real time detection methods developed so far.

5.2 Problem formulation

SSA is a non-parametric method that works well with arbitrary statistical processes and requires no prior assumptions about the stationarity, linearity or normality of the data set. Details of the key concepts of basic SSA have been explained in section 2.2 of the thesis and are not reported here for brevity. The major disadvantage of traditional SSA is that it analyzes data in batches, offline. To alleviate this drawback and to tailor basic SSA towards real time damage detection, recursive implementation of SSA is carried out through the FOEP approach, which is presented next.

5.2.1 RSSA: Theoretical development

Recent research in signal processing and information technology has identified SSA as an efficient damage detection tool [105–107], leading to the development of SSA based structural damage detection algorithms [105–107]. The major challenge towards tailoring SSA towards an online implementation is to perform the EVD of the Hankel covariance matrix at each time instant, which can be

time consuming, thereby impeding its practical applicability towards real time damage detection. This can be alleviated through the use of FOEP approach [134] which provides recursive updates of eigen subspace from the previous eigen-space of the data at a particular time instant. Although this exercise follows the similar notion of the previously conducted theoretical developments on RPCA and RPCA-TVAR based approaches, the subtle differences, in particular, that arise here, are described in detail.

For structural systems dealing with data evolving from zero mean processes, the recursive estimation of the Hankel covariance matrix ($\mathbf{C}_k$) at any instant k can be structured in terms of the current sample vector (X_k) and the previous covariance estimates ($\mathbf{C}_{k-1}$) as follows :

$$\mathbf{C}_k = \frac{k-1}{k}\mathbf{C}_{k-1} + \frac{1}{k}X_k X_k^T \tag{5.1}$$

However, for nonstationary data sets, the recursive mean at each instant of time needs to be accounted for in the estimation of the covariance matrix. The recursive mean at k^{th} instant, μ_k, depends on the mean at the previous instant through the relation: $\mu_k = \frac{k-1}{k}\mu_{k-1} + \frac{1}{k}X_k$. The covariance estimate for cases involving mean shift can be expressed as: $\tilde{\mathbf{C}}_k = \frac{k-1}{k}\mathbf{C}_{k-1} + \frac{1}{k}\left[X_k - \mu_k\right]\left[X_k - \mu_k\right]^T$. In SHM problems, the dynamics of the system evolve predominantly from zero mean processes. Damage detection formulations premised on recursive correction updates of the covariance matrix generally assume to ignore the local non zero means at each time instant. Case studies from previously published works as well as the current work reveal that the aforesaid assumption does not hinder the practical applicability of the online damage detection algorithms. The incorporation of $\tilde{C}$ in the formulation of the covariance estimate is therefore, *inconsequential*. Henceforth, for the remainder of the chapter, $\tilde{C}$ has been dropped for subsequent formulation and analysis.

The current L dimensional sample vector ($X_k = [x_{k-L+1}, x_{k-L+2}, x_{k-L+3}, ...x_k]^T$) comprises of L lagged elements of the one dimensional time series, L being the initial signal length. The objective of pre-selecting a desired initial signal length is to preserve the components with most of the damage information (by selecting components with higher singular values to retain the trend and oscillatory parts) and to eliminate the components of less significance such as noise. The covariance estimate at k^{th} instant can be written in terms of eigen value and eigen vector matrix at a particular time instant

as $\mathbf{C}_k = \mathbf{U}_k \Upsilon_k \mathbf{U}_k{}^T$ with $\varpi_k = \mathbf{U}_{k-1}^T \mathbf{X}_k$, as the projection of the sample vector into the previous eigen subspace. Substituting these expressions in Eqn. 5.1, the following equation is obtained:

$$\begin{aligned} \mathbf{U}_k(k\Upsilon_k)\mathbf{U}_k^T &= (k-1)\mathbf{U}_{k-1}\Upsilon_{k-1}\mathbf{U}_{k-1}^T + \varpi_k\varpi_k^T\mathbf{U}_{k-1}\mathbf{U}_{k-1}^T \\ &= \mathbf{U}_{k-1}\{(k-1)\Upsilon_{k-1} + \varpi_k\varpi_k^T\}\mathbf{U}_{k-1}^T \end{aligned} \tag{5.2}$$

In the above expression, with a finitely large samplesize (k) and low damping estimates [111], the term $((k-1)\Upsilon_{k-1}+\varpi_k\varpi_k^T)$ generally shows a diagonally dominant behavior. The diagonal dominant structure of this term ensures the application of Gershgorin's theorem [132, 134], rendering in the application of FOEP approach admissible to obtain the eigen values and eigen vectors. Interested readers could refer [132–136] for details. The application of Gershgorin's theorem ensures the EVD of the term to be of the form $\mathrm{P}_k\mathbf{\Gamma}_k\mathrm{P}_k^T$, where $\mathbf{P}$ is orthonormal and $\mathbf{\Gamma}$ is diagonal. Substituting the EVD in place of $((k-1)\Upsilon_{k-1} + \varpi_k\varpi_k^T)$ in Eqn. 5.2, a new formulation is obtained as shown below:

$$\mathbf{U}_k(k\Upsilon_k)\mathbf{U}_k^T = (\mathbf{U}_{k-1}\mathrm{P}_\mathbf{k})\mathbf{\Gamma}_\mathbf{k}(\mathrm{P}_\mathbf{k}^\mathbf{T}\mathbf{U}_\mathbf{k-1}^\mathbf{T}) \tag{5.3}$$

From equation (5.3), recursive updates of the eigen subspace are obtained as a function of the previous eigen space as:

$$\begin{aligned} \mathbf{U_k} &= \mathbf{U}_{k-1}\mathrm{P}_\mathbf{k} \\ \Upsilon_k &= \mathbf{\Gamma}_k/k \end{aligned} \tag{5.4}$$

Eqn. 5.4 provides an iterative relation between eigen spaces at consecutive time instants. On using FOEP approach, the recursive eigen vectors obtained at each time instants are not ordered in the same sequence as the previous time instant, thus presenting the problem of permutation ambiguity. This can be resolved by arranging the obtained eigen vectors according to the decreasing order of the corresponding eigen values in $\mathbf{\Gamma}_k$. For the working of RSSA algorithm, this is one of the key steps as eigen values of the covariance Hankel matrix need to be ordered before proceeding with the evaluation of PCs and reconstruction of Hankel matrix using them. The contribution factor for a particular i^{th} eigen vector U_i is given by $\frac{\beta_i^2}{\sum_{i=1}^{n}\beta_i^2}$, where β_i^2 is the eigen value corresponding to U_i. After obtaining the eigen space updates at a particular time instant from the previous eigen space and current sample vector, principal component values of the time series at a particular time series

can be extracted as below:

$$\psi_i(k) = (U_i^T(k))_{1\times L}(\mathbf{X}_k)_{L\times 1} \tag{5.5}$$

Using the above equation, the i^{th} principal component value at particular time instant is obtained. Depending upon the relative contribution of the eigen vectors, the number of PCs required for reconstruction can be automated. For the present work, at any instant k, the PCs of eigenvectors that explain more than 90% of the system's variance is used for reconstruction. In the reconstruction step, the i^{th} PCs are projected back into its original subspace to obtain last column of the corresponding elementary matrix.

$$\mathbf{R}_i(k) = (U_i(k))_{L\times 1} \times (\psi_i(k))_{1\times 1} \tag{5.6}$$

It is to be noted here that the last entry of the $\mathbf{R}_i(k)$ vector, denoted here as $r_i(k)$ is used to obtain the value of the reconstructed time series entry at the k^{th} instant of time as shown below:

$$x(k) = \frac{1}{n}\sum_{i=1}^{n} r_i(k) \tag{5.7}$$

where n denotes the number of eigen values explaining more than 90% of the variance. The reconstructed signal values as per equation (5.7) is recursively obtained at each instant of time as and when the vibration data streams in. The importance of this reconstructed signal is that it has simpler components, making it amenable towards a lower AR order model, deemed sufficient [51] to capture the dynamics of the structure and more sensitive towards singular events like damage. TVAR modeling is subsequently performed on this reconstituted signal.

5.3 Recursive damage indices

In the present framework, RSSA facilitates online processing of data producing recursive updates of eigen vectors and eigen values, referred to as eigen subspace. Despite the absence of noise from the reconstituted signal obtained after the RSSA algorithm, the eigen subspace by itself cannot exhibit the change in system properties inflicted due to damage, if not processed by a set of damage markers commonly referred to as DSFs. In the preceding chapters, the concept of DSFs have been rigorously

deal with, where the theoretical development, key features and practical utility have been repeatedly discussed. As the present RSSA based framework also utilizes the concepts of TVAR coefficients as the key DSFs for identifying damage in real time, a detailed description of TVAR is intentionally not reported here for brevity. However, *in lieu* of the RREs that were used for detecting damage for the RPCA-based approaches, a new DSF, known as eigen ratio difference (ERD) is employed here to further validate the instant and location of damage obtained form the TVAR plots. In this context, a brief description of ERD and its recursive implementation is provided next.

5.3.1 Damage detection using recursive eigen ratio difference

The application of RSSA provides a set of singular values and singular vectors that are eventually utilized in providing recursive updates of the eigenspace at each instant of time. In this context, the ratio of two singular values, delineating the quantification of the level of coupling between them is considered as the secondary DSF, known as the ERD. The use of this quantity as a possible indicator of instability was first adopted for monitoring volcanic activity [101]. The principle behind the use of this marker is that structural damage or instability induces a low frequency component in the signal, creating a de-coupling between the two most significant PCs. This decoupling, can intuitively be represented in the form of ratio between their corresponding singular values. This concept of decoupling has been utilized in the present context to formulate an online damage index known as recursive ERD in order to accurately identify the instant of damage, given as:

$$\delta(k) = \left[\frac{(\lambda_1(k) - \lambda_2(k))}{\sum_{i=1}^{L} \lambda_i} \right] \tag{5.8}$$

At the instant of damage, recursive ERD shows an alteration in its mean level to indicate the de-coupling between the two most significant singular values. The potential of ERD to be implemented online towards damage detection demonstrates its capability to detect damage even for cases of a nonstationary nature of input data. ERD when examined in a recursive framework supplements the use of TVAR coefficients as an effective damage detection tool for the proposed framework. This is shown at a later stage of the thesis.

5.4 Multichannel singular spectrum analysis (MSSA)

This section describes the basic multichannel singular spectrum analysis (MSSA) and its recursive implementation, suitable for online implementation. MSSA is a data-driven technique arising from research on alternative tools for the analysis of multichannel time series and can be considered as a natural extension of the basic SSA algorithm [123–126]. SSA, albeit being an efficient algorithm for extracting the principal patterns in time, becomes computationally demanding for structures with significantly large number of DOF (e.g. UCLAFB, [63]). MSSA uses a *multivariate time series* with all state variables of the coupled systems in the construction of the augmented trajectory matrix. The plethora of literature in MSSA [123–126] shows that the variable chosen to analyze the system will have significant impact on the robustness of the algorithm to capture the dynamics of the system under study. The conventional eigen vector or PCA is a special case of the MSSA when no time lags are introduced. According to Richman [97], the eigen vectors show distortions that contribute to inaccurate representation of the physical relationships in the data. In the presence of data gaps in the data series, the resulting modes of the decomposition of the data are not strictly orthogonal.

Consider the multivariate time series of length N and D channels, $\mathbf{x} = \{\mathbf{x}_n^d : d = 1, ..., D; n = 1, ..., N\}$. Similar to SSA, the first step of MSSA algorithm is to create an augmented trajectory matrix with data from the concerned channels. Each channel d is embedded into an L dimensional phase space by using lagged replicates $X_1^i, X_2^i, ..., X_k^i$, where i ranges from 1 to D, D being the number of channels considered for MSSA. Hence if there are D channels, each embedded into an L dimensional phase space system, the number of rows of the augmented matrix will be $L \times D$ and number of columns will be $K = N - L + 1$. The structure of the trajectory matrix is as shown

below:

$$\mathbf{X}_D = \left[\begin{array}{ccccccccccccccccc} & & & & & & & & & & & & & & & & \\ x_1^1 & x_2^1 & x_3^1 & . & x_L^1 & x_1^2 & x_2^2 & x_3^2 & . & x_L^2 & . & . & . & x_1^D & x_2^D & x_3^D & . & x_L^D \\ x_2^1 & x_3^1 & x_4^1 & . & x_{L+1}^1 & x_2^2 & x_3^2 & x_4^2 & . & x_{L+1}^2 & . & . & . & x_2^D & x_3^D & x_4^D & . & x_{L+1}^D \\ . & . & . & . & . & . & . & . & . & . & . & . & . & . & . & . & . & . \\ . & . & . & . & . & . & . & . & . & . & . & . & . & . & . & . & . & . \\ \underbrace{x_K^1 \quad x_{K+1}^1 \quad x_{K+2}^1 \quad . \quad x_N^1}_{Channel-1} & & & & & \underbrace{x_K^2 \quad x_{K+1}^2 \quad x_{K+2}^2 \quad . \quad x_N^2}_{Channel-2} & & & & & . & . & . & \underbrace{x_K^D \quad x_{K+1}^D \quad x_{K+2}^D \quad . \quad x_N^D}_{Channel-D} & & & & \end{array}\right]^{\mathbf{T}} \tag{5.9}$$

The formulation for MSSA is similar to the steps provided in Section 2.2.3, for a basic SSA algorithm. Applying SVD on the augmented trajectory covariance matrix yields $L \times D$ eigen values and eigen vectors. As the number of channels increases, MSSA becomes computationally expensive. However, MSSA shows good results in interpreting damage events, which is illustrated in the later parts of the study. Hence, projecting the data set onto the eigenvectors simplifies the picture of a possibly high-dimensional complex system by viewing it in an optimal subspace [100]. It is well understood that there will be D sets of $L \times L$ eigen value matrix and eigen vector matrix. Consequently, there will be D sets of L PCs, each accounting for correlation between different data sets taken as input to the algorithm. For TVAR modeling, only one signal is required, but MSSA algorithm gives D reconstructed signals as output. Hence, to tailor the basic MSSA algorithm towards damage detection using TVAR modeling, it is envisioned that the first two PCs of every D channels can be utilized, towards building a composite signal that accounts for all the D input channels. The composite signal contains the maximum information to aid towards the detection problems, obtained using the most significant PCs. Let $\mathbf{\Psi}_D = \left[\psi_1^1, \psi_2^1, ...\psi_L^1, ..., \psi_1^D, \psi_2^D, ...\psi_L^D\right]^{\mathbf{T}}$ represent the PCs obtained from Step 3 as mentioned in Section 2.2.3. Using only the first two PCs of each channel, the trajectory matrix is reconstructed as below:

$$\mathbf{R}_i = \frac{\left\{\sum_{j=1}^{D}\sum_{i=1}^{2} U_i^j \times \psi_i^j\right\}}{D} \tag{5.10}$$

The composite signal from the trajectory matrix is obtained using the same diagonal averaging as

explained in Eqn. 2.53. The reconstructed composite signal has the maximum information contained towards TVAR modeling and subsequent damage detection. The signal is generated based on the principal components containing the maximum variance, in each channel.

5.4.1 Recursive multichannel singular spectrum analysis (RMSSA)

The main disadvantage of MSSA algorithm is that when the number of channels increases, it becomes computationally more involved. This becomes an impeding factor even for developing a recursive version of basic MSSA algorithm towards processing real time multi degree of freedom data. In this section, an attempt is made to modify the formulations of the RSSA algorithm in order to make it amenable towards a multi-channel implementation. Following the similar lines of development, as in Eqn. 5.1, the RMSSA algorithm can be proposed as follows:

$$\mathbf{C_k} = \frac{k-1}{k}\mathbf{C_{k-1}} + \frac{1}{k}\widetilde{X}_{k_D}\widetilde{X}_{k_D} \tag{5.11}$$

where $\widetilde{X}_{k_D} = \left[x^1_{k-L+1}, x^1_{x-L+2}, x^1_{x-L+3}...x^1_k, \quad x^2_{k-L+1}, x^2_{x-L+2}, x^2_{x-L+3}...x^2_k, ..., x^D_{k-L+1}, x^D_{x-L+2}, x^D_{x-L+3}...x^D_k\right]^T$
Once the recursive equation is ready, all the other steps from Eqn. 5.2 to Eqn. 5.7 follows. The key steps of the formulation include the updating of the covariance matrix formed at each time stamp and providing eigen decomposition so as to tailor the basic MSSA algorithm towards its recursive version. As discussed in the preceding sections, the proposed algorithm could be applied for non-stationary cases involving mean shift as well. The recursive update of the covariance matrix could be expressed as: $\tilde{\mathbf{C}}_k = \frac{k-1}{k}\mathbf{C}_{k-1} + \frac{1}{k}\left[\tilde{X}_{k_D} - \mu_k\right]\left[\tilde{X}_{k_D} - \mu_k\right]^T$, where, the recursive mean at each instant of time, $\mu_k = \frac{k-1}{k}\mu_{k-1} + \frac{1}{k}\tilde{X}_{k_D}$. As the data evolves from zero mean process, following similar lines of development, the eigen decomposition of the covariance matrix at the k^{th} time instant could be written as $\mathbf{C}_k = \mathbf{W}_k\Omega_k\mathbf{W}_k^T$. On substituting to the covariance update Eqn. 5.11, with $\beta_k = \mathbf{W}_{k-1}\tilde{X}_{k_D}$, and performing simple algebraic calculations, the following equation is obtained:

$$\mathbf{W}_k\Omega_k\mathbf{W}_k^T = \mathbf{W}_{k-1}\left[(k-1)\,\mathbf{\Omega}_{k-1} + \beta_k\beta_k^T\right]\mathbf{W}_{k-1}^T \tag{5.12}$$

For finitely large samplesize k and low damping estimates [122], the term $((k-1)\Omega_{k-1} + \beta_k \beta_k^T)$ generally shows a diagonally dominant behavior. The diagonal dominant structure of this term ensures the application of Gershgorin's theorem, rendering in the application of FOEP approach admissible to obtain the eigen values and eigen vectors [136]. The application of Gershgorin's theorem ensures the EVD of the term to be of the form $\mathrm{T}_k \mathbf{\Lambda}_k \mathrm{T}_k^T$, where $\mathbf{T}$ is orthonormal and $\mathbf{\Lambda}$ is diagonal, similar to the previous approach. Substituting the EVD in Eqn. 5.12, the covariance matrix update could be simplified as follows:

$$\mathbf{W}_k k \Omega_k \mathbf{W}_k^T = (\mathbf{W}_{k-1}\mathbf{T}_k)(\mathbf{\Lambda}_k)(\mathbf{W}_{k-1}\mathbf{T}_k)^T \tag{5.13}$$

which yields the following iterative update equations:

$$\left.\begin{aligned} \mathbf{W}_k &= \mathbf{W}_{k-1}\mathrm{T}_k \\ \mathbf{\Omega}_k &= \tfrac{\mathbf{\Lambda}_k}{k} \end{aligned}\right\} \tag{5.14}$$

Eqn. 5.14 provides an iterative relation between eigen spaces at consecutive time instants. Following a similar approach, the principal component values of the time series at a particular time series can be extracted as below:

$$\psi_i(k) = (W_i^T(k))(\mathbf{X}_{k_D}) \tag{5.15}$$

The recursively updated trajectory matrix is reconstructed by utilizing the first two signal PCs of all the D input channels as shown below:

$$\mathbf{R}_i(k) = \frac{\left\{\sum_{j=1}^{D}\sum_{i=1}^{2} W_i^j(k) \times \psi_i^j(k)\right\}}{D} \tag{5.16}$$

The composite signal value at k^{th} instant of time is obtained as explained in Eqn. 5.7. This is subsequently utilized for TVAR modeling to track damage sensitive features in real time.

5.5 Proposed RSSA based framework

The identification of spatio-temporal damage in a single framework remains one of the proposed key objectives of this research. Adhering to this purpose, the RSSA based methodology is attuned to operate in a single framework to identify both temporal and local damage, online. This takes place in two separate modules. The first module deals with the temporal damage detection, where the raw acceleration data is processed by the RSSA algorithm as the data streams in real time. This accounts for an online global damage detection framework as the data is not gathered in batches to form a baseline. TVAR modeling is carried out on the updated first principal component, yielding TVAR coefficients at each instant of time. As previously explained, these TVAR coefficients are tracked online for any major and minor changes. DSF such as recursive ERD is utilized to further validate the instant of damage, obtained from the TVAR coefficients. Once the damage instant is detected, the spatial damage detection module further resolves the location of damage.

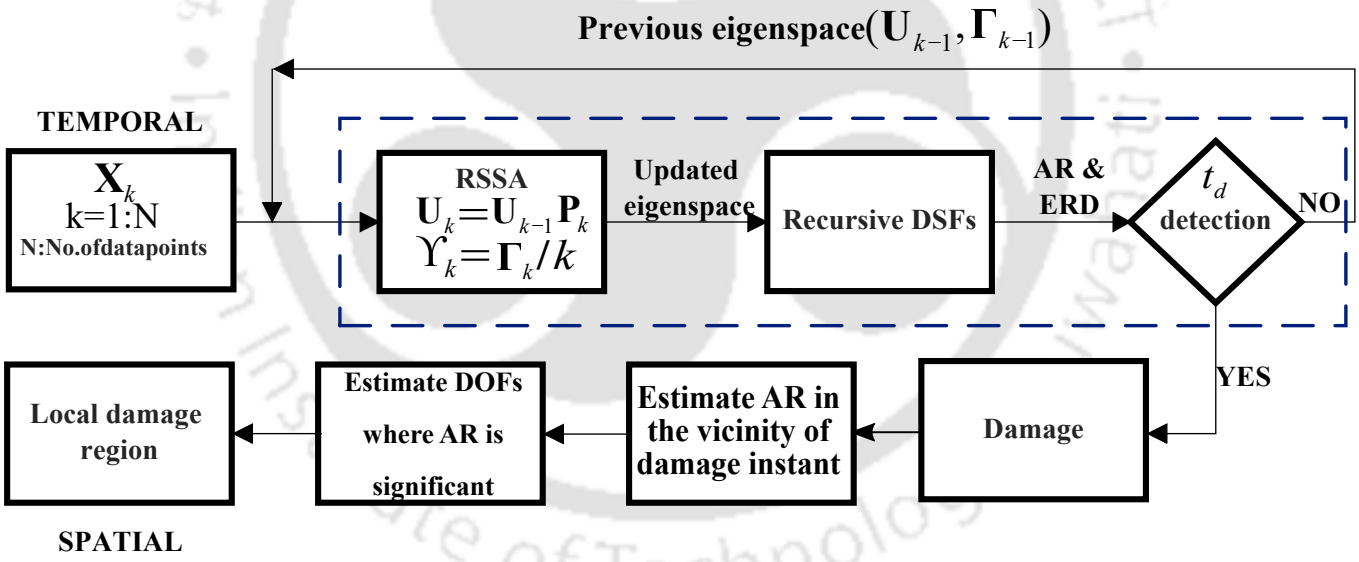

Figure 5.1: Basic framework of the proposed RSSA-TVAR algorithm

To facilitate easy understanding of the flowchart, a summary of the key steps of the RSSA algorithm is enumerated as follows:

1. First, traditional SSA is employed on some initial data points (around 100 in number) in order to estimate the initial eigen vector and eigen value matrices. The number of data points

chosen here is arbitrary and considered only to stabilize the algorithm for subsequent real time damage detection.

2. The RSSA algorithm then operates online on the real time input of the streaming data. This generates a Hankel matrix out of the set of physical responses.

3. Using the recursive gain depth parameter, the covariance estimate of the Hankel matrix at the present time instant is derived using the covariance estimate at preceding time instant. From the recursive updates, the eigen vector and eigen value matrices are updated using FOEP approach and the transformed responses (principal components) are obtained using the RSSA algorithm.

4. During the reconstruction phase, an approximate time series is obtained according to the relative order of significance as given by the decreasing order of the corresponding eigen values.

5. The proposed time series models are generated based on the approximated time series and a TVAR model is fit. The DSFs are tracked real time in order to extract the changes in the model coefficients, thereby revealing the faults in the system.

6. Once the instant of damage is determined, the algorithm shifts on to the next module where the spatial detection of damage takes place. DSFs are tracked online, recursively, to capture the spatial effect of the damage. To further validate the instant of damage obtain from the AR plots, recursive ERD is utilized to show changes in the mean level at the instant of damage.

The flowchart shown in Fig. 5.1 outlines the proposed damage detection scheme. Vibration responses are processed by the RSSA algorithm to obtain the transformed responses and TVAR modeling is utilized to extract time-varying coefficients through which damage instant is detected. Appreciating the fact that recursively updated methodologies are essentially *baseline free* and *parameter independent* processes, the RSSA algorithm complies with the above notion, thereby providing recursive eigenspace at each instant of time.

5.6 Hybrid FOEP based RPCA-RSSA framework

The damage detection strategies based on FOEP methods such as RPCA-RRE, RPCA-TVAR and RSSA-TVAR, have shown that the FOEP approach can be easily improvised for systems involving various complexities. Problems in dynamical systems involving single and multi-channel inputs, linear and nonlinear systems with changes in linear stiffness and /or nonlinear force term, quantified as damage [1–3], can be addressed using the FOEP based framework, to an accurate degree of identification in real time. In this work, a novel hybrid framework is proposed which serves as an ideal paradigm as to how FOEP technique can be improvised to create a hybrid approach towards a SHM problem. It can be understood that the FOEP approach is an efficient method to utilize the eigenspace updates obtained in real time for damage detection purposes. It is worth mentioning the fact that the proposed algorithm accommodates the use of a low model order for TVAR modeling. A recently established real time damage detection strategy has shown significant promise in detecting structural damage of the order of around 15%. In comparison, the main advantage of the hybrid method is the *finer detectability* of structural damage in real time, that has been successfully reported to be of the order of 10%, shown in the later stages of this chapter. In the backdrop of FOEP approach, the estimated eigenspace retains necessary information pertaining to the spatial and temporal patterns of damage, that is tracked through the DSFs for identifying damage in real time.

The proposed framework involves the sequential use of RPCA and RSSA as an application of the FOEP technique on the raw vibration response in order to obtain a transformed response online as and when the data streams in. The physical response matrix is provided as input to the hybrid FOEP algorithm where the response is first transformed using the RPCA scheme. The RPCA algorithm provides a set of transformed response ($\mathbf{X}_{tr}$), updated covariance estimates and recursive eigenspace updates at each time stamp, which can be obtained by carefully scrutinizing the FOEP derivations as previously shown. The transformed response obtained at each instant of time is then provided as input to the RSSA module, where the following recursive update equation gives the covariance estimate:

$$\mathbf{C}_k = \frac{k-1}{k}\mathbf{C}_{k-1} + \frac{1}{k}X_{tr}^{1}X_{tr}^{1^T} \tag{5.17}$$

where X_{tr}^1 is the top floor acceleration obtained after RPCA transformation of the physical response matrix. Following the FOEP approach, the recursive eigenspace updates can be easily obtained from Eqn. 5.4. Following similar lines of development, the reconstructed signal (Y_R^1) can be obtained by projecting the PCs back to the original subspace and averaging it over the eigen values that explain more than 90% of the variance.

Based on the aforesaid perception of spatio-temporal damage detection carried out in a single framework, the hybrid approach also strives to similarly meet the requirements of an efficient recursive algorithm that provides eigenspace updates at each instant of time. The overall methodology is outlined in Fig. 5.2. The crucial point of contrast for the implementation of the hybrid method is that while the RPCA and RSSA modules work in *tandem* to provide eigenspace updates successively, the individual RPCA or the RSSA based procedures utilize only one set of iterative equations to provide the eigenspace in real time. The hybrid algorithm commences by processing the raw acceleration data using the RPCA-RSSA module, that provides a set of transformed responses. TVAR modeling is carried out on the transformed response, yielding TVAR coefficients at each instant of time that are tracked online for any major and minor changes. The final form of Eqn. 4.15 therefore, becomes:

$$Y_R^1(k) = a_1(k)Y_R^1(k-1) + a_2(k)Y_R^1(k-2) + V(k) \tag{5.18}$$

The changes in the mean level of the plots of the TVAR coefficients indicate the exact instant of damage to the system. DSFs such as RRE are employed to further corroborate the instant of damage. Considering the damage at the end of k^{th} instant, the subspace spanned by the eigenvector $\mathbf{G}_{k+1}$ deviates in comparison to the subspace spanned by the eigen vectors at the previous time stamp $\mathbf{G}_k$. To identify global damage to the structure, the temporal RRE can therefore, be evaluated as:

$$\chi_{RR-1} = \left\| \mathbf{G}_k^1 * \mathbf{G}_{k+1}^{1^T} * Y_R^1(k) - \mathbf{G}_{k+1}^{1^T} * \mathbf{G}_k^1 * \mathbf{G}_{k+1}^{1^T} * Y_R^1(k) \right\|^2 \tag{5.19}$$

Once the damage instant is detected, the spatial module is invoked that further resolves the location of damage. Following the similar lines of development, the time series corresponding to each DOF, can be expressed as:

$$\varepsilon_{RR-Y_i}(t) = \left| y_R^{1^{*^2}}(k) - y_R^{1^2}(k) \right| \tag{5.20}$$

Concluding, the spatial RRE used for localizing the damage can be expressed, according to:

$$\langle \varepsilon_{RR-Y_i}(t) \rangle = \frac{\sum_{k=1}^{K} \left| y_R^{1^*^2}(k) - y_R^{1^2}(k) \right|}{K} \tag{5.21}$$

A summary of the key steps involved in the proposed FOEP based example are enumerated below, for simplification:

1. First, batch PCA is applied on some initial points (around 100 in number) in order to obtain the initial eigenvector and eigenvalue estimates. It should be noted that the number of data points chosen here is arbitrary and considered only to stabilize the algorithm to facilitate subsequent real time damage detection. Similarly, batch SSA is also employed on approximately 100 sample points to get the initial eigen estimates for the RSSA algorithm.

2. The RPCA algorithm then operates online on the real time input of the streaming data. This provides the set of transformed response at each instant of time. The sample covariance update at the present time instant is derived using the covariance estimate at the preceding time instant, employing the use of the recursive gain depth parameter. From the recursive updates shown in Eqn. 5.14, the eigenvector and the eigenvalue matrices are updated using the FOEP approach and the transformed responses (principal components) are obtained using the RPCA algorithm.

3. The transformed response obtained from the previous steps are now provided as input to the RSSA algorithm, that generates a *Hankel matrix* out of the set of the input responses. Using the FOEP approach, the recursive updates of the eigenvector and the eigenvalue matrices are updated at each time instant and a new set of transformed responses are obtained, evident from the Eqn. 5.4.

4. During the reconstruction phase, an approximate time series is obtained according to the relative order of significance as given by the decreasing order of the corresponding eigen values. The proposed time series models are generated based on the approximated time series and a TVAR model is fit. The DSFs are tracked real time in order to extract the changes in the

model coefficients, thereby revealing the faults in the system, facilitating real time temporal damage detection.

5. On identifying the damage instant, the algorithm shifts on to the next module where the spatial damage detection takes place. DSFs are tracked online recursively to capture the spatial effect of the damage. To further validate the instant and location of damage, local RREs are tracked recursively to provide information about the exact location of damage in the structure.

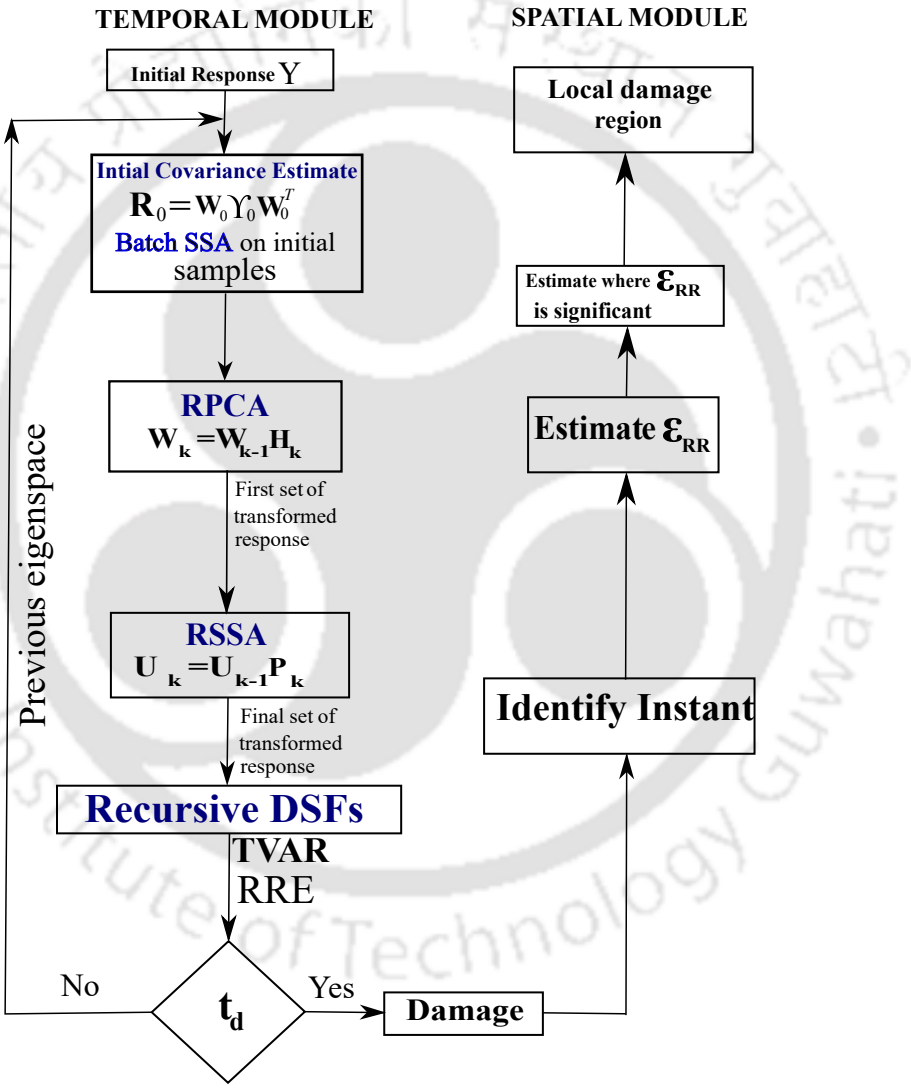

Figure 5.2: Basic framework of the proposed algorithm

5.7 Numerical studies

The main objective of incorporating the hybrid methodology into the framework of the current recursive damage identification algorithm is to unify the provisions of carrying out detection studies through both *single* and *multi-channel* sensor inputs. Towards this, it becomes imperative to understand the performance of the newly proposed methods in this chapter for detecting real time spatio-temporal damage for previously described numerical systems, such as the B-W system. In this context, this section mainly deals with the detection studies for the B-W system and also for some newly developed numerical systems, that are distinct from the B-W system in terms of dimensionality as well as the nature of the system, described next in detail.

5.7.1 Numerical case studies using RSSA

In this section, the proposed RSSA algorithm is implemented on first on the B-W system. Subsequently, as the method uses the input from only a single sensor, a newly developed single-storey modeled with a Duffing oscillator is put into perspective. The description of the B-W system has already been provided in the preceding chapters and no modifications whatsoever are carried out for the present RSSA analysis. However, the SDOF Duffing oscillator model is a relatively fresh conceptualization at this stage and calls for a detailed description.

The Duffing oscillator is one of the prototype systems of nonlinear dynamics. The system has been successfully used to model a variety of physical processes such as stiffening springs, beam buckling, nonlinear electronic circuit. The source of the nonlinearity in a structural system that results in its dynamic behavior being modeled by the Duffing equation is the stiffness. In this section, a simple model involving a single storey structure with a Duffing oscillator at its base is described through the following equation of motion:

$$m\ddot{X} + c\dot{X} + k(X + \alpha X^3) = F(t) \tag{5.22}$$

The excitation $F(t)$ is zero-mean white noise with spectral density S_0. Solving the equation of motion numerically, the statistics of the response $X(t)$ can be obtained. The numerical values for

system and excitation parameters considered here are $k = 1$, $m = 1$, $c = 0.1$, $\alpha = 0.05$ and S_0 =1.

5.8 Detection results using RSSA

5.8.1 Temporal damage detection results for the 5 DOF B-W system using RSSA

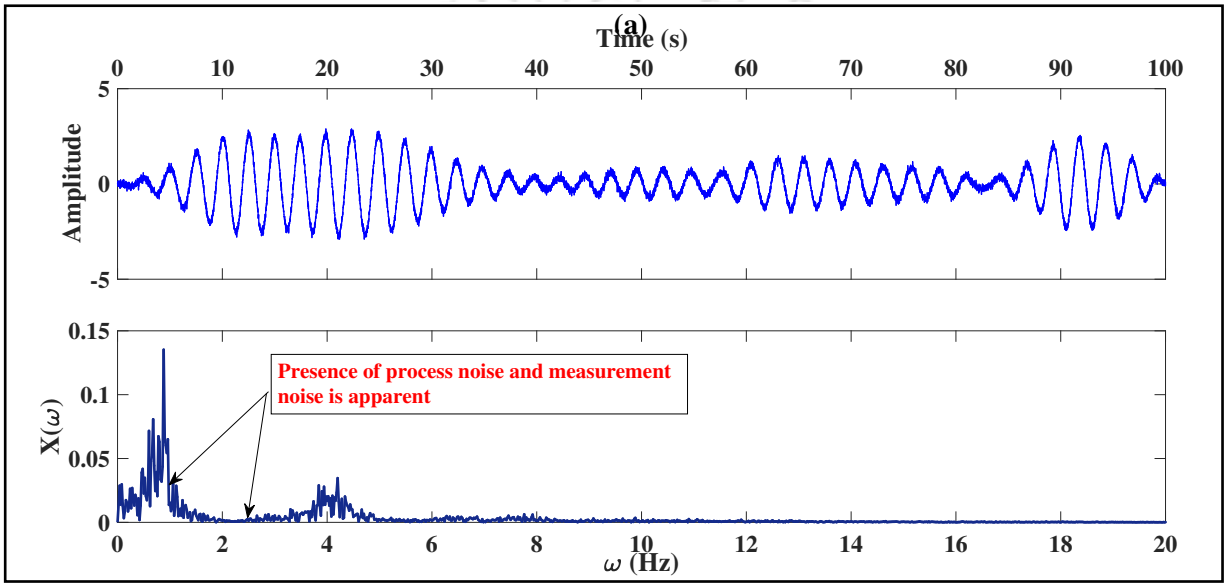

Figure 5.3: Plots of reduced order response (a) and the corresponding FFT (b)

In this section, detection studies are conducted for 15% and 30% change in nonlinearity for the B-W system. It is shown in this chapter that detection results for 15% change in nonlinearity using the real time acceleration response from a *single channel* as input can be successfully obtained. Since the transformed responses obtained using the RSSA algorithm consists of simpler components, a relatively low model order (which is *2* in the present context) can be used. It can be observed from Fig. 5.3 that the reduced order response obtained after the RSSA algorithm is not completely devoid of noise. The presence of both process noise and measurement noise could be discerned from the figure. An additional observation that could be inferred is that both the time series and the FFT plots of the response clearly indicates the presence of process noise as well as measurement noise in the signal.

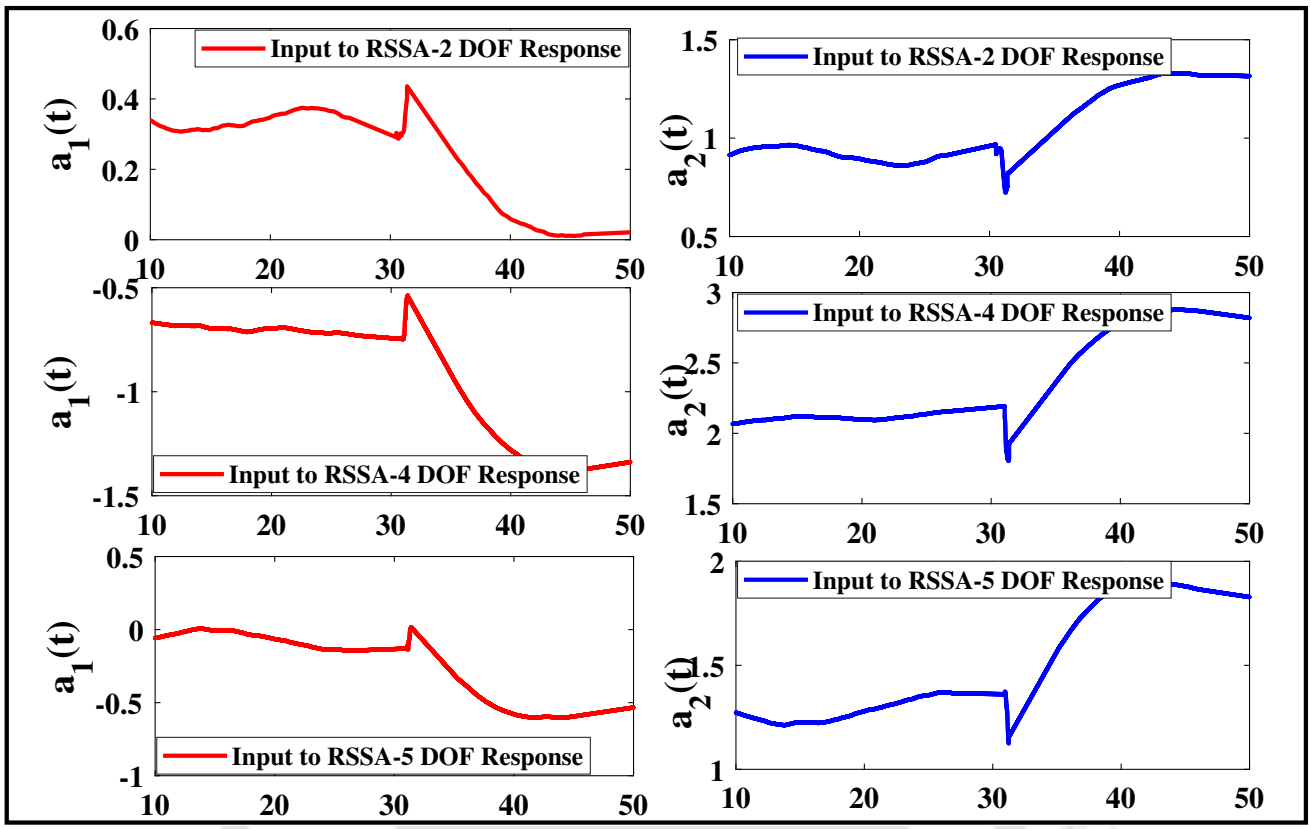

Figure 5.4: AR1 & AR2 plot for 30% global damage

The damage is detected using AR coefficients and ERD as DSFs shown in Fig. 5.4 and Fig. 5.5, respectively. From both the figures, a damage instant at 31s can be easily detected using AR coefficients by observing the sudden changes of the mean level of the plot. This confirms the use of TVAR modeling towards online detection of damage in a recursive framework. To further validate the efficacy of the proposed methodology, ERD, when examined in a recursive framework, detects the instant of damage for 15% nonlinearity change at 31s, as observed in Fig. 5.5. While a change in the mean level of the TVAR plot verifies the damage instant to be at 31s, a distinct peak shown in the recursive ERD plots indicating the exact instant of damage further reinforces the efficacy and robustness of the algorithm.

The efficacy of the DSFs for less than 15% damage is slightly questionable which indicates that the current online framework is less reliable when the extent of damage suffered is low (i.e., less than 15%). The results are therefore, not reported here for brevity. A recently investigated venture of real time damage detection using RPCA in conjunction with TVAR modeling has reported global damage detection in the order of 15%. Thus, it suffices to say that both RPCA and RSSA algorithms

are efficient in detecting low levels of damage in real time, but the performance of RSSA algorithm surpasses the performance of the RPCA algorithm as it takes the streaming data from a *single channel* as input, as compared to the RPCA algorithm, that requires *multi-channel* data as input. Therefore, the key novelty of the work arises due to the utilization of the streaming data available from a *single channel* that provides real time damage detection.

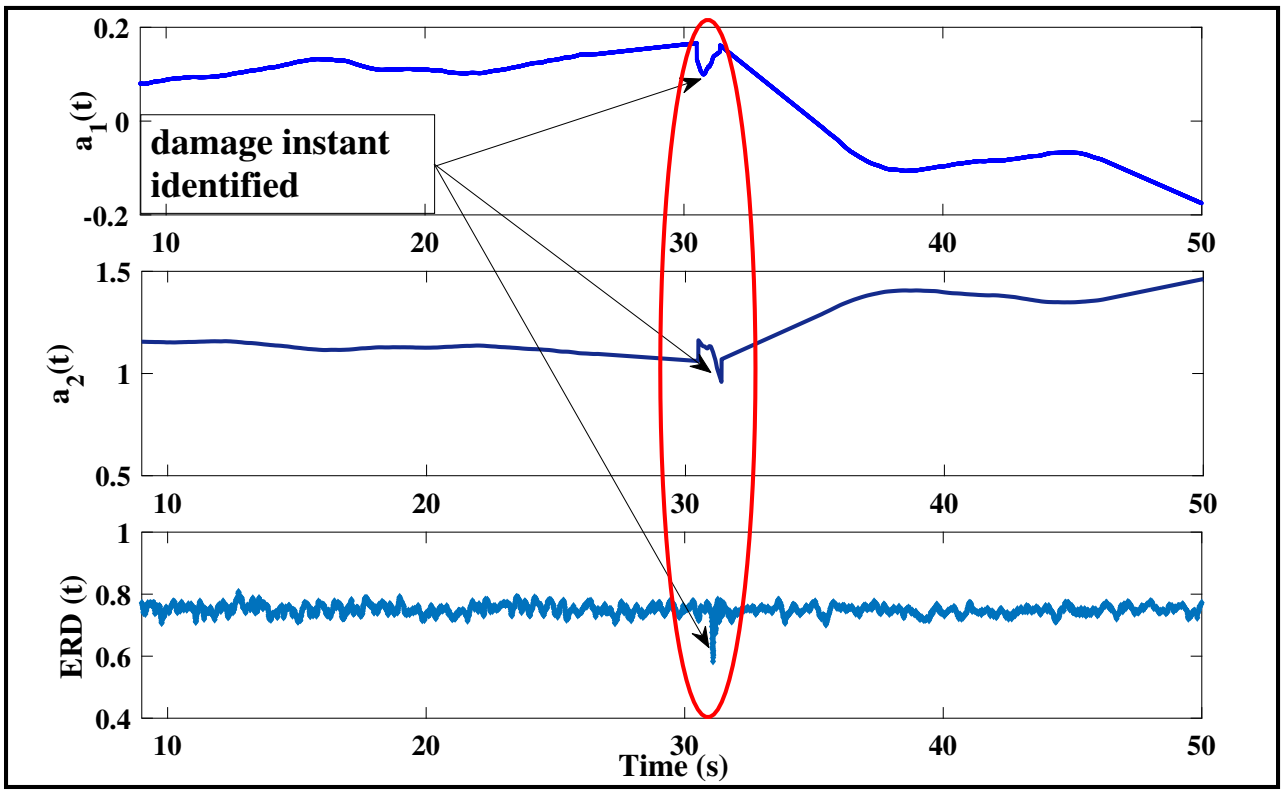

Figure 5.5: Recursive DSF plot for 15% global damage

A separate case study has been carried out taking into consideration the incorporation of mean corrected covariance estimates for real time damage detection. Although the covariance estimate for such cases differs slightly from the updates obtained for zero mean processes, it can be observed from Fig. 5.6 that the variation in the DSF plots is not significant. On comparing Fig. 5.5 and Fig. 5.6, it is evident that the proposed algorithm could efficiently detect real time damage for cases involving mean shifts as well. It can be clearly understood that the usage of $\tilde{C}$ for incorporating recursive mean estimate does not alter the detectability of the proposed algorithm significantly. For brevity, analysis for the cases involving mean shifts have been subsequently dropped for the remainder part of the thesis.

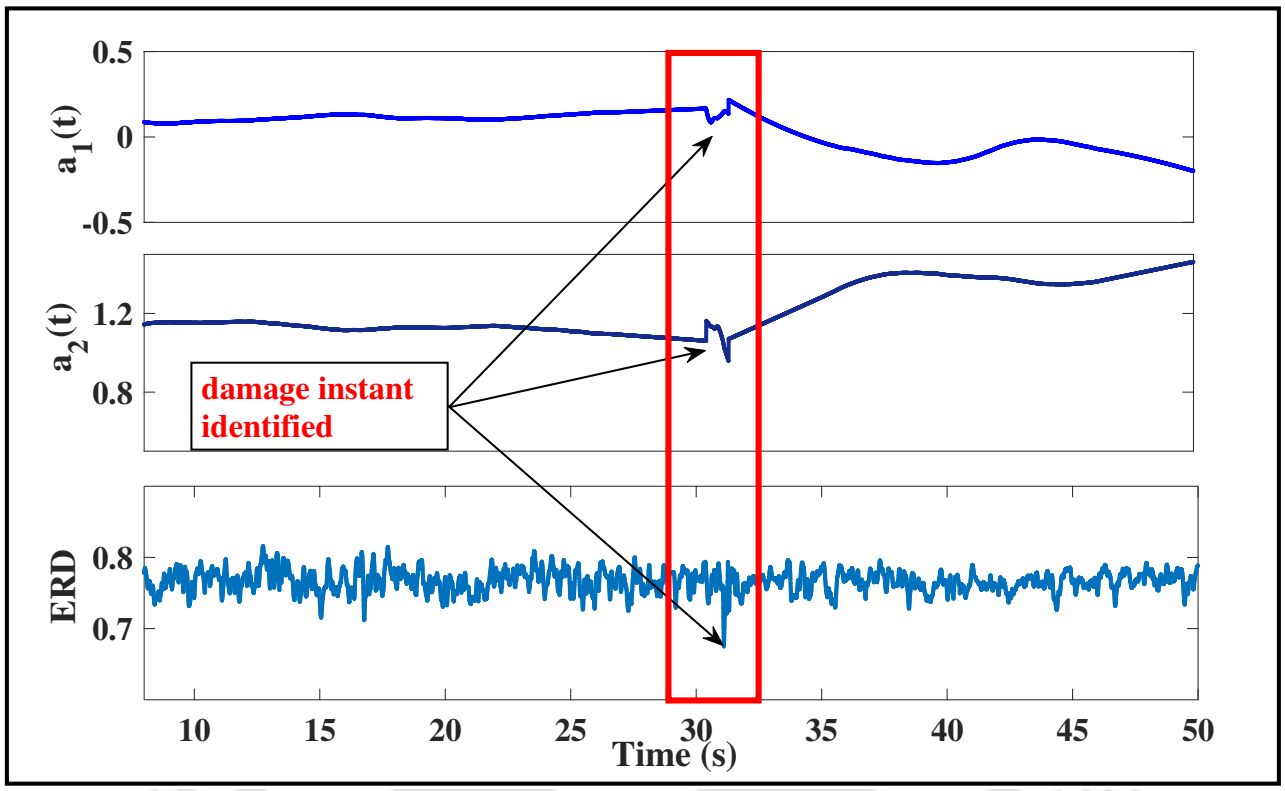

Figure 5.6: Mean corrected DSF plot for 15% global damage

An important aspect of any recursive damage detection strategy is its time complexity. For the present case, the time taken for one complete run of the algorithm is found to 1.18s, which approximately emulates a real time process. The implementation of recursive eigenvalue decomposition consumes 10ms, which is 0.85% of the total time consumed for a complete single iteration. However, the expended time depends upon the computational power of the system used and is more efficient for systems with superior processing power, higher gigabytes of RAM, multiple cores, etc.

5.8.2 Local damage detection results for 5 DOF B-W system using RSSA

In this section, the local damage detection results using the RSSA algorithm is presented. The local damage is induced to the B-W system through a change in the linear storey stiffness at each floor level. The salient feature developed in the local (or spatial) damage detection scheme is consistent with events where a structure undergoes varying changes in stiffness with the progression of time, for example, during an earthquake. Case studies for successive floor-wise local damage at different

instants of time are provided that are validated through the use of TVAR plots and ERD as recursive DSFs for real time damage detection. To this effect, case studies are carried out based on possible simulations closely emulating a real life event where the stiffness of each storey reduces over time.

The simulation cases considered reducing the linear stiffness of individual storey by 15% at each 10 second span. Damage was numerically induced to the fifth floor at 10 seconds from the start, to the fourth floor at 20 seconds, to the third floor at 30 seconds, to the second floor at 40 seconds and to the first floor at 50 seconds. The acceleration response from individual floor levels are provided as input to the algorithm sequentially. The use of the same set of recursive DSFs for simultaneous global and local damage detection demonstrates the robustness of the proposed method. The results for local damage detection is presented next in detail.

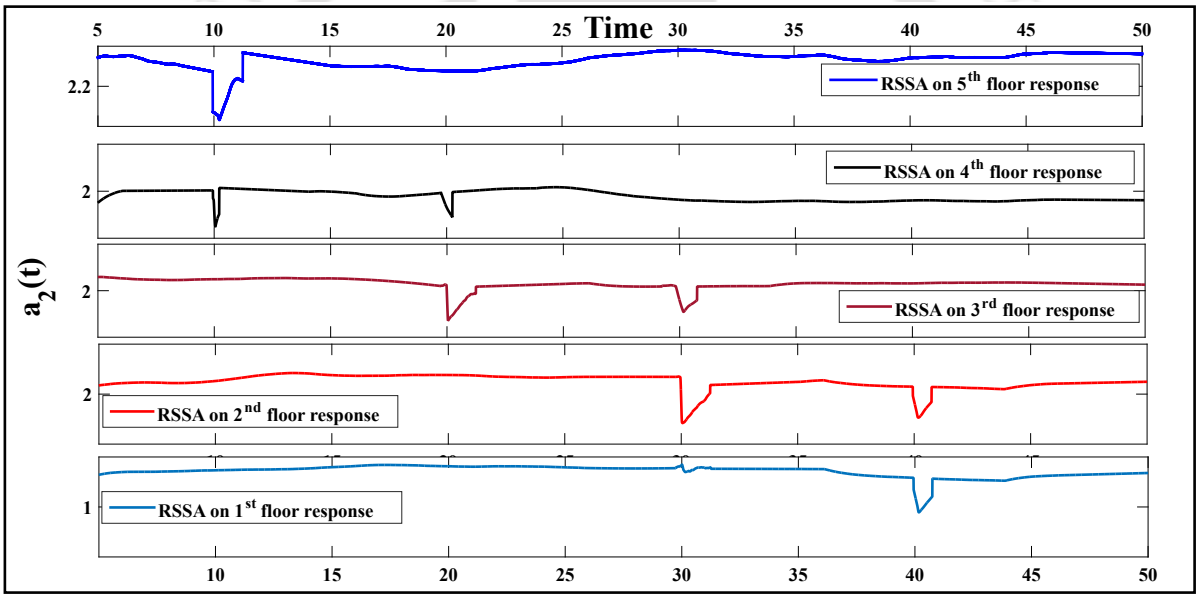

Figure 5.7: Local damage detection using AR coefficient - All floors

The response from the fifth floor is provided as input to the algorithm and is processed by the recursive DSFs to indicate the local damage in the structure. From Fig. 5.7, it can be observed that the change in the mean level of the TVAR plot occurs at $10s$, indicative of a linear stiffness change at that instant of time, for the fifth floor. On providing the acceleration response of the fourth floor as input, the sudden change in the mean level of the AR plot occurs at $20s$, that can be interpreted as a local damage. However, an *additional change* in the mean level could be seen at $10s$ from the start. This observation can be inferred from the fact that the fifth and the fourth

floors are connected through the same column where the damage has occurred, and hence, show simultaneous peaks at both the damage instants. Hence, the cumulative event for both the fifth and the fourth floors, clearly show that the damage has occurred to the fourth floor at $20s$ from the start of the event. Considering the response from the third floor as input for the algorithm, two peaks are observed at $20s$ and at $30s$ respectively, that indicate the progression of local damage in the structure, over time. Considering the cumulative event of the fifth, fourth and the third floor, the TVAR coefficients indicate the damage to the third floor at $30s$ through a change in the mean level of the plot. The proposed algorithm is now applied on the response from the second storey and is

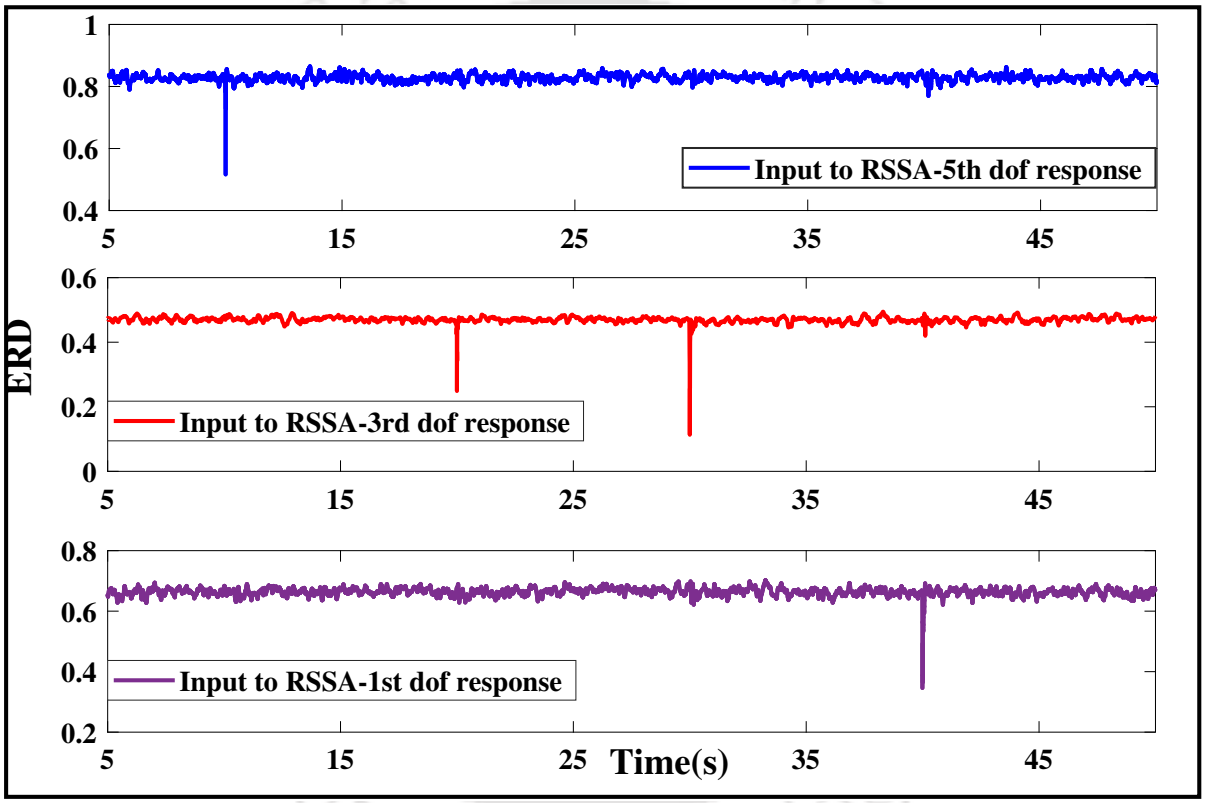

Figure 5.8: Local damage detection using ERD

processed by the set of recursive DSFs. The change in the mean level of the AR plot occurs at $40s$ from the start. As observed from the figure, the plot shows two peaks simultaneously at $30s$ and at $40s$ on considering the individual response of the second floor. However, taking into consideration the cumulative response of the fifth, fourth, third and the second floors, the local damage at the second floor can be clearly inferred from the AR plot at $40s$. The response from the first floor when provided as input to the algorithm, show change only at $40s$ from the start of the event. This result

can be clearly concluded from the fact that the column connecting the second and the first floor has already suffered damage at $40s$. The cumulative event of all the floors combined indicate the damage to be at $40s$ and as the damage has stopped its progression over time, the mean level of the AR plot provide a distinctive change only at $40s$ from the start. To show the efficacy of the recursive ERD in detecting the successive floor-wise local damage, the plots of ERD for different input cases is shown in Fig. 5.8. It can be observed from the figure that the ERD plots behave in the same manner as the AR plots for indicating the progressive damage to the structure.

5.8.3 Performance of the RSSA algorithm against recently established damage detection schemes: A comparative study

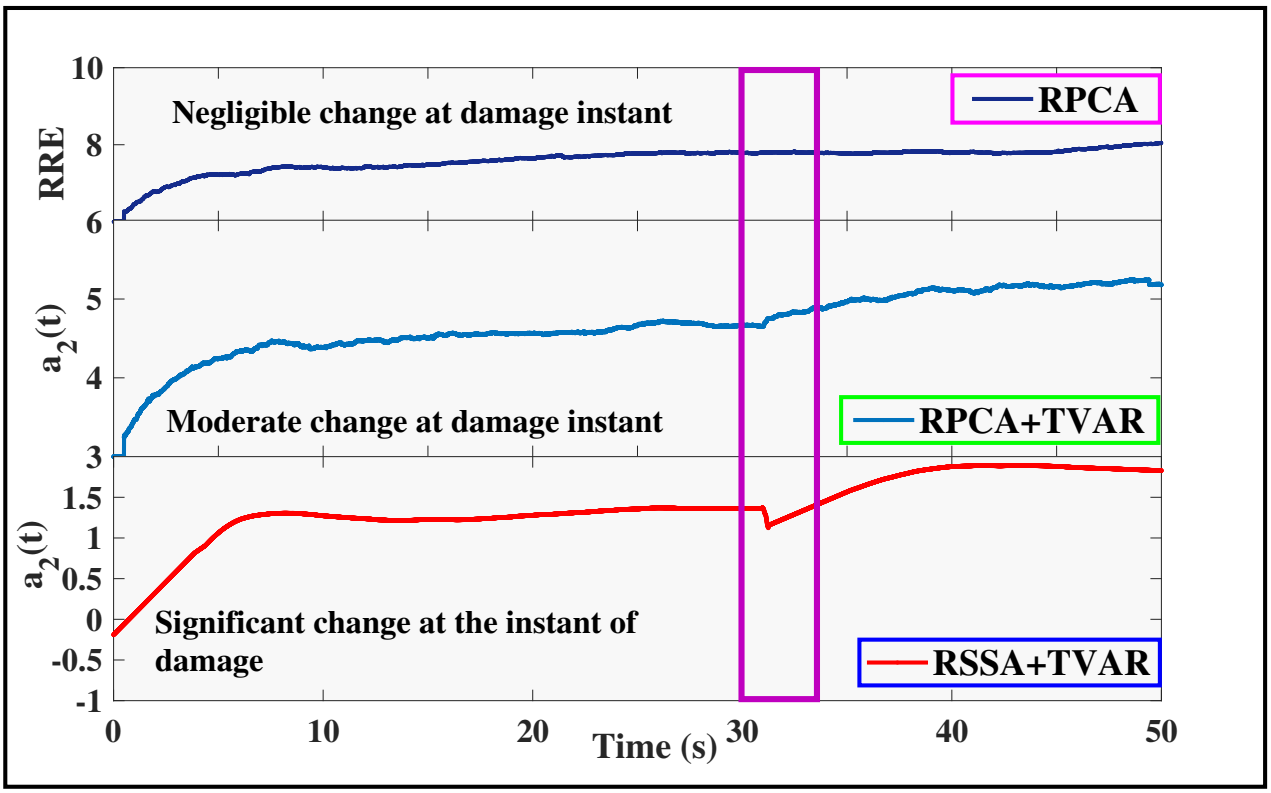

Figure 5.9: Comparison of the various methods for local damage detection

In this section, the performance of the proposed method is compared with the recently-established online RPCA based damage detection schemes. One of the key findings of this research is the *finer detectability* of real time damage through improved theoretical derivations and modifications in the

Table 5.2: Comparison of existing damage detection methods with the proposed algorithm

Local damage (%)	RPCA-RRE	RPCA-TVAR	Proposed algorithm
35.00	Yes	Yes	Yes
25.00	Yes	Yes	Yes
20.00	No	Yes	Yes
15.00	No	No	Yes

formulations. However, establishing these facts on a conceptual level alone is not enough. This necessitates that the algorithms established during the course of this dissertation are applied on the same system (numerically simulated or otherwise) and identifying the events corresponding to fine levels of damage. Conforming to this notion, the ground work has been established by providing certain key detection results of the RPCA based approaches on the B-W system. the present section is devoted to understanding the performance of all the algorithms established so far towards an improved detectability of damage in real time.

The proposed algorithm is compared against RPCA and its recursive residual error (RRE) and RPCA in conjunction with TVAR modeling. As the damage detection methods are purely *online* in nature, comparison with traditional methods such as PCA, is not justified, since PCA is inherently an *offline* algorithm that requires data to be processed in batches. Windowing of the data is necessary for executing batch PCA based damage detection which prevents any possibility of online implementation of the method. A crucial point of contrast of the RSSA algorithm with the established detection methods is the use of a *single sensor* data as input for damage detection process. RPCA based detection schemes use a bare minimum of 2 sensors as inputs for proper functioning of the algorithm. In addition, RPCA involves updating of the covariance matrix of the *data set* at each time stamp, contrary to the functioning of the RSSA algorithm where the covariance update of the *Hankel* matrix takes place at each instant of time.

In the present context, the comparative study is conducted on the B-W system described in the earlier chapters, using a white noise excitation of 50s duration. On excitation, the third floor of the model undergoes a change in the linear stiffness by 15% at 31s. The basis of comparison of the algorithms is to detect the change in the spatial orientation of the system in real time. As evident from previously elucidated case studies, the damage detection potential of the RPCA algorithm is

confined to the order of 25% for spatial damage. Fig. 5.9 clearly indicates that the efficacy of both RPCA-RRE and RPCA-TVAR algorithms is slightly questionable for 15% spatial damage. While the RRE and TVAR plots for both the RPCA based detection algorithms fail to show any detectable change in the mean level of the plots, the proposed RSSA algorithm captures the exact instant of damage at 31s even for a 15% linear local storey stiffness change. This confirms the superiority of the proposed RSSA algorithm over the aforesaid damage detection schemes. In line with the above findings, a tabular comparison of the algorithms towards percentage change in linear storey stiffness (termed as spatial damage) is provided in Table 5.2. It can therefore be concluded that the proposed RSSA algorithm is advantageous over RPCA based damage detection methods in terms of an improved detectability of spatial damage in real time.

5.8.4 Results for the SDOF Duffing oscillator model

To verify the accuracy of the RSSA method, the algorithm is implemented on a single set of acceleration data, unlike the multi-channel datasets necessary for functioning of the RPCA based processes. In this approach, the damage is induced through a change in the α parameter of the governing differential Eqn. 5.22. The change in the parameter α is analogous to a change in the value of κ (Eqn. 3.22) that indicates an alteration in the nonlinear force term. Similar to the B-W system, the single storey modeled with the Duffing oscillator also undergoes a global damage when the force parameter controlling the effect of nonlinearity is changed at a particular instant of time. The damage is induced to the model at $26s$ from the start, through a 25% change in the nonlinear force term of Eqn. 5.22.

A plot of Hilbert-Huang spectrum (HHS) for the SDOF Duffing oscillator is shown in Fig. 5.10. Empirical mode decomposition (EMD) applied to the acceleration response yields intrinsic mode functions (IMFs) [77–79] for application of Hilbert spectral analysis. Although plots of both FFT and HHS are approximate spectral representations of a signal evolving from a nonlinear system, the use of HHS to study nonlinear systems and signals is well documented in literature [79,80]. Therefore, spectral representations of nonlinear systems are studied through HHS plots in this work. In the present context, IMFs having significant energy content were chosen for the subsequent plotting of

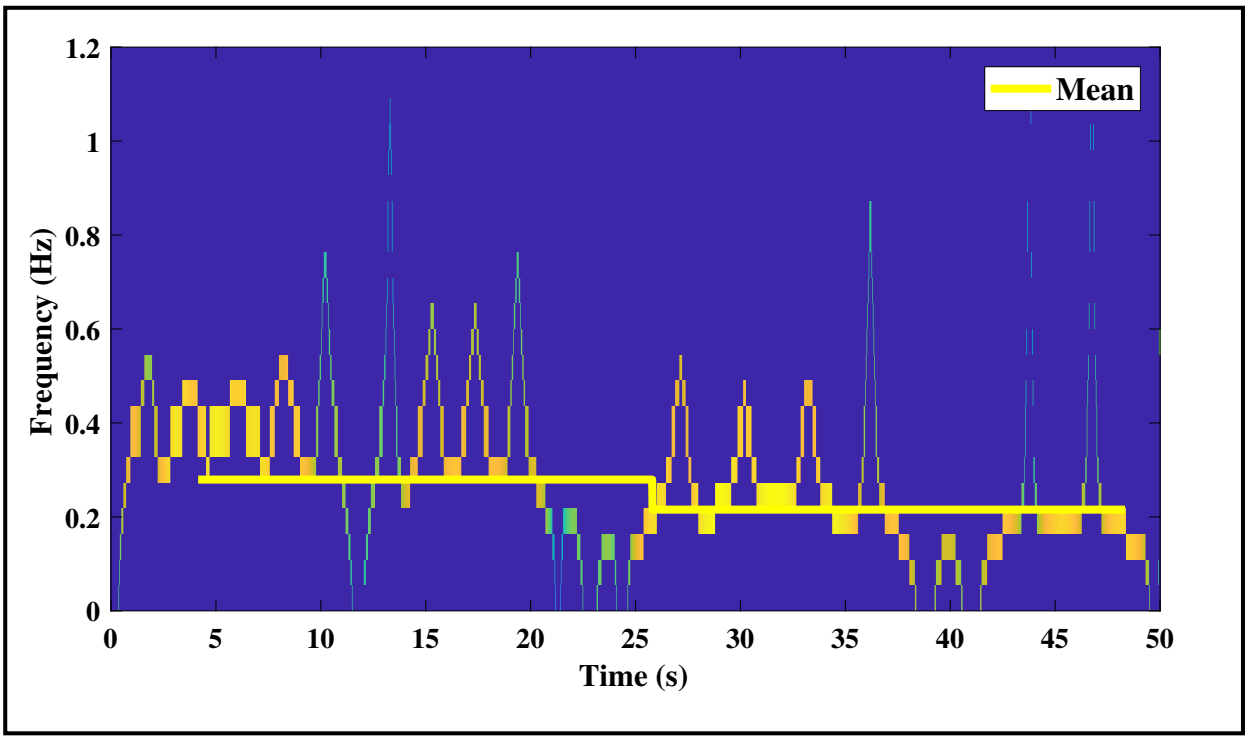

Figure 5.10: Hilbert Huang spectrum for SDOF Duffing oscillator

the HHS. The mean frequency is calculated on the basis of the average of the frequencies obtained from the instantaneous values of the Hilbert phase, considered event to event in time. Fig. 5.10 shows the variation in the mean frequency content of the system which roughly corroborates to the changes in the system occurring due to a possible damage at a certain instant of time. A noticeable feature of the HHS is the change in the mean level of the frequency band only at $26s$, thereby, indicating the possible event at $26s$. However, it should be noted that the purpose of these plots is purely to serve as a visual aid for identifying the instant of damage and does not play any role in the real time functioning of the algorithm. Using the proposed algorithm, the detection results for the Duffing oscillator is shown in Fig. 5.11. It is evident from the figure that the plots of AR-1 and AR-2 clearly indicate an accurate damage instant at $26s$. Fig. 5.11 (a) and (b) show a discernible change in the mean level of the AR plots at the instant of damage. A change in the mean plot verifies the efficacy of the DSF to detect damage even for a single storey structure with a nonlinear parameter associated with it. Based on these interpretations, it becomes very clear to explain the sudden change in the mean level of the ERD plot shown in Fig. 5.11 (c). The exact instant of

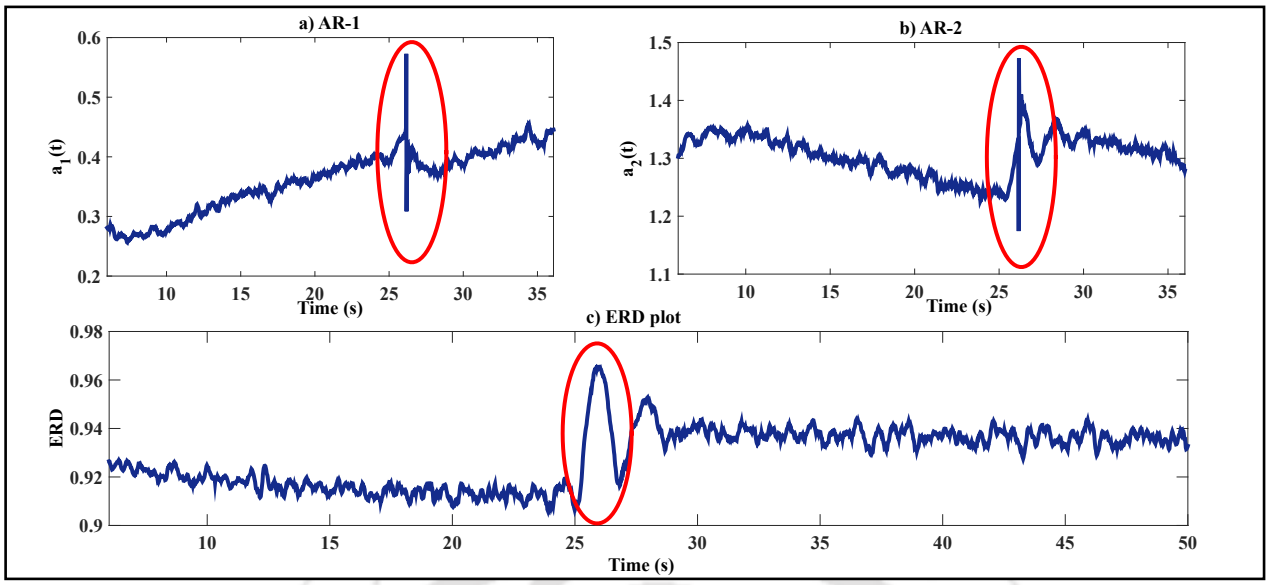

Figure 5.11: Damage detection for SDOF Duffing oscillator

damage at 26s, clearly evident from the ERD plot, further substantiates the use of the proposed methodology towards solving global damage detection problems for a category of nonlinearities that might be associated with systems.

5.9 Detection results using RMSSA

In this section, the RMSSA algorithm is applied on the vibration response obtained from the B-W system. RMSSA, an extension of the RSSA approach, is effective in analyzing inputs from two or more channels from a system. The method is receptive towards temporal damage and indicates the exact instant of damage occurred due to a linear change in the storey stiffness. At a particular instant of time, the linear stiffness of the third storey is reduced by 30%. As the third column is affected, the neighboring DOFs are expected to show distortions as previously discussed using the RSSA approach (kindly refer Fig. 5.7 for further details). Since the RMSSA algorithm uses multi-channel floor response as inputs at the *same time*, it cannot be used for localization of the damage that is confined only to a single storey. This drawback can be alleviated by implementing the single channel RSSA approach multiple times towards localizing the damage. It should, however, be noted that the sensor used for capturing the spatial patterns of damage should be instrumented in the

storey where the damage actually takes place. This is a minor impediment for a practical scenario as the occurrence of damage can never be predicted to be confined to a particular storey for effective placement of the sensor. Therefore, only the temporal damage detection is demonstrated in this section using RMSSA.

To this effect, response obtained from the 2^{nd} and 4^{th} floor are provided as inputs to the RMSSA algorithm. The initial signal length is selected as 6. The data processed after RMSSA is fit with TVAR models to be tracked in real time. Fig. 5.12 provides clear detection results for a damage occurring at $31s$ through deviations in the TVAR plots. To further substantiate the instant of damage provided by the TVAR coefficients, ERD is applied over the processed data and tracked in real time, as discussed in the preceding sections. From Fig. 5.12 (a) and (b) it can be observed

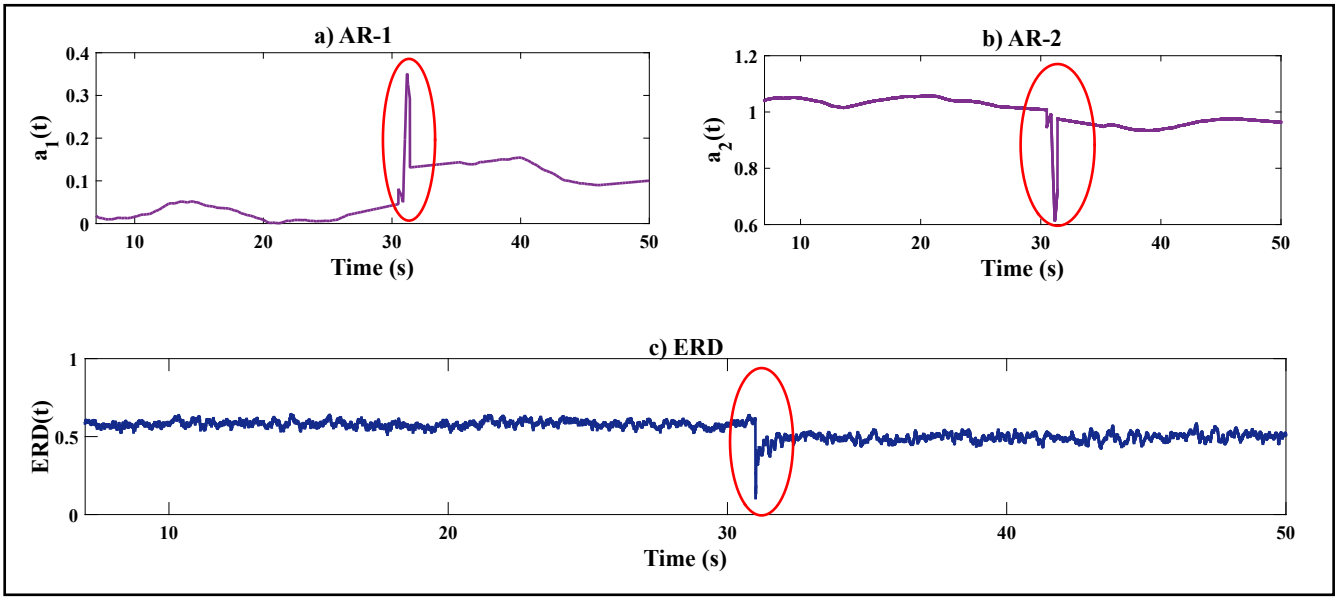

Figure 5.12: Detection results using RMSSA

that the AR plots show changes in the mean level at $31s$, precisely indicating the instant of damage. Additionally, the ERD plot (Fig. 5.12 (c)) further validates the instant of damage to be the same as that observed from the AR plots. Thus, based on the above result, it is safe to interpret that RMSSA is consistent with RSSA towards an online implementation. The DSFs developed for the RSSA algorithm are amenable towards damage detection for RMSSA as well, showing good detection results for multi channel inputs developed towards this study.

5.10 Numerical case studies using hybrid RPCA-RSSA algorithm

The applicability, robustness as well as a comparative understanding of the FOEP based hybrid algorithm are discussed here in the light of a fairly representative class of numerical models. Numerical simulations are carried out on (i) a 2 DOF Duffing system having Duffing oscillator on both the floors; (ii) a 2 DOF system with the base modeled with a Duffing oscillator and a linear top storey and (iii) the previously described B-W system. The notion of global damage is introduced through the changes in the nonlinear force term governing the equation of motion of the systems. This is verified through the use of an empirical damage index (DI) in conjunction with hysteresis plots that validate the changes in the nonlinear force term as indicators of damage to the system, extensively elucidated in chapter 2. The description of the models are presented next, followed by the results of the numerical simulation towards damage detection studies.

5.10.1 Description of the 2-storey modeled with Duffing oscillator on both floors

The differential equation that governs this oscillator has a cubic nonlinearity, and it has been named after the studies of G. Duffing in the 1930's. The nonlinear force term is associated with the stiffness parameter, which is altered at certain pre-selected time instances that define global damage to the system. A simple two storey model involving Duffing oscillator on both the floors is described through the following equation of motion:

$$\mathbf{M}\ddot{X} + \mathbf{C}\dot{X} + \mathbf{K}X + \tilde{\mathbf{\Omega}}\tilde{\mathrm{Z}} = F(t) \tag{5.23}$$

The excitation matrix consists of two statistically independent Gaussian white noise processes sampled at $100Hz$ having zero mean and standard deviation σ_1 and σ_2 for the vectors $f_1(t)$ and $f_2(t)$, respectively. M, C and K are the assembled mass, damping and stiffness matrices, respectively. $X(t)$ and $F(t)$ are $n \times 1$ stochastic vectors describing the displacement and excitation, respectively.

Each individual elements of the matrix $\tilde{\mathbf{\Omega}}$ denotes Duffing parameter value at contributing at each floor. The governing stochastic differential equation is discretized using the *Taylor's 1.5 strong scheme* [155] with a time step Δ= 0.01s. Solving the equation of motion numerically, the statistics of the response vectors $x_1(t)$ and $x_2(t)$ can be obtained. Brief details of this procedure are given in the APPENDIX B. The interested readers are referred to other pioneering references on this topic [155] for details. The system information contained in the mathematical model of the dynamical system expressed using the aforementioned discretization scheme leads to the development of the real time damage detection strategy decreed by the hybrid algorithm. The numerical values for the system and excitation parameters are: mass of each floor, m_1=m_2=10 kg, linear stiffness coefficient, k_1=k_2=1 kN/m with Duffing constants, α_1=1 kN/m^3 and α_2=2 kN/m^3. The detection results for the model are provided later on.

5.10.2 Description of the 2-storey modeled with a base Duffing oscillator

A 2-storey system modeled with a Duffing oscillator at its base with a linear top floor is numerically simulated with a zero mean Gaussian white noise excitation on both the floors. The matrix $\mathbf{\Xi}$ describes the Duffing action at the bottom DOF, expressed as: $\Xi = \alpha X_1^3$. The governing equation of motion is recast as an Ito's stochastic differential equation and subsequently discretized using Taylor's 1.5 strong scheme [155] with a step size Δ= 0.01s. Interested readers are kindly referred to APPENDIX C for details. The governing equation of motion is obtained as:

$$\mathbf{M}\ddot{X} + \mathbf{C}\dot{X} + \mathbf{K}X + \Xi = F(t) \tag{5.24}$$

Here, σ_1 and σ_2 impart energy to the stationary white noise excitation at each of the floor levels. The symbols M, C and K represent the mass, damping and stiffness matrices for the system. From the numerical solution of the above equation, the response vectors $x_1(t)$ and $x_2(t)$ can be obtained. Upon

expanding the governing differential equation term by term, the following equations are obtained:

$$\left.\begin{aligned} &m_1\ddot{X}_1 + c_1\dot{X}_1 + k_1X_1 + \alpha X_1^3 \\ &+c_2\left(\dot{X}_1 - \dot{X}_2\right) + k_2\left(X_1 - X_2\right) = F_1(t) \\ &m_2\ddot{X}_2 + c_2\left(\dot{X}_2 - \dot{X}_1\right) + k_2(X_2 - X_1) = F_2(t) \end{aligned}\right\} \tag{5.25}$$

A short note on the nature of the numerically simulated systems. It is worth noting the fact that the above mentioned systems are modeled using Duffing oscillator on either or both the floors; hence, these systems are *strongly nonlinear* in nature. From a different standpoint, it is a well understood phenomena that the damage occurred due to the change in the nonlinear parameter will immediately affect the neighboring DOF, thereby propagating at a faster rate as compared to the 5 storey B-W system. Being an inherently weakly nonlinear system, the B-W system preserves its temporal change in the nonlinear parameter that progresses at a comparatively slower rate on account of the higher number of DOF. An important point to note here is that the global damage eventuating in the systems are permanent in nature whose affects do not wear off as time progresses. This clearly certifies the fact that the systems undergoing global damage have certainly not repaired over the progression of time.

5.11 Temporal damage detection results using the hybrid algorithm

5.11.1 Detection results for the 2-storey Duffing oscillator model using hybrid algorithm

The results for damage detection for the 2 storey modeled with duffing oscillator on both floors using the hybrid approach is presented in this section. In this method, the damage is induced through a change in the nonlinear parameter α_1 as shown in Eqn. 5.23. As previously described, the change in the nonlinear parameter at a particular instant of time induces a global damage to the structure that does not wear off as time progresses. For the current study, the damage is induced to the model

through change of nonlinearity by 10%, 15% and 25% at a particular time instant of 35s from the start.

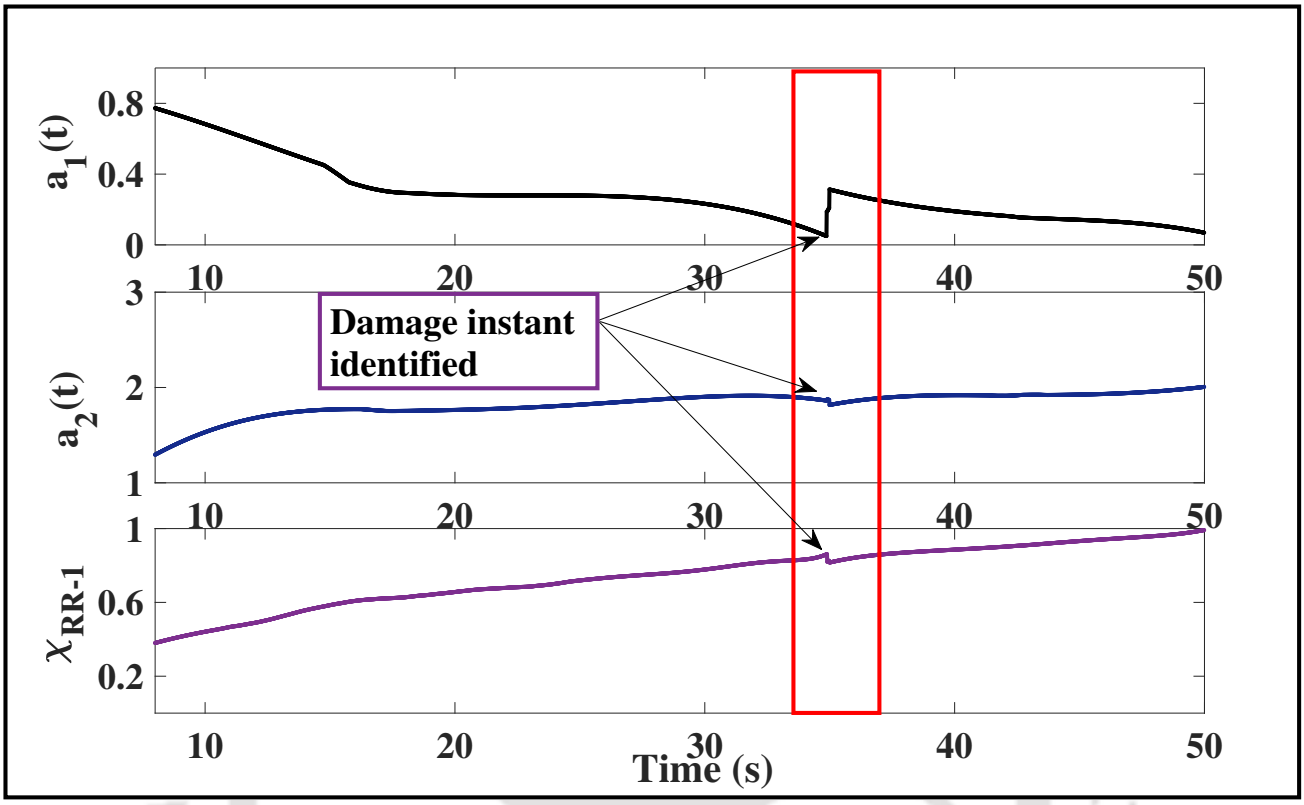

Figure 5.13: DSFs for 25% change in nonlinearity for 2 DOF Duffing oscillator

The detection results for 25% damage is shown in Fig. 5.13. It is evident from the figure that the plots of AR-1 and AR-2 clearly indicate an accurate damage instant at 35s, through a discernible change in the mean level at the instant of damage. The figure also shows the performance of χ_{RR-1} towards indicating the damage instant. It is imperative to note that the temporal RRE plots serve as a visual confirmation for the exact damage instant for the system. From the AR-2 plot, it can be observed that there occurs a period of activity even after 35s, that could be solely attributed to the nonlinear nature of the response and not a possible event indicating damage, which is verified from the use of the RRE plots that show distortion only at the damage instant. The detection results for 15% are clearly observable from fig. 5.14. The change in the mean level of the AR plots at 35s indicate the possible damage event for the system. From the AR plots, the presence of spurious peaks indicate of period of activity prior to the instant of damage. As previously explained, this arises due to the instabilities present in the system due to the nonlinearities involved. The distortion

in the temporal RRE plot at 35s confirms the exact instant of damage to the system corresponding to a 15% nonlinear change. Thus, it can be safely concluded that albeit these instabilities, the algorithm is equipped to address detection scenarios for nonlinear systems as well. The absolute percentage change in the mean level before and after damage is provided in Table 5.3. It can be observed that the absolute percentage change in the mean level decreases as the damage becomes finer, thereby indicating the efficacy of the proposed algorithm towards detecting lower percentage of damage in real time.

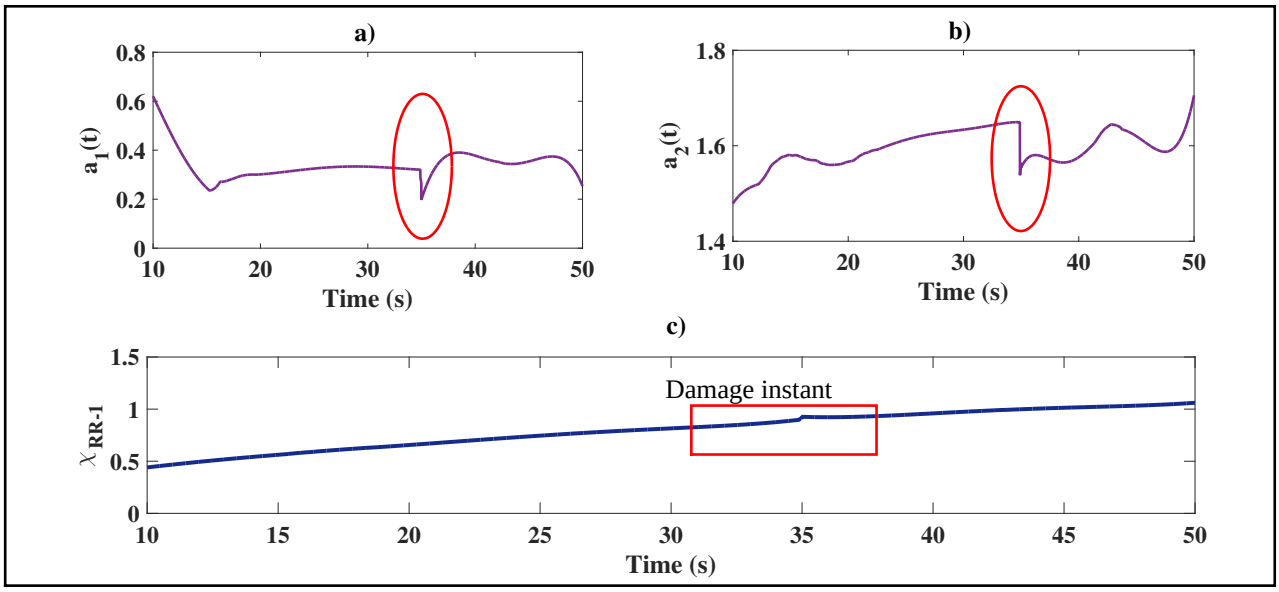

Figure 5.14: DSFs for 15% change in nonlinearity for 2 DOF Duffing oscillator

Previous damage identification studies have reported real time damage detection of the order of 15% for a single sensor data input using a FOEP based algorithm, RSSA. The FOEP based method, RPCA, is not expected to perform well for such a strongly nonlinear system and hence the detection results using RPCA have not been reported here for brevity. In addition, RPCA-TVAR FOEP based algorithm provides successful identification results for weakly nonlinear systems up to 15% global damage cases. Therefore, it can be well understood that the proposed hybrid approach fares better than the recently established online damage detection methods, extensively dealt with in chapters 2 and 3. The present study successfully identifies real time damage of the order as low as 10%, which is difficult, especially in an online framework. To the best of the knowledge of the author, this level of damage detection has not been reported in real time damage detection literature. The

results of damage detection for a 10% damage are displayed in Fig. 5.15. Although there appears to be a certain amount of activity before the instant of damage, the DSFs detect the exact instant of damage through a change in the mean level of the plots at 35s. As evident from the figure, the distortion in the RRE plot further confirms the efficacy of the DSFs as a potential tool for detecting real time damage as low as 10%. Although it can be understood from the figure that the efficacy of the RREs for lower percentage of damage is slightly questionable, it does not pose any impediment towards the current framework.

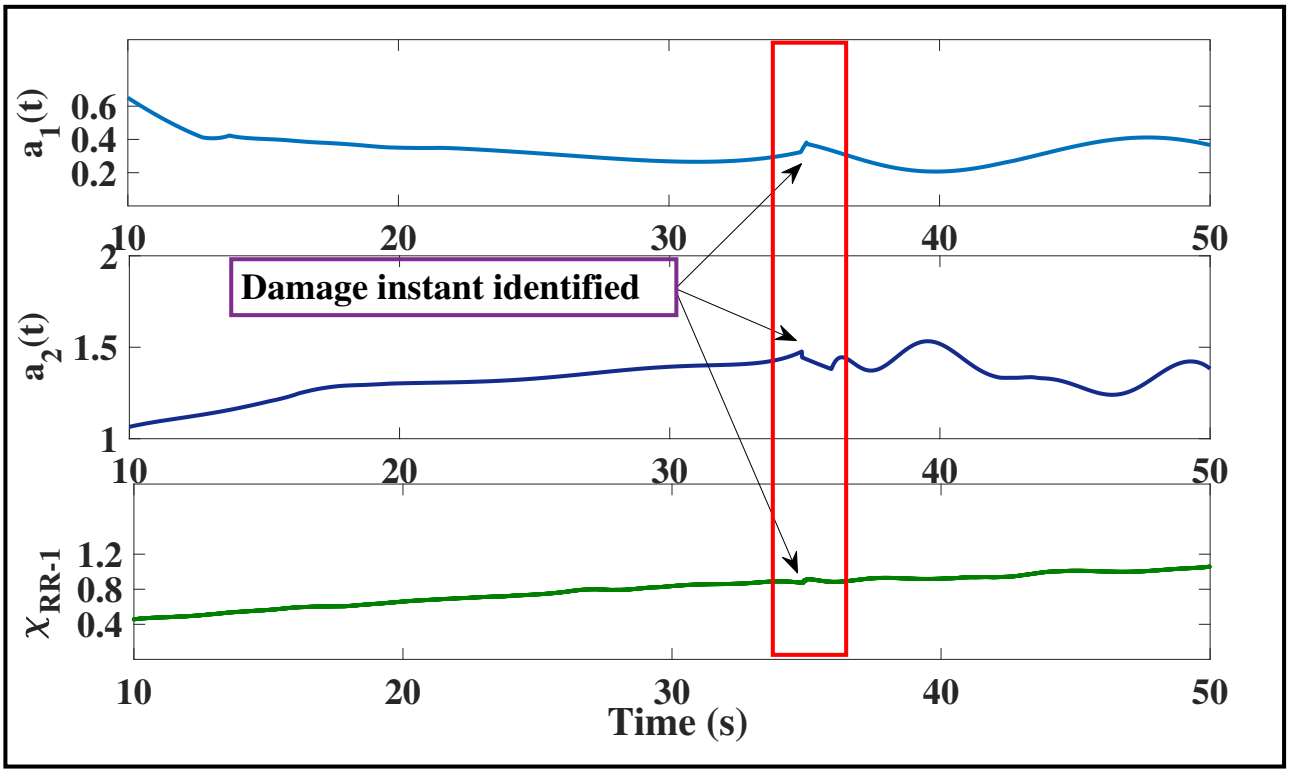

Figure 5.15: DSFs for 10% change in nonnlinearity for 2 DOF Duffing oscillator

5.11.2 Temporal damage detection results for the 2-storey modeled with Duffing oscillator at the base

Following the same lines of development, damage detection for changes in 20%, 15% and 10% nonlinear force term are sequentially presented. An important note to be considered here is the fact that the changes to the system are global in nature that do not wear off over time which indicates that the system has certainly not repaired from the effects of the damage as time progresses. The

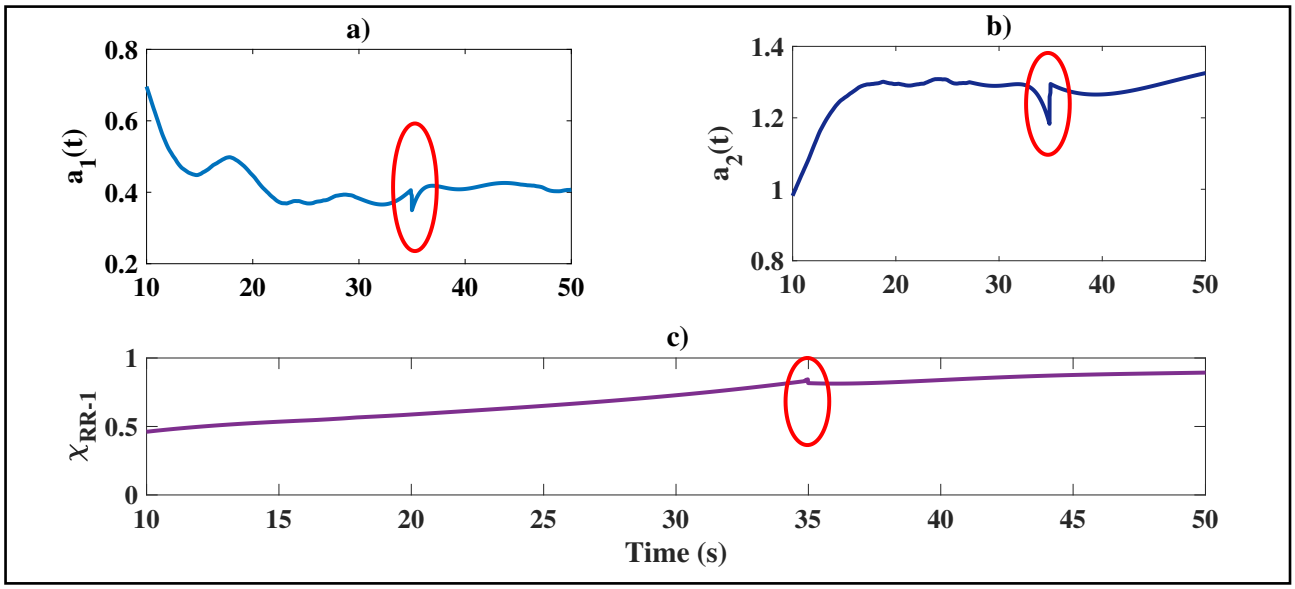

Figure 5.16: Damage detection using AR coefficients for 20% nonlinearity change

FOEP based example is applied to the raw vibration data in order to identify the exact instant of damage. Consider the first case where the damage is simulated for a 20% change at 35s. After the streaming data is processed by the algorithm, the DSFs are tracked online, recursively, in order to identify the exact instant of damage. Upon examination of the identification results shown in fig. 5.16, it is clear that the algorithm detects the exact instant of damage at 35s through the change in the mean level of the DSF plots. To verify these findings, the RRE plot clearly shows distortions at exactly 35s, thereby rendering the instabilities observed from the AR plots before damage as indicators of nonlinearities associated with the system. Thus, it can be safely concluded that the hybrid method detects damage exactly for the aforesaid percentage change in nonlinearity. While a change in the mean level of the TVAR plot verifies the damage instant to be at 35s, a distortion in the RRE plot indicating the exact instant of damage further reinforces the efficacy and robustness of the FOEP based hybrid approach. Through these discussions, it can be well understood that the proposed algorithm gives provides better detectability for an increased percentage of damage. The results, therefore, have not been reported here for brevity.

Proceeding to the next case, detection results for a 15% change in nonlinearity is provided in Fig. 5.17. As observed from the figure, the TVAR plots serve as a robust DSF for identifying damage. While approaching the damage instant, the plots show a sudden change in the mean level of the

graph that indicates a possible damage instant at 35s. The RRE plot shows a distortion at 35s, thereby validating the exact instant of damage for the system. To illustrate the potential application of the hybrid approach for a finer level of detection, the algorithm is applied for a 10% change in the nonlinear force term of the system. Through the TVAR plots, it can be seen that the exact instant of damage is identified at 35s for even a 10% change in the nonlinearity, which now establishes a finer level of detection as compared to the existing literature. Although the presence of certain system instabilities account for a gradual change in the mean level of the plot before the instant of damage is reached, the exact damage instant can be clearly observed at 35s from the plots. The RRE plot further verifies the damage instant through a sharp peak indicating the distortion in the subspace that occurs due to the presence of damage.

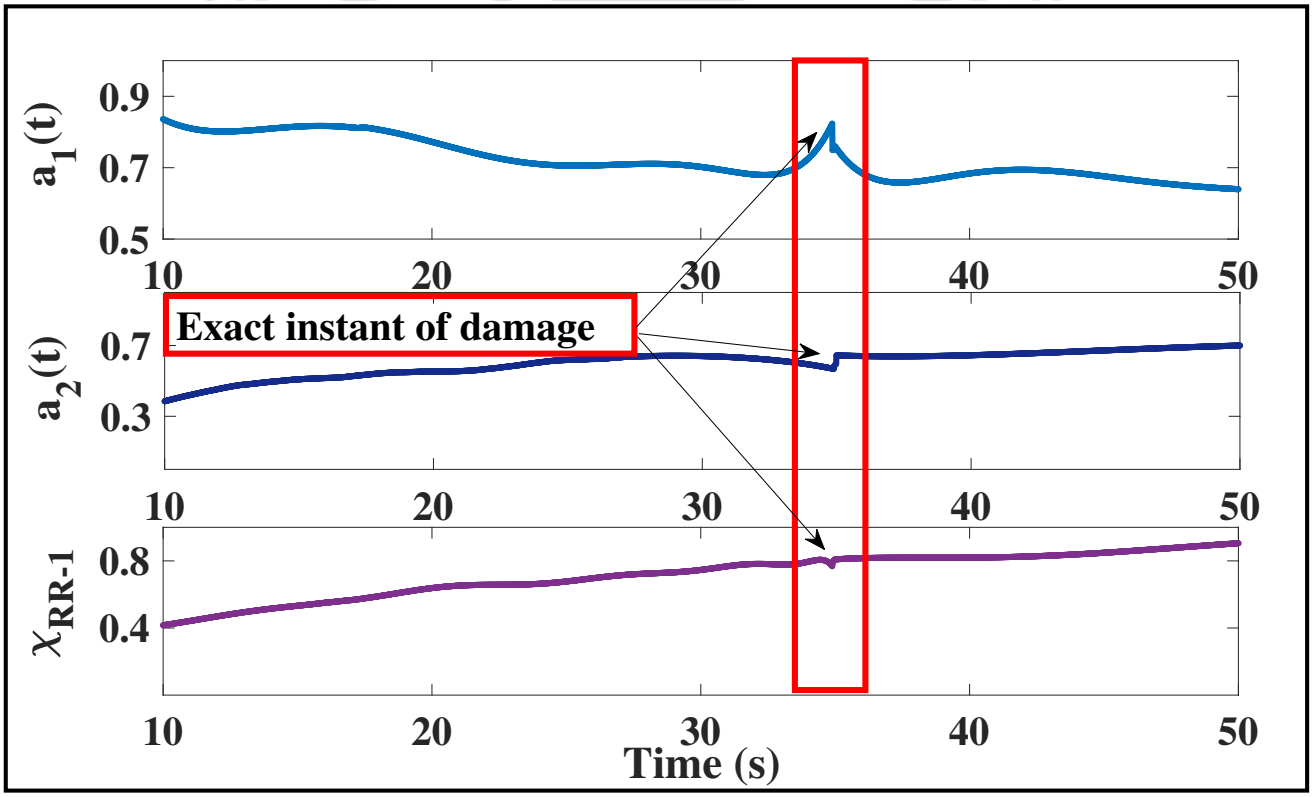

Figure 5.17: Recursive DSF plot for 15% damage

From the previously explored online damage detection studies, it is clear that RPCA-RRE based algorithm does not provide successful identification for such a low percentage of real time damage. It can also be perceived from prior case studies that the RPCA-TVAR algorithm fails to detect damage lower than 15% nonlinearity change. As the system under consideration is strongly nonlinear, the

RPCA-TVAR algorithm is not expected to perform under the specified changes in nonlinearity. From the present results, it can be concluded that the hybrid method provides better detectability than reported in the currently available literature [51]. It is well understood that the instant of damage can be accurately detected by the algorithm for the aforementioned changes in the nonlinear force term. However, it should be noted that a fine level of detectablility (such as 10%) for a nonlinear system is a difficult feat considering the essentially online nature of the implementation. The consistent evolution of the TVAR coefficients and the distinct change in the mean level of the plots at the instant of damage validates the efficacy of the said DSF. It can be observed from Table 5.3 that the absolute percentage change in the mean values lower gradually corresponding to the finer levels of damage. This provides ample evidence regarding the efficiency of the proposed method in detecting finer levels of real time damage. The time taken for a complete run of the algorithm is found to be 2.16s, that approximately emulates a real time process. The recursive implementation of the RPCA-RSSA module takes 10ms which is 0.46% of the total time consumed for a single iteration. However, the time consumed depends on the computational power of the system used and is more efficient for systems with superior processing power of the console used for computation.

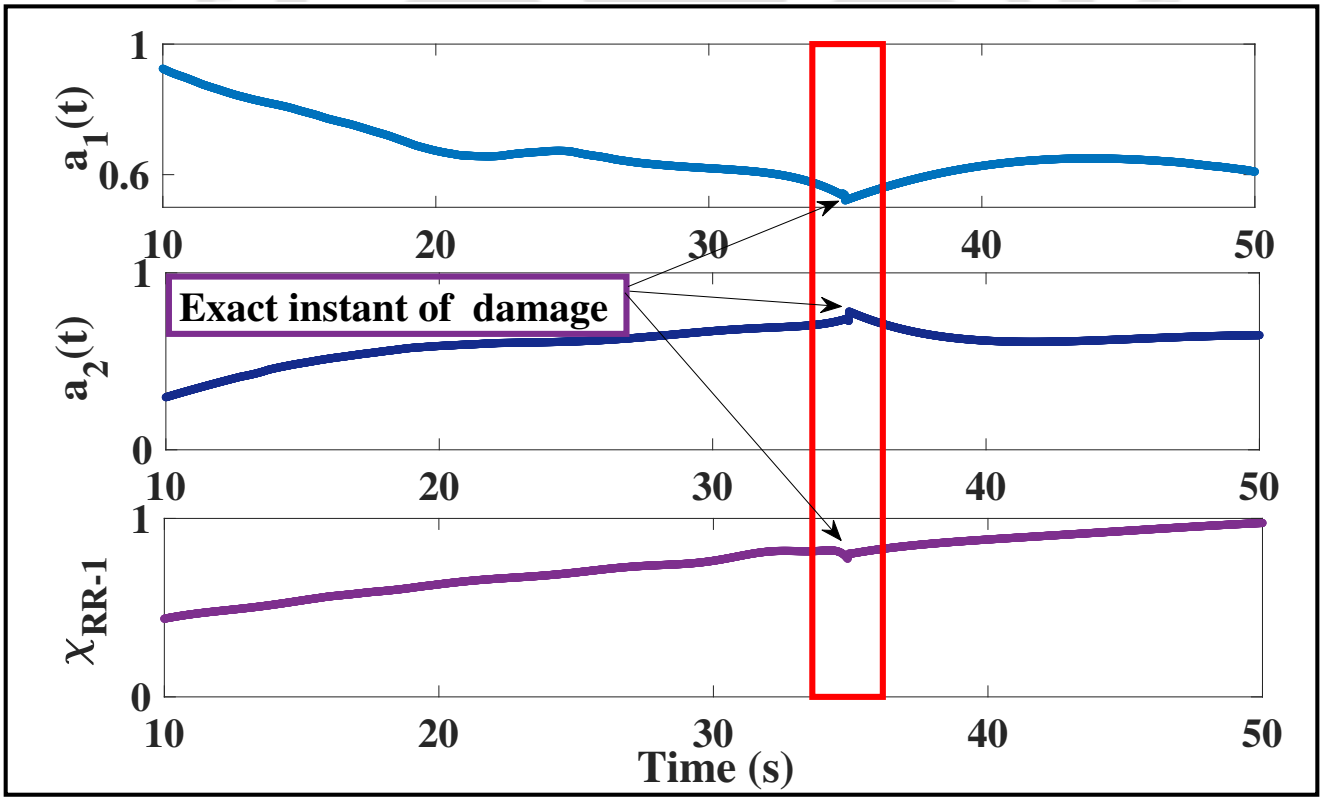

Figure 5.18: Recursive DSF plot for 10% damage

5.11.3 Temporal damage detection results for the 5 DOF B-W system

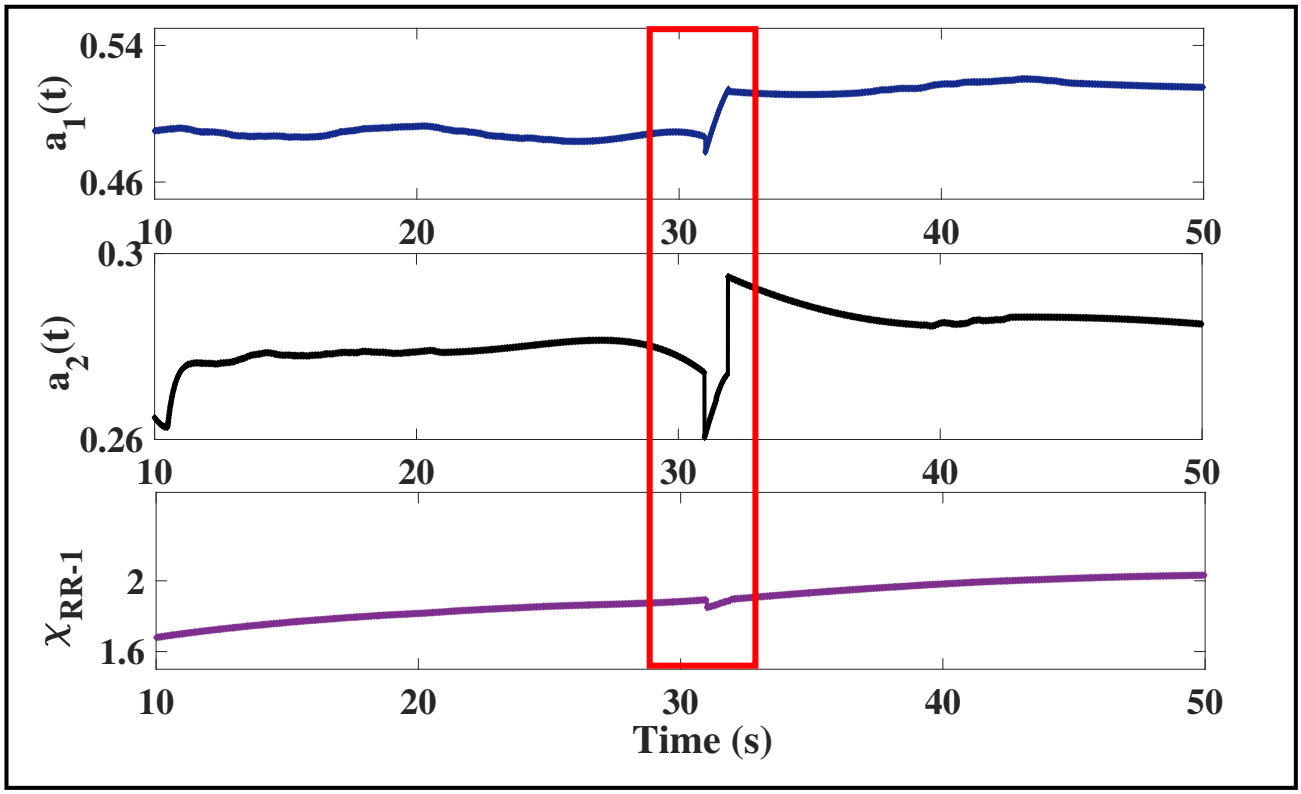

Figure 5.19: Recursive DSF plot for 15% damage for the B-W system

Case studies for 10% and 15% change in nonlinearity are provided in this section. A survey of the existing damage detection literature reveals that damages of the order of 15% have often been reported as a lower limit for real time vibration based damage detection [51]. However, FOEP based example successfully captures a damage as low as 10% for the B-W system previously described. From Fig. 5.19, a damage instant at 31s for 15% change in nonlinearity can be easily detected using the AR coefficients by observing sudden changes in the mean level of the plot. This confirms the use of TVAR modeling towards online damage detection for the B-W system in addition to the aforementioned nonlinear systems. To further validate the efficacy of the proposed methodology, temporal residual error when examined in a recursive framework, detects the instant of damage at 31s, as observed in Fig. 5.19. The absolute percentage change in the mean level of the recursive DSFs is provided in Table 5.3. A separate figure dedicated towards real time damage detection for a 10% change in nonlinearity is shown in Fig. 5.20. As observed from the figure, the plots of the TVAR coefficients show changes in the mean level of the plot around the 31s mark, indicating

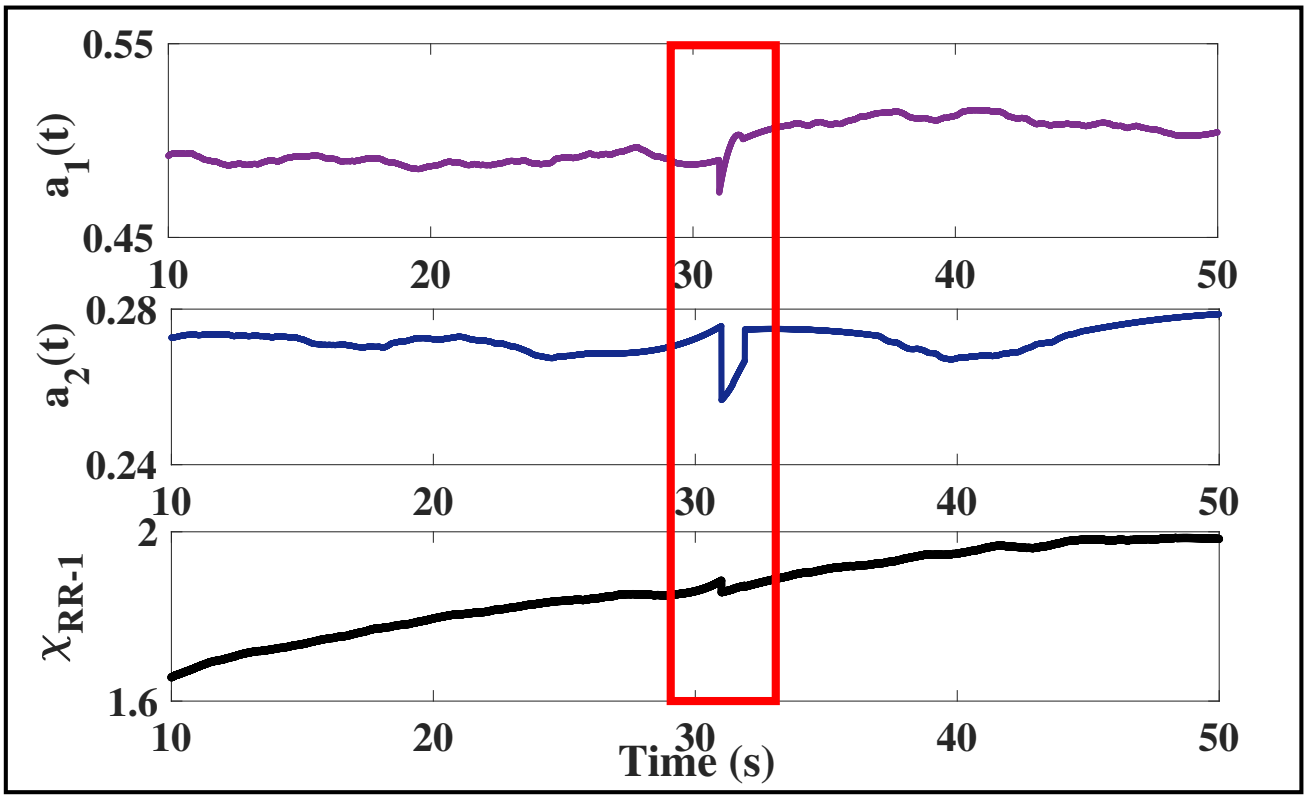

Figure 5.20: Recursive DSF plot for 10% damage for the B-W system

a possible event. In order to validate these findings, RRE is employed to check for distortions in the eigen subspace. It is clear from Fig. 5.20 that the distortions indicated by the RRE plot confirms the exact instant of damage at 31s. It can therefore, be concluded that the hybrid method is efficient in determining global damages as low as 10% for nonlinear systems in a recursive framework. The performance of the FOEP based example towards detecting spatial damage in a simultaneous recursive framework is described in the following section.

5.11.4 Spatial damage detection results for the B-W system

The concept of global damage discussed in the previous sections, pivots around the idea of changing the nonlinear parameter of the system. In the present section, the notion of local damage is presented by a change in stiffness for a particular floor which brings out the concept of online spatio-temporal damage detection. As already mentioned, only when the instant of damage in ascertained, the proposed algorithm shifts on to spatial damage detection module in order to find out the exact location of the damage. Previously reported literature suggests that a lower limit of 25% for spatial

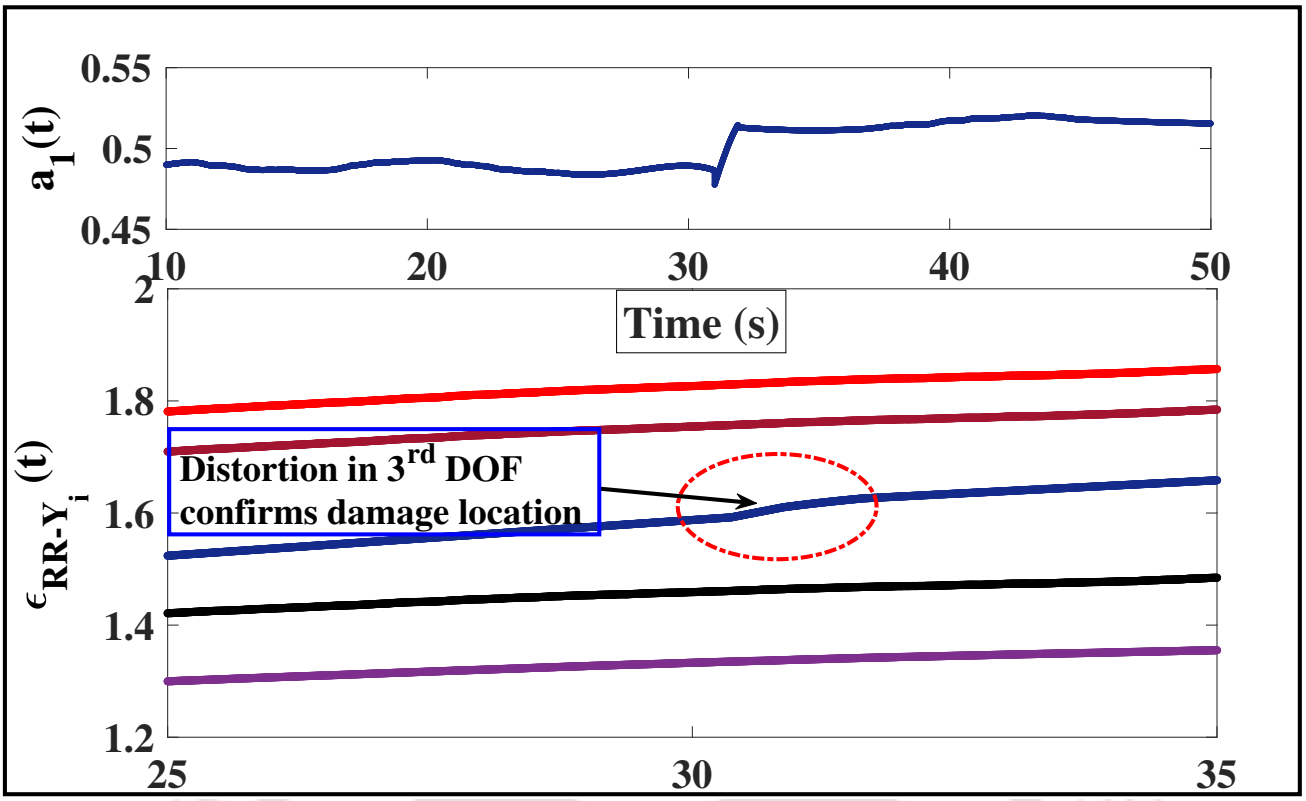

Figure 5.21: Recursive DSF plot for 15% spatio-temporal damage for the B-W system

damage detection case has been successfully reported through a standalone RPCA based formulation. An improvement of the detection potential to 15% has been observed from a recently published work that focuses on the spatio-temporal damage detection using only RSSA on the raw vibration response. One of the key entitlements of the present work is the development of the hybrid algorithm that provides an improved detectability towards real time simultaneous spatio-temporal damage detection in a single framework. Case studies are carried out on the B-W system that deals with 10% and 15% change in linear stiffness of the third storey at 31s. The system is assumed to be fully nonlinear by scaling the value κ to 1.

Once the instant of damage is detected, the proposed algorithm shifts on to the spatial detection module to localize the position of damage occurred to the system. From Fig. 5.21 it can be seen that a clear damage instant is identified for 15% damage through the deviation in the AR plot. As the damage instant is now ascertained from the AR plot, the spatial RRE in the neighborhood of the vicinity of damage (say 25s-35s) is examined. From the same figure, it can be clearly observed that the spatial RRE for the third DOF shows a significant distortion at 31s, as compared to the other

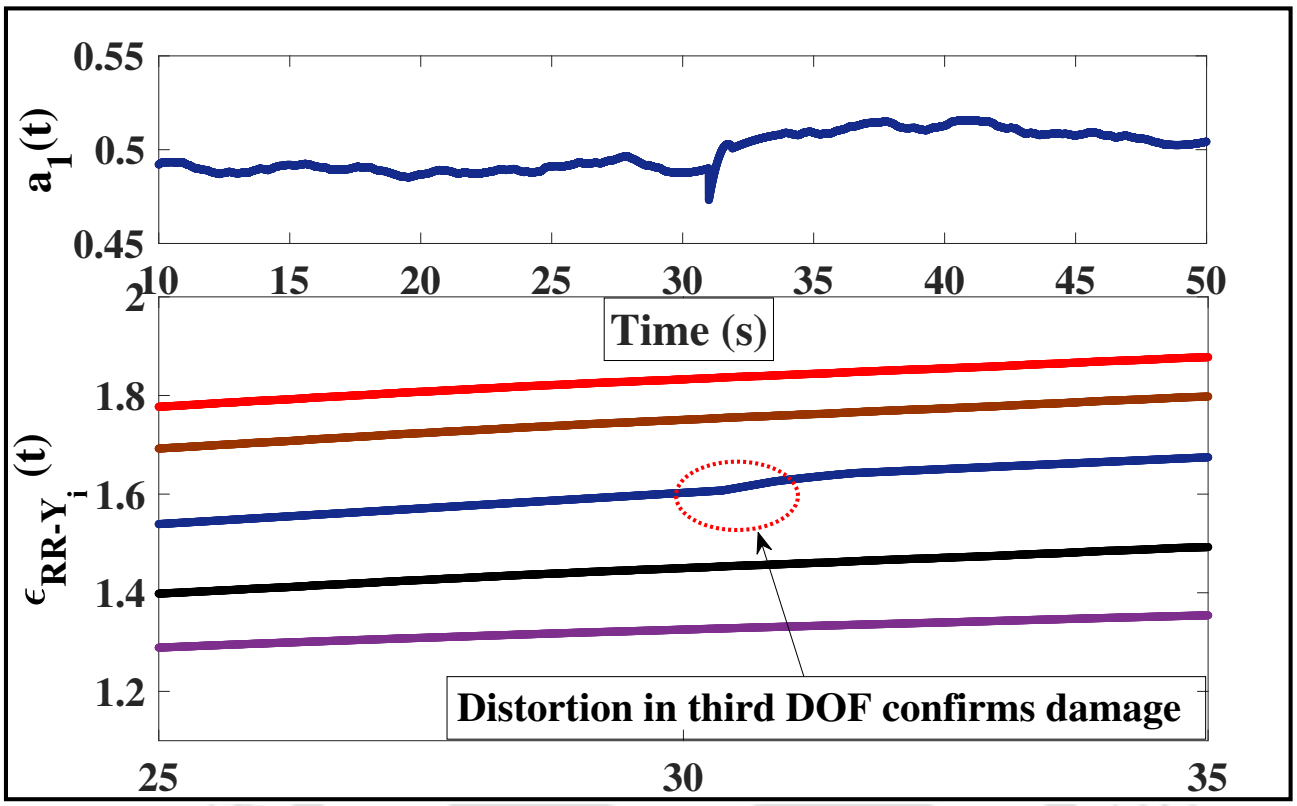

Figure 5.22: Recursive DSF plot for 10% spatio-temporal damage for the B-W system

set of responses originating from the corresponding floors. This validates the fact that damage has indeed occurred in the third storey of the structure. From Fig. 5.22, it is evident that the spatial RRE for 10% damage clearly indicates a significant distortion in the third DOF at 31s. As outlined before, the temporal and spatial detection module should run simultaneously. The changes in the TVAR coefficients and the local RRE are tracked online recursively in order to capture the essence of temporal and spatial damage detection, respectively. Albeit certain instabilities arising due to the nonlinear nature of the system and the real time nature of the proposed implementation, the distortions corresponding to the other DOFs is of minor importance and can be safely neglected. Moreover, these distortions are generally crowded around the 24s–27s mark, which does not even correspond to the exact instant of damage and could be safely ignored. An important point to be noted is that as the extent of stiffness degradation decreases, it becomes increasingly difficult to conduct spatio-temporal damage detection simultaneously in a single framework. The underlying complexity in determining damage location for lower percentage of stiffness degradation arises due to minor distortions of the eigenspace which becomes inconsequential as time progresses.

5.12 Results for El Centro ground excitation

The applicability of the FOEP based hybrid approach towards nonstationary excitation is an important aspect to ensure its robustness towards solving an expansive range of damage identification problems. There exists significant literature where established real time damage identification strategies have consistently failed to detect damage for nonstationary cases with a reasonable degree of confidence. This is primarily attributed to the inherent formulation of the damage detection algorithms that impede their possible execution for nonstationary events such as earthquakes. However, time series models work extremely well in capturing the key patterns of any data series without assuming any stationarity associated with the data. In addition, TVAR models capture the nonstationarity involved with any data that arises due to its inherent nature or due to the damage induced in the structure. In the present context, the numerical simulation is performed on the

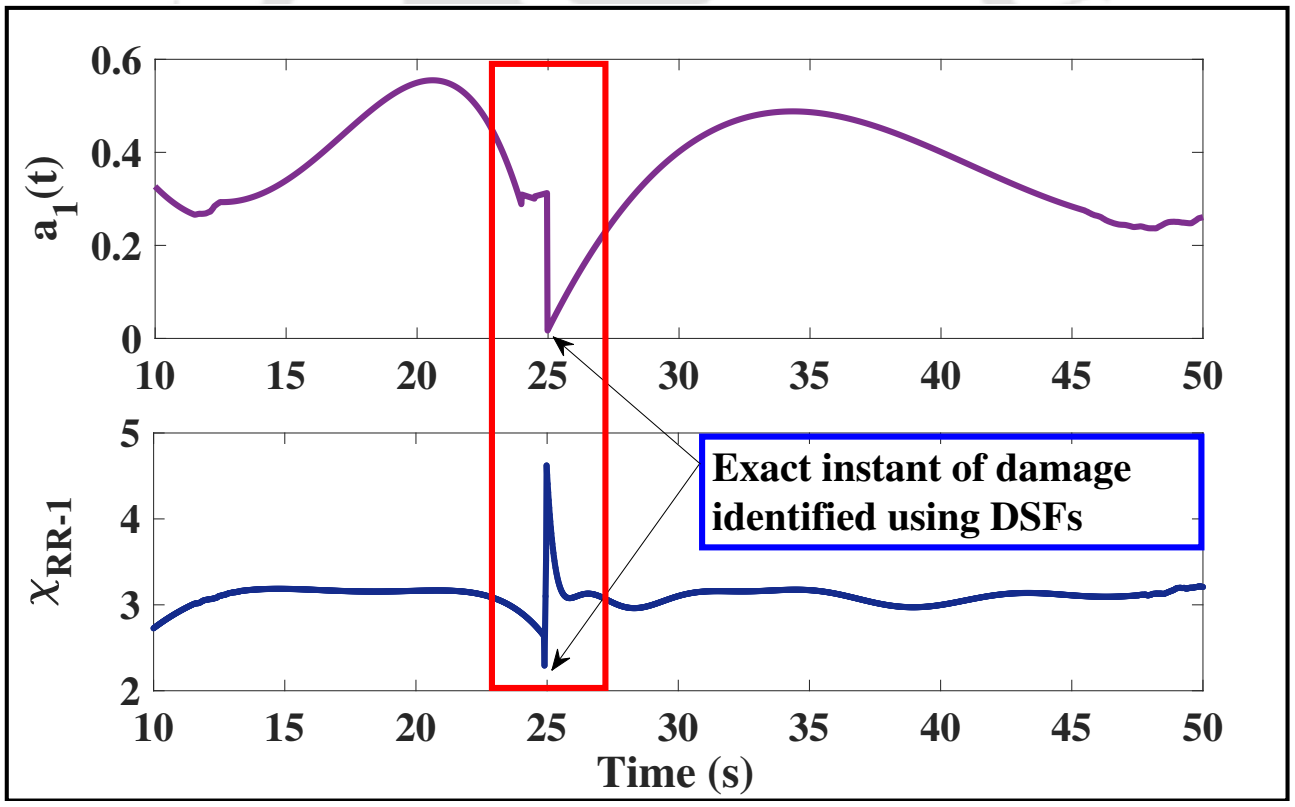

Figure 5.23: Recursive DSF plot for 25% temporal damage for the B-W system under El Centro excitation

B-W system using El Centro excitation data for a 25% linear stiffness change in the third floor at 25s. The proposed hybrid algorithm processes the data and the simultaneous tracking of the DSF

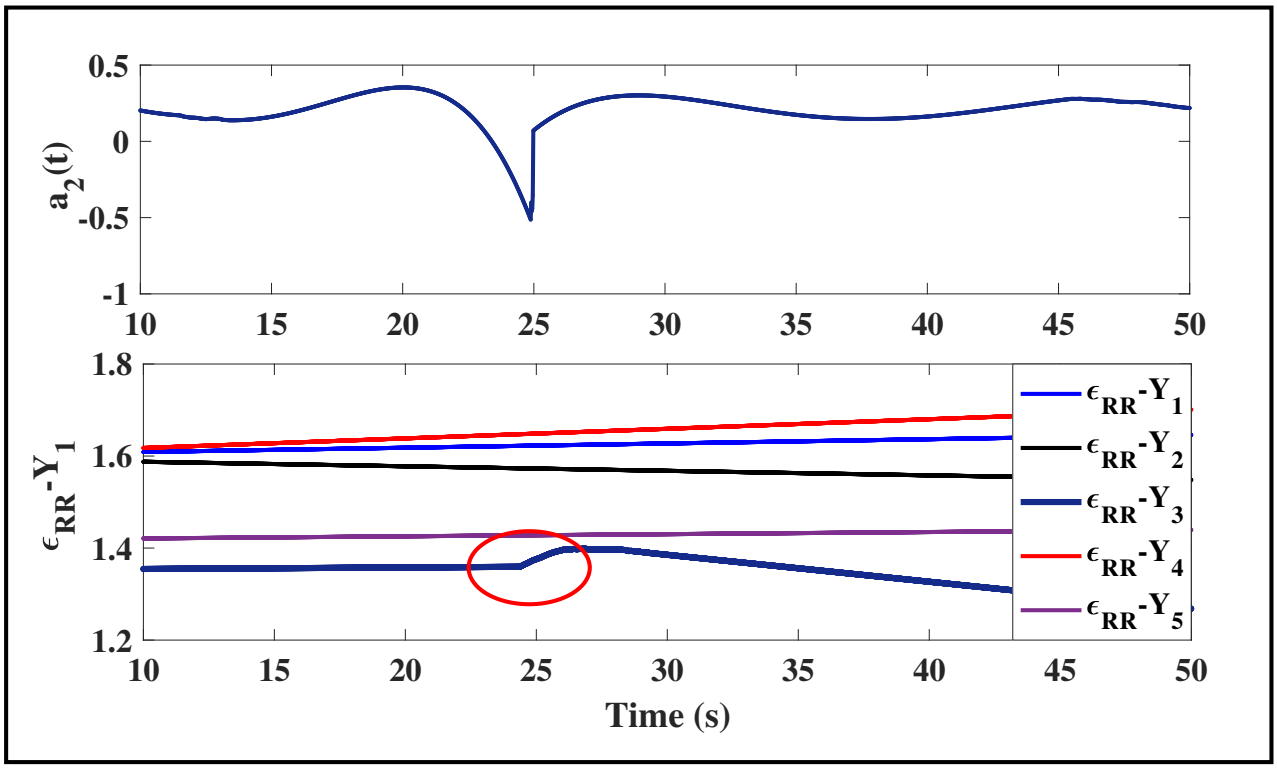

Figure 5.24: *Spatio-temporal* damage detection for 25% damage for the B-W system under El Centro excitation

are done online, recursively, in order to accurately identify the damage instant. In order to mask the behavior of the non-stationarity of the data, the TVAR models have shown successful results towards detecting the instant of damage, as observed from Fig. 5.23. In addition to the DSF plots, it is clear from the RRE plot that the deviation in the subspace due to damage is indicated through the distortion exactly at 25s, further reinforcing the fact that damage has induced in the structure at 25s. In the present damage scenario, once the damage instant is ascertained by tracking a change in the AR coefficients, the algorithm invokes the spatial detection module through the spatial RRE as DSFs. The spatial RRE in the neighborhood of damage is examined recursively. As observed from Fig. 5.24, the spatial RRE for the third degree of freedom shows a significant change at 25s as compared to the other set of responses which behave almost linearly throughout the excitation phase. This is a clear illustration of the localization of damage, manifested through a deviation in the spatial RREs for the structure. As evident from the literature, simultaneous spatio-temporal damage detection for nonstationary excitation has not been attempted in the purview of a real time fervor in a single framework. In a separate work, the author has successfully reported temporal

damage exclusively for nonstationary excitation for a 30% damage case. In the current scenario, spatio-temporal damage detection embedded into a single recursive framework for nonstationary excitation for a 25% damage case has been successfully reported. This confirms the superiority of the proposed method over the existing detection strategies currently available in the literature.

Table 5.3: Summary of real time damage detection results

Type of system	Excitation used	% change in nonlinearity	DSFs used	Mean (Undamaged)	Mean (Damaged)	Absolute % change in mean
2-storied Duffing oscillator	White noise	25%	AR1	0.46	0.27	41.30
			AR2	1.48	1.92	29.73
			RRE	0.56	0.64	14.29
		15%	AR1	0.48	0.29	39.60
			AR2	1.16	1.44	24.14
			RRE	0.55	0.65	18.18
		10%	AR1	0.5	0.32	36.00
			AR2	1.07	1.38	22.46
			RRE	0.56	0.64	14.29
		20%	AR1	0.49	0.30	38.78
			AR2	1.17	1.41	20.51
			RRE	0.72	0.83	15.28
2-storey with Duffing oscillator at the base	White noise	15%	AR1	0.83	0.66	20.48
			AR2	0.42	0.67	59.52
			RRE	0.54	0.85	57.41
		10%	AR1	0.79	0.67	15.19
			AR2	0.42	0.60	42.86
			RRE	0.54	0.86	59.26
B-W system	White noise	15%	AR1	0.49	0.51	4.08
			AR2	0.25	0.28	12
			RRE	1.50	1.81	20.67
B-W system	El Centro	25%	AR1	0.39	0.41	5.13
			AR2	0.27	0.19	29.63
			RRE	2.83	3.07	8.48
			spatial RRE	1.33	1.35	1.5

5.13 Comparison of all the developed FOEP based techniques

5.13.1 Performance check using B-W system

In one of the recently established works, the prospects of damage detection using RPCA in conjunction with TVAR modeling has successfully reported global damage detection in the order of 15%. In yet another work, damage detection using RSSA treating TVAR modeling as a DSF has also reported the same percentage of detectability, with an added advantage of single sensor input for damage identification. Thus, it suffices to say that both the aforementioned algorithms are efficient in detecting low levels of damage in real time. However, the performance of the RPCA-RSSA hybrid method surpasses the performance of the aforesaid damage detection schemes in terms of detecting even a lower percentage of damage, of the *order of 10%*. In addition, the proposed method has been successfully applied to strongly nonlinear systems to good results, as described in the previous sections. Therefore, one of the key novelty of the work arises due to the successful identification of a finer percentage of damage in real time. To the best knowledge of the author, such a fine level of detectability for strongly nonlinear systems in real time has not been reported in the literature so far.

In this section, the performance of the proposed method is compared with the recently established online RPCA and RSSA based damage detection schemes. The proposed hybrid method is compared against RPCA and its RRE, RPCA in conjunction with TVAR and RSSA considering TVAR coefficients as recursive DSFs for damage identification. It should be noted that as the proposed hybrid method is purely *online* in nature, comparison with traditional methods such as PCA [93], is not justified, since PCA is fundamentally different due to its inherent formulation that makes it essentially an *offline* algorithm. As PCA requires data to be processed in batches, windowing of the data becomes absolutely necessary for conducting damage identification studies which prevents any possibility of online implementation of the method. While RPCA updates the sample covariance matrix at each time stamp [135], the functioning of the RSSA algorithm involves the updating of the Hankel covariance matrix at each instant of time. A crucial point of contrast of the proposed

method with the established real time damage detection schemes is that the individual essence of real time updating of the matrices are done sequentially, viz., updating the sample covariance estimate at each time stamp followed by the updating the Hankel covariance matrix upon obtaining the transformed response from the RPCA algorithm. The key results using the newly proposed method

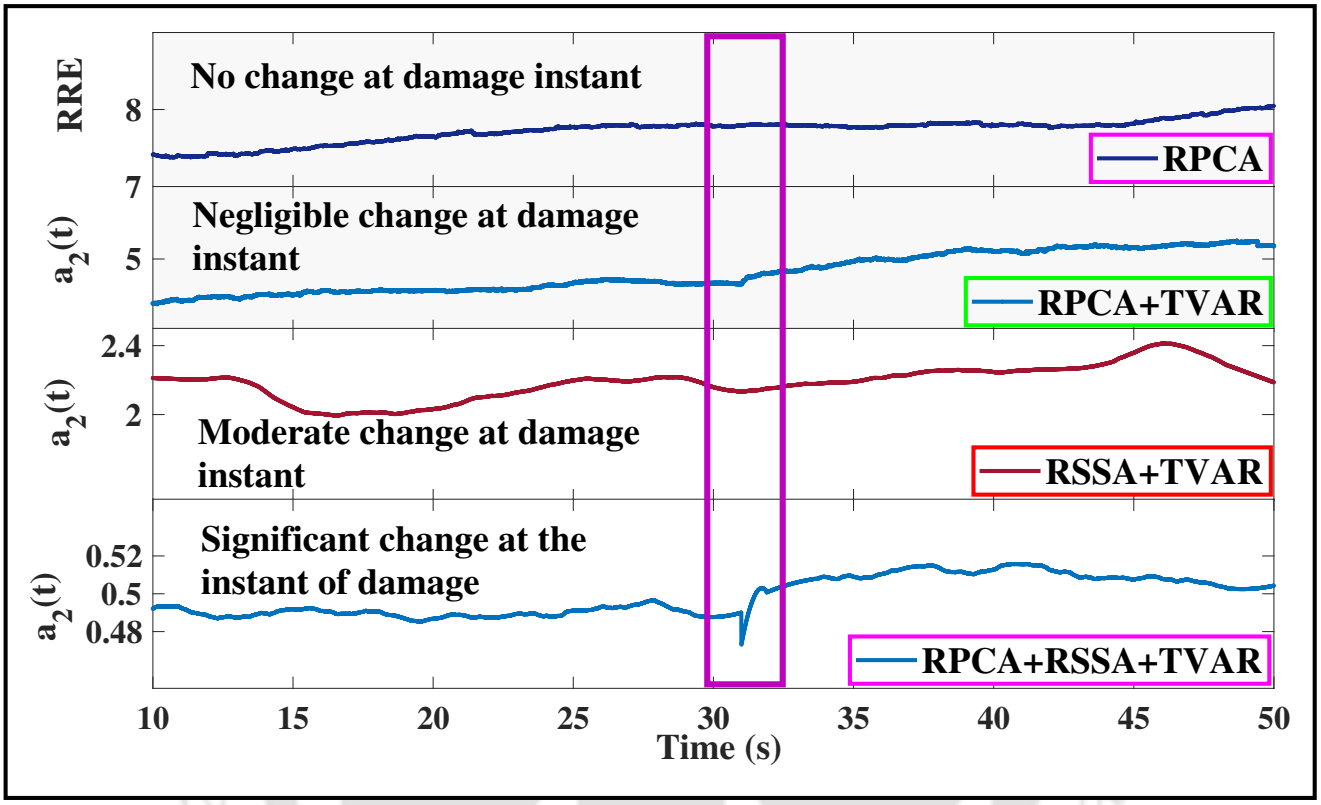

Figure 5.25: Comparison of the recently established damage detection methods with the proposed algorithm

are summarized and compared against the recently established damage detection strategies. In the present context, the comparative study is conducted on the 5 DOF B-W system under a zero mean Gaussian white noise excitation of 50s duration. A change in the third storey linear stiffness by 10% at 31s induces a local damage to the structure. The basis of comparison of the algorithms is to detect a change in the spatial orientation of the system in real time. As evident form the literature, the damage detection potential of the RPCA algorithm is confined to the order of 25% for spatial damage [41]. In addition, recently published works on RSSA towards damage detection indicate a lower limit of 15% for detecting local damage scenarios. As observed from the Fig. 5.25, the efficacy of RPCA-RRE, RPCA-TVAR and RSSA-TVAR algorithms is slightly questionable for 10% damage. While the RRE and AR plots corresponding to both RPCA and RSSA based algorithms fail

to show any significant deviation in the mean level at the instant of damage, the proposed method captures the instant of damage accurately and show a significant change in the mean level of the DSF plot. This confirms the superiority of the proposed algorithm over the established damage detection schemes. In line with the above findings, a tabular comparison of the algorithms towards percentage change in linear storey stiffness is provided in Table 5.4. From the results, it can be concluded that the hybrid algorithm is advantageous over the individual RPCA and RSSA based damage detection strategies in terms of an improved detectability of spatial damage in real time.

Table 5.4: Comparison of the existing damage detection methods with the proposed algorithm

Local damage (%)	RPCA-RRE	RPCA-TVAR	RSSA-TVAR	Proposed algorithm
35.00	Yes	Yes	Yes	Yes
25.00	Yes	Yes	Yes	Yes
20.00	**No**	Yes	Yes	Yes
15.00	**No**	**No**	Yes	Yes
10.00	**No**	**No**	**No**	Yes

5.13.2 Performance check using a 5 DOF structure with the third storey modeled as Duffing Oscillator

In this section, the FOEP improvised examples are applied a 5 DOF system modeled with a Duffing oscillator at the third floor. The purpose of modeling the third DOF with a Duffing spring is to induce nonlinearity to the structure through a storey stiffness and to ensure the robustness of the algorithm towards a more practical scenario as well. In the previous assumptions, the nonlinearity was confined at the base of the model that allowed the change in the nonlinear term to induce a global damage to the structure. As the damage induced affected the entire structure as a whole, the induced damage was reported to be global in nature whose affects did not wear out over the progression of time. Following similar thoughts, the present numerical model is also excited with a zero mean Gaussian white noise. The governing equation of motion is modeled as Ito's stochastic differential equation and subsequently discretized using Taylor's 1.5 strong scheme [155] considering a step size Δ= 0.01s. The governing equation of motion can be written as:

$$\mathbf{M}\ddot{X} + \mathbf{C}\dot{X} + \mathbf{K}X + \mathbf{\Psi}\mathrm{Z} = \mathbf{F}(t) \tag{5.26}$$

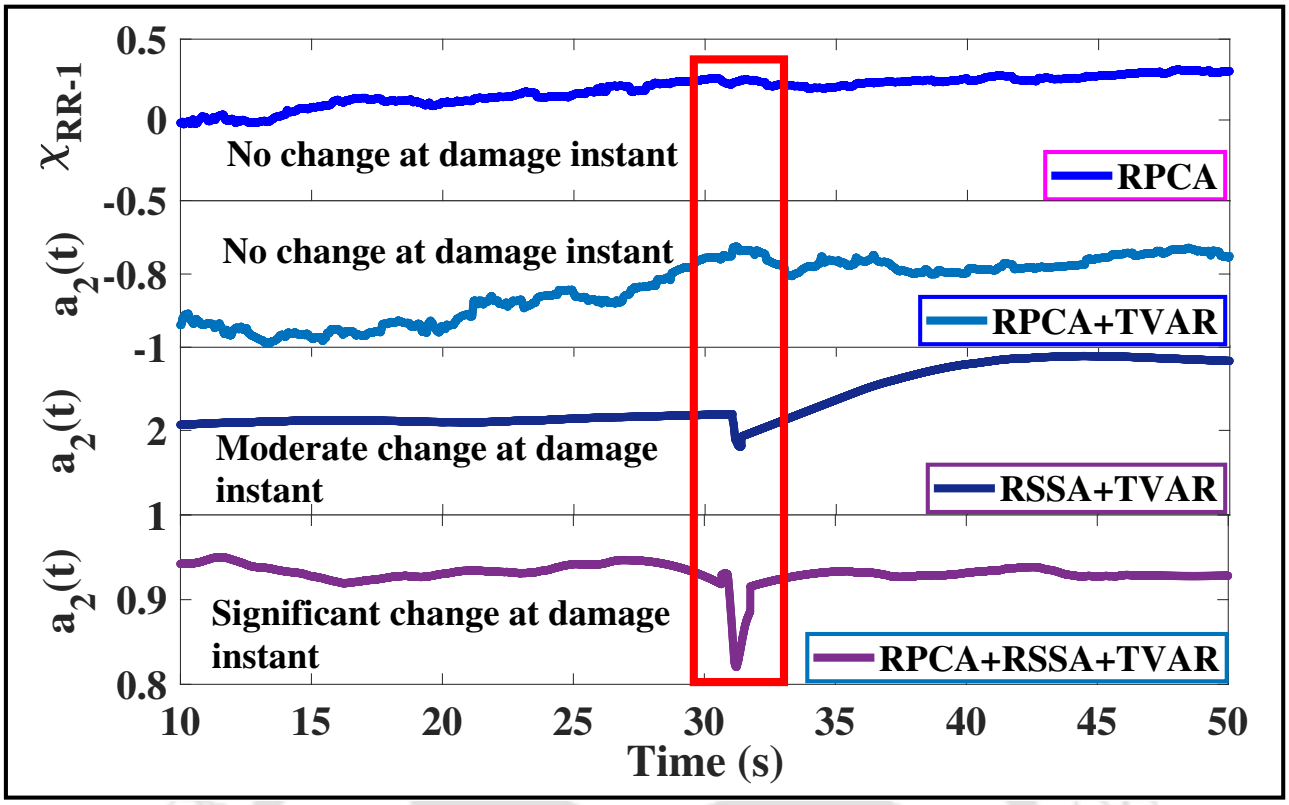

Figure 5.26: Comparison between the methods for a strongly nonlinear system

where **M**, **C** and **K** follow the similar notations as before. Ψ represents the location of DOF modeled with the Duffing oscillator and its neighboring DOF involved towards the formulation of the equation of motion. The vector Z represents a curtailed version of the operation $(X_2 - X_3)^3$ that arises due to the coupling of the DOF while obtaining the equation of motion. Interested readers are kindly referred to APPENDIX E for a brief derivation of the response using Taylor's scheme and the dynamical considerations of the same.

From Table 5.4, it is ensured that RPCA-RRE algorithm fails to detect spatial damage finer than 25%. Considering an even comparison among the established online damage detection methods for a 20% spatial damage, it is safe to conclude that RPCA-RRE algorithm can be ignored from the comparison scheme. As the system is strongly nonlinear, finer levels of damage detection is difficult, especially when applied in an online framework. The performance of the participating algorithms towards a localized event corresponding to a 20% damage is illustrated in Fig. 5.26. As observed from the figure, RPCA-TVAR algorithm does not indicate a significant change at the instant of damage. Although RSSA-TVAR algorithm shows a certain amount of distortion in the mean level of the plot at

the damage instant, the associated caveat with the methodology is the optimum placement of sensors that necessitates sensor instrumentation at the damage-induced DOF for capturing local damage. However, the proposed hybrid algorithm surpasses the performance of the established methods both in terms of detection potential in real time as well as placement of sensors, since a complete set of sensor response is adequate to detect local damage in the structure. A clear change in the mean level of the plot of the TVAR coefficient clearly distinguishes the efficacy of the proposed method as compared to its contemporaries. Thus, it can be concluded that the proposed methodology is advantageous over the established real time detection schemes even for systems having nonlinearity at individual storey level, in terms of an improved detectability of spatial damage in real time.

5.14 Experimental verifications

While addressing the facets of numerical case studies for the RSSA and hybrid approaches, the sequential treatment for each of the algorithms provided a steady development of thoughts which ultimately culminated into the effective comparison of the established real time damage detection schemes. Following similar trend, experimental case studies verified using RSSA are first presented, subsequently followed by the trials undertaken for verifying the efficacy of the hybrid method, discussed next in detail.

5.14.1 Experimental verifications using RSSA

Experimental studies were conducted in a laboratory environment to verify the applicability of the proposed algorithm towards solving real time damage detection problem. To substantiate the robustness of the proposed algorithm, two case studies have been presented:

1. An experimental model setup in a laboratory environment comprising of an aluminium beam excited by a ground motion, having a rubber strip attached to its free end.

2. A single degree of freedom (SDOF) system modeled as a cart attached to springs on either side of the mass experimented with a Gaussian white noise to detect damage through a change in the stiffness of the system.

Aluminum beam experiment

In this section, the applicability of the RSSA method is verified using the aluminum model, extensively described in the preceding chapters. The RSSA algorithm is applied on the raw acceleration data streaming in real time, acquired by the QuantumX DAQ. It can be observed from Fig. 5.27 that TVAR coefficient $a_1(t)$ shows a significant change in mean level of the plot at *33*s and persists with the same mean level till the end of the acquisition (experiment). This indicates the occurrence of damage at *33s* which is further validated by the use of ERD (Fig. 5.27 (b)) estimated in a recursive fashion over the data set processed by the RSSA algorithm. As observed in Fig. 5.27 (b), the peak at 33s clearly indicates the instant of damage. Thus, it is safe to conclude that the proposed method is effective in identifying the instant of damage in real time under experimental conditions.

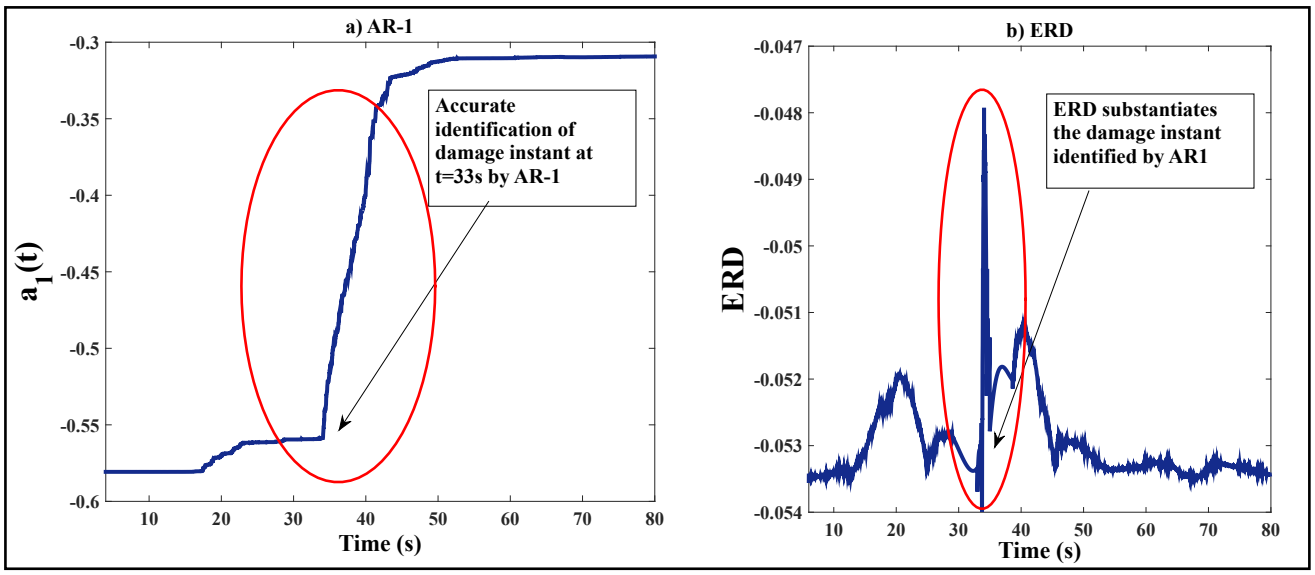

Figure 5.27: DSFs for the aluminium beam experiment

Toy cart experiment

Figure 5.28 shows the setup consisting of an SDOF system which is physically modeled as 100g mass cart attached with three springs on either side whose other end is connected to fixed supports. The combined stiffness of the attached spring assembly is calculated as 0.379 N/mm. The whole

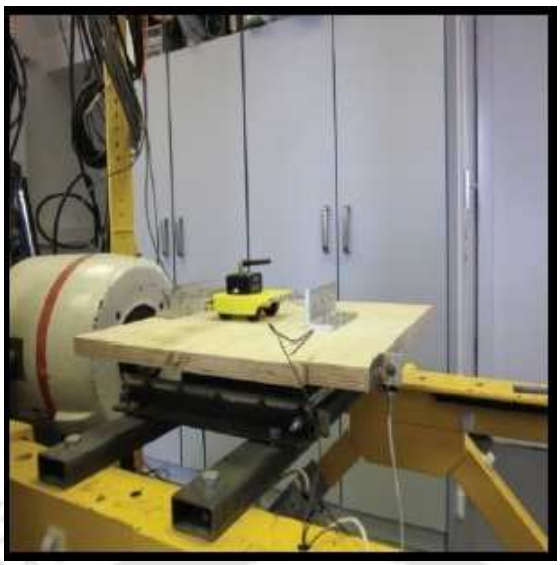

Figure 5.28: Setup for the toycart experiment (adapted from [153])

setup is arranged on top of a vibration bench which is excited by an input force of suitable intensity. The structural damping is usually considerably below critical damping and the system undergoes forced vibration. While assuming the damping of the simulated model, free vibration decay of the physically built model was considered and an estimated value of 2% equivalent viscous damping ratio was used. Accelerometers placed on top of the vibration bench and the mass cart measured the input acceleration and the output response data, respectively, at a sampling rate of 830Hz. In order to ensure the accuracy of the measured data, Laser Doppler Vibrometer (LDV) attached to the cart measured the velocity of motion at a sampling rate of 128Hz, to obtain the output acceleration data through integration. Although the springs are linearly calibrated in tension under static loading and to a certain displacement, the combined system is not guaranteed to exhibit linear model behavior as obtained from linear or weakly nonlinear simulations.

The experiment is carried out by subjecting the vibration bench to a Gaussian white noise excitation and the response data sampled at a prefixed frequency. During the vibrational motion of the mass cart, the springs are carefully sheared at a particular time instant, in order to simulate a real time damage scenario [153]. In the present study, two damage instances are created by shearing two different springs at different time instants. The first damage instant, at $t = 13$ seconds, reduces the overall stiffness from 0.378 N/mm to 0.303 N/mm (stiffness reduction of around 19%). The second break induces a stiffness alteration of around 17%, by reducing the equivalent stiffness from

0.303 N/mm to 0.249 N/mm at $t = 38$ seconds [153]. The detailed analysis using the proposed RSSA based framework is considered next.

The raw vibration data streaming from the accelerometer and LDV is accurately recorded at a fixed sampling rate using suitable DAQ. The proposed algorithm is applied to the acceleration data in order to identify the exact instant of damage. The damage instant is accurately identified by the DSF as observed from the Fig. 5.29. It is clear from the figure that TVAR coefficients $a_1(t)$ and $a_2(t)$ both show changes in the mean level at the instants of damages ($13s$ and $38s$, respectively). The proposed experimental verification further validates the sensitivity of the current framework to detect structural damages as low as 17%, for a practical scenario. As clearly observed from Fig. 5.29 (a) and (b), TVAR coefficients provide good indicators of damage for the observed damage cases. It should be noted that although the presence of noise during an experiment is inevitable, the algorithm still detects the damage instants to a fairly good level of accuracy. The successive instants of damage are efficiently captured by the recursive coefficients, indicating that the algorithm works well even for cases with multiple damage.

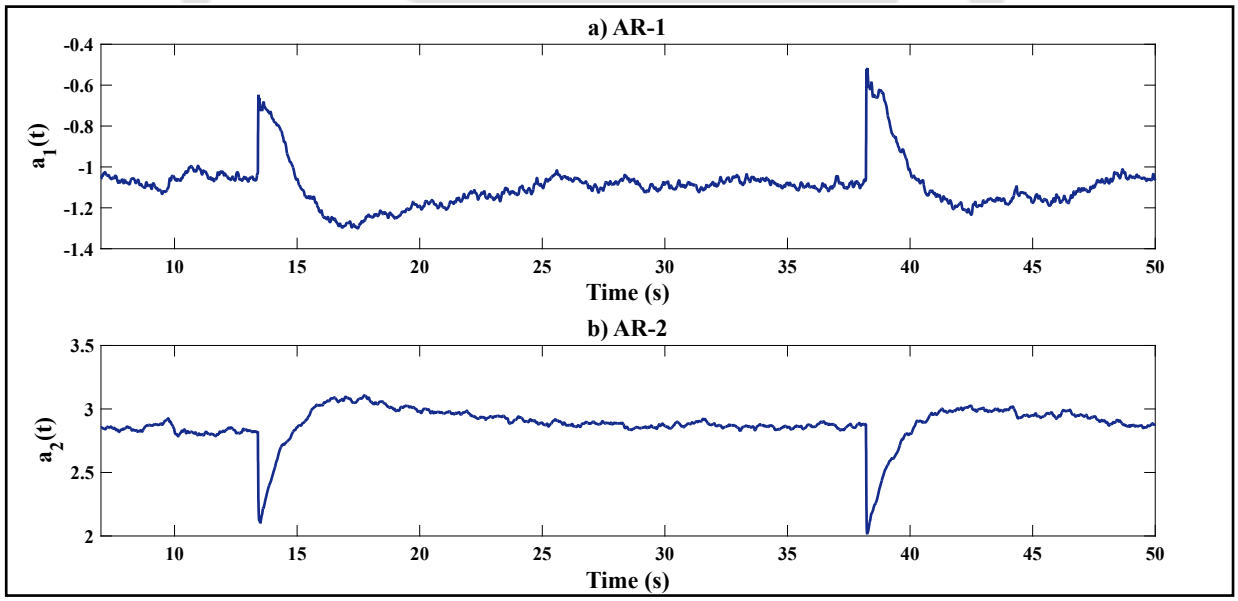

Figure 5.29: DSFs for the toy cart experiment

It should be noted that for slowly decaying mechanisms such as corrosion, the impact of the embedded variables play a significant role in determining the accurate instant of damage, leading to a mixing of the original and the newer states. The embedded variables need to be processed in batches.

The difficulty in measuring the real time changes in environmental and operational conditions (such as temperature, humidity, wind, etc.) arises due to cost factors, complexity in determining the optimal locations of sensors and susceptibility towards false detections. These slow varying processes might hinder the applicability of the proposed algorithm towards real time implementation and might lead to the masking of environmental variations. The potential implementations of the proposed algorithm range from real time damage detection of civil structures, to data-driven mechanical and aerospace applications where the acquisition of time series data is possible. Multiple real life possibilities range from fault detection of gear boxes, detection of cracks in airplane to nonlinear damage detection in structures, instrumented with either a single sensor or even a dense array of sensors located at strategic points for health monitoring. The proposed algorithm shows effective results even for multi-channel inputs, in a recursive framework, closely emulating real life instances where the structures are subjected to low levels of damage due to external excitations.

5.14.2 Experimental verifications using the hybrid approach

Vibro-impact experiment

Vibro-impact systems are encountered in many engineering applications such as vibro-impact response of heat exchanger tubes to aerodynamic excitation impact of floating ice with ships, slamming of ocean waves on off-shore structures, ships colliding against fenders, and so on. The concept for analyzing near-elastic vibro-impact problems using contact force over a test specimen greatly motivates the current experimentation scheme. Fig. 5.30 shows the setup consisting of an aluminum beam with a steel impactor attached to the free end. The entire setup is mounted on top of a fixed bench that restricts the sliding movement during the vibration testing procedure for the beam. The experimental setup is similar to the one described in the previous section, exclusive of the latex strip that was attached to the free end. Three accelerometers placed on the beam record the streaming vibration data that is acquired by the DAQ for real time processing through the proposed method.

The experiment is carried out by subjecting the aluminum beam to a scaled white noise of 0.7 intensity. The impactor is fixed at a vertical gap of 5mm from the initial rest position of the beam and is maintained throughout the experiment duration. Upon externally exciting the beam, the

Figure 5.30: Vibro-impact experimental setup

occurrence of repeated impact of the beam on the steel impactor was observed. However, it was found that the recurrence of impact was not uniform due to the randomness present in the input excitation. The impact mechanism continued for a period of 20s after which the vertical distance between the steel impactor and the aluminum beam was increased in order to avoid continued impacts on the beam-impactor system. The entire experiment lasted for a duration of 50s. The analysis of the data through the proposed method is described next in detail.

The proposed method is applied on the streaming vibration data acquired by the DAQ in real time in order to identify a change of state for the system. As previously mentioned, one of the key contributions of this work is to assess the *state of the system* (linear or nonlinear) along with detecting damage in real time. It can be very well understood from the experiment description that the entire setup was exposed to a nonlinear regime, attributed to the fact that the steel impactor provided the basis of nonlinearity in the setup. On removing the impactor after a period of 20s, the linear vibration of the beam due to external excitation continued for 30s. As clearly observed from Fig. 5.31, the TVAR plots show significant activity in the region from 0-20s, indicating a nonlinear state of the system. After 20s, due to the removal of the impactor, the setup was transformed

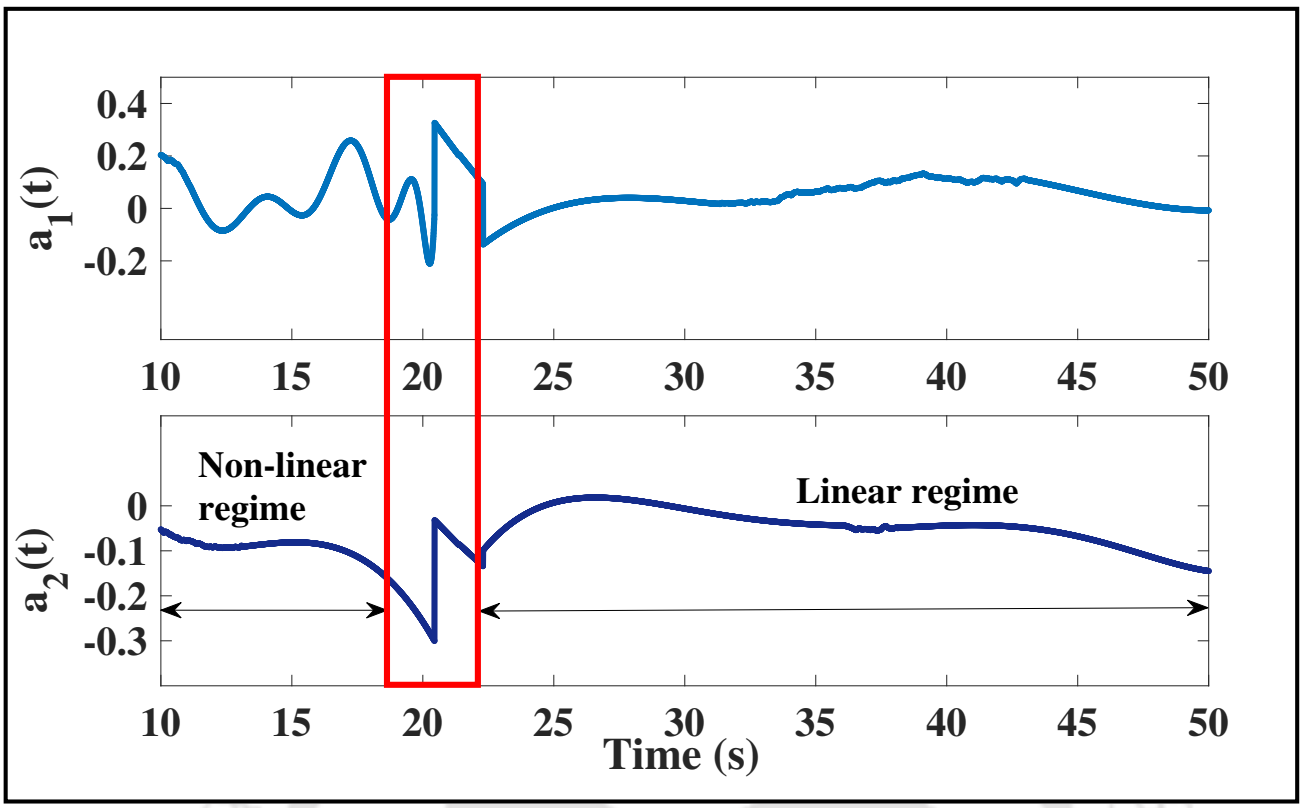

Figure 5.31: DSFs for the vibro-impact experiment

into a linearly vibrating system, reflected by slowly varying undulations of the TVAR plots. The change in the mean level after 20s is gradual, as compared to the nonlinear state of the setup, which demonstrates the efficacy and robustness of the algorithm towards distinguishing between contiguous states of the system.

5.15 Practical case studies

The applicability of the proposed FOEP based algorithms towards large data dimension is an important aspect to ensure their robustness towards practical problems as well. In this regard, it becomes imperative to assess the performance of these algorithms individually for a crisp understanding of what the detection results actually entail. Based on the previous detection studies on UCLAFB using the RPCA based approaches, it was easy to distinguish between the onset of the Parkfield earthquake and its pronounced damage effects on the floors of the structure. The present detection study involving RSSA algorithm provides a similar visualization through the DSFs. However, the

advanced hybrid approach clearly identifies the change of state of the system, the details of which are presented next.

5.15.1 Case study for the UCLAFB using RSSA

In order to examine the efficacy and damage detection potential of the proposed algorithm, floor accelerations due to the combined ambient data and earthquake data response are considered. The vibration response obtained from the data-base server suggests that a considerable incidence of nonstationary activity in the vicinity of t=360s indicates the onset of the Parkfield earthquake. Out of the 48 responses obtained from the data set, the translational responses are utilized for online processing using the proposed algorithm. The acceleration response of the roof and third floor for the E-W component are considered for a close analysis through the proposed RSSA based algorithm.

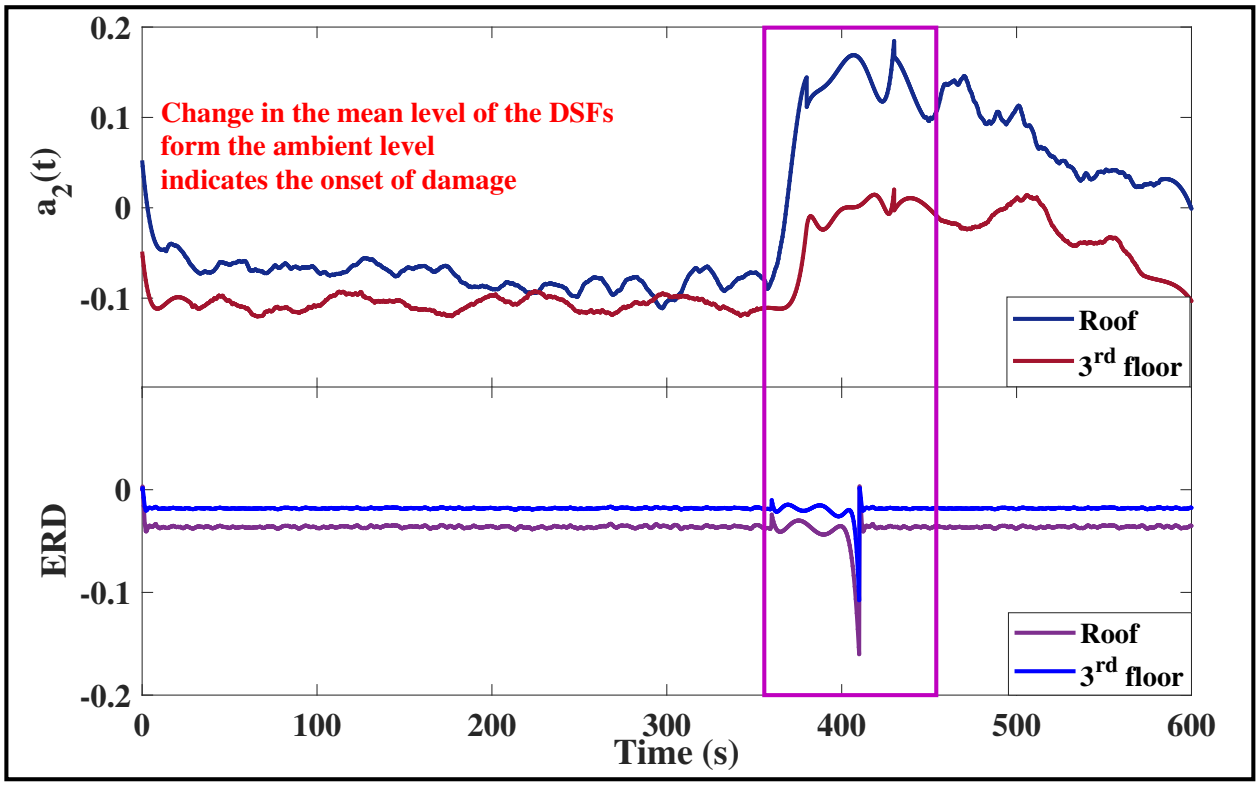

Figure 5.32: DSFs for the UCLAFB

It is evident from Fig. 6.31 that the change in the mean level of the AR plot for both the floor responses around t=380s indicates the onset of the earthquake that continues upto t=410s,

indicative of pronounced structural damage. It is normal to expect these two instants to be different from each other because it takes a finite time for the structure to undergo significant changes, reflected through a change in stiffness. In addition to the AR plots, ERD plots (Fig. 6.31) examined in a recursive framework, show deviation from the ambient regime at around t=380s and significantly in the vicinity of t=410s indicating the occurrence of damage. Hence, it can be concluded that the proposed algorithm could be extensively used for damage detection of real life structures involving large data dimension under nonstationary cases as well.

5.15.2 Case study for the UCLAFB using the hybrid RPCA-RSSA approach

In line with the previous discussions, the set of translational responses are provided as input to the proposed hybrid algorithm. TVAR modeling is carried out on the transformed response and the eigenspace obtained is tracked using the proposed DSFs. While the entire dataset is required for evaluating the eigenspace using RPCA, the transformed response obtained from the *roof* is eventually taken into consideration for the RSSA module. It is evident from Fig. 5.33 that the ambient regime continues until the 380s mark, after which the mean values of the DSFs begin to deviate. The mean values of the TVAR plots, examined in a recursive framework, show significant deviation around 410s, indicating the occurrence of pronounced structural damage. It is worth noting the fact that while the recently established real time damage detection schemes provide ample evidence to differentiate between the onset of occurrence of earthquake and its effects, the hybrid approach provides a utilitarian distinction of the change of state due to the earthquake. The DSFs portrayed in Fig. 5.33 clearly distinguishes the change of state from the ambient regime of the response to the one affected by the onset of earthquake. Hence, it can be concluded that the hybrid algorithm is well suited to handle practical situations involving large data dimension under nonstationary cases as well.

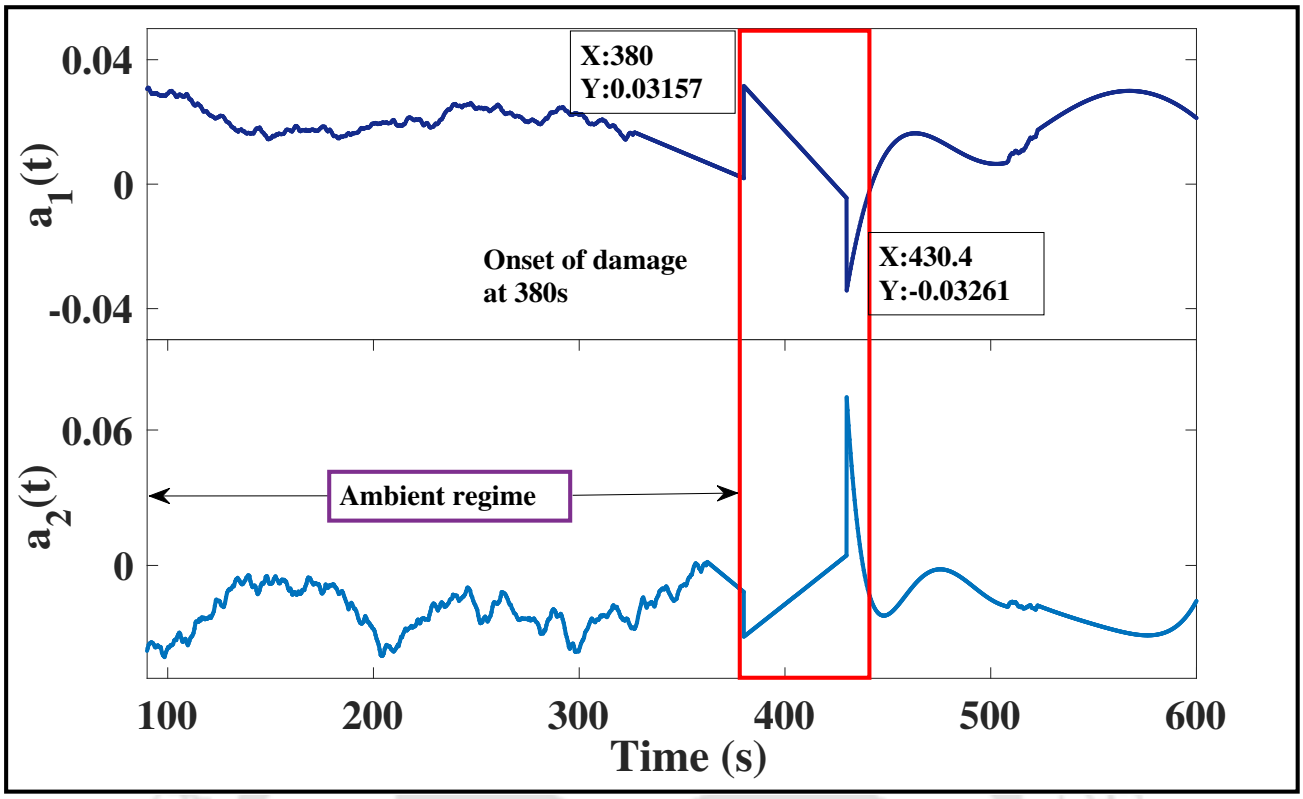

Figure 5.33: DSFs for UCLAFB

5.16 Summary

Real time damage detection algorithms for vibrating systems premised on RSSA in conjunction with TVAR model and a hybrid approach using RPCA-RSSA is presented. Recursive updates of the eigen subspace using rank one perturbation facilitated real time evolution of the principal components, eliciting the maximum information contained for damage detection. Subsequent modeling of principal components explaining maximum variance makes the transformed response amenable to a low order TVAR model which is a key step of the proposed framework. The use of TVAR coefficients as viable DSFs facilitated real time damage detection for the system. The potential of ERD towards an online implementation provided substantial evidence to validate the damage instants detected through the use of TVAR coefficients. The proposed framework provided successful detection results for damages even up to 15% for the white noise excitation and up to 17% stiffness reduction for the experimental case. RMSSA provides good detection results upto 30% linear stiffness change for a particular storey. The RSSA method shows accurate damage instants through changes in the mean level of the plots for numerically simulated systems. Case studies show that the algorithm is equally

capable of detecting damage online through experimental setups based on global damage schemes.

One of the key objectives of this study was to unify the RSSA based framework to improvise it for detecting finer levels of damage without compromising on the time complexity and at the same time catering to application specific problems. This has been successfully carried out in this chapter using the hybrid RPCA-RSSA framework and applied for numerical simulations, verified using experimental case studies and implemented on practical problems as well. Based on the conclusions, it can be certified that the hybrid algorithm is well equipped to detect real time damage as fine as 10% even for nonlinear systems. In addition, the applicability of the method towards practical scenarios demonstrate its effectiveness in determining the transition of state. Hence, it can be concluded that the proposed methods have shown to perform well for nonlinear systems excited with both stationary and nonstationary datasets which is clearly advantageous from a real time damage detection standpoint. The following chapter deals with the exhaustive development of a new recursive algorithm, RCCA, inherently formulated on the utilization of multi-directional datasets towards recursive damage identification.

Chapter 6

Real time structural damage detection using recursive canonical correlation analysis

In this chapter, a new real time structural damage detection strategy is developed that aims at identifying spatio-temporal damage patterns, online. The method, known as *recursive canonical correlation analysis* (RCCA), is a direct recursive extension of the traditional *canonical correlation analysis* (CCA). The chapter begins with a brief introduction to the need for using the algorithm and moves on to the detailed methodology developed for detecting damage in real time. Numerical simulations carried out on both weakly and strongly nonlinear systems demonstrate the applicability of the method and its exclusive superlative performance over the previously discussed RPCA algorithm, that greatly motivates the scope for implementing the proposed method. Experimental verifications on an idealized 2 DOF shear building model, followed by a full-scale demonstration of the method on the UCLAFB, demonstrate the robustness of the algorithm . The key results and discussions are presented next, followed by some important conclusions. The important acronyms used in this chapter are provided in Table 6.1.

Table 6.1: Important acronyms

CCA	Canonical Correlation Analysis
RCCA	Recursive Canonical Correlation Analysis
ICA	Independent Component Analysis

6.1 Motivation

A majority of the response based detection schemes comprise of data-driven statistical techniques developed primarily in the field of classical time series analysis, signal processing algorithms and multi-variate statistics, that show enormous potential in identifying the key patterns of these series. In this context, algorithms premised on EVD of the covariance matrix of the physical response, such as PCA [92], have enormously contributed to a multitude of structural dynamics applications. A powerful statistical technique developed in the recent years, CCA, utilizes the block covariance matrix of the physical responses in order to measure the underlying correlation between two sets of multidimensional variables [139–150]. The primary objective of CCA is to find projections such that the mutual correlation coefficient is maximized [148–152]. In addition to multivariate statistical analysis [143, 144], statistical imaging [146, 147], social and behavioral depiction studies [141], the underlying concepts of CCA are utilized in finding key patterns of time series [150] for both linear and nonlinear systems [151], and are also applied in meteorological studies [145] and flood frequency estimation [149]. The method takes into account the eigenspace characteristics, which could be globally tracked to ascertain the damage occurred to the system [152]. The plethora of SHM literature provides ample instances where CCA based applications involving BSS algorithms have been implemented in the context of modal identification of structures subjected to ambient vibrations [53,63]. CCA promises to incorporate a mathematically general structure consistent with the theoretical advancements in structural dynamics that can possibly accommodate both damage detection and modal identification in a single framework. To date, the attempt at using CCA in its unabridged version at identifying damage patterns in real time, is a novel work undertaken in this research. Again, addressing the facets of real time modal identification still poses a big challenge, owing to permutation ambiguity. The aspect of unifying CCA to address both modal identification and damage detection in real time in a simultaneous framework poses a formidable challenge that is

beyond the scope of this research and is kept as a possible extension to be dealt with in the future.

The utility of CCA as a structural damage detection tool can be envisaged from the successful implementation of BSS towards modal identification [53, 63] and damage detection [51, 68], in the recent times. Techniques involving separation of modes, such as BSS and ICA, emerge as potential candidates for modal identification algorithms. Since a class of BSS methods come under the category of CCA based schemes [154], direct application of CCA towards modal identification and damage detection is imperative. However, it is worth noting the fact that the majority of the available damage detection schemes are *offline*, requiring windowing of the data in order to compare the newer set of the response to the baseline values. An indispensable requisite for any detection algorithm to identify fine levels of damage, is its ability in comparing the recorded data at continuous intervals, from which the damage to the structure can be detected. This necessitates that the algorithms must work *online*, an aspect that has rarely been reported in the context of damage detection literature. As damage is a real time event, it further warrants that the detection algorithm must work online, which motivates the utilization of RCCA, a direct extension of the traditional CCA approach using the previously slated FOEP theory [134, 135]. In line with the previous salient theoretical treatment of the topic, the FOEP technique provides the rank-one eigenvector updates at each instant, as and when the vibration data streams in real time. The use of RCCA as an effective damage detection tool emanates from the conceptualization of the distortion of the eigenspace, that can be modeled using TVAR and utilized to identify the spatio-temporal damage in a simultaneous framework.

The implementation of the recently established method, RPCA, is based on the principles of orthogonal transformation of the data covariance matrix arising from an uniaxial vibration. The CCA method, however, generates a block covariance matrix utilizing multi-directional data, that arise mostly during field studies and experimental setups. It is observed that the RPCA based methodologies consistently fail to perform using multi-directional data, as opposed to the CCA based methods, where the inherent formulation of the technique pivots around this concept. It can therefore, be surmised, that the RCCA method should provide better detectability results for multi-directional dependencies and flexible structures with torsionally coupled systems as compared to the previously discussed RPCA scheme, which motivates the present study. Due to its more robust and accommodative essence, the RCCA method can be applied for a diversified range of excitations for

both linear and nonlinear systems. In order to examine the efficacy of the proposed algorithm as a suitable candidate for baseline-free SHM, numerical simulations are conducted for damage detection to the aforementioned 5 DOF B-W system for varying levels of nonlinearity change. Additionally, a numerically simulated 7 DOF B-W system is adopted in order to assess the performance of the proposed scheme against the increase in the DOF. This provides a test bed to evaluate the robustness of the methodology for a more practical case in which tall, flexible structures might be encountered and the detection results needs to be established with the ground truth. The detailed theoretical derivations are presented in the ensuing sections.

6.2 Background

CCA is an exploratory method for determining the relationship between two multivariate sets of vectors by extracting information from the *cross-covariance* matrices. Developed in the late 1930's by Hoteling, CCA is a standard tool in statistical analysis that finds its application in econometrics, meteorology, medical studies and in the fields of signal processing as well. To the best of the knowledge of the author, the present work is one of the cardinal attempts at integrating CCA into a structural damage detection framework. The method finds two bases, one for each variable, that are optimal with respect to correlations and simultaneously obtains the corresponding correlations. Mathematically, it finds two basis vectors in which the correlation matrix between the variables is diagonal and mutually maximized by projecting the original set of variables onto an optimum subspace. An important feature of the method is that the dimensionality of these new bases is equal to or less than the dimensionality of the individual variables. In order to utilize the concepts of CCA into a structural dynamics framework, consider two column vectors $X = (x_1, x_2, ..., x_n)^T$ and $Y = (y_1, y_2, ..., y_n)^T$ of random variables with finite moments. Projecting these variables onto the basis vectors, the linear combinations $\mathcal{X} = X^T \hat{w}_x$ and $\mathcal{Y} = Y^T \hat{w}_y$ need to be mutually maximized

which is given by:

$$\begin{aligned}\rho &= \frac{E[\mathcal{X}\mathcal{Y}]}{\sqrt{E[\mathcal{X}^2]E[\mathcal{Y}^2]}} \\ &= \frac{E[\hat{w}_x^T X Y^T \hat{w}_y^T]}{\sqrt{E\left[\hat{w}_x^T X X^T \hat{w}_x\right] E\left[\hat{w}_y^T Y Y^T \hat{w}_y\right]}} \\ &= \frac{\mathbf{w}_x^T \mathbf{C}_{xy} \mathbf{w}_y}{\sqrt{\mathbf{w}_x^T \mathbf{C}_{xx} \mathbf{w}_x \mathbf{w}_y^T \mathbf{C}_{yy} \mathbf{w}_y]}}\end{aligned} \tag{6.1}$$

It is a well understood concept that the covariance matrix of the random variables (centered to zero mean) can be expressed as:

$$\mathbf{C} = \begin{bmatrix} \mathbf{C}_{xx} & \mathbf{C}_{xy} \\ \mathbf{C}_{yx} & \mathbf{C}_{yy} \end{bmatrix} \tag{6.2}$$

The covariance matrix is essentially a block matrix where $\mathbf{C}_{xx}$ and $\mathbf{C}_{yy}$ are the within-set covariance matrices of $\mathcal{X}$ and $\mathcal{Y}$ respectively and the relation $\mathbf{C}_{xy} = \mathbf{C}_{yx}^T$ holds true for the cross-set covariance matrices. The aim of this methodology is to obtain the canonical correlations between $\mathcal{X}$ and $\mathcal{Y}$, that can be easily obtained by solving the following sets of eigen decomposition equations:

$$\left.\begin{aligned}\mathbf{C}_{xx}^{-1}\mathbf{C}_{xy}\mathbf{C}_{yy}^{-1}\mathbf{C}_{yx}\hat{\mathbf{w}}_x &= \rho^2\hat{\mathbf{w}}_x \\ \mathbf{C}_{yy}^{-1}\mathbf{C}_{yx}\mathbf{C}_{xx}^{-1}\mathbf{C}_{xy}\hat{\mathbf{w}}_y &= \rho^2\hat{\mathbf{w}}_y\end{aligned}\right\} \tag{6.3}$$

where the eigenvalues ρ^2 are the squared *canonical correlations* and the corresponding eigenvectors $\hat{\mathbf{w}}_x$ and $\hat{\mathbf{w}}_y$ represent the normalized the canonical correlation *basis vectors*. In practice, Eqn. 6.3 can be recast into a single eigenvalue equation, given by:

$$\mathbf{B}^{-1}\mathbf{A}\hat{\mathbf{w}} = \rho\hat{\mathbf{w}} \tag{6.4}$$

where the matrices involved in the eigenvalue decomposition (EVD) are obtained as:

$$\mathbf{A} = \begin{bmatrix} \mathbf{0} & \mathbf{C}_{xy} \\ \mathbf{C}_{yx} & \mathbf{0} \end{bmatrix}, \quad B = \begin{bmatrix} \mathbf{C}_{xx} & \mathbf{0} \\ \mathbf{0} & \mathbf{C}_{yy} \end{bmatrix} \quad and \quad \hat{\mathbf{w}} = \begin{pmatrix} \mu_x\hat{\mathbf{w}}_x \\ \mu_y\hat{\mathbf{w}}_y \end{pmatrix} \tag{6.5}$$

It is worthy noting that a slightly different structure of the covariance matrix will give rise to the *traditional PCA* based approach, a concept that has consistently exhibited its potential in identifying the spatial and temporal patterns of structural damage, over the recent years. PCA, a special instance of CCA, can be formulated on substituting the matrices $\mathbf{A}$ and $\mathbf{B}$ as: $\mathbf{A} = \mathbf{C}_{xx} \quad and \quad \mathbf{B} = \mathbf{I}$. PCA is a dimensionality reduction approach that projects the data onto principal subspace, such that the variance of the projected data is maximized. In carrying out the projection, PCA reveals some simplified structures relevant to the dataset that could be obtained by EVD on the covariance matrix. Prior to getting into the details of the proposed methodology, it is imperative to review the concepts of PCA through a structural dynamics viewpoint, profoundly discussed in *chapter 2*. To tailor the basic CCA into a recursive framework, it becomes essential to revisit certain key theoretical developments that center around covariance estimates and FOEP techniques. In the backdrop of recursive implementation, the detailed formulation of FOEP presented in *chapter 2*, provides an in-depth know how about incorporating eigenspace update through the rank-one perturbation theory. The readers are advised to acquaint themselves with the FOEP formulations previously described, prior to getting into the theoretical attributes of the present recursive approach.

6.3 RCCA: Detailed derivation

The use of CCA as a structural damage detection tool is a relatively nascent topic that has garnered certain attention among the researchers. The major drawback of using CCA is that it analyzes data in batches, primarily rendering it an offline approach. In order to detect finer levels of damage, it is essential to estimate the eigenspace recursively, thereby providing iteartive updates at each instant of time. The formulation of the basic CCA approach necessitates that the covariance matrix obtained from the set of recorded responses is essentially a block matrix, that needs to be updated for its online implementation. The major challenge towards tailoring the basic CCA towards an online implementation is to perform EVD on the block covariance matrix, which is particularly cumbersome and memory consuming. This can be alleviated through the use of the FOEP based approach which provides recursive updates of the eigenspace obtained from the previous eigenspace of the data at a particular instant. An important aspect to be considered here is that the FOEP

based recursive approach updates the eigenspace characteristics at each time instant, instead of updating the covariance matrix as a whole, thereby reducing the time complexity of the recursive implementation.

The theoretical development of RCCA is premised on the objective of finding a recursive update of the eigenspace characteristics at each instant of time, a central idea envisaged from FOEP improvisation. The individual lower dimensional matrices shown in Eqn. 6.2 needs to be updated at each time stamp, providing recursive eigenspace estimates through the FOEP strategy. In this context, the response covariance matrix $\mathbf{C}_{xx}(k)$ at any instant k can be expressed as a function of the covariance matrix at the previous time stamp, $\mathbf{C}_{xx}(k-1)$ and the response vector X_k at the k^{th} instant, according to:

$$\mathbf{C}_{xx}(k) = \frac{k-1}{k}\mathbf{C}_{xx}(k-1) + \frac{1}{k}X_k X_k^T \tag{6.6}$$

As previously mentioned, the FOEP based approach is a versatile idealization that does not take into consideration the nature of the dataset. The applicability of the method for nonstationary datasets involves the consideration of the recursive mean at each instant of time. The recursive mean update at k^{th} instant, μ_k, depends on the mean at the previous time stamp through the relation: $\mu_k = \frac{k-1}{k}\mu_{k-1} + \frac{1}{k}X_k$. The covariance estimate for cases involving mean update can be expressed as:

$$\tilde{\mathbf{C}}_{xx}(k) = \frac{k-1}{k}\mathbf{\Sigma}_k^{-1}\mathbf{\Sigma}_{k-1}\tilde{\mathbf{C}}_{xx}(k-1)\mathbf{\Sigma}_{k-1}\mathbf{\Sigma}_k^{-1} + \mathbf{\Sigma}_k^{-1}\Delta\mu_k\Delta\mu_k^T\mathbf{\Sigma}_k^{-1} + \frac{1}{k}\left[\mathbf{X}_k - \mu_k\right]\left[\mathbf{X}_k - \mu_k\right]^T \tag{6.7}$$

The eigen decomposition of the covariance estimate shown in Eqn. 6.7 can be written in terms of $\tilde{\mathbf{C}}_{xx}(k) = \tilde{\mathbf{W}}_k\tilde{\Upsilon}_k\tilde{\mathbf{W}}_k^T$. Eqn. 6.7 can be recast as:

$$\tilde{\mathbf{W}}_k\tilde{\Upsilon}_k\tilde{\mathbf{W}}_k^T = \frac{k-1}{k}\mathbf{\Sigma}_k^{-1}\mathbf{\Sigma}_{k-1}\tilde{\mathbf{C}}_{xx}(k-1)\mathbf{\Sigma}_{k-1}\mathbf{\Sigma}_k^{-1} + \mathbf{\Sigma}_k^{-1}\Delta\mu_k\Delta\mu_k^T\mathbf{\Sigma}_k^{-1} + \frac{1}{k}\left[\mathbf{X}_k - \mu_k\right]\left[\mathbf{X}_k - \mu_k\right]^T \tag{6.8}$$

The POC vector at the k^{th} time instant can be estimated as: $\tilde{\psi}_k = \tilde{\mathbf{W}}_{k-1}^T X_k$. Carrying out proper

substitutions in Eqn. 6.8, one obtains:

$$\tilde{\mathbf{W}}_k \tilde{\Upsilon}_k \tilde{\mathbf{W}}_k^T = \frac{k-1}{k} \boldsymbol{\Sigma}_k^{-1} \boldsymbol{\Sigma}_{k-1} \tilde{\mathbf{W}}_{k-1} \tilde{\Upsilon}_{k-1} \tilde{\mathbf{W}}_{k-1}^T \boldsymbol{\Sigma}_{k-1} \boldsymbol{\Sigma}_k^{-1} + \boldsymbol{\Sigma}_k^{-1} \Delta\mu_k \Delta\mu_k^T \boldsymbol{\Sigma}_k^{-1} \tag{6.9}$$

$$+ \frac{1}{k} \left[\mathbf{W}_{k-1} \tilde{\psi}_k - \mu_k \right] \left[\mathbf{W}_{k-1} \tilde{\psi}_k - \mu_k \right]^T \tag{6.10}$$

Scaling the data to unit variance, the above equation translates to:

$$\tilde{\mathbf{W}}_k \tilde{\Upsilon}_k \tilde{\mathbf{W}}_k^T = \frac{k-1}{k} \tilde{\mathbf{W}}_{k-1} \tilde{\Upsilon}_{k-1} \tilde{\mathbf{W}}_{k-1}^T + \Delta\mu_k \Delta\mu_k^T + \frac{1}{k} \left[\mathbf{W}_{k-1} \tilde{\psi}_k - \mu_k \right] \left[\mathbf{W}_{k-1} \tilde{\psi}_k - \mu_k \right]^T \tag{6.11}$$

For structural systems in particular, data is assumed to consistently evolve from zero mean processes. Therefore, the above equation can be simplified as:

$$\tilde{\mathbf{W}}_k k \tilde{\Upsilon}_k \tilde{\mathbf{W}}_k^T = \tilde{\mathbf{W}}_{k-1} \left[(k-1) \tilde{\Upsilon}_{k-1} + \tilde{\psi}_k \tilde{\psi}_k^T \right] \tilde{\mathbf{W}}_{k-1}^T \tag{6.12}$$

An important conclusion that could be drawn from the aforementioned discussion is the fact that the term $[(k-1)\,\tilde{\boldsymbol{\Upsilon}}_{k-1} + \tilde{\psi}_k \tilde{\psi}_k^T]$ should diagonally dominant, for the RPCA algorithm to be stable and robust. Subsequently, as the system consists of very low to moderate levels of damping, the EVD can be evaluated using the Gershgorin's theorem [122]. The term $\tilde{\psi}_k \tilde{\psi}_k^T$ represents the correlation between the POC estimates at a particular instant. Substituting from Eqn. 4.3, the covariance between POC estimates can be written as (to an arbitrary scale factor):

$$\begin{aligned} \tilde{\psi}_k \tilde{\psi}_k^T &= \tilde{\mathbf{W}}_{k-1}^T X_k {X_k}^T \tilde{\mathbf{W}}_{k-1} \\ &= q_{k-1} {q_{k-1}}^T + \gamma {q_{k-1}}^T + \gamma^T q_{k-1} + \gamma\gamma^T \end{aligned} \tag{6.13}$$

As far as the dynamics of structural systems are considered, the error term in the Eqn. 6.13 can be neglected as the number of sampling points increases and under moderate to low damping [122]. Recognize the similarity of the first term in Eqn. 6.13 that closely resembles the covariance of the normal coordinates at the instant $(k-1)$. Thus the term $q_{k-1} {q_{k-1}}^T$ represents a matrix whose diagonal terms dominate its off-diagonal terms; hence, the term $\tilde{\psi}_k \tilde{\psi}_k^T$ can be safely assumed to be diagonally dominant. This in turn, ensures the diagonal dominance of the matrix $\left[(k-1) \tilde{\Upsilon}_{k-1} + \tilde{\psi}_k \tilde{\psi}_k^T \right]$, fa-

cilitating straightforward application of Gershgorin's theorem. Hence for a structural system, the recursive eigenspace update is obtained using FOEP approach which provides a less computationally intensive algorithm in a recursive framework. The EVD of the matrix $\left[(k-1)\tilde{\Upsilon}_{k-1} + \tilde{\psi}_k\tilde{\psi}_k^T\right]$ can be substituted as $\mathbf{H_k}\mathbf{\Lambda}_k\mathbf{H}_k^T$ into Eqn. 5.12 as,

$$[\tilde{\mathbf{W}}_k][k\tilde{\Upsilon}_k][\tilde{\mathbf{W}}_k]^T = [\tilde{\mathbf{W}}_{k-1}\mathbf{H}_k][\mathbf{\Lambda}_k][\tilde{\mathbf{W}}_{k-1}\mathbf{H}_k]^T \tag{6.14}$$

yielding the following iterative update equations:

$$\left.\begin{aligned} \tilde{\mathbf{W}}_k &= \tilde{\mathbf{W}}_{k-1}\mathbf{H}_k \\ \mathbf{\Upsilon}_k &= \tfrac{\mathbf{\Lambda}_k}{k} \end{aligned}\right\} \tag{6.15}$$

The recursive algorithm of Eqn. 6.6 is transformed to obtain the values of H_k and Λ_k. As previously described, the term $(k-1)\,\tilde{\mathbf{\Upsilon}}_{k-1} + \tilde{\psi}_k\tilde{\psi}_k^T$ is diagonally dominant, which ensures that the eigen values are the diagonal entries of the matrix. therefore, the i^{th} diagonal entry of the term Λ_k can be represented as $(k-1)\,\lambda_i + \tilde{\psi}_i^2$, where λ_i is the (i,i) element of $\tilde{\mathbf{\Upsilon}}_{k-1}$ and $\tilde{\psi}_i$ is the i^{th} entry of the POC estimate. Once the eigen values are obtained, the corresponding eigen vectors can be found out, leading to H_k.

Based on the above discussion, the recursive eigenspace estimate of a single set of response (more particularly, the responses obtained in a single direction) is achieved. The block covariance matrix shown in Eqn. 6.2 consists of the covariance matrices obtained from the responses in the orthogonal direction as well. Further, the block matrix comprises of the cross covariance matrices, that needs to be recursively updated as well. In line with the above derivations, a similar presentation of the recursive eigen estimation can be arrived at, which is repetitive and therefore, omitted here for brevity. Once each of the individual covariance estimates are obtained, the next task is to implement these matrices onto a recursive framework prescribed by the eigenvalue problem shown in Eqn. 6.4.

At any time instant k, the fundamental matrices involved in the eigen decomposition of Eqn. 6.4

can be expressed as:

$$\mathbf{A}(k) = \begin{bmatrix} \mathbf{0} & \mathbf{C}_{xy}(k) \\ \mathbf{C}_{yx}(k) & \mathbf{0} \end{bmatrix}, \quad \mathbf{B}(k) = \begin{bmatrix} \mathbf{C}_{xx}(k) & \mathbf{0} \\ \mathbf{0} & \mathbf{C}_{yy}(k) \end{bmatrix} \tag{6.16}$$

The recursive updates of the covariance estimates can be substituted in to the above equation. These updates follow the similar structure as shown in Eqn. 6.6 and can be expressed as:

$$\left.\begin{aligned} \mathbf{A}(k) &= \begin{bmatrix} \mathbf{0} & \frac{k-1}{k}\mathbf{C}_{xy}(k-1) + \frac{1}{k}X_k Y_k^T \\ \frac{k-1}{k}\mathbf{C}_{yx}(k-1) + \frac{1}{k}Y_k X_k^T & \mathbf{0} \end{bmatrix} \\ \mathbf{B}(k) &= \begin{bmatrix} \frac{k-1}{k}\mathbf{C}_{xx}(k-1) + \frac{1}{k}X_k X_k^T & \mathbf{0} \\ \mathbf{0} & \frac{k-1}{k}\mathbf{C}_{yy}(k-1) + \frac{1}{k}Y_k Y_k^T \end{bmatrix} \end{aligned}\right\} \tag{6.17}$$

An important feature of the FOEP based techniques is its ability in reducing time complexities by a significant margin. As evident from the literature, the step wise update of the covariance matrix at each iteration is cumbersome [88] and calls for efficient techniques to perform the recursive updates. Additionally, performing an iterative estimation in the backdrop of a generalized eigenvalue problem is more involved and complicated. A simplified route that could be envisioned is through the structural modification of the equation under study and then performing the recursive updates. Based on this premise, consider a simplified version of Eqn. 6.4 at the k^{th} time instant, given by:

$$\mathbf{A}(k)\hat{\mathbf{w}}(k) = \rho(k)\mathbf{B}(k)\hat{\mathbf{w}}(k) \tag{6.18}$$

From a thorough understanding of the FOEP approach, it is clear that Eqn. 6.18 needs to be updated for every sample. As evident from Eqn. 6.15, the rank-one update of the covariance matrix provides the recursive estimations at each instant. Similar to this notion, consider the rank-one perturbation of the eigen decomposition given by Eqn. 6.18:

$$\left(\mathbf{A} + \Delta\mathbf{A}\right)\left(\hat{\mathbf{w}} + \Delta\hat{\mathbf{w}}\right) = \left(\rho + \Delta\rho\right)\left(\mathbf{B} + \Delta\mathbf{B}\right)\left(\hat{\mathbf{w}} + \Delta\hat{\mathbf{w}}\right) \tag{6.19}$$

Considering the fact that the perturbed matrices are of low magnitude, each of the small perturbations correspond to evaluating the matrix at the $k+1^{th}$ instant. This translates to evaluating the EVD at the $k+1^{th}$ time stamp, which is precisely the basic objective of the FOEP methodology:

$$\mathbf{A}(k+1)\hat{\mathbf{w}}(k+1) = \rho(k+1)\mathbf{B}(k+1)\hat{\mathbf{w}}(k+1) \tag{6.20}$$

From the aforementioned discussions, it is obvious that the individual matrices involved in the EVD can be recursively updated following the similar notion expressed in Eqn. 6.17. A key feature of this update is the recursive estimation of the eiegnspace, which can be readily obtained by following the same methodology as in Eqn. 5.14. This demonstrates that the eigenspace updates can be obtained through the FOEP technique without actually performing EVD on the subsequent data points, thereby reducing the time complexity and memory consumption, to an enormous extent.

6.4 Recursive damage sensitive features

The current framework exploring the concepts of RCCA facilitates online processing of the data and yields the recursive updates of the eigenvalues and the eigenvectors, referred to as the 'eigenspace', in a pedantic sense. The eigenspace by itself is inadequate in exhibiting the deviations inflicted at the onset of the damage. Therefore, certain damage markers, known as DSFs, are employed to ascertain the presence of damage and its location, visually or otherwise. The key characteristics of a good DSF lies in its potential to detect the presence of damage, locate and estimate the severity of damage and effectively distinguish between the damaged and undamaged states of the structure. Further, the auxiliary attributes of these DSFs arise from their ability to function online, in order to identify the change of states in real time. In this context, the aforementioned TVAR coefficients and the RRE vectors are utilized as appropriate DSFs for identifying the spatio-temporal patterns of damage in time. The detailed derivation for the same has already been encountered in *chapter 3* and hence, not reported here for brevity.

6.5 Proposed algorithm

The comprehensive methodology followed in this chapter for identifying and localizing the damage in real time entails two contributing modules: *temporal* and the *spatial* module, working simultaneously in a single framework. The primary course of action followed is to first identify the instant of damage, and then proceed on to detecting its location. The first module deals with identifying the instant of damage where the recorded vibration data is provided as input to the RCCA algorithm, in order to obtain the transformed responses. These responses, consequently modeled using TVAR, produces TVAR coefficients which are indicative of damage to the system. On ascertaining the instant of damage, the spatial module is invoked where the spatial RRE is tracked over each DOF to identify the location of damage. A distortion in the RRE plots confirms the exact location of damage in the structure. For an easy comprehension of the detailed process, the basic steps of the algorithm are enumerated as follows:

1. First, a block covariance matrix incorporating the individual auto- and cross-covariance matrices is fabricated from the set of physical responses. Traditional CCA is applied on some initial data points (around 100 in number) in order to estimate the initial eigenspace. The number of data points chosen here is arbitrary and considered only to stabilize the algorithm for subsequent real time damage detection. The batch implementation comprises the EVD updates shown in Eqn. 6.3, yielding the eigenspace represented by ρ and $\hat{\mathbf{w}}$.

2. The recursive gain depth parameter is employed to estimate the covariance estimate at the present time instant using the covariance estimate at preceding time instant. From these recursive updates, the eigenvector and eigenvalue matrices are updated using FOEP approach and the transformed responses (principal components) are obtained using the RCCA algorithm. While the covariance updates for the matrices are given by Eqn. 6.17, the iterative set of eigenspace updates carried out after the initial batch implementation can be easily obtained through Eqn. 5.14.

3. The transformed responses are fit using TVAR models of appropriate model order. This provides a set of TVAR coefficients that evolve with the progression of time and aid in identifying

the exact instant of damage, governed by the Eqn. 4.15. In addition, the temporal RRE plot, given by Eqn. 3.14, further substantiates the damage instant corroborated by the TVAR plots.

4. Once the instant of damage is determined, the algorithm shifts on to the next module where the spatial detection of damage takes place. The mathematical expressions administering its implementation can be clearly obtained from Eqn. 3.18. The local RRE is tracked over the entire system as a whole that generates distortions in the plot, indicative of damage at that particular location.

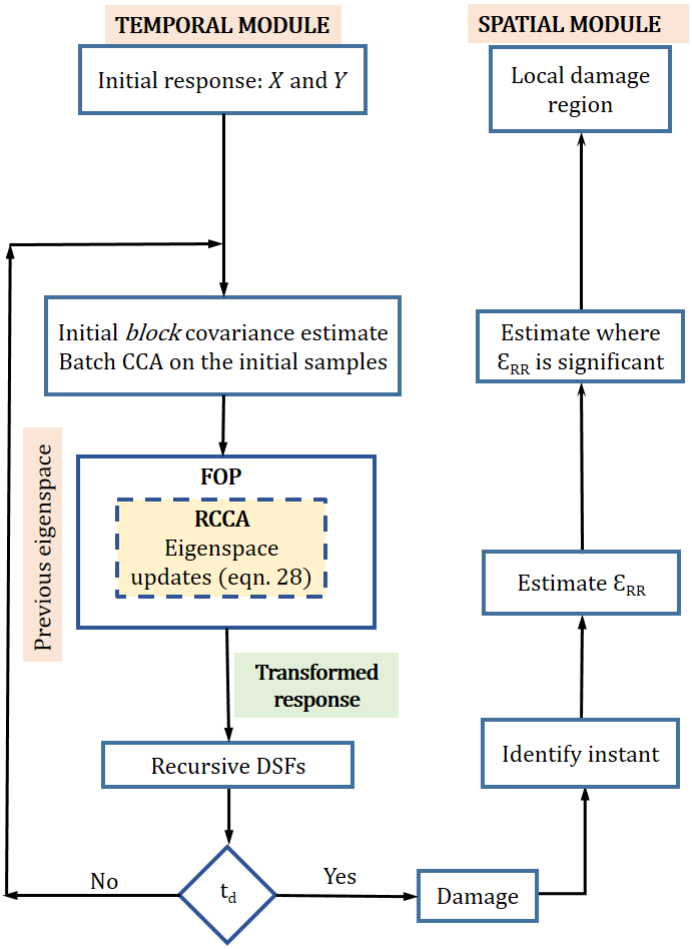

Figure 6.1: Flowchart of the RCCA method

The aforementioned steps for the proposed method are shown in the form of a stepwise flowchart in Fig. 6.1. Based on the theoretical derivations, the TVAR coefficients and RRE show deviations in the mean level of the plots, that visually aid in identifying the instant of damage. A few impor-

tant characteristics of the proposed algorithm include: (i) implementation on the data obtained at each time stamp, as and when the data becomes available; signifying that the algorithm essentially operates *online* (ii) detection of damage instant and its location without ad-hoc windowing or gathering of any sort of baseline data, making it *baseline-free* and (iii) absence of parameters controlling the functioning of the algorithm, rendering it *parameter independent*. These characteristics of the proposed algorithm makes it an ideal candidate for real time structural damage detection framework.

6.6 Detection results using proposed algorithm

Case studies are undertaken for both global and local damage detection using the proposed algorithm in the context numerical simulations and verified using experimental studies. In this context, two numerically simulated systems are considered here: (i) a 5 DOF B-W system and (ii) a 7 DOF B-W system. The source of nonlinearity for both the systems is through the nonlinear force parameter at the base of the models, controlled by the nonlinear force term κ. It can be conjectured at this stage that the effect of change of the value of κ for the latter case will not be as pronounced as compared to the 5 DOF model, primarily due to the increasing DOF of the structure, that constraints the nonlinearity propagation throughout the model. The temporal damage detection cases are obtained by changing the value of the nonlinear force term κ for the B-W system at a specified instant of time, sequentially followed by the cases for real time spatial damage detection.

6.6.1 Temporal damage detection studies for the B-W systems excited using *white noise*

A brief numerical study on aforementioned systems has been carried out using Gaussian white noise as a excitation. Temporal damage detection cases are studied first by sequentially changing the κ corresponding to 15% and 10% changes in nonlinear characteristics respectively.

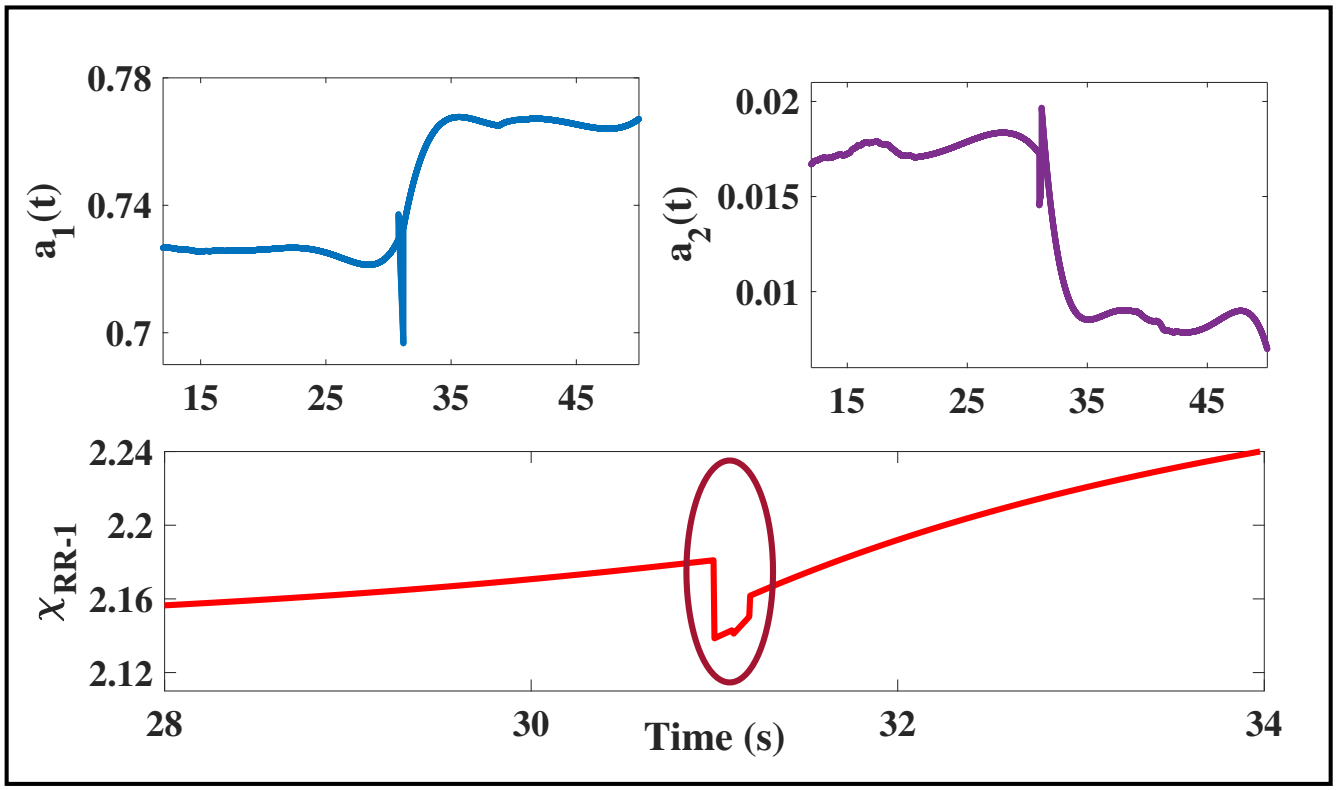

Figure 6.2: Recursive DSF plot for 15% temporal damage for the 5 DOF B-W system (using white noise excitation)

Temporal damage detection results for the 5 DOF B-W system

Case studies using 5 DOF B-W system for 10% and 15% change in nonlinearity are reported in this section. Recent investigation has revealed that damages of the order of 15% have often been reported as a lower bound for real time vibration based damage detection. However, the proposed algorithm provides successful detection results for finer levels of damage, as low as 10%, for the 5 DOF B-W system. The detection results using the proposed DSFs are presented next in detail.

From Fig. 6.2 a damage instant at 31s can be clearly observed for 15% change in nonlinearity. The sharp peak discerned at the damage instant primarily attributes to the sudden change in the mean level of the TVAR plot, an event that is consistent for both the coefficients. In order to validate these findings, the temporal RRE plot clearly substantiates the instant of damage through a sharp distortion at 31s. A separate figure dedicated towards real time damage detection for a 10% change in nonlinearity is shown in Fig. 6.3. From both Fig. 6.2 and 6.3 it can be observed that, the plots of the TVAR coefficients show changes in the mean level of the plot around the 31s mark, indicating a

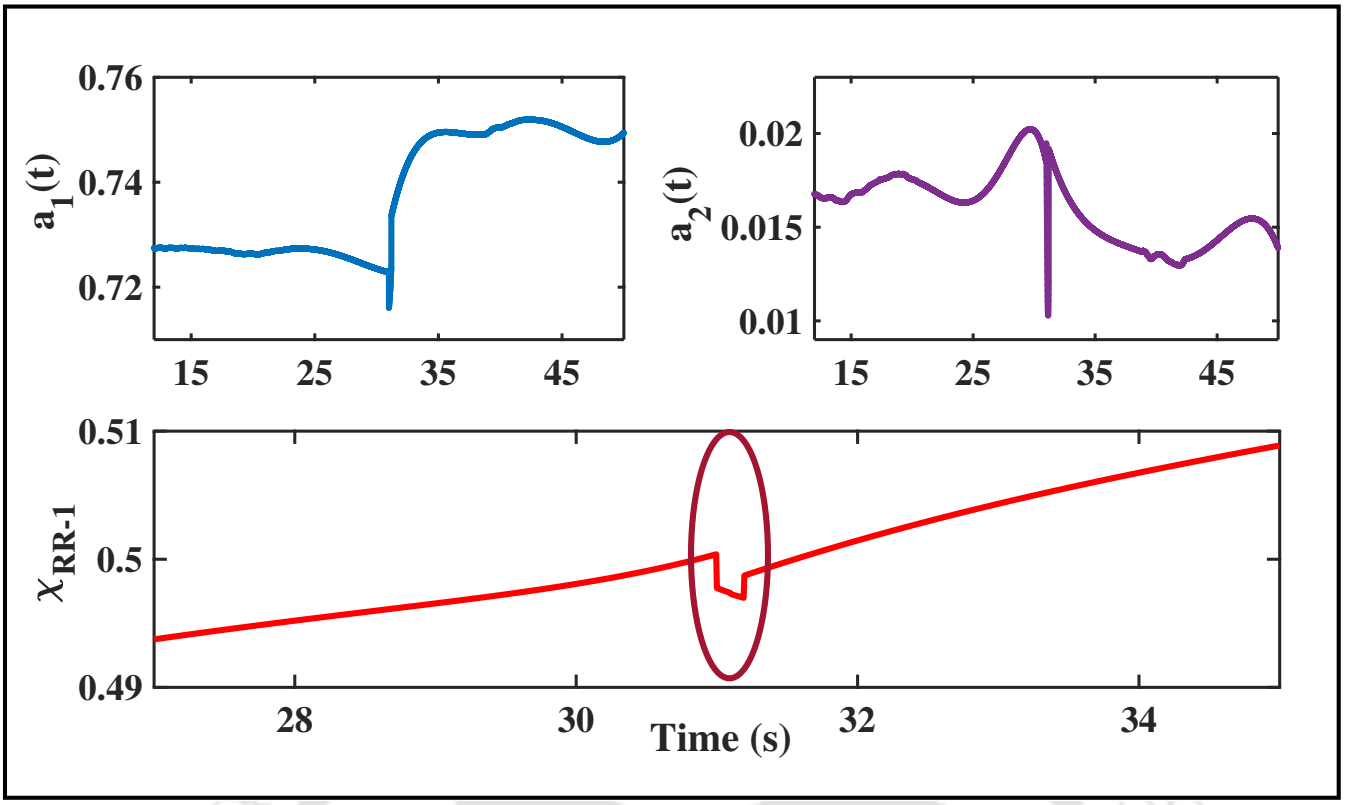

Figure 6.3: Recursive DSF plot for 10% temporal damage for the B-W system (using white noise excitation)

possible event of damage. Further, residual error when examined in a recursive framework, detects the instant of damage at 31s, clearly observed from the figures, thereby validating the inferences concluded from the TVAR plots. In line with the above findings, it can be very well established that the proposed RCCA algorithm is efficient in determining fine levels of damage in real time, a feat that has only been reported in a recently established hybrid algorithm using an association of the RPCA-RSSA strategies.

Spatial damage detection results for the Bouc-Wen 5 dof model

The present section deals with the performance of the proposed algorithm towards simultaneously detecting a spatio-temporal damage in real time, which is one of the key entitlements of the current work. The notion of local damage is brought about by a change in linear storey stiffness of a particular DOF for an MDOF system, that forms the key cornerstone for processing online spatio-temporal damage. It is worth noting that the proposed algorithm invokes the spatial module only

when the instant of damage has been previously ascertained in the temporal constituent. A through investigation of the recently established real time damage detection literature reveals that detection studies using the RPCA algorithm could be traced back to a lower limit of 25% in real time. Motivated by this key shortcoming, the proposed method focuses on the detection potential for the weakly nonlinear B-W system for a spatial damage of both 10% and 15%, the results of which are presented next in detail. The key consideration to be incorporated here is the fact that the system is made fully nonlinear by scaling up the value of the nonlinear parameter κ to unity and the linear storey stiffness of the third floor are reduced by 10% and 15%, respectively, at 31s from the start of the excitation.

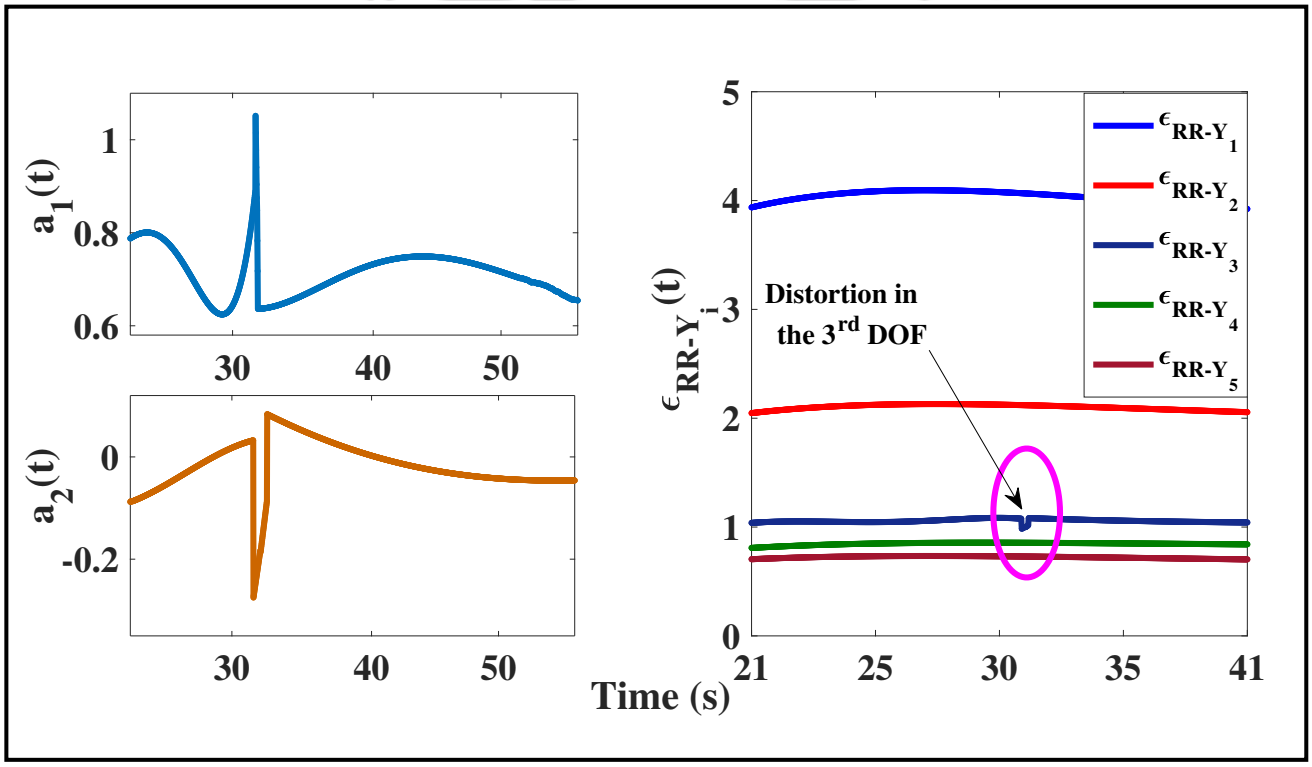

Figure 6.4: Recursive DSF plot for 15% spatio-temporal damage for the B-W system

From Fig. 6.4, it can be visualized that a clear damage instant is identified for 15% reduction in storey stiffness through the deviation in the TVAR plot. After the damage instant is established from TVAR plot, the spatial RRE in the vicinity of damage (say 21s-41s) is examined. The spatial RRE plots for all the DOFs are portrayed beside the TVAR coefficients clearly indicate a distortion in the 3^{rd} DOF, thereby conforming to the previous consideration of the occurrence of damage at 31s confined to that floor. Furthermore, a sharp change in the mean level of the TVAR plots at 31s is

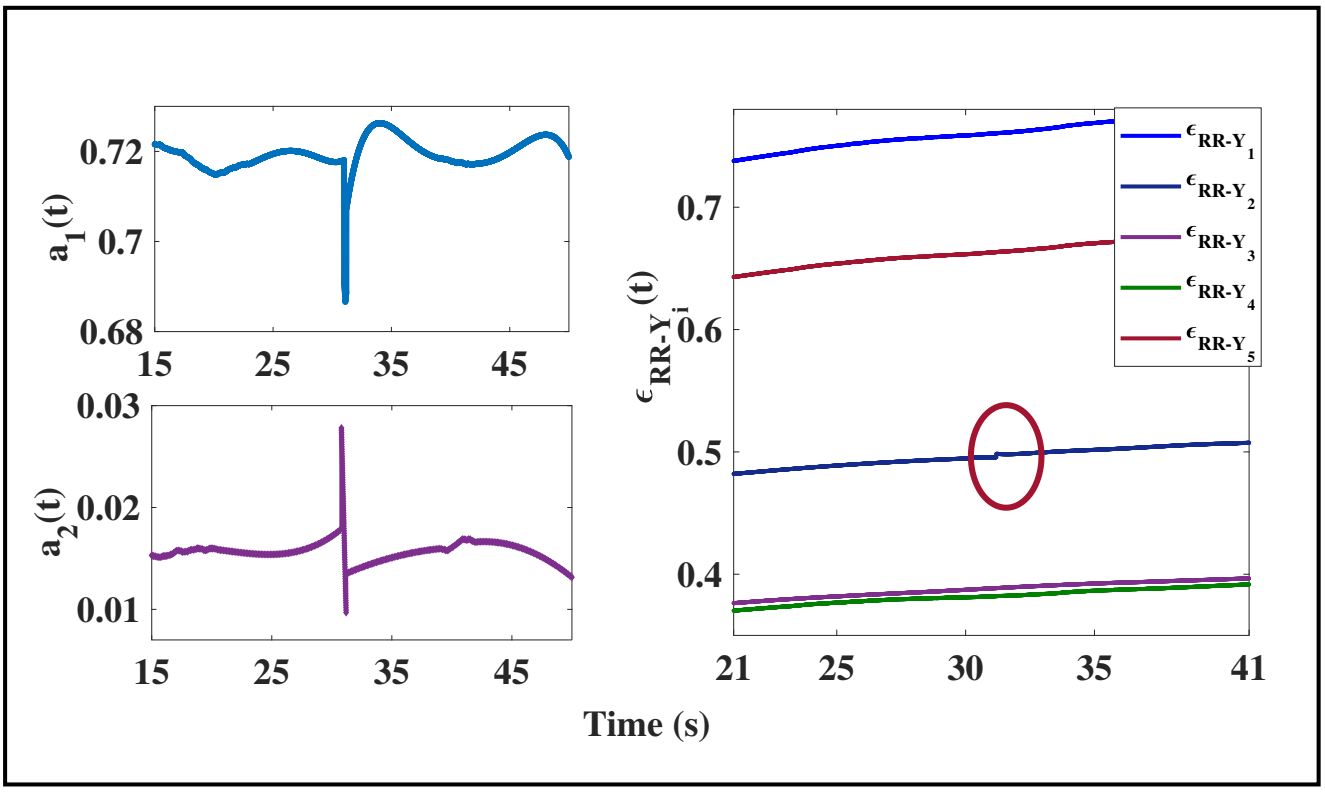

Figure 6.5: Recursive DSFs for 10% spatio-temporal damage for the B-W system (under white noise excitation)

clearly evident from Fig. 6.5, thereby establishing the fact that the proposed method is well suited at identifying the local patterns of damage for as low as 10%, which is clearly a major accomplishment considering the online nature of the algorithm. Such a low percentage of spatio-temporal damage has only been reported in a recently established hybrid scheme incorporating RPCA-RSSA based methods. However, the key shortcoming of the said method is its time complexity as opposed to the proposed scheme that independently identifies such a finer aspect of damage. This is one of the major entitlements of the current study.

6.6.2 Detection results for the 5 DOF B-W system excited by El Centro ground motion

The robustness of the proposed RCCA algorithm towards solving a wide range of damage identification problems can ensured with its application towards a wide range of excitation that includes nonstationary cases as well. Some of the well published literature on damage detection have consis-

tently failed to detect damage for nonstationary cases with a reasonable degree of confidence. This situation arises primarily due to the inherent formulation of the damage detection techniques which are mostly pivoted around linear systems excited using stationary events such as white noise. However, the proposed method has successfully identified real time damage for the aforesaid nonlinear system and is conjectured to provide good results for case studies involving nonstationary excitations as well. To this effect, the use of TVAR modeling on the transformed responses substantially aid in the damage detection scheme, by masking the nonstationary effect of the input excitation.

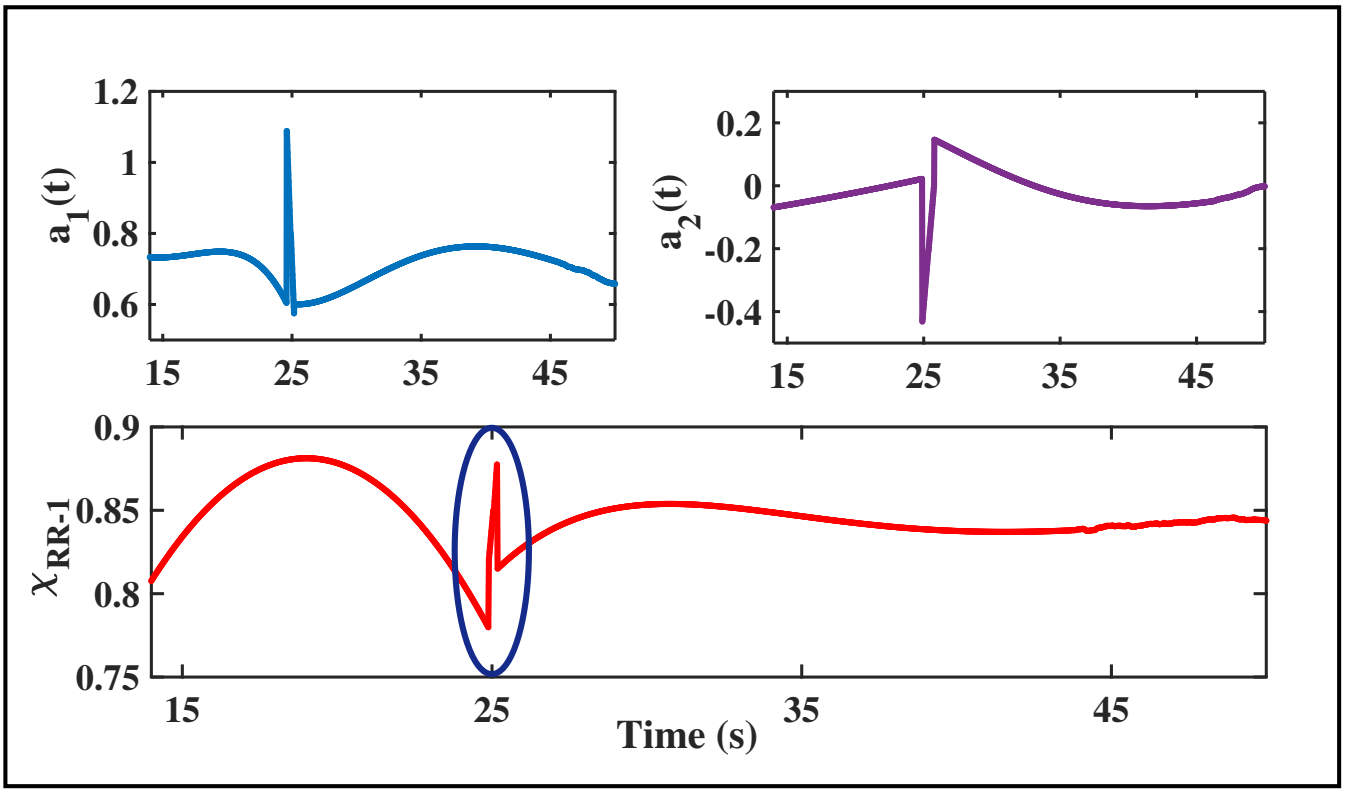

Figure 6.6: Recursive DSF plot for 25% temporal damage for the B-W system under El Centro excitation

To ensure the versatility of the proposed RCCA algorithm, the B-W system is excited using El Centro ground motion and the detection results are presented. The damage to the model is numerically simulated through a 25% and a 20% change in the nonlinear force term at the base of the model, that eventually contributes to a global damage to the system. Recently established RPCA algorithm provides a real time detection of 30% for the El Centro excitation case, thereby confirming the superiority of the proposed RCCA based scheme over the previously established ones.

In the subsequent sections, a thorough comparison of the two said methods will be provided, that

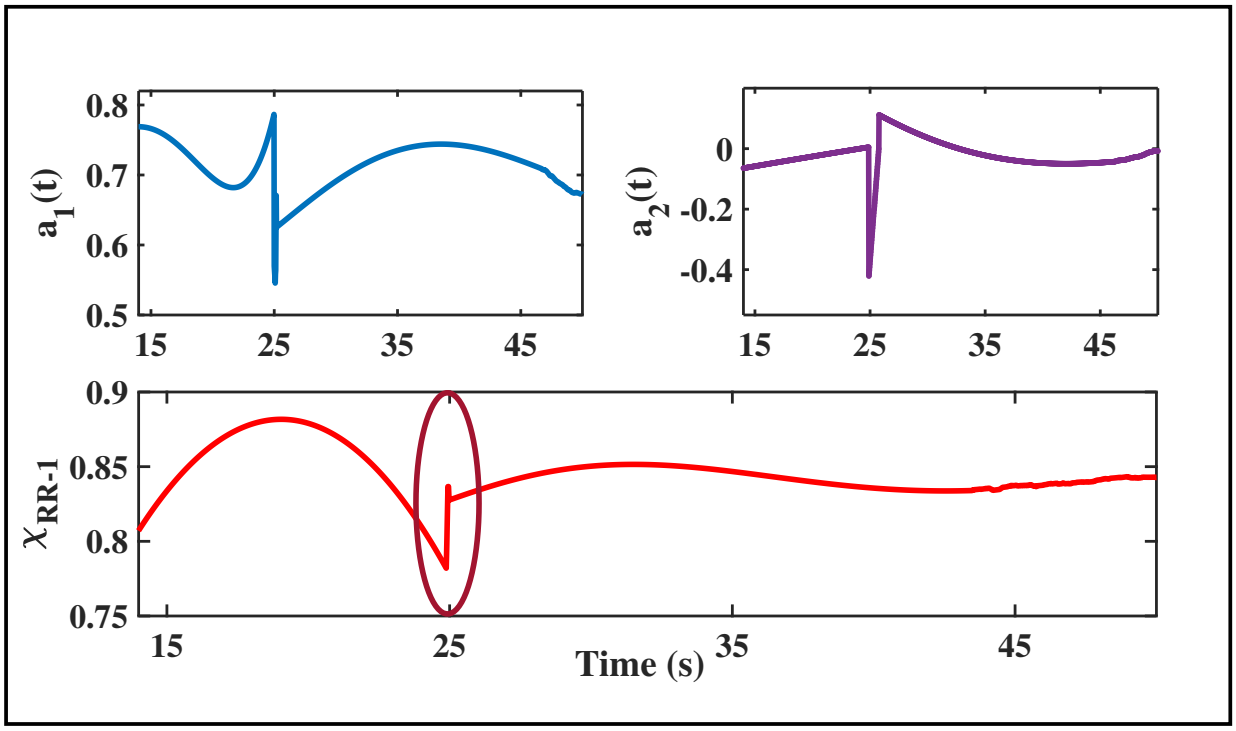

Figure 6.7: Recursive DSF plot for 20% temporal damage for the B-W system under El Centro excitation

sheds a light on the efficacy of the proposed algorithm over the recently established schemes. The detection results displayed in Fig. 6.6 and 6.7 clearly indicate the exact instant of damage at 25s from the start of the excitation. The temporal RRE plots, in addition to the TVAR coefficients, aptly validates the damage instant for both cases.

The local damage is simulated for the B-W system by numerically reducing the linear storey stiffness of the 3^{rd} floor by 25% and 20%, respectively, at 25s from the commencement of the excitation. The plots of the TVAR coefficients shown in Fig. 6.8, indicate a clear instant of damage at 25s. The spatial module of the algorithm gets invoked at the determination of the damage instant, due to which, the spatial RREs are tracked at each of the floor levels. In the neighborhood of the damage instant, the spatial RREs are evaluated for each floor, displayed in Fig. 6.8, which show distortion at 25s for the 3^{rd} storey. This confirms the localization of damage at the 3^{rd} floor of the system, corroborated from the spatial RRE plots. Similar results are obtained from Fig. 6.9 that indicates spatio-temporal damage in real time for a 20% change in the linear storey stiffness. Recently established detection schemes such as RPCA has reported a lower limit of detectability of *30% global damage* for a nonstationary input excitation; hence, a key contribution of the present

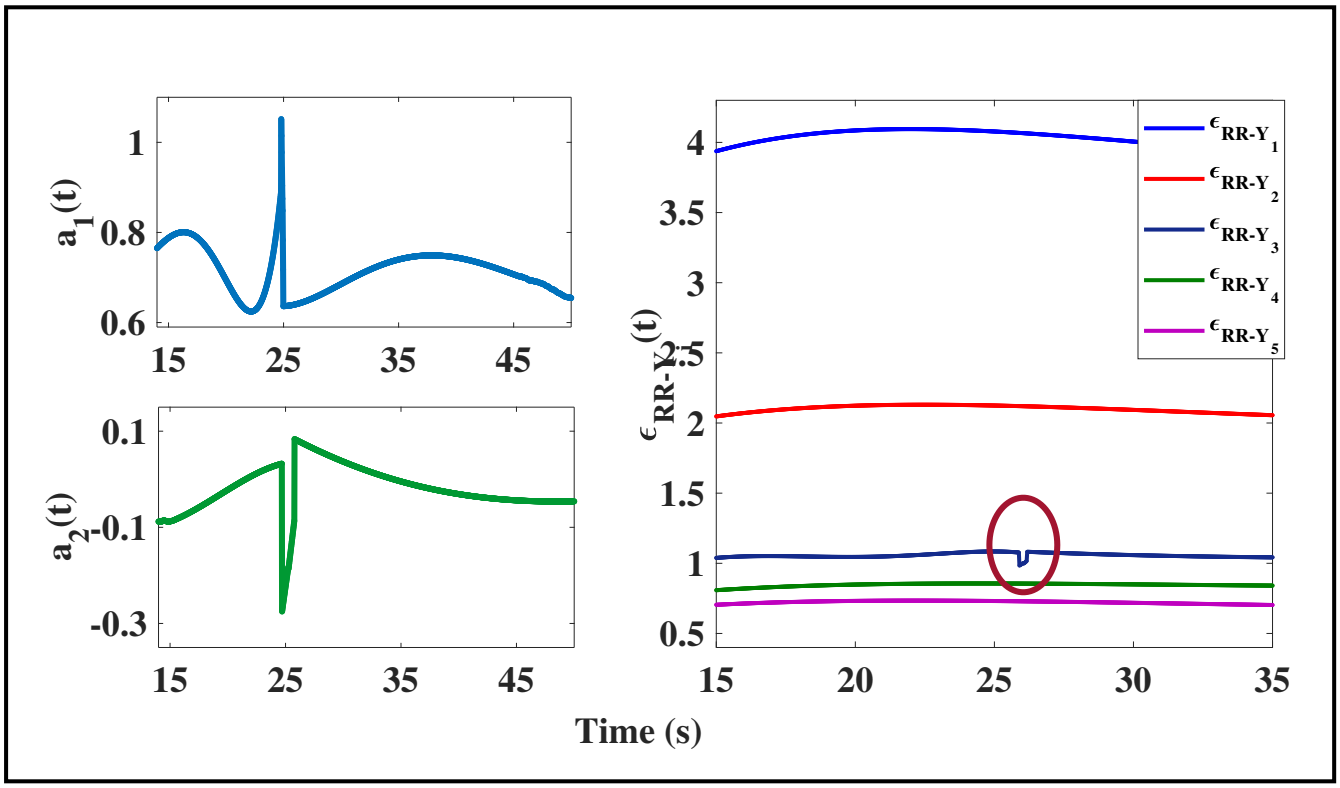

Figure 6.8: Recursive DSF plot for 25% spatio-temporal damage for the B-W system under El Centro excitation

work is the development of a framework that successfully reports *sptio-temporal damage* as low as *20%* for a nonstationary excitation.

6.6.3 Case study for an underdetermined system

It is worth noting that the covariance matrix generated from the physical responses obtained from the structure are usually full rank in nature. In practical scenarios, cost, improper accessibility and unavailability of good quality sensors, impede the possible instrumentation of all the physical DOF of the structure. This results in an *underdetrmined case*, where the number of instrumented sensors is less than the number of DOF, thereby fabricating a rank deficit matrix of the physical responses. The applicability of any damage detection scheme towards such continuous health monitoring and condition based maintenance lie in the performance assessment of the methods towards effectively identifying the damage patterns for underdetermined cases as well. In this context, the proposed method is examined in a recursive framework to effectively determine the instant and location of

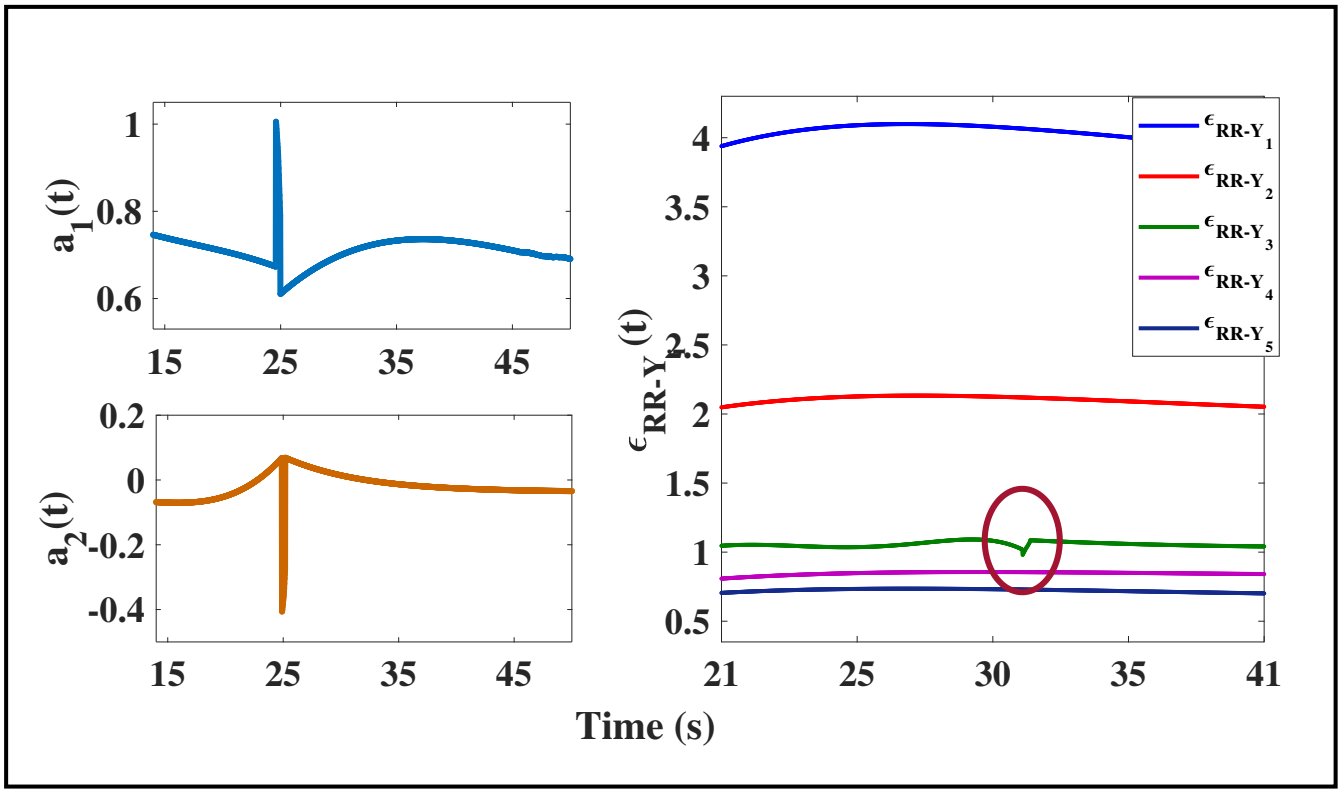

Figure 6.9: Recursive DSF plot for 20% spatio-temporal damage for the B-W system under El Centro excitation

damage for such a case. The performance check mainly assesses the functioning of the algorithm to determine damage from a subset of sensors, considered below:

1. Case 1: Generating a block covariance matrix using a subset of sensors instrumented at the 3^{rd}, 4^{th} and 5^{th} floors.

2. Case 2: Generating a block covariance matrix using the first set of responses obtained from 3^{rd}, 4^{th} and 5^{th} floors and the other set obtained from 2^{nd}, 3^{rd} and 5^{th} floors

For both these case studies, the previously described B-W system is considered that undergoes a temporal damage of 20% and 15% at 31s from the start. From a theoretical standpoint, the number of instrumented sensors must equal the number of actively participating modes, which is 3 in the present context. Thus the resultant underdetermined system is expected to produce POMs and POVs corresponding to the reduced system order. Once the block covariance matrix is created, the RCCA algorithm operates on the reduced order physical responses to provide a set of corresponding transformed responses, on which the TVAR models are fit. In this context, two cases are considered:

(i) a global damage considering 15% change in nonlinearity and (ii) a local damage case considering reduction of the linear storey stiffness by 20%, at 31s from the start of the excitation.

Detection results for Case 1:

The first case considers the streaming input data obtained from 3^{rd}, 4^{th} and 5^{th} floors that is required for creating a block covariance matrix. Once the transformed responses are obtained, the TVAR modeling is adopted that provides the key DSFs for identification of damage. The TVAR plots shown in Fig. 6.10 depict the exact instant of damage by indicating a change in the mean level at 31s. In order to validate these findings, the temporal RRE plot shows a distortion that confirms the damage event occurring at 31s. It is obvious that the present results are invariant of any instabilities that might arise due to the underdetermined nature of the responses, thereby demonstrating the superior prowess of the proposed scheme over recently established methods such as RPCA, that are prone to instabilities, even for a 20% global change in nonlinearity.

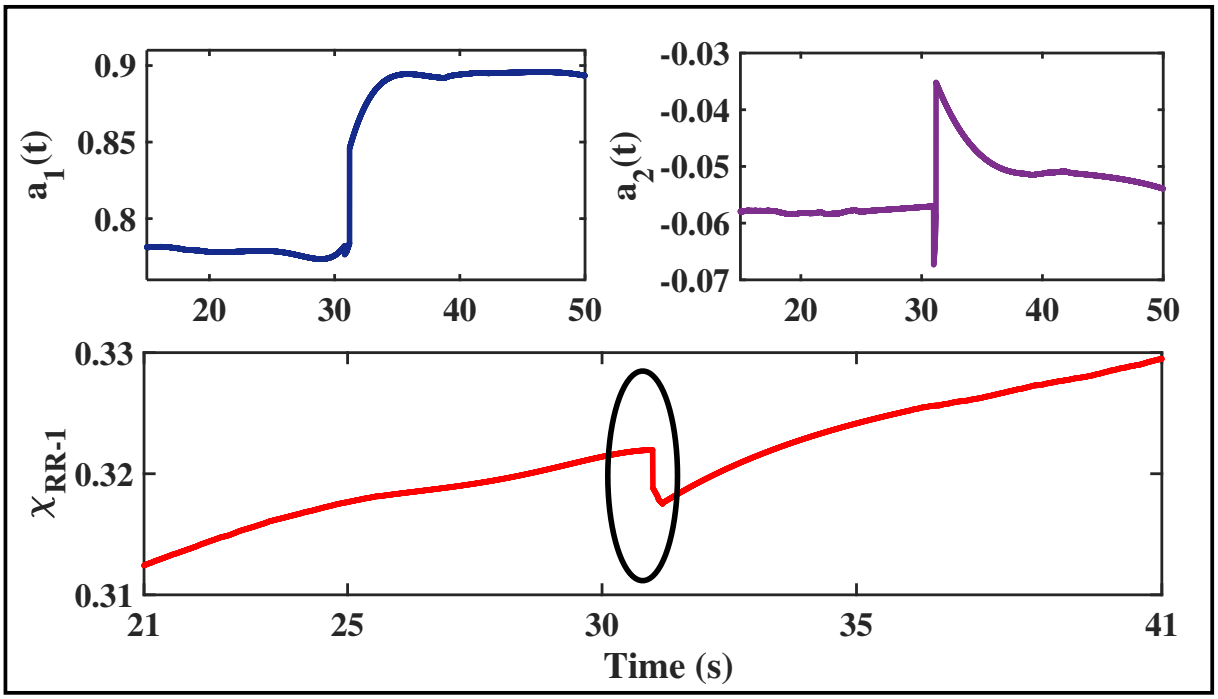

Figure 6.10: Recursive DSF plot for Underdetermined case-1, Global damage, 15% change in nonlinearity excited by white noise

Detection results for Case 2:

The present case provides an insight into the efficacy of the proposed scheme in determining spatio-temporal damage for an underdetermined case. The *first instance* considers the block covariance

matrix to be formed by the set of the physical responses obtained from 3^{rd}, 4^{th} and 5^{th} floors. The linear stiffness of the 3^{rd} storey is reduced by 20% at 31s from the start. The transformed responses are modeled using TVAR coefficients, portrayed in Fig. 6.11. The exact instant of damage is identified at 31s from TVAR plots. On determining the exact instant of damage, the spatial module of the algorithm is invoked where the local RRE for the reduced number of floors are tracked over time. It is clear from Fig. 6.11 that the local RRE corresponding to the 3^{rd} floor provides a significant distortion at 31s. It can therefore be interpreted that the absence of a similar pattern of distortion from the other floor levels validates the exact localization of damage, a phenomenon indeed confined only to the 3^{rd} storey of the system.

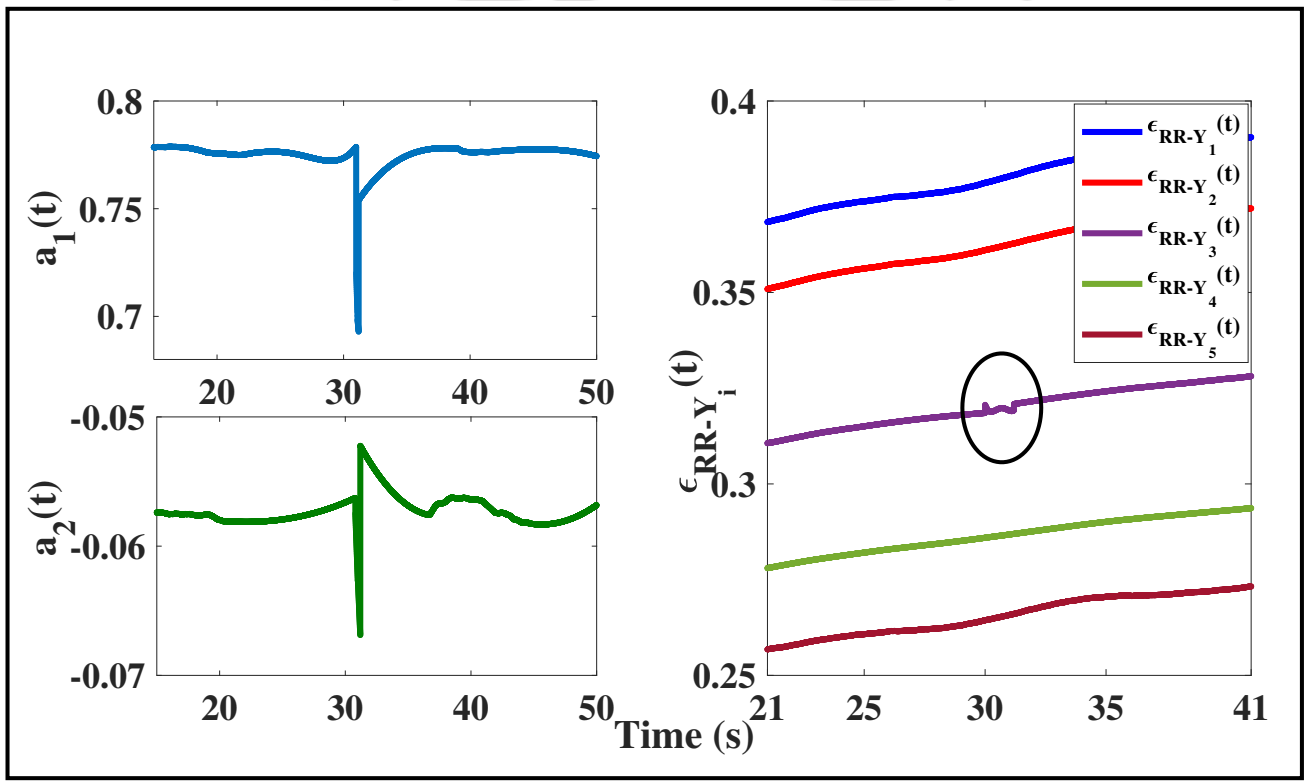

Figure 6.11: TVAR plot for Underdetermined case-2, first instance

The *second instance* considers the inputs two sets of response: the first set obtained from the 3^{rd}, 4^{th} and 5^{th} floor, while the other set is acquired from the 2^{nd}, 3^{rd} and 5^{th} floor response. The block covariance matrix is generated based on these inputs. It can be conjectured that the detectability of the proposed scheme under a non-identical set of responses might be affected, primarily due to the divergent nature of the input processes, which makes the individual covariance matrices dissimilar. The plots of recursive DSFs shown in Fig. 6.12 provides a clear insight into the matter. Although

the exact damage instant of 31s can be observed from the TVAR plots, the spatial module fails to provide adequate detection results for localizing the damage in real time. It is clearly visible that the distortions in the 3^{rd} DOF are not as noteworthy as the ones reported in the previous detection estimates, thereby rendering the spatial localization scheme inconsequential for this case. A review of the recently established RPCA based detection strategy provides a 20% and 30% lower limit of detectability for the global and local damage cases, respectively. Based on the above inferences, the proposed method successfully identifies comparatively finer levels of spatio-temporal damage, which is a key contribution, considering the real time essence of the algorithm.

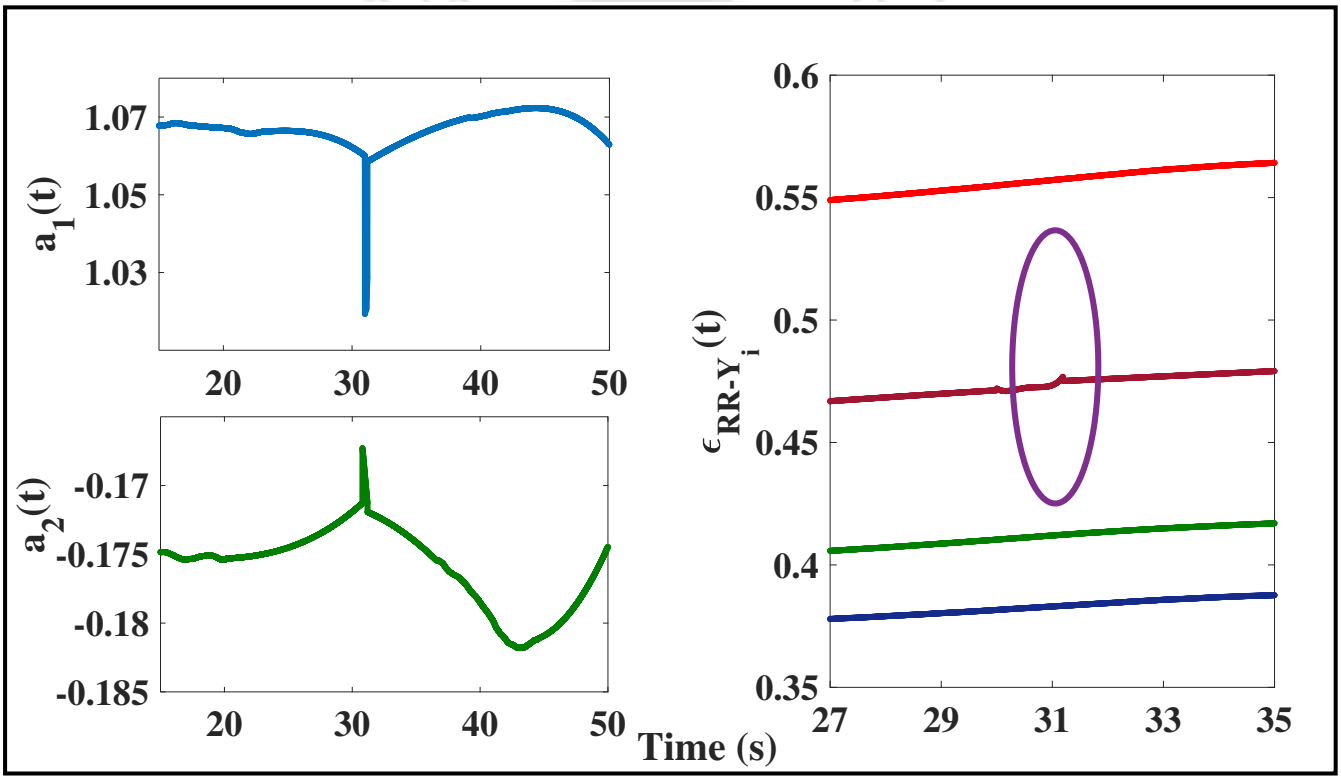

Figure 6.12: TVAR plot for Underdetermined case-2, second instance

6.6.4 Case study of a 7 DOF B-W system excited using white noise

A numerically simulated 7 DOF B-W system is excited using a Gaussian white noise of 50s duration, sampled at 100 Hz. An extension of the previously inspected 5 DOF B-W system, the key motivation of using this system for real time damage detection studies is to assess the performance of the method against an increase in the DOF. It is well understood that the nonlinear change at the base of the

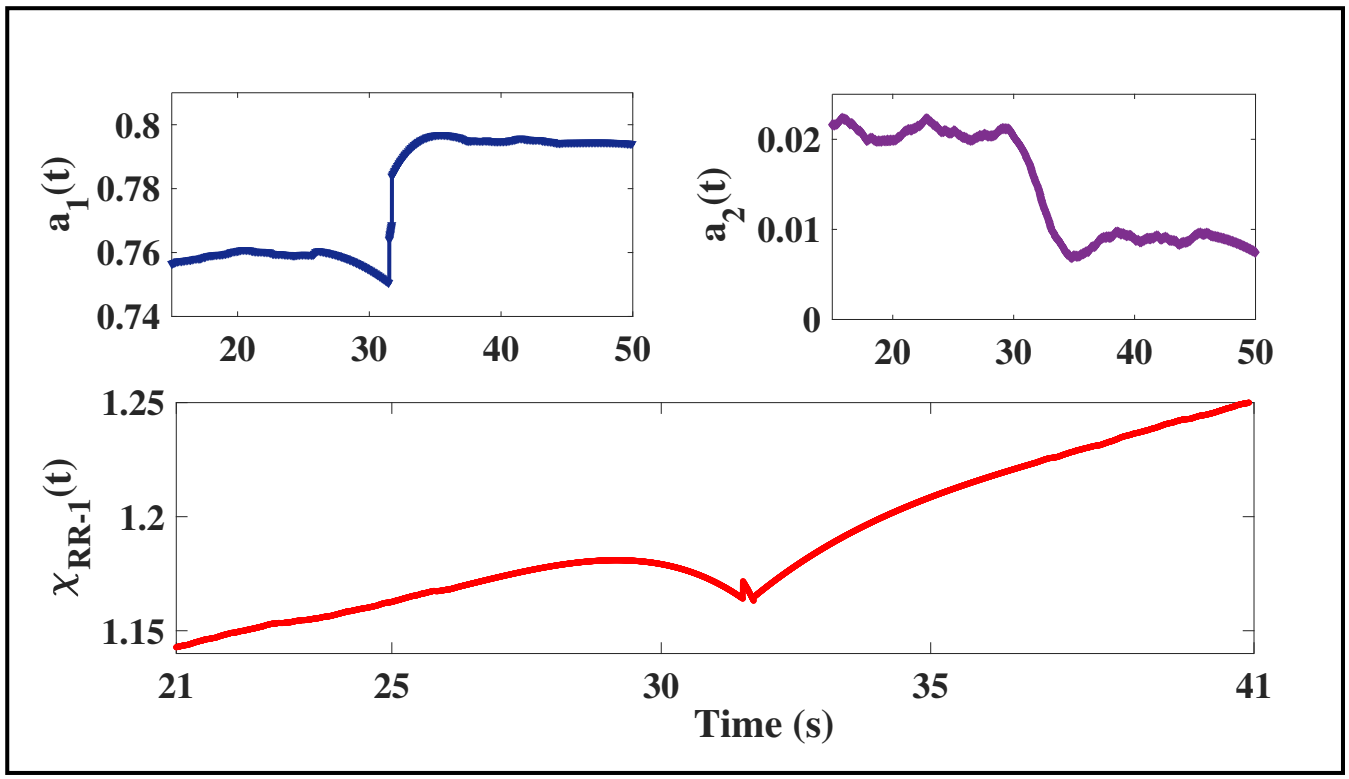

Figure 6.13: Recursive DSF plot for 20% damage for the B-W 7 DOF system under white noise excitation

model propagates strongly to the vicinity of the damage. Therefore, the nonlinear propagation throughout the model is an arduous task and can effect only a few of the neighboring DOF of the superstructure. In order to clearly understand the aspects of damage for an increased number of DOF, keeping all other factors invariant, the proposed method is applied on to the model under consideration and the detailed results are reported. In this context, the nonlinear force parameter κ is varied by 20% and 15%, individually, at 31s from the commencement of the excitation. The recursive DSFs shown in Fig. 6.13 clearly portray the exact instant of damage through a sharp change in the mean level at 31s. Additionally, Fig. 6.14 provides successful detection results for a 15% real time damage to the 7 DOF B-W system.

A salient feature of the DSFs can be observed here. A recently established real time damage detection algorithm, RPCA, has provided successful results for a 15% temporal damage case. The study, conducted on a 5 DOF B-W system failed to show significant distortions in the global RRE plots. The robustness of the DSFs lie in their ability to determine damage for a wide range of applications, including a varied class of nonlinear systems as well. One of the key features of the

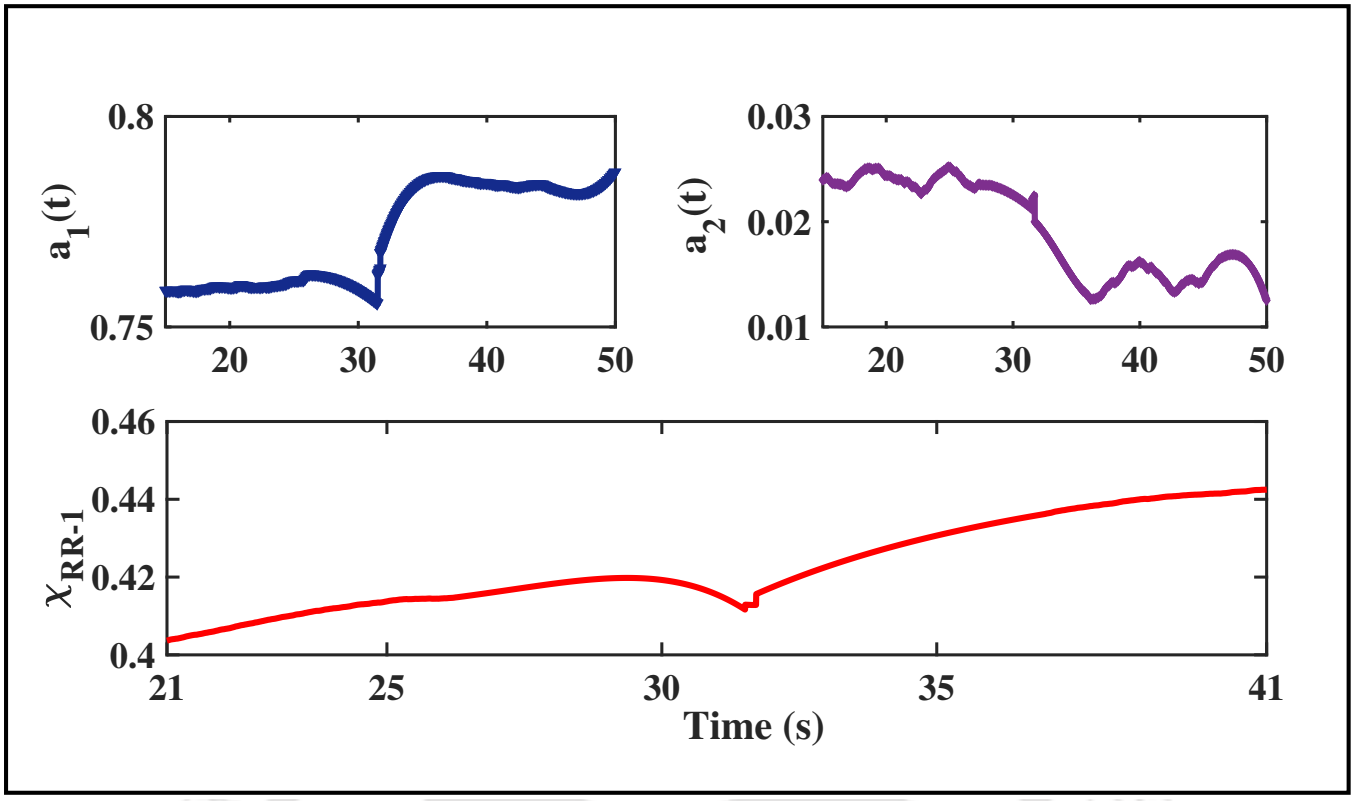

Figure 6.14: Recursive DSF plot for 15% damage for the B-W 7 DOF system under white noise excitation

proposed scheme is to incorporate the same specific set of DSFs for a wide class of problems dealt within the scope of this study, without compromising on the time complexity or the efficacy of the proposed methodology. Therefore, the significant distortion in the RRE plots displayed in both the Fig. 6.13 and 6.14 is of key importance and provides extensive evidence towards the effectiveness of the proposed methodology and thereby, the DSFs.

The key entitlement of the work lies in the ability of the method to identify spatio-temporal damage in real time. Following a similar notion, the proposed RCCA method is examined for a local damage case for the 7 DOF B-W system. From the previous detailed discussions, it is clear that the change in the linear storey stiffness remains confined to a single DOF; therefore, the proposed method is expected to provide credible results for spatio-temporal damage for the current model as well. Hence, it is envisioned that the RCCA scheme will provide successful detection results for a similar percentage of local damage in real time. In this regard, the linear storey stiffness of the 3^{rd} floor is reduced by 15% and 10% and studied extensively in separate case studies. For the first case, the sharp peak of the TVAR plots shown in Fig. 6.15, indicate a clear damage instant at 31s.

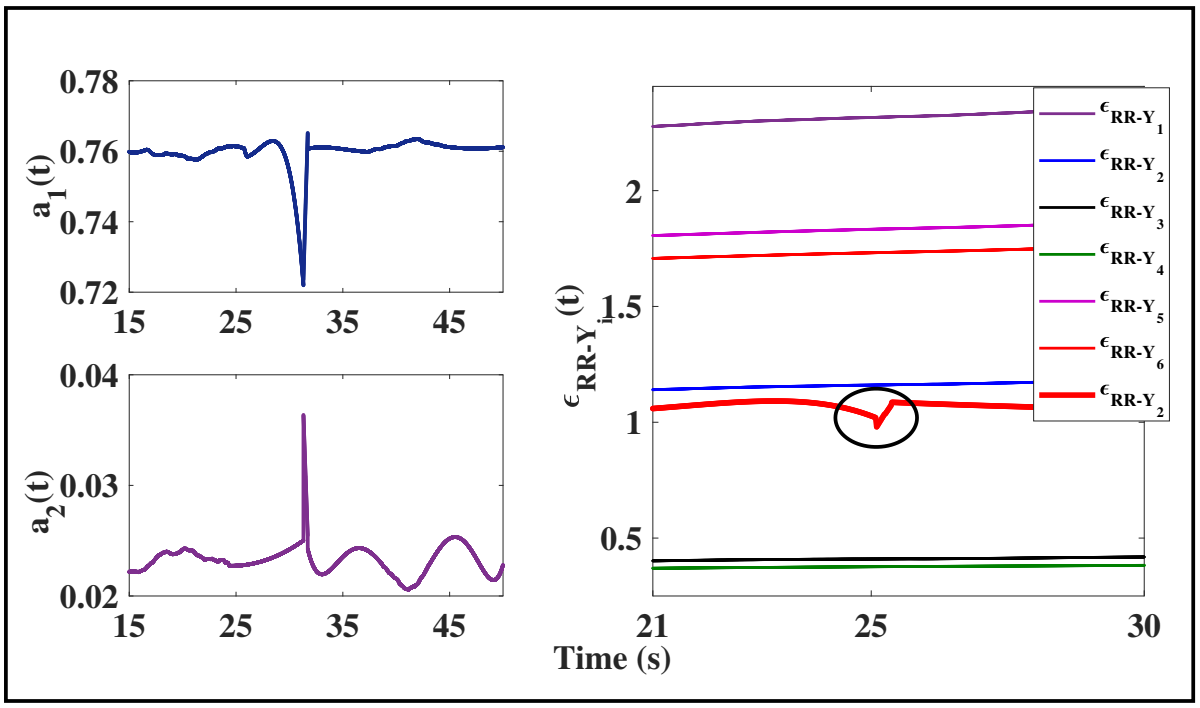

Figure 6.15: Recursive DSF plot for 15% spatio-temporal damage for the B-W 7 DOF system under white noise excitation

While the spatial RREs of all the other floors fail to indicate a distortion, the significant deviation that occurs in the 3^{rd} storey of the system, validate the exact occurrence of damage, recursively, in a simultaneous framework. Detection results for a 10% linear storey stiffness change is provided in Fig. 6.16 that clearly brings out the spatio-temporal aspect of the proposed framework. Based on the above discussions, some of the key conclusions that can be drawn are:

1. The propagation of the change in nonlinearity for an increased number of DOF is comparatively less, an concept that is discussed in details in the later stages of the chapter.

2. The use of RRE as an efficient DSF even for fine level of damage of the order of 10% is a key entitlement of the work, which readily provides an authentication to the efficacy of the proposed algorithm in addition to recognizing the utility of the said DSFs.

3. The algorithm provides almost similar results for local damage detection for both the above mentioned B-W systems. The purpose of carrying out a separate case study for the 7 DOF system is to effectively recognize the utility of the RCCA method against similar conditions of damage in real time.

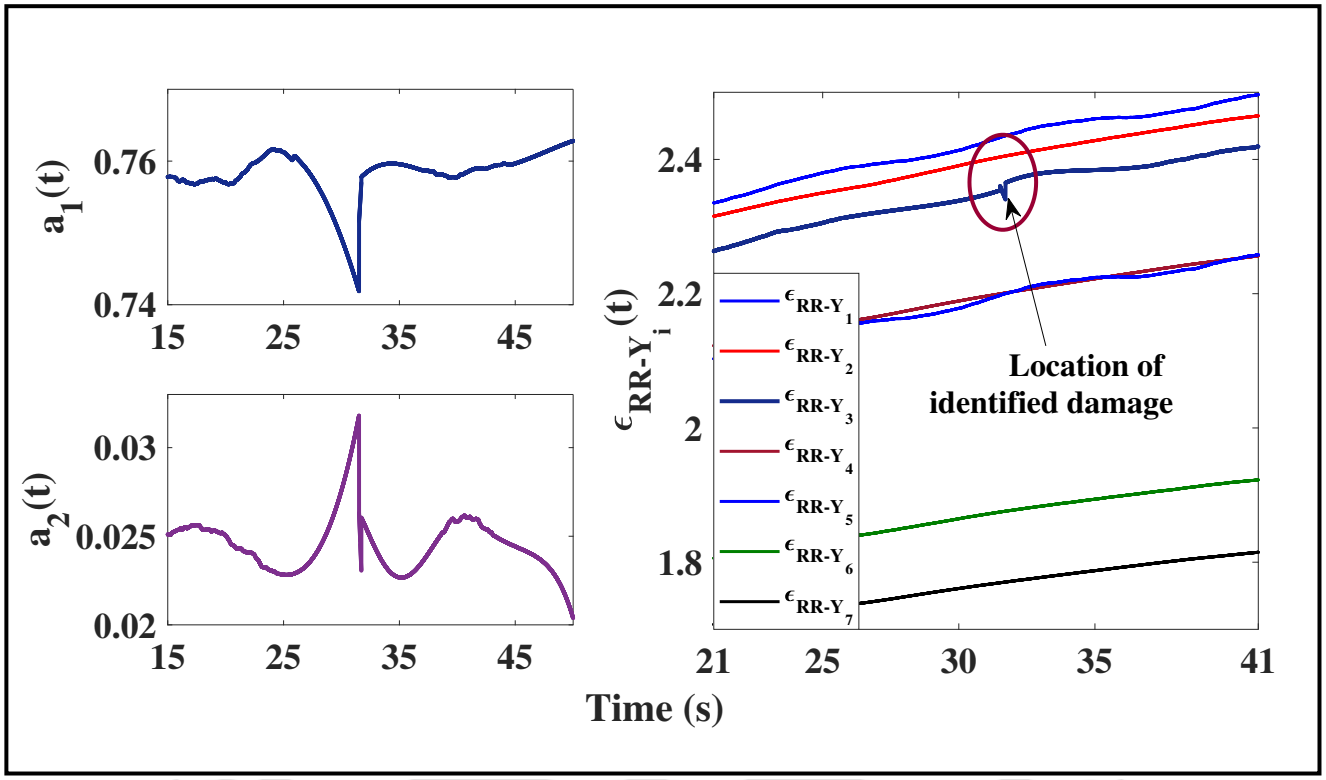

Figure 6.16: Recursive DSF plot for 10% spatio-temporal damage for the B-W 7 DOF system under white noise excitation

6.6.5 A note on the effect of the increased DOF on the detection results using the proposed algorithm

The central idea to the development of this section is to investigate the detection potential of the proposed RCCA algorithm towards an increased number of DOF. The 7 DOF B-W system is simulated based on the consideration that the two newly added floors exhibit a linear storey stiffness, that could be altered to induce a local damage to the system. The global damage cases, however, adhere to the previous notion of the change of the nonlinear force parameter at the base of the model, thereby imparting a temporal damage to the model. The detection results using the proposed algorithm have already been presented in the preceding sections and are not repeated here for brevity. Considering the figures 6.2 and 6.14, it can be very well established that the TVAR plots provide information regarding the exact damage instant to the system. However, the RRE plots presented in Fig. 6.14 provides an approximate estimation of the damage instant. As previously mentioned, the propagation of the change of the nonlinearity throughout the model is comparatively

reduced due to an increased DOF of the system. Therefore, although the effect of global damage is appropriately captured by the TVAR coefficients for both the cases, the RRE plots provide an rough estimation for the 7 DOF B-W system, which can be considered as a direct implication of the increased number of DOF.

The local damage cases, however, are expected to show similar results for both the systems in context. A summary of the detection results for the systems can be obtained from Figu, 6.4 and 6.15 for a 15% change in the linear storey stiffness. As the proposed method successfully provided consistent detection results for a 10% saptio-temporal damage for the 5 DOF B-W system (Fig. 6.5), it is expected that the method should present similar results when the model is replaced with an increased number of linear DOF, depicted in Fig. 6.16. It can therefore be well concluded that due to the confinement of the damage to a single storey, the proposed method provides similar spatio-temporal damage detection results for both the aforesaid models, in real time.

6.6.6 Case study for a strongly nonlinear system: A 5 DOF structure modeled with Duffing oscillator on its 3^{rd} floor

In this section, the efficacy of the proposed method is assessed against a strongly nonlinear 5 DOF system, modeled with a Duffing oscillator on its 3^{rd} floor. While the source of nonlinearity is provided by the Duffing parameter α, obtained from the governing differential equation of motion for the system, the other 4 floors are idealized as having linear storey stiffness. The concept of global damage emanates from the previous notion of changing the nonlinear force term that brings about a state of temporal damage throughout the system and the local damage is numerically simulated by altering the linear storey stiffness of a floor at a particular instant of time. The system is excited using Gaussian white noise for a duration of 50s, sampled at 100 Hz. The cases of global and local damage are separately discussed next in detail.

The numerical simulation of global damage is carried out by changing the value of the nonlinear force parameter α at 31s, presented in two individual case studies of 20% and 15% change. In the later stages of the chapter, the performance evaluation of RPCA is also provided that inspects its potential to identify damage for a strongly nonlinear system. For the first case, TVAR modeling is

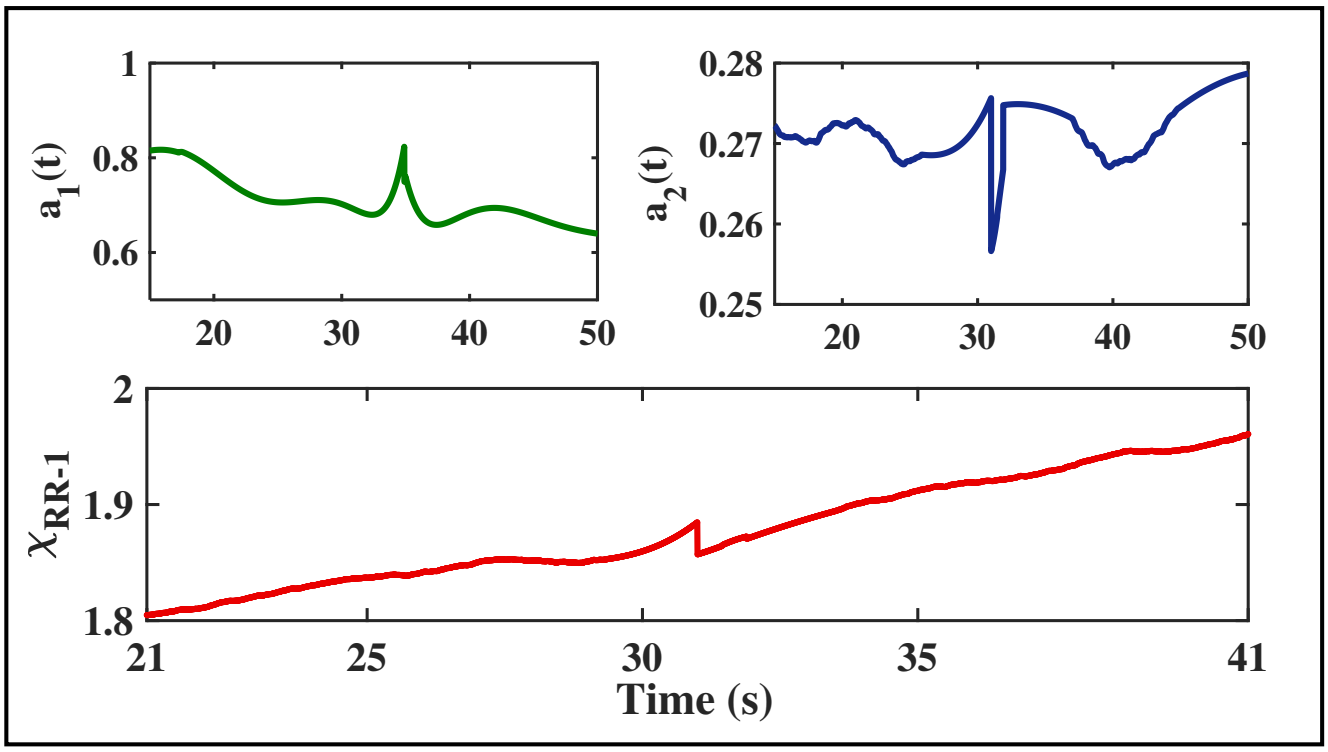

Figure 6.17: Detection results for 20% temporal damage for the strongly nonlinear system

adopted on the transformed responses to yield the TVAR coefficients, clearly shown in Fig. 6.17. The sharp peak of the TVAR coefficients, accompanied by a significant distortion in the temporal RRE plots confirms the exact instant of damage at 31s. On reducing the α value by a fine level of 15% in real time, the generated recursive DSF plots are shown in Fig. 6.18. It can be clearly understood from the figure that the proposed algorithm is able to effectively identify the instant of damage for a fine level as low as 15%, which is a tough accomplishment considering the strongly nonlinear nature of the system and the recursive essence of the proposed method. It can be envisaged that the performance of the RPCA algorithm in evaluating damage for a strongly nonlinear system might not show consistent results, based on the premise that the RPCA methodology is pivoted around identifying damage patterns of linear to weakly nonlinear system. Nevertheless, a fare comparison of these methods in the subsequent sections of the manuscript is attempted.

Proceeding to the next case, the spatio-temporal damage detection prowess of the proposed method is examined in a simultaneous framework. conforming to the previous notion of change in linear storey stiffness as an indicator of local damage, the 2^{nd} floor of the model undergoes a stiffness

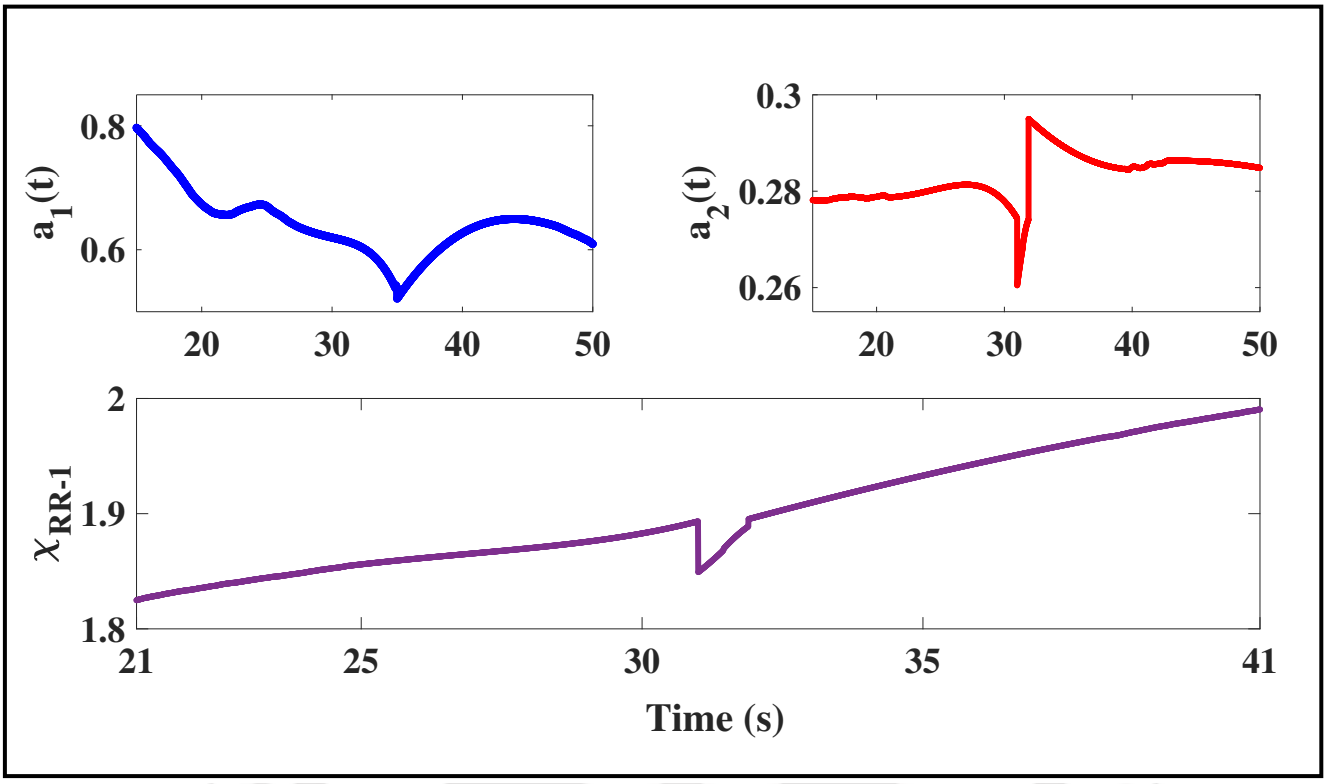

Figure 6.18: Detection results for 15% temporal damage for the strongly nonlinear system

change at 31s from the start. The damage cases of 20% and 15% are discussed next in detail. The detection results for the first case are displayed in Fig. 6.19, from which the exact instant of damage at 31s is clearly visible through the TVAR plots. Once the temporal damage is ascertained, the RCCA algorithm shifts to the spatial module where the local RREs for all the floors are tracked recursively. A significant distortion in the 2^{nd} floor RRE and its absence in others, confirms the location of the damage, confined to the 2^{nd} storey. Similar to these findings, the 15% spatio-temporal damage detection case also provides adequate evidence to suggest the instant of damage at 31s and its localization in the 2^{nd} storey of the system. Considering the strongly nonlinear behavior of the system and the simultaneous spatio-temporal damage detection capability of the proposed method, the above findings hold a major entitlement of this research.

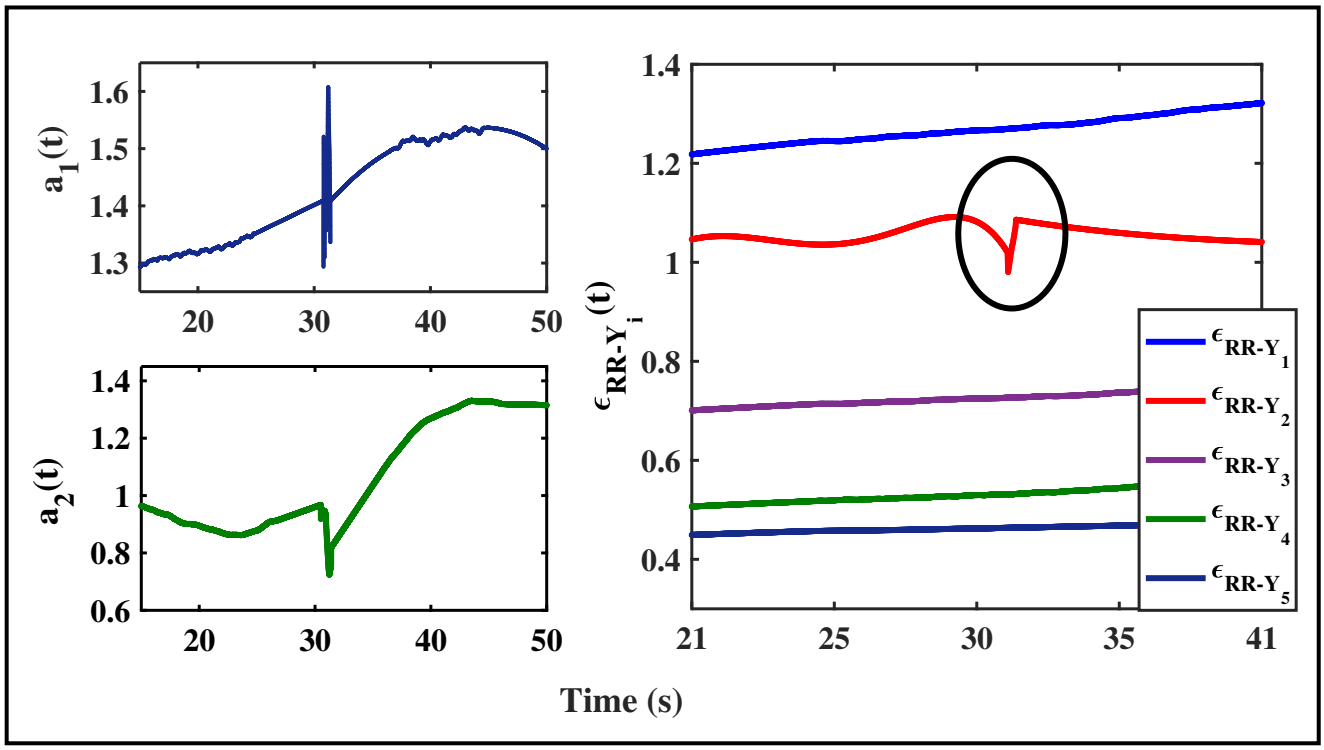

Figure 6.19: Spatio-temporal damage detection for strongly nonlinear system for 20% damage

6.6.7 A case study with negligible non-linearity: Spatial damage detection

In this section, the potential of the proposed RCCA towards an almost linear system is examined. The previous discussions were mainly centered around nonlinear systems and therefore, it becomes imperative to understand the applicability of the method towards a linear system as well. Obtaining a purely linear system is impractical, considering the material properties and the geometric nature of the system; hence, the nonlinear parameter α of the above mentioned model is scaled down to 0.005, which is negligible and can closely emulate to a linear state of the system. The spatio-temporal damage detection case is studied by considering a 20% damage to the system at 31s from the start, to the 2^{nd} storey of the model. It can be clearly observed from Fig. 6.21 that the TVAR plots are effective at identifying the temporal damage instant through a sharp peak at 31s. Once the spatial module gets invoked, the local RREs for the 2^{nd} floor shows a significant distortion that confirms the presence of damage confined to that storey. Hence, it can be concluded that the proposed method is effective in identifying the spatial and temporal patterns of damage for both linear and nonlinear

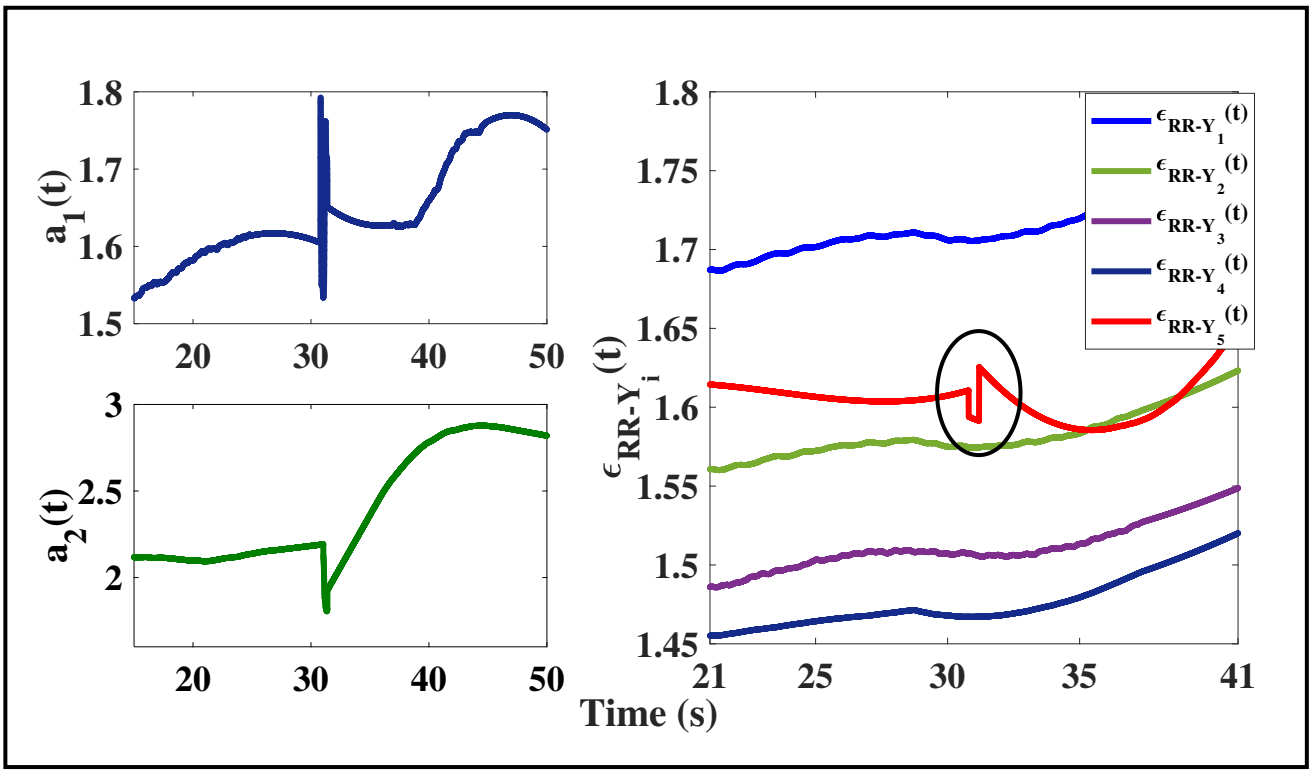

Figure 6.20: Spatio-temporal damage detection for strongly nonlinear system for 15% damage

systems to a fair degree to accuracy, as evident from the underlying findings.

6.7 Performance check of the proposed method against RPCA: A comparative study

In this section, the performance check of the proposed method against a recently established real time damage detection scheme, utilizing the concepts of RPCA, is provided. The performance evaluation of the proposed method against its recently established counterpart takes place in three major case studies:

1. Global and local damage detection case studies for the 5 DOF B-W system excited using white noise

2. Global damage detection studies for the 5 DOF B-W system excited using El Centro ground motion

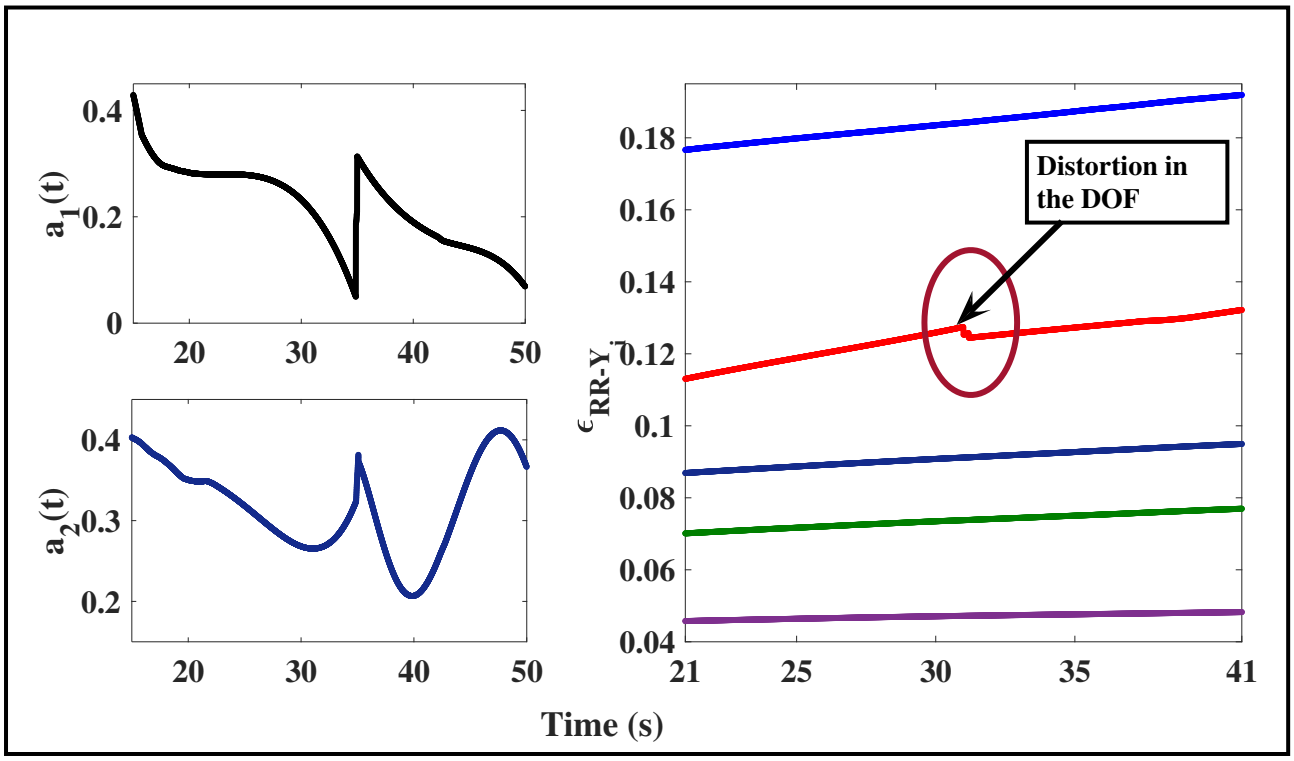

Figure 6.21: Spatial damage detection for almost negligible non-linearity (α =0.05)

3. Local damage detection studies for the 5 DOF system modeled using a Duffing oscillator on the 3^{rd} floor, excited using white noise

6.7.1 Case studies for the 5 DOF B-W system using white noise

The 5 DOF B-W system previously described is taken into consideration to examine the real time damage detection performance of both RCCA and the RPCA algorithms. The RPCA algorithm is a recently established real time scheme that has been published in the Journal of Mechanical Systems and Signal Processing, and is an important contribution in the context of real time damage identification of structures. The basic premise of the method was centered around finding damage for linear to weakly nonlinear systems. Since RPCA and RCCA both consider the EVD of the covariance matrices through their formulations, it becomes imperative to understand the performance of both the said methodologies for the same damage conditions. In this context, the global damage cases are first presented, followed by the results of the local damage detection.

Case study for 15% global damage detection using 5 DOF B-W system

The global damage is carried out by changing the nonlinear force term κ at 31s by 15%. Detection results obtained using RCCA can be found in Fig. 6.4. The RPCA algorithm operates in a similar fashion by first creating a covariance matrix out of the physical responses, performing a batch PCA on the initial samples and then using FOEP to estimate the eigenspace updates at each instant of time. Using TVAR coefficients, the transformed responses are modeled and the detection results using both the algorithms are shown Fig. 6.22. It is evident from the plot that the RPCA algorithm shows certain instabilities for such a low percentage of damage in real time, which can be primarily attributed due to the nature of the covariance matrix obtained from the physical responses. In comparison, the RCCA method creates a block covariance matrix that provides eigenspace updates at each time instant, and therefore, devoid of instabilities of any kind. Moreover, the RPCA algorithm is premised mostly linear system theory and its applicability towards a weakly nonlinear system is its direct extension. Therefore, it can be concluded that the RCCA method provides better estimates of detectability even for a fine level of damage in real time as compared to the RPCA scheme. However, it should be noted that both the algorithms provide a reasonable first-hand representation of the instant of damage in real time.

Case study for 25% local damage detection using 5 DOF B-W system

In this section, the performance of the FOEP based RPCA and RCCA methods are examined for a 25% spatio-temporal damage. A snapshot of the comparative study is provided in Fig. 6.23. It can be observed from the plot that both the recursive algorithms are able to identify the exact instant of damage at 31s that occurs in the 3^{rd} storey of the system. However, from a straightforward visual inspection of the figure, it can be understood that the RPCA algorithm is susceptible to certain instabilities that might arise due to the inherent nonlinear nature of the system. Contrary to this, the RCCA method provides smooth detection results and therefore, preferred in identifying damage for a nonlinear system over the recently established RPCA framework.

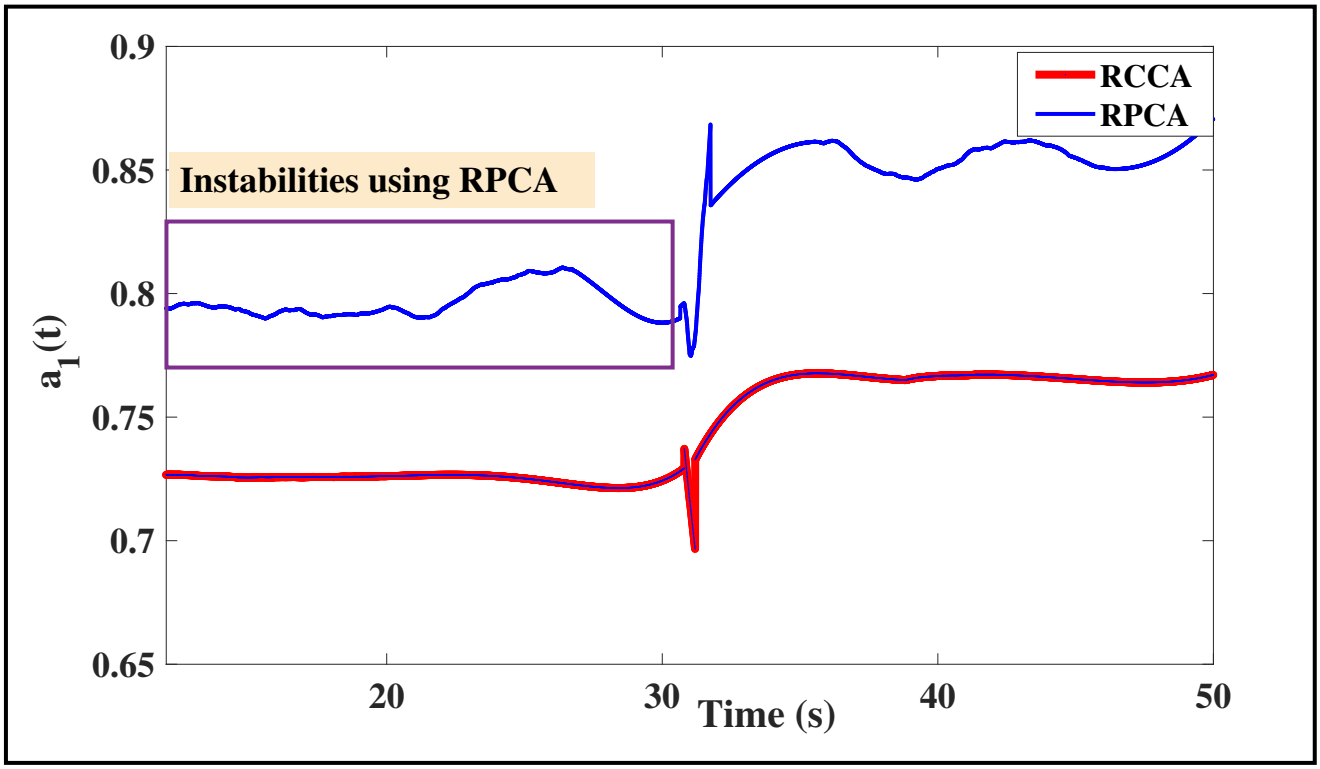

Figure 6.22: Comparison between RCCA and RPCA for 15% global damage using 5 DOF B-W system (under white noise excitation)

6.7.2 Case study for the 5 DOF B-W system excited using El Centro ground motion

A review of the recently established real time damage detection literature reveals that a 30% global damage for a nonstationary excitation is reported as the lower limit of detectability. However, the present work has successfully proposed *spatio-temporal* damage detection studies as fine as 20%, in real time. Based on these discussions, an even comparison with the RPCA method can only be justified at its lower limit of detectability, i.e, at 30% global damage. The detection results provided in Fig. 6.24 show a clear instant of damage at 31s using both the algorithms. While the TVAR plots using RCCA provide impeccable detection results, the plots obtained using RPCA is highly susceptible to the nonstationarities that arise due to the input excitation. This creates a zone of significant instability in the TVAR plot, thereby rendering the application of RPCA under nonstationary environment, ineffective. Hence, it can be safely concluded that the proposed RCCA algorithm provides better damage detection results in real time even for a nonstationary excitation

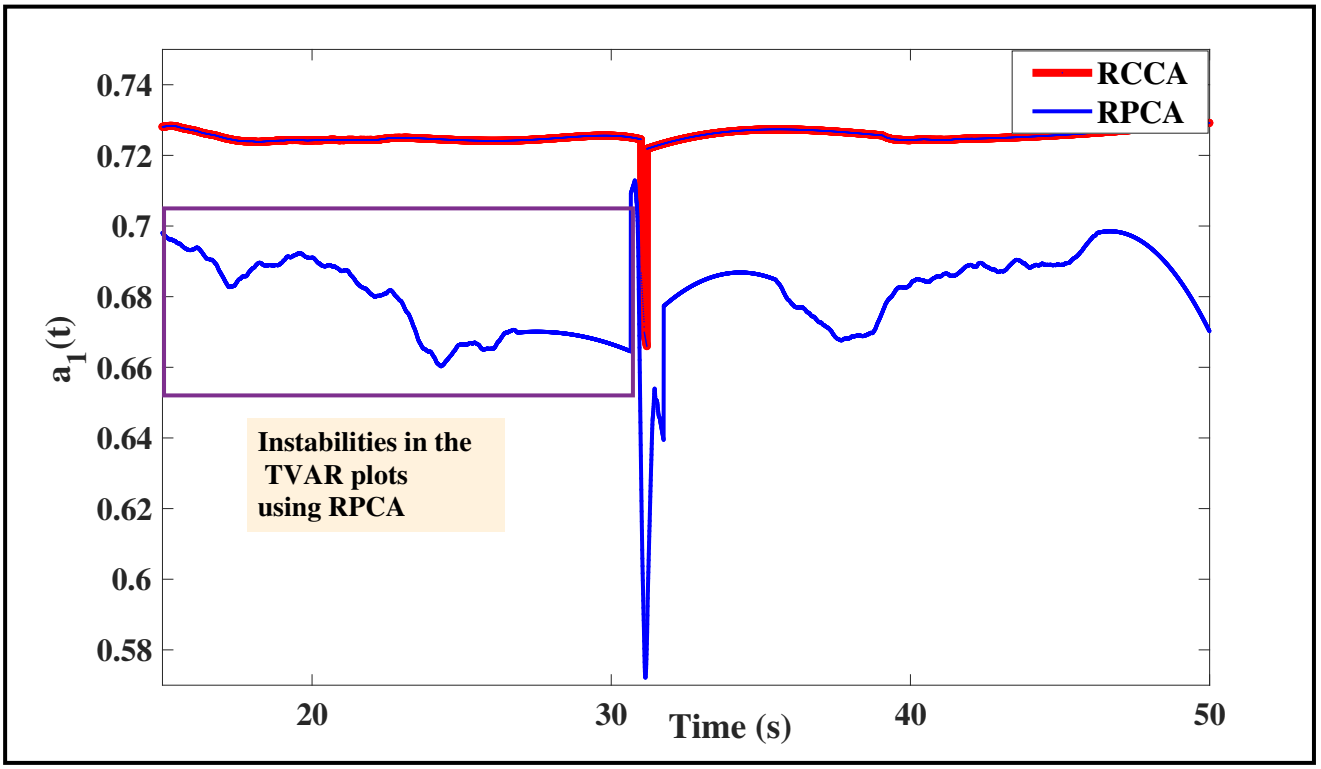

Figure 6.23: Comparison between RCCA and RPCA for 25% local damage using 5 DOF B-W system (under white noise excitation)

for a nonlinear system as well.

Table 6.2: Percentage changes in statistical mean of TVAR coefficients

Damage condition	Method	Mean (undamaged)	Mean (damaged)	% change	Mean+SD (undamaged)	Mean+SD (damaged)	% change
15% global (WN)	RCCA	0.71	0.76	6.72	0.78	0.77	0.85
	RPCA	0.79	0.85	7.70	0.85	0.86	1.06
25% local (WN)	RCCA	0.68	0.69	1.47	0.73	0.70	4.92
	RPCA	0.67	0.69	2.98	0.72	0.69	4.98
30% global (El Centro)	RCCA	-0.01	-0.008	20	-0.009	-0.005	45.56
	RPCA	0.13	0.005	64.54	0.14	0.051	62.22

The percentage changes in the mean level of the TVAR coefficients are shown in Table 6.2. It is well understood the wavy modulations indicated by the fluctuations in the TVAR plots obtained from the RPCA transformed responses can be accounted through the recursive standard deviations (SD) pre and post damage. It can be inferred from the statistical descriptions shown in Table 6.2 that the RPCA algorithm provides a significantly higher percentage change of the recursive SD before and after damage. This can mostly be attributed due to the inconsistent modulations in the TVAR

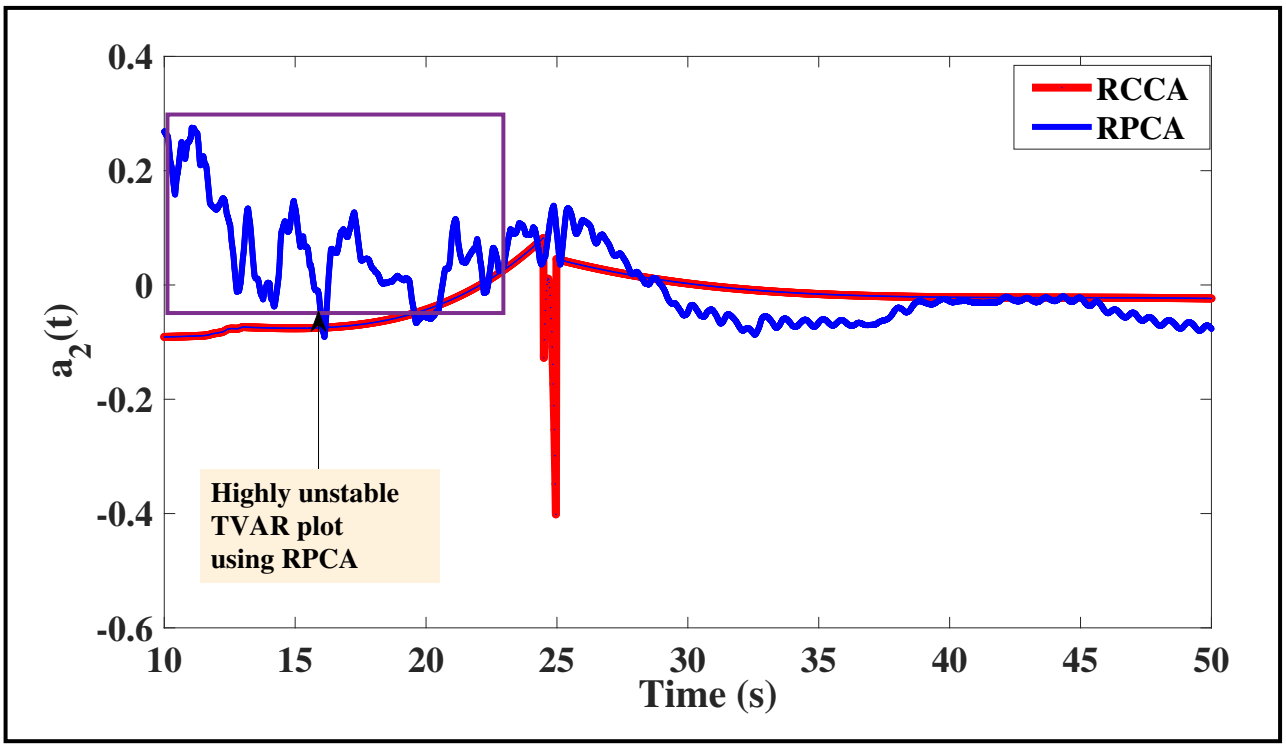

Figure 6.24: Comparison between RCCA and RPCA for 30% global damage using 5 DOF B-W system (under El Centro excitation)

plots obtained from the RPCA algorithm, clearly depicted in Fig. 6.22, 6.23 and 6.24. A change in the mean level of the TVAR coefficients obtained from both the algorithms correspond to the occurrence of damage inflicted to the system at 31s. The higher percentage change of the statistical parameters reflected by the RPCA-TVAR algorithm characterize the presence of instabilities in the recursive DSF plots.

6.7.3 Performance check of the proposed method against RPCA for a strongly nonlinear system

In order to inspect the performance of a recently established real time damage detection scheme, RPCA, is applied on the streaming vibration data obtained from the strongly nonlinear system. The 5 DOF system modeled with a Duffing oscillator on its third floor experiences a reduction of stiffness in its 2^{nd} storey by 20%, considered as a local damage to the structure. It is well understood that both the real time detection schemes, RCCA and RPCA, will provide transformed

response at each time stamp, on which the TVAR models are subsequently fit. The comparative study considers the performance of the TVAR coefficients, shown in Fig, 6.25. It is evident from the plots that the RCCA algorithm provides a distinct identification of the instant of damage at 31s from the straightforward change in the mean level of the TVAR coefficients. In contrast, the TVAR plots obtained from the RPCA response show numerous peaks even before the instant of damage is attained, which correspond to local change in the mean levels. This primarily occurs due to the presence of strong nonlinear component in the vicinity of damage that affects the detection prowess of the RPCA algorithm, which is premised mostly on linear and weakly nonlinear systems. This aspect has already been previously demonstrated through the aforesaid comparative studies presented in the chapter. It can therefore be conclusively inferred that the proposed RCCA algorithm provides better detection results in real time, even for a strongly nonlinear systems, in comparison to the recently established RPCA scheme, that has consistently shown improper identification results for the same.

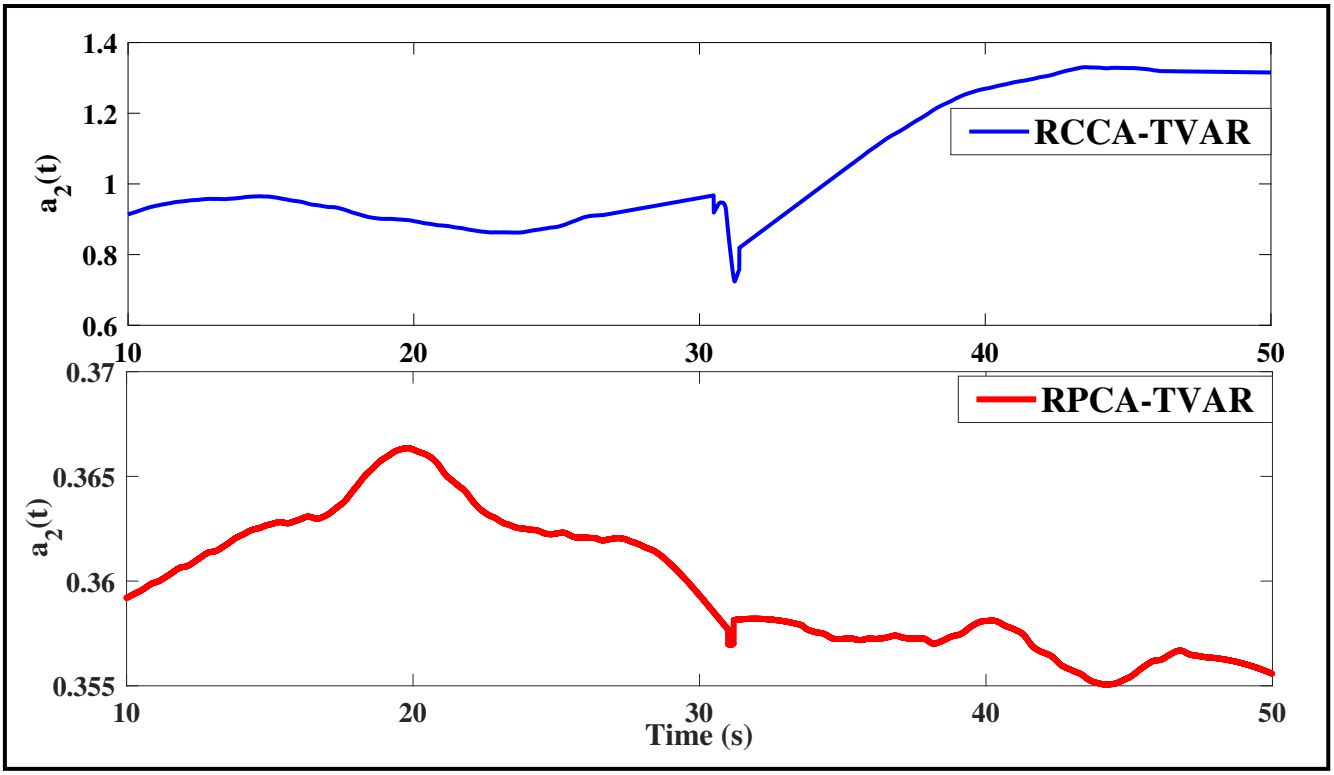

Figure 6.25: Comparison between RCCA and RPCA for strongly nonlinear system

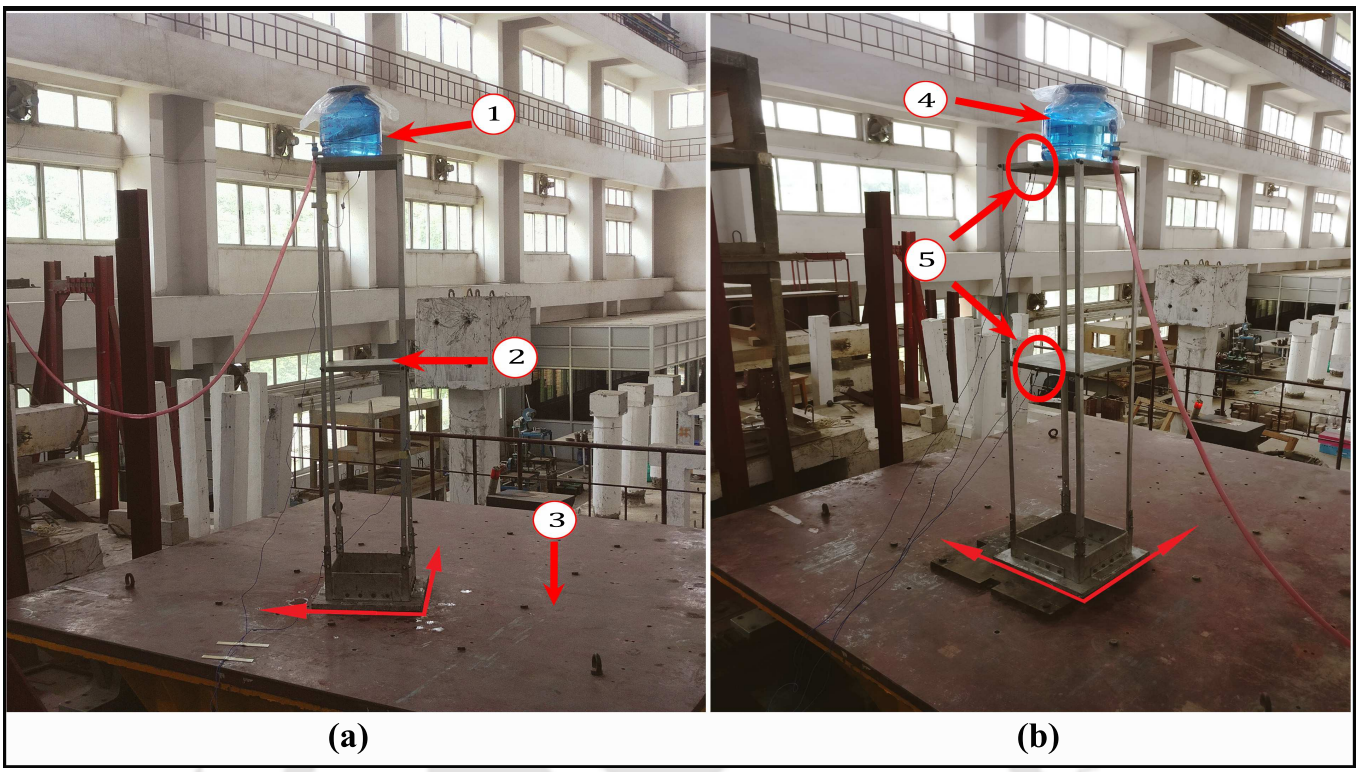

Figure 6.26: Details of the experimental setup: (a) biaxial and (b) orthogonal directions

6.8 Experimental verifications

A crucial feature of any algorithm is to assess its effectiveness by validation through experimental case studies, carried out under controlled laboratory environment. In the recent years, numerous experimental setups have been developed that closely emulate real time damage scenarios. In the present work, the focus has shifted towards detecting the change of state from a linear to nonlinear regime and vice versa, through an extensive experimental setup. To substantiate the robustness of the proposed approach, an experimental setup is devised consisting of a two-storey aluminum shear building prototype placed with a water dispenser at its top floor. The aluminum model is of height $1.5m$ with inter-storey distance of $0.74m$ fixed on a base plate that is bolted on top of a shake table. The cross section of the base measures $0.3m \times 0.3m \times 0.02m$ placed on the $0.15m$ thick base plate and firmly bolted against the shake table. The water dispenser of height $0.26m$ is firmly affixed to the roof plate using commercially available epoxy resin. The model is subjected to scaled Gaussian white noise excitation and the acceleration data are collected using QuantumX MX410 HBM Data Acquisition (DAQ) system at a sampling frequency of $400Hz$. The shear building

model is instrumented at the floor levels in orthogonal directions using PCB Piezotronics triaxial acceleormeters of sensitivity $100mV/g$, bearing a frequency range of $0.5 - 10000Hz$. The dispenser when filled with water provides nonlinearity to the setup. This comes into effect when the water sloshes against the walls of the dispenser as the model is subjected to scaled vibration excitation. The flow valve of the dispenser emancipates water at the rate of $1L/30s$ during the run-time of the experiment.

The experimental trials were conducted at two different alignments of the shear building model (Fig. 6.26): **Alignment A**: The model is placed along the axis of the shake table with the local x-axis coinciding with the global x-direction and **Alignment B**: The model positioned at a non-orthogonal orientation with respect to the global x- and y-axes. For each of these cases, the experiment is carried out by allowing the water to drain out of the dispenser at 0s and at 20s in separate trials, that continued for the remainder of the excitation. The time stamp of the trial was captured using a stop watch and the experiment was also recorded in the form of videos, in order to gain an immaculate insight about the dynamics of the process. The streaming acceleration data is recorded and the proposed algorithm is applied in real time that yields the transformed responses. As the water drains out from the system, the sloshing of the water leads to a variable mass loss that accounts for the transition from nonlinear to linear state, which can be distinctly identified using the proposed method, described next in detail.

In addition to demonstrating the detection potential of the RCCA algorithm, the performance of the recently established RPCA method is also dealt with in detail. Based on the previous discussions, it can be easily understood that the RPCA algorithm premises on the concept of orthogonal transformations for data gathered from linear to weakly nonlinear systems. Its performance for a multi-directional case can therefore, be expected to falter as the formulation of the algorithm does not take into consideration the effects of torsionally coupled systems involving multi-directional dependencies. In this regard, the application of both the algorithms on the streaming dataset from the experimental trials generate eigenspace updates at each time instant, from which the transformed responses are modeled using TVAR approach. The comparative study of the performance of these recursive algorithms are discussed in the following section.

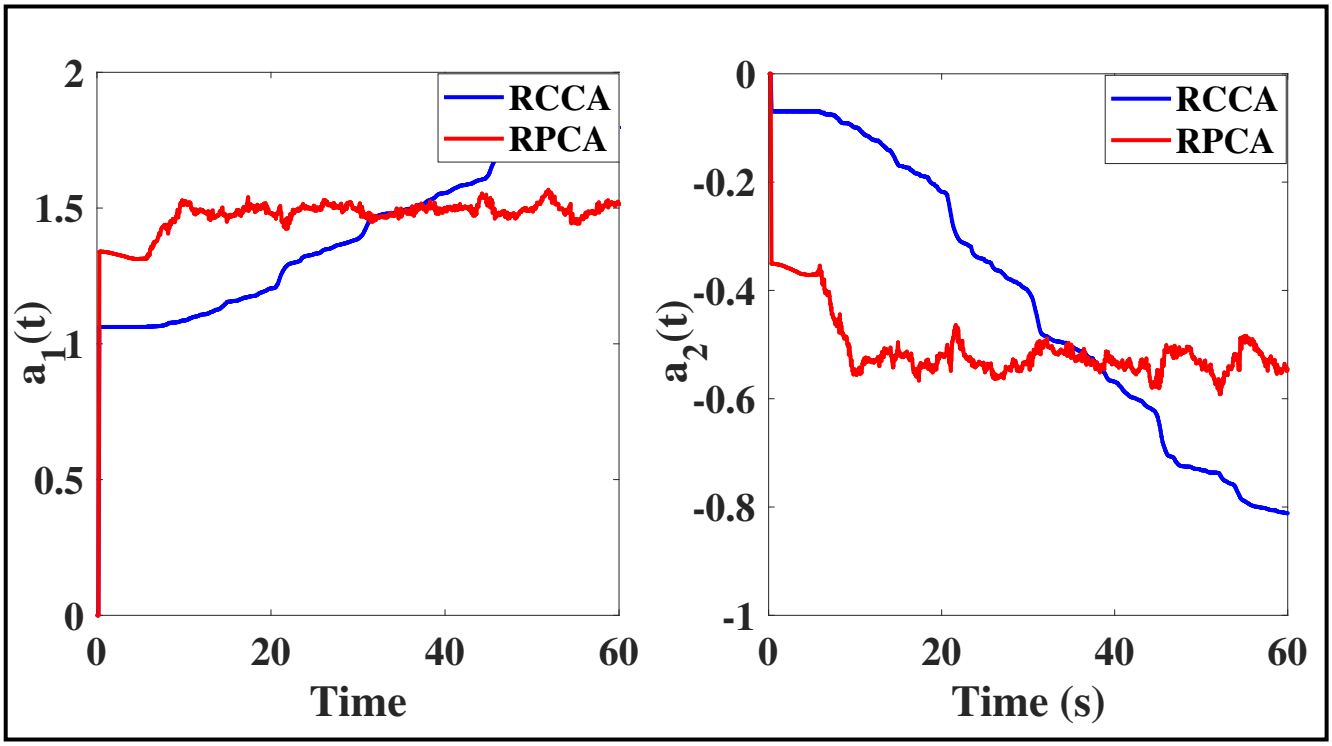

Figure 6.27: DSFs for mass loss at 0s, Alignment A

6.8.1 Detection results for the experimental trials: A comparative study with RPCA

The behavior of the recursive DSFs for Alignment A are illustrated in Fig. 6.27 and 6.28, for the mass loss at 0s and 20s, respectively. For the case where the water drains out at 0s from the start, Fig. 6.27 shows a gradual change in the mean level of the TVAR coefficients. The draining of water is a continuous event, which necessitates that the recursive damage markers should be able to illustrate a similitude through their representations. This conceptualization can be exactly inferred from the TVAR coefficients where the consistent changes in the mean level of the plots correspond to a gradual loss of water from the system. This clearly depicts the transition from a nonlinear to a linear state of the model, validated by the DSF plots. Considering the TVAR plots obtained from the RPCA algorithm, the coefficients displayed in Fig. 6.27 indicate the initial regime, but the inconsistency of the plots gradually impedes its expected utility. The loss in mass due to water drainage is a gradual event, a fact corroborated by the DSFs obtained from RCCA transformed response. In the present case, RPCA algorithm fails to provide any substantial evidence of the

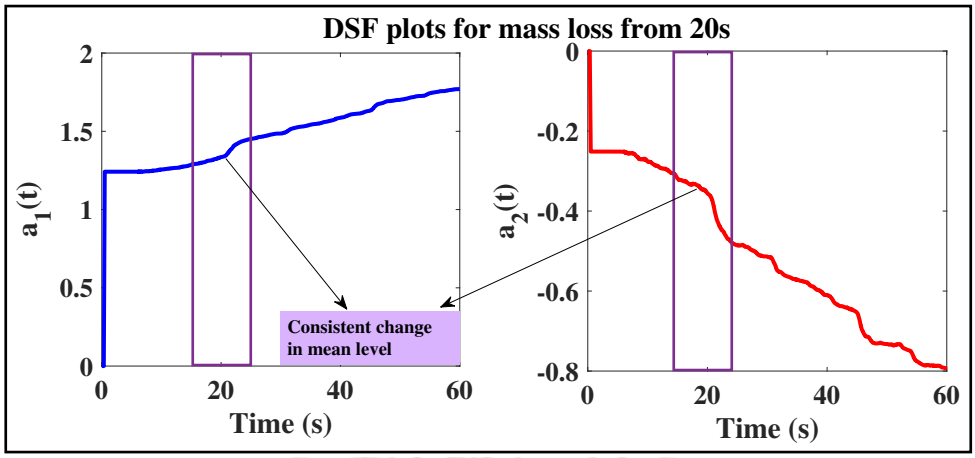

Figure 6.28: DSFs for mass loss at 20s, Alignment A

gradual mass loss scheme, conducted through the experiment. However, the global change in the mean level from the 0s mark until the entire experimental duration is indicative of a variable mass loss and can be roughly interpreted as a transition of state of the system. In line with the above findings, the DSFs shown in Fig. 6.28 clearly identifies the commencement of the water loss from 20s from the start of the excitation. It can be inferred that the water loss from 20s represents a gradual event, evident from the consistent shifts in the mean level of the TVAR plot. An interesting feature to observe here is that the graph maintains an apparent horizontal alignment until the commencement of water loss at 20s, illustrating the fact that the transition from the nonlinear to the linear regime is aptly depicted by the proposed algorithm. The detection results using RPCA are not expected to show consistent changes indicating the phenomena of the mass loss, the results of which are omitted here for brevity.

The subsequent trials on the experimental setup were conducted by aligning the model in a non-orthogonal orientation with respect to the shake table (Alignment B). A similar procedure is adopted where the variable mass loss takes place at 0s and 20s, for two individual case studies. The main objective of this experimental trial is to assess the efficacy of the proposed algorithm for a multi-directional case, closely emulating a practical scenario, where the ground motions might excite a structure from a non-orthogonal alignment. Motivated by this objective, the RCCA method is applied on to the biaxial (non-orthogonal) datasets obtained from the streaming vibration response. From the experimental trials, it was observed that the sloshing of water due to the excitation in the aligned direction had a greater magnitude compared to the mutually orthogonal oriented cases. Fig.

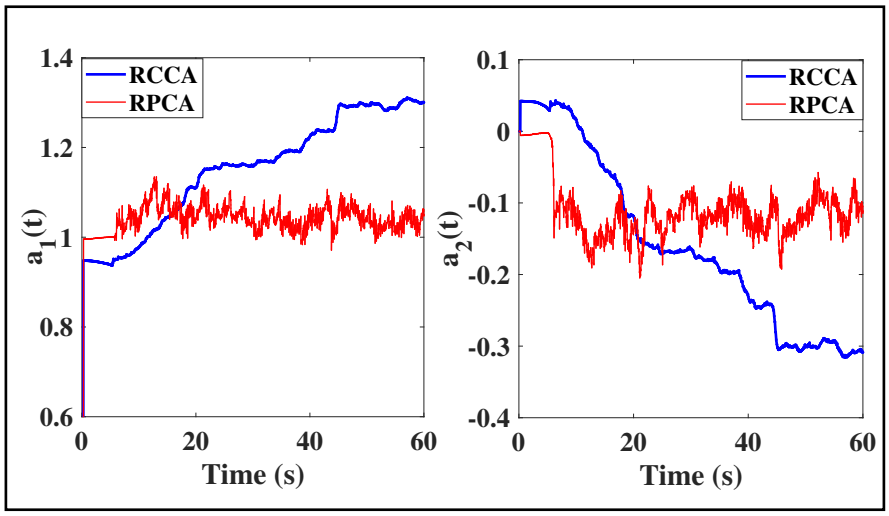

Figure 6.29: DSFs for mass loss at 0s, Alignment B

6.29 clearly shows that the change in the mean level of the DSF plot takes place from 0s, thereby conforming to the fact that the water loss commences exactly at the beginning of the excitation. However, it is observed that the shifts in the mean level of the TVAR coefficients is not uniform, which can be attributed to the multi-directional nature of the recorded responses. The torsional component generated during the vibration of the shake table allowed a rapid sloshing of water with a greater magnitude, compared to the previous case. It can be clearly observed from Fig. 6.29 that the TVAR coefficients obtained using RPCA algorithm fail to show consistent deviation in the mean level, an occurrence that had immaculately been corroborated by the RCCA algorithm. Furthermore, the gradual transition of state from the 0s mark is not obvious, attributed primarily due to the global non-orthogonal pairs of vibration input. The comparative study with the recently established RPCA method conclusively indicates that the RCCA algorithm provides better detection results even when the input features are locally orthogonal with respect to each other.

A similar case study for the DSFs involving water loss at 20s is reported in Fig. 6.30. While the change in the mean level of the plots is pronounced from 20s, the shifts in the level is not consistent. It can therefore, be concluded that the proposed RCCA based approach provides better identification results when the vibration data streams in from a pair of globally orthogonal sensors, as opposed to the ones obtained from the pair of multi-directional locally orthogonal datasets.

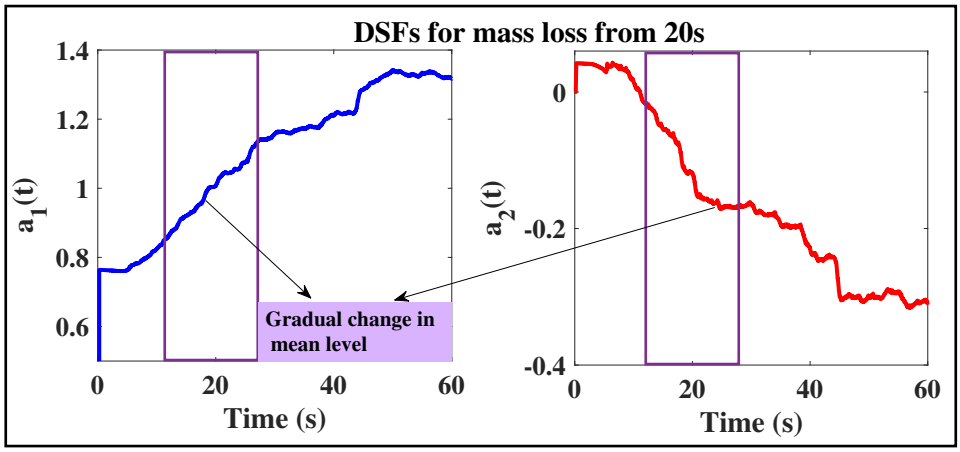

Figure 6.30: DSFs for mass loss at 20s, biaxial orientation

6.9 Case study for the UCLAFB: A practical problem

In order to ensure the robustness of any proposed methodology, it is imperative to understand its behavior towards real life scenarios that generally involves data sets of large dimensions. The proposed RCCA based approach is now applied to the mutually orthogonal pair of E-W and N-S recorded vibration data of the UCLAFB. The continuous monitoring of the structure provides a rich test bed for blind identification, damage detection and condition based monitoring processes by making the data globally available through a remote database server. The data is sampled at $100Hz$. In order to examine the efficacy and damage detection potential of the proposed algorithm, floor accelerations due to the *combined ambient vibration* and *earthquake data* (with Mw = 6.0, on 28 September 2004, 10:15 AM PDT from Parkfield, CA) are considered.

In the present context, the proposed algorithm is applied on the entire dataset obtained from the pair of mutually orthogonal directions. The set of translational responses are provided as inputs to the algorithm and the transformed responses are obtained at each time stamp and the TVAR model is fit. It can be clearly observed from the TVAR plots shown in Fig. 6.31, that the algorithm could effectively distinguish between the ambient regime and the occurrence of earthquake. It is well understood that the ambient regime lasts upto 380s, following which, the mean values of the DSFs begin to change. The time stamp 380s marks the onset of the earthquake and the steady change in the mean level continues until 410s, where the damage to the structure is pronounced. This is certified through the peaks of the TVAR coefficients that slowly begin to change after 410s, marking

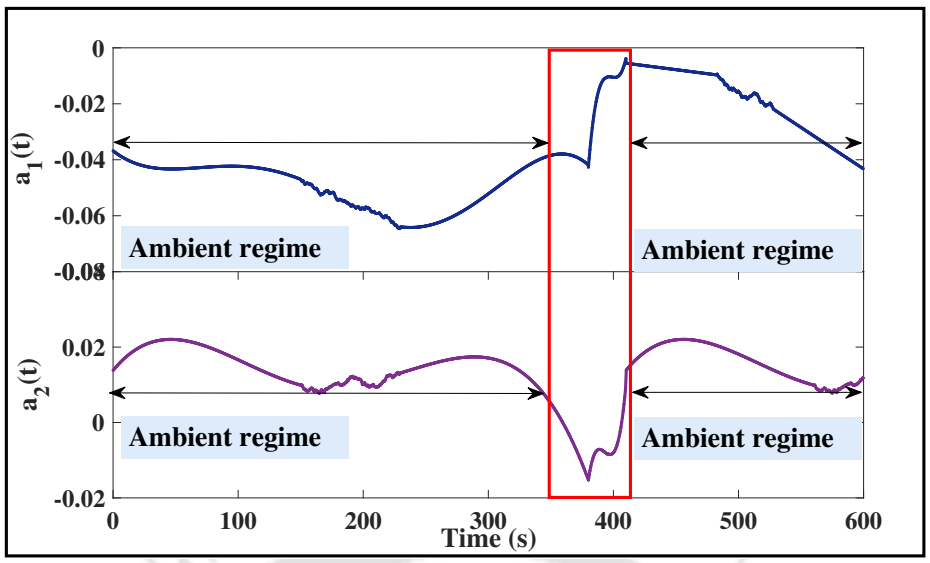

Figure 6.31: DSFs for the UCLAFB

the steady reduction in the intensity of the earthquake, thereby entering into a post-damage ambient zone, clearly demarcated in Fig. 6.31. UCLAFB has also been recently studied in the purview of damage detection through RPCA [35, 41] based algorithm. Previously reported detection results using RPCA have consistently failed to identify the exact onset of the damage around the 410s mark, due to the high nonstationary nature of the dataset. Recently established RPCA method have also shown certain inconsistencies in identifying damage for numerical cases as well, a topic that has already been reported in the earlier stages of the thesis. Additionally, in the context of RPCA, the TVAR plot alone shown in Fig. 6.32, could not identify the exact onset of the earthquake at the 380s mark, a feat clearly achieved by the DSFs in the present context. It can therefore, be very well concluded that the proposed method is well adept at identifying the change of states even for a practical system, that greatly enhances its robustness and efficacy.

6.10 Summary

A novel real time damage detection scheme based on recursive canonical correlation analysis principles, is proposed in this chapter. The method yields transformed responses at each instant of time and the eigenspace updates are iteratively obtained. The method applied to both weak and strongly nonlinear systems provides successful detection results of the order of finer damages of 10%, in real

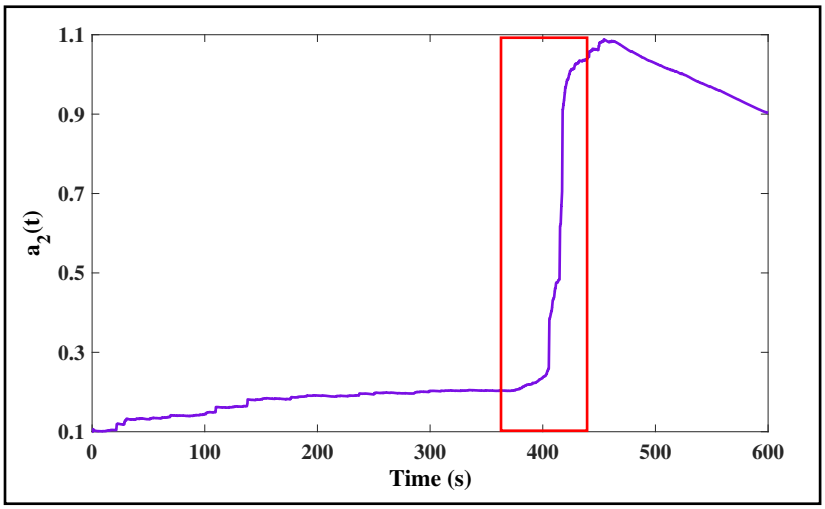

Figure 6.32: DSFs for the UCLAFB using RPCA

time. From the detailed comparative assessments, it is shown that the proposed RCCA based detection scheme provides better results than the recently established RPCA methodology, and can be extended for both full and partial sensor inputs as well. Furthermore, experimental validations using the proposed method have provided successful evidence to perceive the applicability of the method from a practical standpoint. Real time detection studies on the recorded ambient and vibration response data from the UCLAFB is provided that sheds a light onto the efficacy and robustness of the proposed scheme in determining the transition of state at the onset of the Parkfield earthquake, in real time.

Chapter 7

Conclusions and Recommendations

An extensive study of the real time damage detection techniques has been undertaken in this dissertation, with special emphasis towards simultaneous spatio-temporal damage detection conducted in a single recursive framework. En-route, several milestones have been achieved in the context of damage identification of structures, in a real time fervor. The key contributions of this thesis are briefly summarized as follows:

1. A new real time damage detection strategy known as recursive principal component analysis (RPCA) has been developed that extends the concepts of basic PCA towards online damage detection of structures subjected to an assortment of excitations. Specifically, the issues of detecting real time damage even for an underdetermined system is addressed in this framework. This work got published in the Journal of Smart Materials and Structures, IOP Publishers [156].

2. A novel approach amalgamating the concepts of RPCA and TVAR modeling has been introduced. This method provides a finer level of detectability of structural damage in real time as compared to the previous findings. This indicates a steady development of a newer set of detection strategies solely directed towards real time health monitoring of structures. This work got published in the Journal of Mechanical Systems and Signal Processing, Elsevier [157].

3. An important practical aspect of continuous health monitoring arises from the instrumentation of the structure under consideration. Due to impediments such as cost, unavailability and

improper accessibility, sparse instrumentation, the present work invested in the development of a real time damage detection scheme considering input from a single sensor and proposed an algorithm known as recursive singular spectrum analysis (RSSA). To the knowledge of the author, this is a completely new development in the field purely from an algorithmic perspective. This is also extended to incorporate a multivariate version known as RMSSA. Results clearly demonstrate the applicability of the aforementioned algorithms to a wide range of applications. This work got published in the Journal of Structural Health Monitoring, SAGE Publications [158].

4. The concept of recursive canonical correlation analysis (RCCA) is incorporated into a damage detection framework that provides substantial refinement of the detection due to the incorporation of multi-directional data, and systems with torsional coupling, nonlinear systems of higher dimensions, where the above methods fail to exhibit consistent performance. The work is under review in the Journal of Mechanical Systems and Signal Processing.

7.1 Conclusions

Having highlighted the important contributions of the current work, the key conclusions can be enumerated as follows:

1. Most of the traditional damage detection schemes operate in batches, *offline*. In addition to performance issues, the damage detetability of such methods is questionable for complex systems. In this regard, the RPCA based algorithms provide *finer levels of detection* compared to the existing approaches. RPCA outperforms traditional PCA in terms of exact identification of damage even for nonlinear systems subjected to varying levels of nonlinearity and a plethora of input excitation.

2. In terms of finer detectability, the RPCA based method in conjunction with TVAR modeling provide better results as compared to the RPCA-RRE approach, thereby justifying the use of *TVAR modeling* as an efficient tool for real time damage detection. The method successfully

provides better detection results in the event of nonstationary excitations and handles an underdetermined scenario with fine levels of accuracy, which is clearly an advantage while dealing with practical economics of condition based monitoring of real full-scale structures.

3. The applicability of RSSA in the backdrop of sparse sensor economics provide key detection results considering the inputs available from a *single sensor*, which is sometimes a practical situation, considering the associated cost and other factors, that impede full instrumentation of the structure. The development of the RSSA based method has certainly been a significant advancement towards solving practical problems even for non-stationary excitations and large data dimension. Furthermore, the hybrid RPCA-RSSA algorithm provides finer levels of damage that could be catered to application specific problems, without demanding a computational complexity or a steadfast increase in the resource consumption.

4. A novel real time damage detection algorithm based on RCCA principles, is used to identify damage patterns for systems excited using both stationary and nonstationary input excitations. The usefulness of this method is justified in its strengthened damage detection potential as compared to the RPCA algorithm. It is shown that the method performs well for various input excitations and provides adequate results while handling an underdetermined case. furthermore, it is shown that the new damage detection method fares well even with an increase in the linear DOF of the structure.

7.2 Recommendations for future study

In course of the research work, some aspects of online structural damage detection using the principles of RPCA have been unraveled. However, to achieve the objectives set for the entire course of study, some of the possible extensions of the current work can be summarized as under:

1. Extension of the current RCCA algorithm towards conducting *recursive modal identification and real time damage detection* in an unified adaptive framework.

2. A thorough quantification of damage alongside the *behavior of eigenspace distortion* in real time through the development of certain real time damage indices that could possibly unify the framework for both linear and nonlinear systems and extend to hybrid systems as well.

3. Extending the applicability of the real time damage detection schemes in order to identify spatio-temporal patterns of damage using *wireless sensors*.

4. Examining the performance of sensors and incorporating different types of sensor data for damage detection studies, viz., *strain based measurements*, *image processing data* and *energy harvester data*.

5. Developing real time strategies that aims at adequately estimating the *remaining useful life* of the structure. The current methods could be extended to provide features that aid in retrofitting processes and improving resistance to earthquake by optimizing the strength of the materials used.

APPENDICES

Appendix A

Basic principal component analysis

The goal of this section is to provide both an intuitive feel for PCA, and a thorough discussion of this topic. The objective of PCA is to identify the most meaningful basis to re-express a data set. PCA makes one stringent but powerful assumption: linearity. Linearity vastly simplifies the problem by restricting the set of potential bases [93]. With this assumption PCA is now limited to re-expressing the data as a linear combination of its basis vectors.

Let $\mathbf{X}$ be the original data set of size $m \times n$, where each column is a single sample. Let $\mathbf{Y}$ be another $m \times n$ matrix related by a linear transformation $\mathbf{P}$. $\mathbf{X}$ is the original recorded data set and $\mathbf{Y}$is a new representation of that data set. The linear transformation is expressed as:

$$\mathbf{Y} = \mathbf{PX} \tag{A.1}$$

The following quantities are defined:

- p_i are the rows of $\mathbf{P}$
- x_i are the columns of $\mathbf{X}$ and
- y_i are the columns of $\mathbf{Y}$.

Equation A.1 represents a change of basis and thus can have the following interpretations [93]:

1. $\mathbf{P}$ is a matrix that transforms $\mathbf{X}$ into $\mathbf{Y}$.

2. The rows of $\mathbf{P}$, $(p_1, p_2, ..., p_m)$, are a set of new basis vectors for expressing the columns of $\mathbf{X}$.

3. Geometrically, $\mathbf{P}$ is a rotation and a stretch which again transforms $\mathbf{X}$ into $\mathbf{Y}$.

The matrix $\mathbf{Y}$ can be mathematically expressed as :

$$Y = \begin{bmatrix} p_1.x_1 & \dots & p_1.x_n \\ \vdots & \ddots & \vdots \\ p_m.x_1 & \dots & p_m.x_n \end{bmatrix}$$

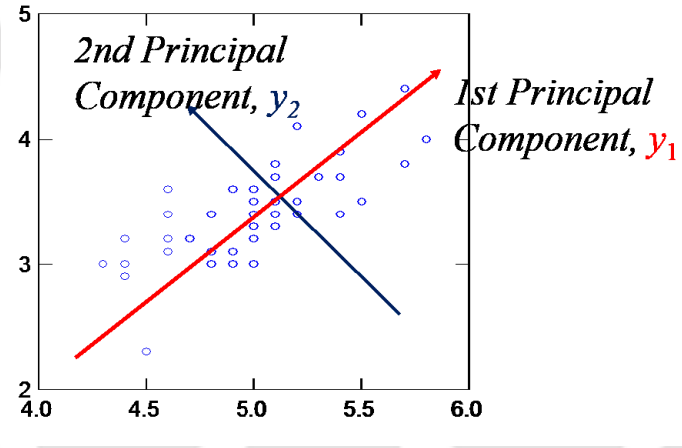

Figure A.1: PCA showing the maximum variance along the direction of the signal

This shows that the j^{th} coefficient of $\mathbf{y_i}$ is a projection onto the j^{th} row of $\mathbf{P}$. Therefore, the rows of $\mathbf{P}$ are a new set of basis vectors for representing of columns of $\mathbf{X}$. Maximizing the variance corresponds to finding the appropriate rotation of the initial basis. This intuition corresponds to finding the direction indicated by the line corresponding to the maximum variance exhibited by the signal. Therefore, on producing a set of decorrelated transform, PCA indicates the direction of maximum variance, which is reflected by the first principal component, as shown in Fig.A.1. In the 2-dimensional case the direction of largest variance corresponds to the best-fit line for the data cloud. The other principal components form an orthonormal basis, indicating the directions of the least variance, supposedly indicated by the presence of noise in a data set [93].

Solving PCA using eigenvalue decomposition

An orthonormal matrix $\mathbf{P}$, for which the linear transformation $\mathbf{Y} = \mathbf{PX}$ holds good, would lead to a covariance estimate of the decorrelated matrix $\mathbf{Y}$ according to: $\mathbf{C}_Y = \frac{1}{n}\mathbf{YY}^T$. The rows of $\mathbf{P}$ are the principal components of $\mathbf{X}$. The above expression could be expanded as shown:

$$\begin{aligned} \mathbf{C}_Y &= \frac{1}{n}\mathbf{YY}^T \\ &= \frac{1}{n}\mathbf{PXX}^T\mathbf{P}^T \\ &= \mathbf{PC}_X\mathbf{P}^T \end{aligned} \tag{A.2}$$

The objective is to recognize that any symmetric matrix $\mathbf{A}$ is diagonalized by an orthogonal matrix of its eigenvectors. For a symmetric matrix $\mathbf{A}$, $\mathbf{A} = \mathbf{EDE}^T$, where $\mathbf{D}$ is a diagonal matrix and $\mathbf{E}$ is a matrix of eigenvectors of $\mathbf{A}$ arranged as columns. The trick is to select the matrix $\mathbf{P}$ to be a matrix where each row $\mathbf{p_i}$ is an eigenvector of $\frac{1}{n}\mathbf{XX}^T$. By this selection, $\mathbf{P} = \mathbf{E}^T$. From the basic theorems of linear algebra, the inverse of an orthogonal matrix is its transpose, therefore, $\mathbf{P}^{-1} = \mathbf{P}^T$. Thus, Eqn. A.2 can be re-written as:

$$\begin{aligned} \mathbf{C}_Y &= \mathbf{PC}_X\mathbf{P}^T \\ &= \mathbf{P}(\mathbf{E}^T\mathbf{DE})\mathbf{P}^T \\ &= \mathbf{P}(\mathbf{P}^T\mathbf{DP})\mathbf{P}^T \\ &= (\mathbf{PP}^{-1})\mathbf{D}(\mathbf{PP}^{-1}) \\ &= \mathbf{D} \end{aligned} \tag{A.3}$$

It is evident that from Eqn. A.3 that the choice of P diagonalizes $\mathbf{C}_Y$. This proves that the i^{th} diagonal value of $\mathbf{C}_Y$ is the variance of $\mathbf{X}$ along $\mathbf{p_i}$. In practice computing PCA of a data set $\mathbf{X}$ entails:

(1) subtracting off the mean of each measurement type and

(2) computing the eigenvectors of $\mathbf{C}_X$.

Appendix B

Dynamical representations of some nonlinear systems

B.1 2 storied Duffing oscillator

The governing stochastic differential equation is discretized using the Taylors 1.5 strong scheme with a time step $\Delta = 0.01s$. The excitation matrix consists of two statistically independent Gaussian white noise processes sampled at $100Hz$ having zero mean and standard deviation σ_1 and σ_2 for the vectors $f_1(t)$ and $f_2(t)$, respectively. Solving the equation of motion numerically [155], the statistics of the response vectors $x_1(t)$ and $x_2(t)$ can be obtained. The numerical values for the system and excitation parameters are: mass of each floor, m_1=m_2=10 kg, linear stiffness coefficient, k_1=k_2=1 kN/m with Duffing constants, α_1=1 kN/m^3 and α_2=2 kN/m^3. The detailed derivation towards obtaining the response of the system is presented next.

Each individual elements of the matrix $\tilde{\mathbf{\Omega}}$ denotes Duffing parameter value at contributing at each floor, given by: $\tilde{\mathbf{\Omega}} = \begin{bmatrix} \alpha_1 & \alpha_2 \\ 0 & -\alpha_2 \end{bmatrix}$. The vector $\tilde{Z}$ is expressed as: $\tilde{\mathrm{Z}} = \begin{Bmatrix} X_1^3 \\ (X_1 - X_2)^3 \end{Bmatrix}$

Upon expanding the governing differential equation (5.23) term by term, the following equations

are obtained:

$$\left.\begin{aligned} &m_1\ddot{X}_1 + c_1\dot{X}_1 + k_1X_1 + \alpha_1X_1^3 + c_2\left(\dot{X}_1 - \dot{X}_2\right) + k_2\left(X_1 - X_2\right) \\ &+\alpha_2(X_1 - X_2)^3 = F_1(t) \\ &m_2\ddot{X}_2 + c_2\left(\dot{X}_2 - \dot{X}_1\right) + k_2(X_2 - X_1) + \alpha_2(X_2 - X_1)^3 = F_2(t) \end{aligned}\right\} \tag{B.1}$$

Towards solving the problem through Taylor 1.5 scheme, it is important that the equations are represented in *state-space* format, for an easier simplification at each step of the derivation.Considering the following substitutions for the first DOF, certain important expressions can be obtained:

$$\begin{aligned} X_1 &= Y_1 \\ \dot{X}_1 &= \dot{Y}_1 = Y_2 \\ \ddot{X}_1 &= \ddot{Y}_1 = \dot{Y}_2 \end{aligned} \tag{B.2}$$

Similarly, the necessary substitutions corresponding to the second DOF can also be carried out. The above sets of equation could be translated to a simpler set of matrix equation as: $dY = \mathbf{a}*Y + \mathbf{b}*dW$. It is to be noted that the variables used here for defining the individual matrices obtained above will be subsequently utilized for formulating the detailed Taylor 1.5 scheme expressions as and when necessary. The matrices **a** and **b** are given by:

$$\mathbf{a} = \begin{bmatrix} 0 & 1 & 0 & 0 \\ \frac{-(k_1+\alpha_1Y_1^2+k_2+\alpha_2(Y_1^2-3Y_1Y_3+3Y_3^2)}{m_1} & \frac{-(c_1+c_2)}{m_1} & \frac{(k_2+\alpha_2Y_3^2)}{m_1} & \frac{c_2}{m_1} \\ 0 & 0 & 0 & 1 \\ \frac{(k_2-\alpha_2(-Y_1^2-3Y_3^2+3Y_1Y_3))}{m_2} & \frac{c_2}{m_2} & \frac{-(k_2+\alpha_2Y_3^2)}{m_2} & \frac{-c_2}{m_2} \end{bmatrix}$$

$$\mathbf{b} = \begin{bmatrix} 0 & 0 & 0 & 0 \\ 0 & \frac{\sigma_1}{m_1} & 0 & 0 \\ 0 & 0 & 0 & 0 \\ 0 & 0 & 0 & \frac{\sigma_2}{m_2} \end{bmatrix} \tag{B.3}$$

At each time instant, the system response can be evaluated using the Taylor 1.5 strong scheme

through a set of discretized equations. Therefore, the basic equation is expressed as follows:

$$\begin{aligned} X_k(n+1) &= X_k(n) + a_k(n)\Delta T + b_k(n)\Delta W + \tfrac{1}{2}\Im^1 b_k(n)\left\{(\Delta W)^2 - \Delta T\right\} \\ &+\Im^1 a_k(n)\Delta Z + \Im^0 b_k(n)\left\{\Delta W \Delta T - \Delta Z\right\} \\ &+\tfrac{1}{2}\Im^0 a_k(n)\Delta T^2 + \tfrac{1}{2}\Im^1\Im^1 b_k(n)\left\{\tfrac{1}{3}(\Delta W)^2 - \Delta T\right\}\Delta W \end{aligned} \tag{B.4}$$

where, n denotes the number of DOF at each floor, k represents the total number of sample points used for the formulation. At each discretization point, the values associated with the each individual element of the matrices **a** and **b** are represented by a_k^n and $b_k^{n.j}$, respectively. In Eqn. B.4, at each time step ΔT, the corresponding incremental white noise is given by $\Delta W^j = \sqrt{\Delta T}.\xi_j$, ξ_j being the white noise term at the j^{th} instant. The operators $\Im^0$ and $\Im^j$ are expressed as:

$$\left.\begin{aligned} \Im^0 &= \frac{\partial}{\partial t} + \sum_{k=1}^{d} a_k \frac{\partial}{\partial x_k} + \frac{1}{2}\sum_{k=1}^{d}\sum_{l=1}^{d} b_k b_l \frac{\partial^2}{\partial x_k \partial x_l} \\ \Im^1 &= \sum_{k=1}^{d} b_k \frac{\partial}{\partial x_k} \end{aligned}\right\} \tag{B.5}$$

Here, ΔW and ΔZ are related as follows:

$$\begin{Bmatrix} \Delta W \\ \Delta Z \end{Bmatrix} = \begin{bmatrix} \sqrt{\Delta T} & 0 \\ \frac{\Delta T^{1.5}}{2} & \frac{\Delta T^{1.5}}{2\sqrt{3}} \end{bmatrix} \begin{Bmatrix} U_1 \\ U_2 \end{Bmatrix} \tag{B.6}$$

with U_1 and U_2 jointly follow normal distribution with zero mean and unit standard deviation: $\begin{Bmatrix} U_1 \\ U_2 \end{Bmatrix} \equiv N\left(\begin{Bmatrix} 0 \\ 0 \end{Bmatrix}, \begin{bmatrix} 1 & 0 \\ 0 & 1 \end{bmatrix}\right)$

The displacement and velocity at each DOF can be evaluated for each discretized point through the following simplified set of equations, arrived after carrying out proper substitutions. The displacement and velocity for the first DOF can be obtained from the following set of equations, respectively.

$$\begin{aligned} Y_1(k+1) &= Y_1(k) + a_1(k)\Delta T + \tfrac{1}{2}\Im^0 a_1(k)\Delta T^2 + \Im^1 a_1(k)\Delta Z^1 + \Im^2 a_1(k)\Delta Z^2 \\ Y_2(k+1) &= Y_2(k) + a_2(k)\Delta T + \tfrac{1}{2}\Im^0 a_2(k)\Delta T^2 + \tfrac{\sigma_1(k)}{m_1}\Delta W^1 + \Im^1 a_2(k)\Delta Z^1 + \Im^2 a_2(k)\Delta Z^2 \end{aligned} \tag{B.7}$$

Following the same lines of development, the response vectors for the second DOF can also be obtained. A few essential parameters required to arrive at the final discretized equation for the

complete response of the system are expressed as follows:

$$\begin{aligned}
\Im^0 a_n(k) &= dA \times A + ddA \times B \\
\Im^1 a_n(k) &= \left\{ b_1(k)\frac{\partial}{\partial Y_1} + b_2(k)\frac{\partial}{\partial Y_2} \right\} a_n(k) \\
\Im^2 a_n(k) &= \left\{ b_3(k)\frac{\partial}{\partial Y_3} + b_4(k)\frac{\partial}{\partial Y_4} \right\} a_n(k)
\end{aligned} \tag{B.8}$$

where $\mathbf{A} = \mathbf{a} * Y \quad \& \quad \mathbf{B} = \mathbf{b} * dW$

The final equation after carrying out these substitutions for the 2 DOF Duffing model can be expressed as follows:

$$Y(:, k+1) = Y(:, k) + \mathbf{A}(k)\Delta T + \frac{1}{2}\Im^0 A(k)\Delta T^2 + \mathbf{B}\Delta W + \Im^1 A(k)\Delta Z^1 + \Im^2 A(k)\Delta Z^2 \tag{B.9}$$

It should be noted that- odd numbers in suffix denotes displacement while the even numbers denote the velocity at each DOF. The acceleration response for each DOF can be numerically obtained by differentiating the velocity vector given by the above equation. Considering an ensemble of 5000 samples, the response acceleration plots for the individual DOF are provided as ready reference: In addition to the acceleration plots, the phasespace diagrams for the first floor is provided below

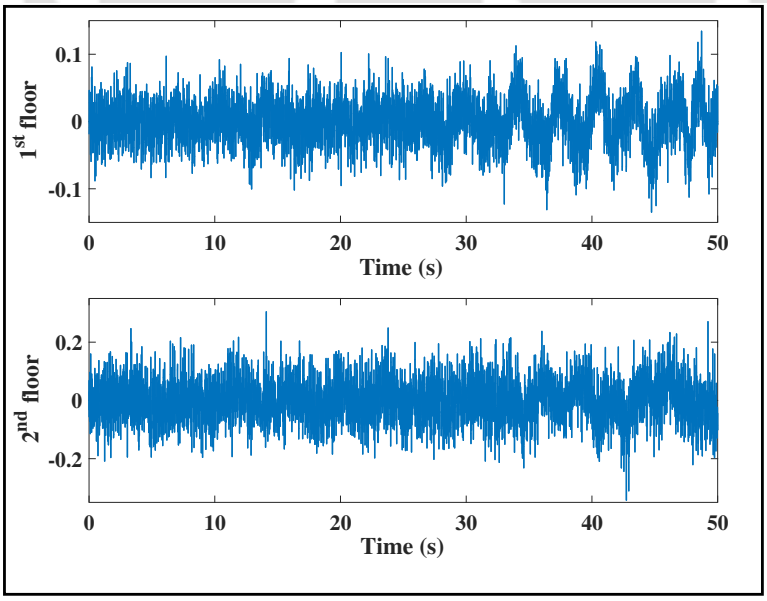

Figure B.1: Acceleration plots for the 2 storied Duffing oscillator

for reference. The unevenness and inconsistency of the plot observed from the Fig. B.2 indicate

that the system is highly nonlinear. A real time damage detection scheme portrayed for a nonlinear system having such a high degree of nonlinearity is a novel attempt addressed in the thesis.

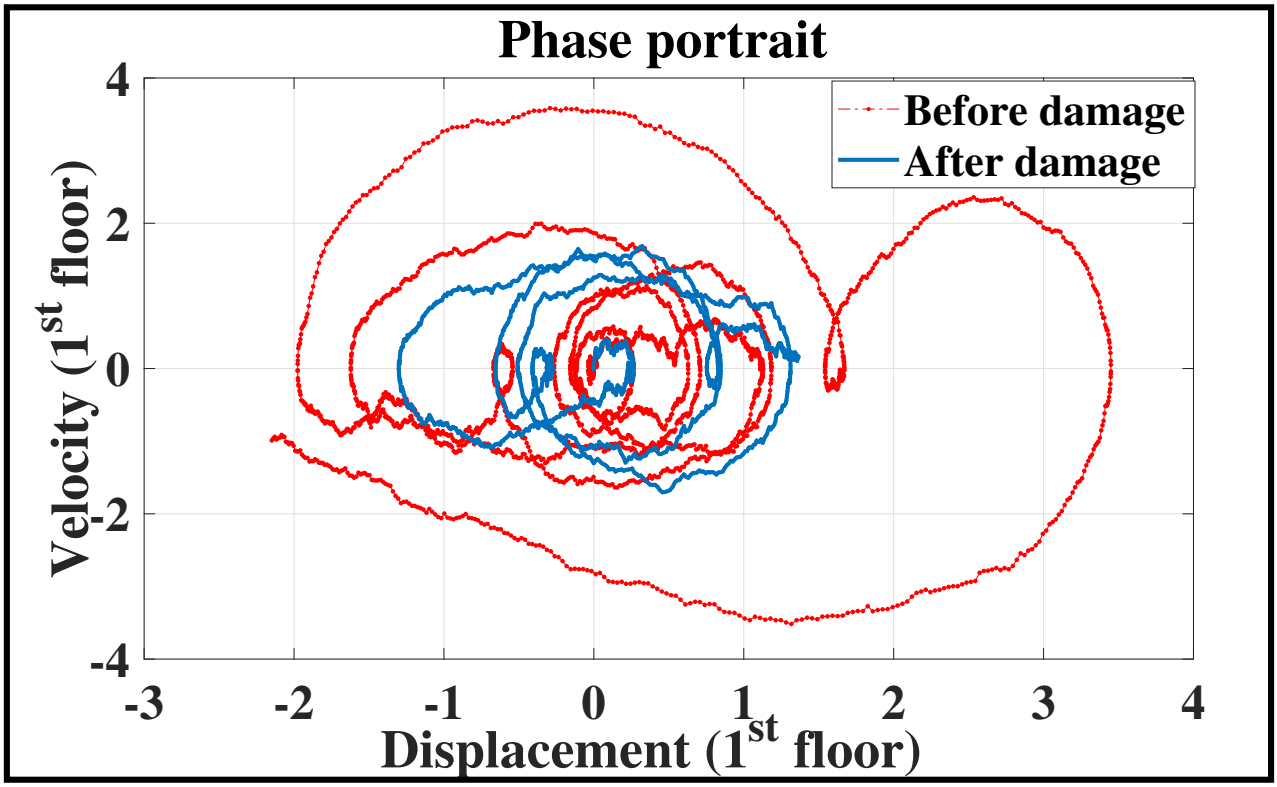

Figure B.2: Phase portrait for the 1^{st} DOF

Considering the damage instant at 35s, it can be well understood from a theoretical perspective that the structure undergoes a change in the frequency composition at the instant of damage. This shift in frequency is time-varying, as the damage occurs in real time. The system being highly nonlinear, approximate spectral representations for the same could only be carried out using HHS plots, that indicate the change in the frequency content over time. Towards this, the HHS plots for the 2^{nd} DOF is shown that indicate a possible event at 35s.

As observed from figure B.3, the shift in the frequency at 35s indicate the exact instant of a possible event. This approximate finding is further analyzed by the recursive algorithm in order to validate the instant of damage due to the change in the nonlinear force term.

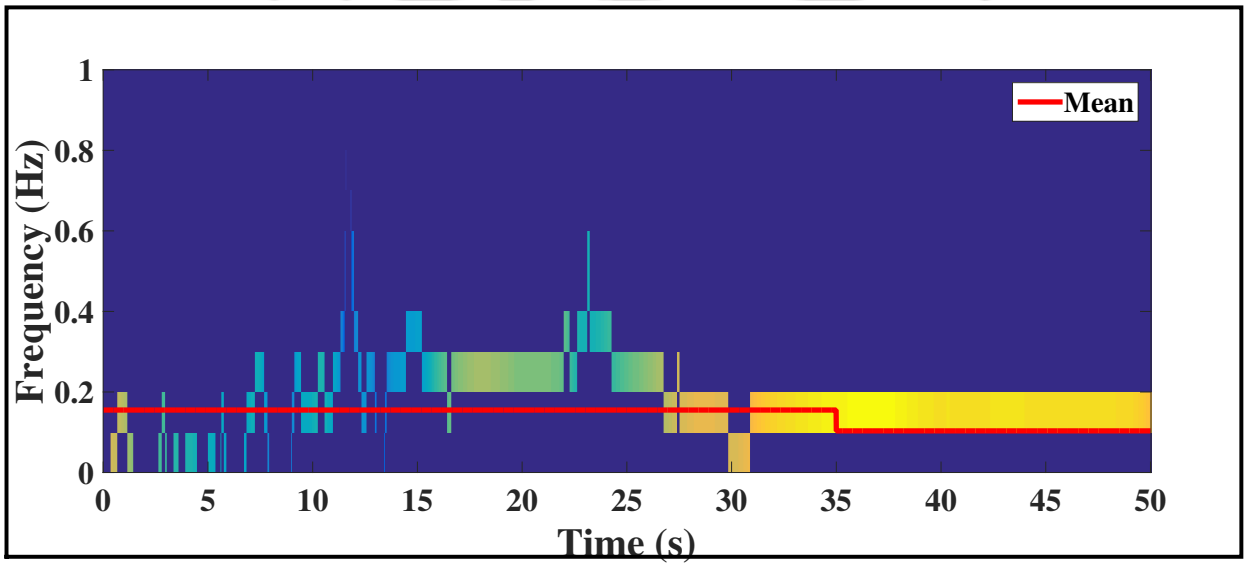

Figure B.3: HHS plot for the second DOF

Appendix C

5 DOF B-W system

The Taylor's 1.5 strong scheme is used to evaluate the responses at the individual DOF for the B-W system. The theoretical derivations are skipped here. However, the acceleration plots are provided for a better understanding:

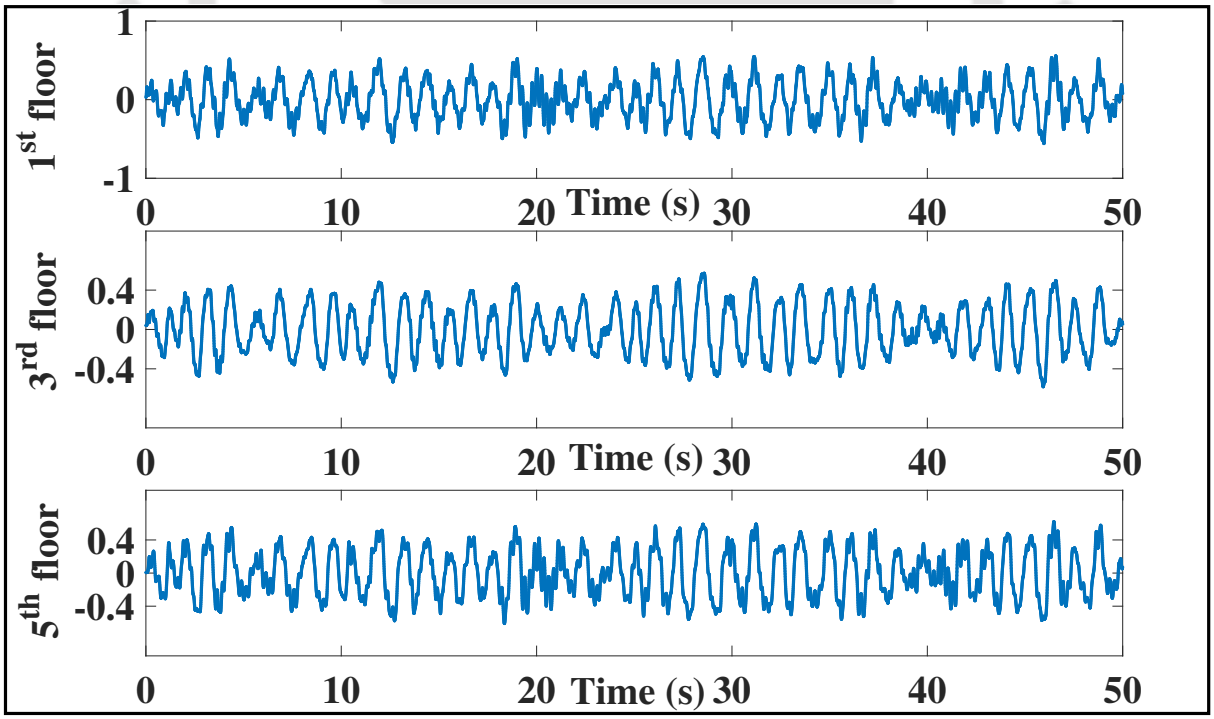

Figure C.1: Acceleration plots for the DOFs

The corresponding phase portraits before and after damage for the individual DOFs are also provided here:

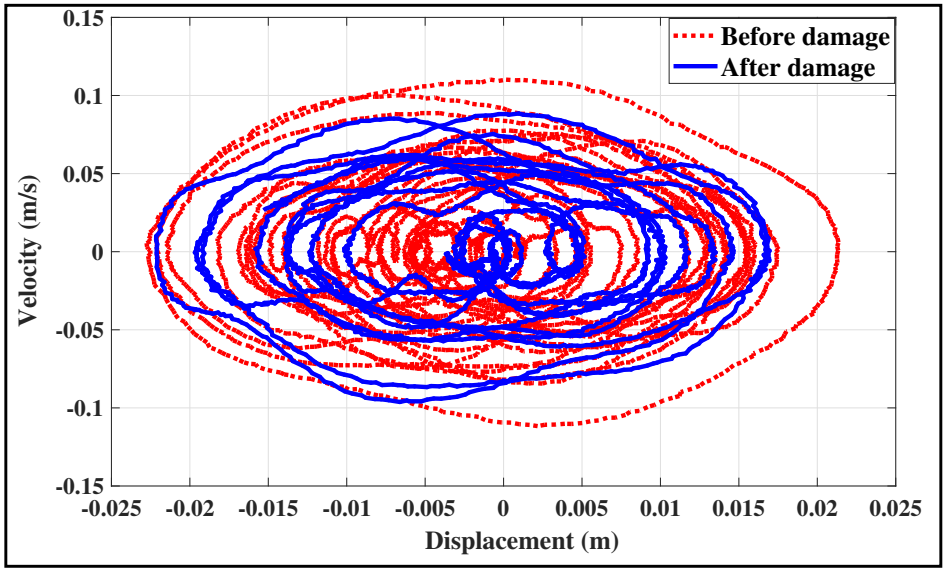

Figure C.2: Phase portrait for first floor

As discussed in the dissertation, the damage to the BW model is induced by changing the nonlinear force term κ at 31s. From the purview of structural dynamics, it can be understood that the change in the nonlinear force term induces a global damage to the structure that affects the frequency content before and after the event. Therefore, a spectral representation of the phenomena would provide a better intuition regarding the nature of the shift in frequency. This is provided by the plots of HHS as shown in Fig. C.7 and C.8, for the top floor and the third floor, respectively. As evident from the figure, the shift in the frequency occurs at 31s, indicating a possible event, which is further verified by the proposed algorithm.

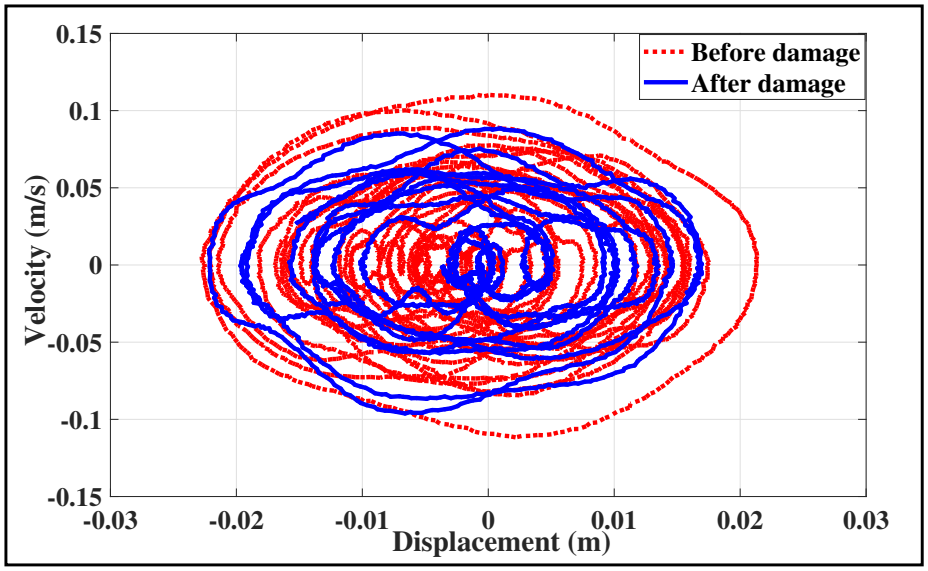

Figure C.3: Phase portrait for second floor

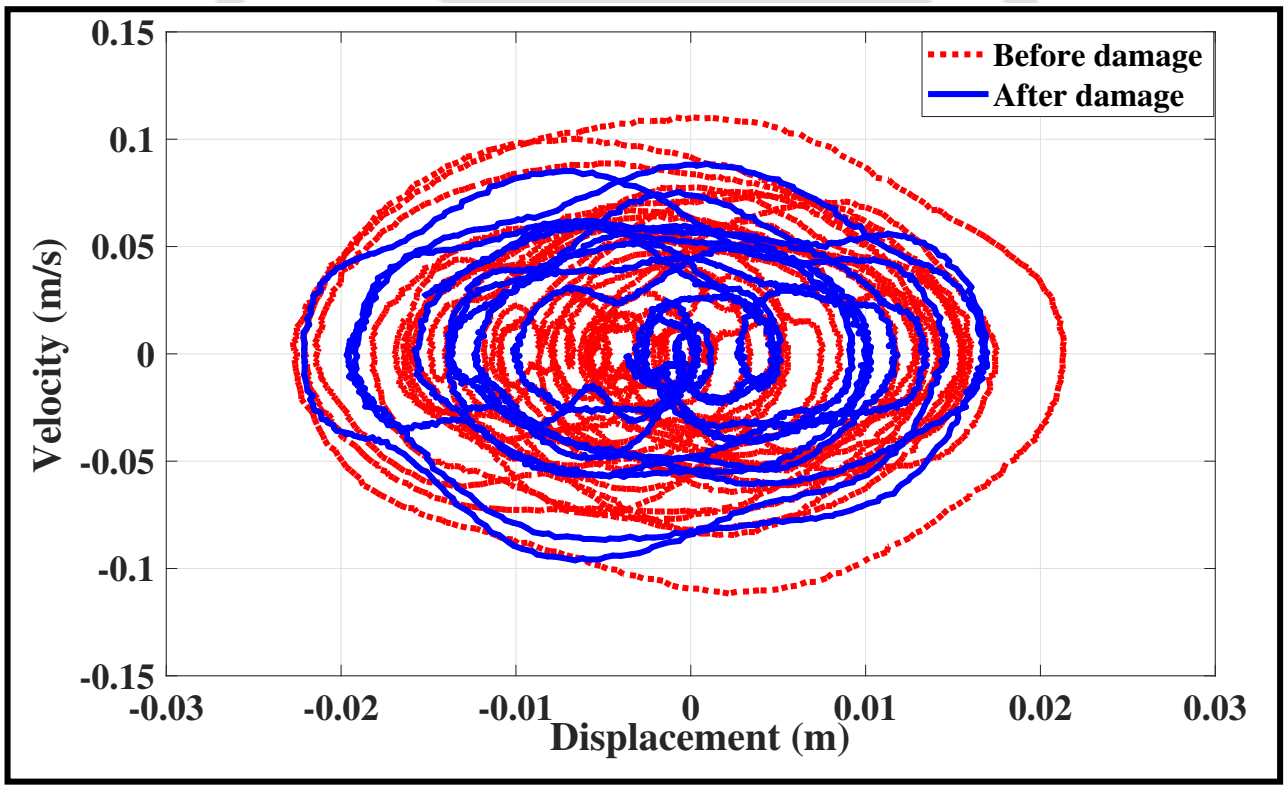

Figure C.4: Phase portrait for third floor

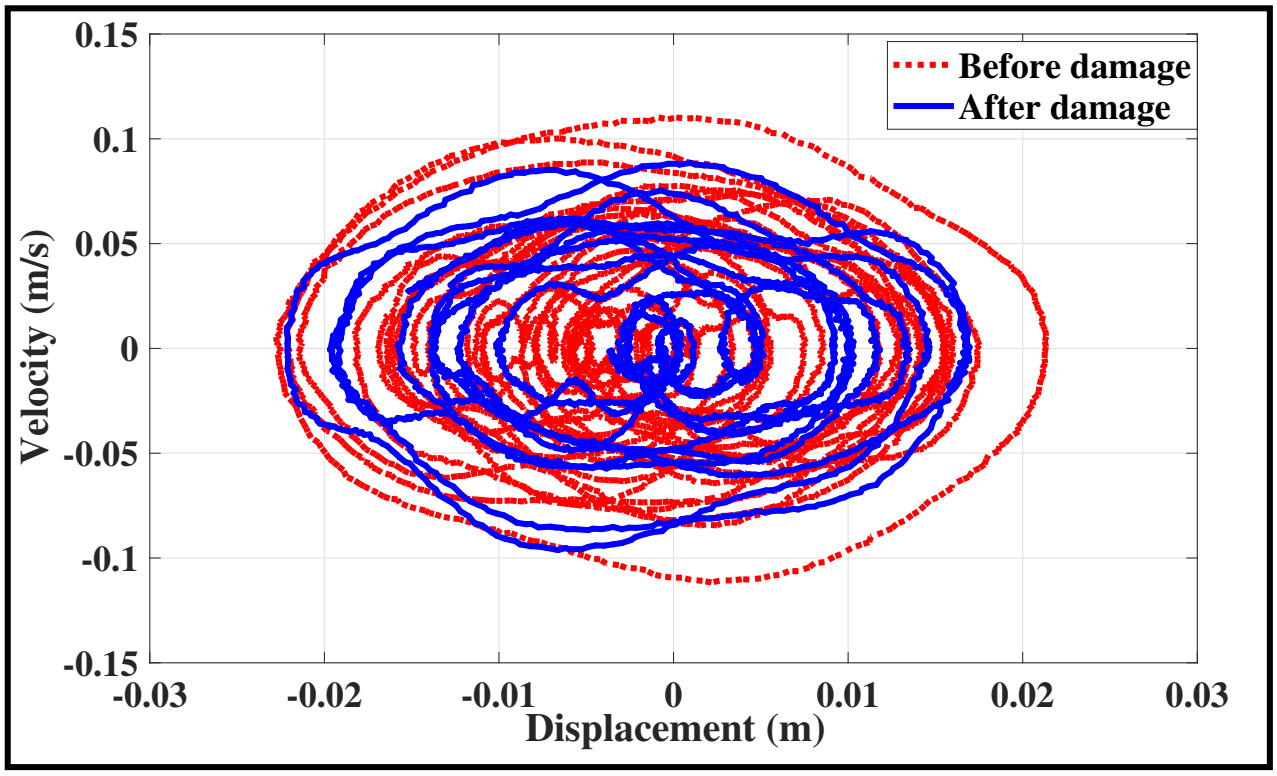

Figure C.5: Phase portrait for fourth floor

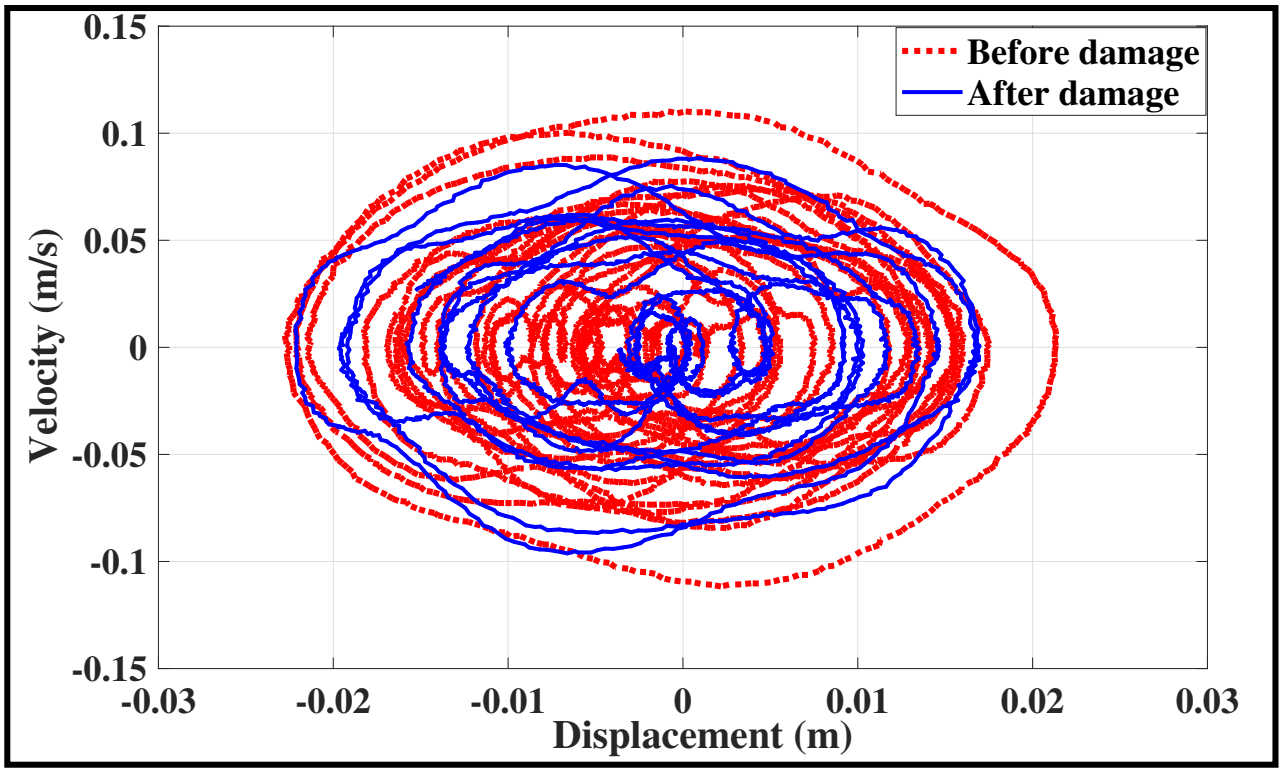

Figure C.6: Phase portrait for fifth floor

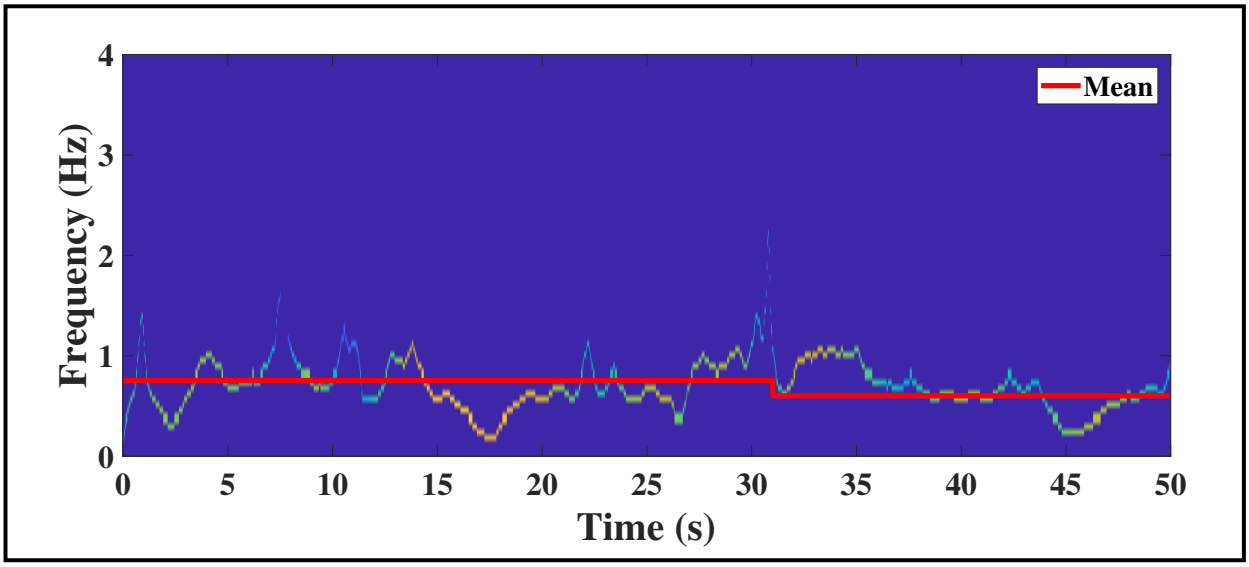

Figure C.7: HHS for fifth floor

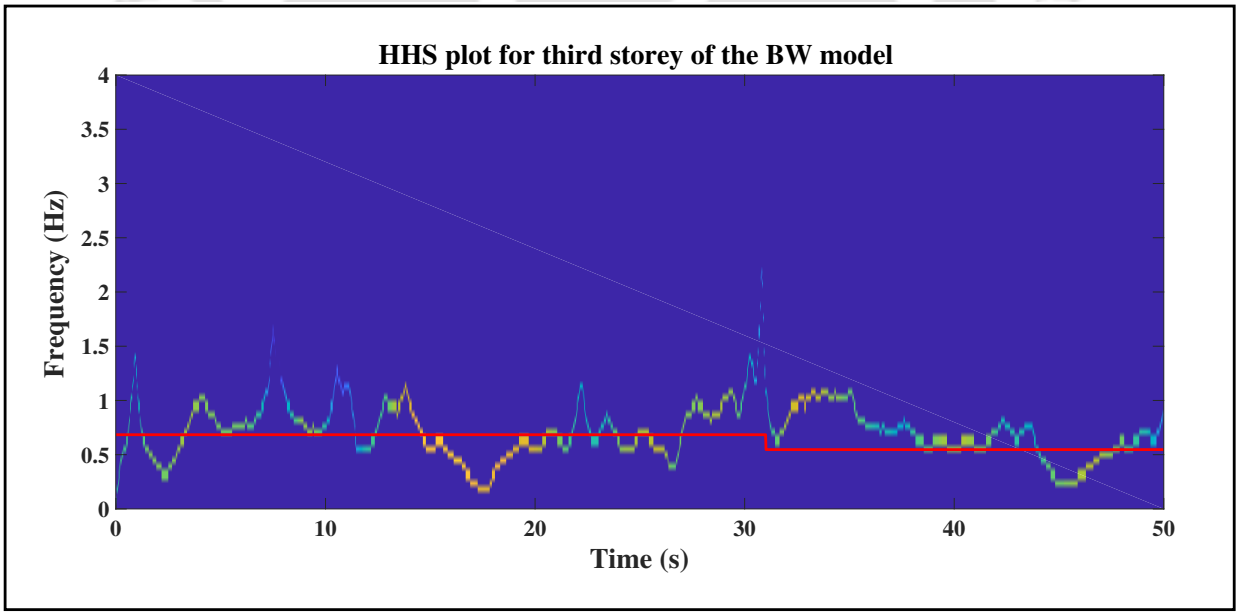

Figure C.8: HHS for third floor

Appendix D

Gershgorin's theorem

One of the primary objectives of a preliminary dynamic analysis of a vibrating system is to evaluate the natural frequencies of each of its components. The trace of a matrix merely provides the sum of its eigenvalues and does not provide insights about the range for those eigenvalues. One of the easier methods is to employ Gershgorin's theorem for the same, which is subsequently discussed in the purview of the dynamics of a structural system.

Prior to getting into the details of the theorem, it is important to review certain key concepts that are essential for its theoretical treatment. The condition in which the individual elements of a matrix $\mathbf{A}_{nn}$ follow the relation

$$|\mathbf{A}_{ii}| > \sum_{j \neq i} |\mathbf{A}_{ij}|, \ for\ i = 1, 2, ..., n \tag{D.1}$$

renders the matrix as a *strictly diagonally dominant* (SDD) matrix. On employing the non-singularity of such type of matrices, it now becomes easy to understand the Gershgorin's theorem.

The theorem states that, every eigenvalue of the SDD matrix $\mathbf{A}_{nn}$ satisfies:

$$|\lambda - \mathbf{A}_{ii}| > \sum_{j \neq i} |\mathbf{A}_{ij}|, \ i \in \{1, 2, ..., n\} \tag{D.2}$$

The proof of this theorem can be stated as follows:

Suppose that λ is an eigenvalue of the matrix $\mathbf{A}$. Then the matrix $\lambda\mathbf{I} - \mathbf{A}$ is SDD if $|\lambda - \mathbf{A}_{ii}| >$

$\sum_{j \neq i} |\mathbf{A}_{ij}|$ for every i. If equation D.2 is not satisfied then $\lambda\mathbf{I} - \mathbf{A}$ is SDD. If $\lambda\mathbf{I} - \mathbf{A}$ is SDD, it automatically implies that the matrix is nonsingular and as a result, λ is not an eigenvalue. For λ to be an eigenvalue, the above stated rule must hold, which forms the key basis of the Gershgorin's theorem. In analyzing the theorem, it can be well understood that every eigenvalue of the matrix $\mathbf{A}$ must be within a distance d of $\mathbf{A}_{ii}$ for some i. Since in general, an eigenvalue can be visualized as a point in the complex plane, it necessitates that the point has to be within distance d of $\mathbf{A}_{ii}$ for some i.

Bibliography

[1] Farrar CR and Worden K (2007) *An introduction to structural health monitoring*, Philosophical Transactions of the Royal Society of London A. 365(1851), 303–315.

[2] Balageas D, Fritzen C-P and Güemes A (2006) *Structural health monitoring*, Wiley Online Library, vol:493.

[3] Farrar CR and Worden K (2012) *Structural Health Monitoring: A Machine Learning Perspective*, John Wiley & Sons, Ltd. 22(10), isbn: 9781118443118.

[4] Doebling SW, Farrar CR, Prime MB and others (1998) *A summary review of vibration-based damage identification methods*, Shock and vibration digest, Citeseer. 30(2), 91–105.

[5] Gul M and Catbas FN (2009) *Statistical pattern recognition for structural health monitoring using time series modeling: thoery and experimental verifications*, Mechanical Systems and Signal Processing, Elsevier. 23(7), 2192–2204

[6] Balsamo, L. and Betti R. (2015) *Data-based structural health monitoring using small training data sets*, Structural Control and Health Monitoring, Wiley Online Library. 22(10), pp: 1240–1264.

[7] Curadelli RO, Riera JD, Ambrosini D and Amani MG (2008) *Damage detection by means of structural damping identification*, Engineering Structures, Elsevier. 30(12), 3497–3504.

[8] Worden, K and Dulieu-Barton, JM. 2004. *An overview of intelligent fault detection in systems and structure*. Structural Health Monitoring, Sage Publications. 3(1), pp. 85–98.

[9] Wahab, MM-A and De Roeck, G. (1999) *Damage detection in bridges using modal curvatures: application to a real damage scenario*, Journal of sound and vibration, Elsevier, 226(2), pp: 217–235.

[10] Pandey AK, Biswas M and Samman MM. (1991) *Damage detection from changes in curvature mode shapes*, Journal of Sound and Vibration, Elsevier. 145(2), 321 - 332.

[11] Hearn, G. and Testa, RB. (1991) *Modal analysis for damage detection in structures*, Journal of structural engineering, American Society of Civil Engineers, 117(10), pp: 3042–3063.

[12] Kim, JT., Ryu, Y-S., Cho, H-M and Stubbs, N. (2003) *Damage identification in beam-type structures: frequency-based method vs mode-shape-based method*, Engineering structures, Elsevier, 25(1), pp: 57–67.

[13] Ratcliffe, CP. (1997) *Damage detection using a modified Laplacian operator on mode shape data*, Journal of sound and vibration, Elsevier, 204(3), pp: 505–517.

[14] Hasrizam, CM., and Noor Fawazi. (2017) *Damage Identification Based on Curvature Mode Shape using Cubic Polynomial Regression and Chebyshev Filters*. IOP Conference Series: Materials Science and Engineering, IOP Publishing. 271(1).

[15] Abdo, MAB., and Hori, M. (2002) *A numerical study of structural damage detection using changes in the rotation of mode shapes*, Journal of Sound and vibration, Elsevier, 251(2), pp: 227–239.

[16] Behmanesh I and Moaveni B (2015) *Probabilistic identification of simulated damage on the Dowling Hall footbridge through Bayesian finite element model updating*, Structural Control and Health Monitoring, Wiley Online Library. 22(3), 463–483, issn: 545-2263.

[17] Brownjohn J-MW, Xia P-Qi, Hao H and Xia Y (2001) *Civil structure condition assessment by FE model updating:: methodology and case studies*, Finite Elements in Analysis and Design . 37(1), 761–775.

[18] Jaishi, B. and Ren, W-X. (2005) *Structural finite element model updating using ambient vibration test results*, Journal of Structural Engineering, American Society of Civil Engineers, 131(4), pp: 617–628.

[19] Teughels A and De Roeck G. 2005. *Damage detection and parameter identification by finite element model updating* Revue européenne de génie civil, Taylor & Francis. 9(1–2), pp.: 109–158.

[20] An Y and Ou, J. 2013. *Experimental and numerical studies on model updating method of damage severity identification utilizing four cost functions.* Structural Control and Health Monitoring, Wiley Online Library. 20(1), pp.: 107–120

[21] Lee E-T and Eun H-C. 2014. *A model-based substructuring method for local damage detection of structure* Shock and Vibration, Hindawi Publishing Corporation.

[22] Pandey, AK and Biswas, M. (1994) *Damage detection in structures using changes in flexibility*, Journal of sound and vibration, Elsevier, 169(1), pp: 3–17.

[23] Skolnik, D., Lei, Y., Yu, E. and Wallace, JW. (2006) *Identification, model updating, and response prediction of an instrumented 15-story steel-frame building*, Earthquake Spectra. 22(3), pp: 781–802.

[24] Posenato D, Lanata F, Inaudi D and Smith, I-FC. 2008. *Model-free data interpretation for continuous monitoring of complex structures* Advanced Engineering Informatics, Elsevier. 22(1), pp.: 135–144.

[25] Fritzen CP and Bohle K. *Application of model-based damage identification to a seismically loaded structure* Smart materials and structures, IOP Publishing. 10(3), pp. 452.

[26] Salawu, OS. (1997) *Detection of structural damage through changes in frequency: a review*, Engineering structures, Elsevier, 19(9), pp: 718–723

[27] Wang, S-Q, and Hua-Jun L.(2012) *Assessment of structural damage using natural frequency changes.* Acta Mechanica Sinica, Springer, 28(1),pp.: 118–127.

[28] Wang, X., Hu, N., Fukunaga, H and Yao, ZH. (2001) *Structural damage identification using static test data and changes in frequencies*, Engineering structures, Elsevier, 23(6), pp: 610–621.

[29] Yan YJ, Cheng L, Wu ZY and Yam LH (2007) *Development in vibration-based structural damage detection technique*, Mechanical Systems and Signal Processing, Elsevier. 21(5), 2198–2211.

[30] Jaksic V, Mandic DP, Ryan K, Basu B and Pakrashi V (2016). *A Comprehensive Study of the Delay Vector Variance Method for Quantification of Nonlinearity in Dynamical Systems*, Royal Society Open Science, 2, 150493-1-24.

[31] Wang, Z., and Lin, RM., and Lim, MK. (1997) *Structural damage detection using measured FRF data*, Computer methods in applied mechanics and engineering, Elsevier, 147(1–2), pp: 187–197.

[32] Zimmerman, DC., and Kaouk, M. (1992) *Eigenstructure assignment approach for structural damage detection*, AIAA journal, 30(7), pp: 1848–1855

[33] Carden E.P and and Fanning P. (2004) *Vibration based condition monitoring: a review*, Structural health monitoring, Sage Publications. 3(4), 355–377.

[34] Fan W and Qiao P. (2011) *Vibration-based damage identification methods: a review and comparative study*, Structural health monitoring, Sage Publications. 10(1), 83–111.

[35] Li YY and Chen Y. (2013) *A review on recent development of vibration-based structural robust damage detection*, Structural Engineering and Mechanics, Techno-Press. 45(2), 159–168.

[36] Yan YJ, Cheng L, Wu, ZY and Yam, LH. 2007. *Development in vibration-based structural damage detection technique*. Mechanical Systems and Signal Processing, Elsevier. 21(5), pp.: 2198–2211.

[37] Laory I, Trinh TN. and Smith I-FC. 2011. *Evaluating two model-free data interpretation methods for measurements that are influenced by temperature* , Advanced Engineering Informatics, Special Section: Engineering informatics in port operations and logistics. 25(3), pp.: 495–506.

[38] Yam, LH., Yan, YJ. and Jiang, JS. (2003) *Vibration-based damage detection for composite structures using wavelet transform and neural network identification*, Composite Structures, Elsevier, 60(4), pp: 403–412.

[39] Peeters, B., Maeck, J. and De Roeck, G. (2001) *Vibration-based damage detection in civil engineering: excitation sources and temperature effects*, Smart materials and Structures, IOP Publishing, 10(3), pp: 518.

[40] Fugate, ML., Sohn, H and Farrar, CR. (2001) *Vibration-based damage detection using statistical process control*, Mechanical Systems and Signal Processing, Elsevier, 15(4), pp: 707–721.

[41] Deraemaeker, A., Reynders, E., De Roeck, G. and Kullaa, J. (2008) *Vibration-based structural health monitoring using output-only measurements under changing environment*, Mechanical Systems and Signal Processing, Elsevier, 22(1), pp: 34–56.

[42] Messina, A., and Williams, EJ., and Contursi, T. (1998) *Structural damage detection by a sensitivity and statistical-based method*, Neural Networks (IJCNN), Journal of sound and vibration, Elsevier, 216(5), pp: 791–808.

[43] Poncelet, F., Kerschen, G., Golinval, JC. and Verhelst, D. (2007) *Output-only modal analysis using blind source separation techniques*, Mechanical Systems and Signal Processing, Elsevier, 21(6), pp: 2335–2358.

[44] Chelidze, D., and Zhou, W. (2006) *Smooth orthogonal decomposition-based vibration mode identification*, Journal of Sound and Vibration, Elsevier, 292(3–5), pp: 461–473.

[45] Yang, Y., and Nagarajaiah, S. (2013) *Blind modal identification of output-only structures in time-domain based on complexity pursuit*, Earthquake Engineering and Structural Dynamics, 42(13), pp: 1885–1905.

[46] Chao, SH., Loh, CH. and Tseng, MH. (2014) *Structural damage assessment using output-only measurement: localization and quantification*, Journal of Intelligent Material Systems and Structures, Sage Publications Sage UK: London, England, 25(9), pp: 1097–1106.

[47] Zou, Y., Tong, LPSG. and Steven, GP. (2000) *Vibration-based model-dependent damage (delamination) identification and health monitoring for composite structures:a review*, Journal of Sound and vibration, Elsevier, 230(2), pp: 357–378.

[48] Salokhe, N, et al. (2016) *Vibration Based Damage Detection using overall frequency response and Time Domain Decomposition.* Engineering and Technology (ICETECH), IEEE International Conference. IEEE.

[49] Ciang, CC., and Lee, JR., and Bang, HJ. (2008) *Structural health monitoring for a wind turbine system: a review of damage detection methods*, Measurement Science and Technology, IOP publishing, 19(12), pp. 122001.

[50] Sohn, H., and Farrar, CR. (2001) *Damage diagnosis using time series analysis of vibration signals*, Smart materials and structures, IOP Publishing, 10(3), pp. 446.

[51] Musafere F, Sadhu A and Liu K. 2015. *Towards damage detection using blind source separation integrated with time-varying auto-regressive modeling.* Smart Materials and Structures, IOP Publishing. 25(1), pp.: 015013.

[52] Nair, KK., and Kiremidjian, AS. (2007) *Time series based structural damage detection algorithm using Gaussian mixtures modeling*, Journal of dynamic systems, measurement, and control, American Society of Civil Engineers, 129(3), pp: 285–293.

[53] Hazra B, Sadhu A, Roffel AJ and Narasimhan S. (2012) *Hybrid Time-Frequency Blind Source Separation Towards Ambient System Identification of Structures*, Computer-Aided Civil and Infrastructure Engineering, 27(5), pp. 314–332.

[54] Yao, R. and Pakzad, SN. (2012) *A structural damage detection indicator based on principal component analysis and statistical hypothesis testing*, Mechanical Systems and Signal Processing, Elsevier, vol. 31, pp: 355–368.

[55] Nair KK, Kiremidjian AS and Law KH. (2006) *Time series-based damage detection and localization algorithm with application to the ASCE benchmark structure*, Journal of Sound and Vibration, Elsevier. 291(1), 349–368.

[56] Trendafilova, I., and Manoach, E. (2008) *Vibration-based damage detection in plates by using time series analysis.* Mechanical Systems and Signal Processing 22(5), pp.: 1092–1106.

[57] Hazra B, Sadhu A and Narasimhan S. (2016) *Fault detection of gearboxes using synchro-squeezing transform*, Journal of Vibration and Control, SAGE Publications. pp:1077546315627242.

[58] Hamilton, JD. (1994) *Time series analysis*, Princeton university press Princeton, vol.:2.

[59] Morovati V and Kazemi MT. 2013. *Detection of sudden structural damage using blind source separation and time–frequency approaches.* Smart Materials and Structures, Wiley Online Library. 42(8), pp.: 1221–1242.

[60] Nagarajaiah, S., and Basu, B. (2009) *Output only modal identification and structural damage detection using time frequency & wavelet techniques*, Earthquake Engineering and Engineering Vibration, Springer, 8(4), pp: 583–605.

[61] Kesavan, KN. and Kiremidjian, AS. (2012) *A wavelet-based damage diagnosis algorithm using principal component analysis*, Structural Control and Health Monitoring, Wiley Online Library. 19(8), pp: 672–685.

[62] Rucka, M. and Wilde, K. (2006) *Application of continuous wavelet transform in vibration based damage detection method for beams and plates*, Journal of Sound and Vibration, Elsevier, 297(3–5), pp: 536–550.

[63] Hazra B and Narasimhan S (2010) *Wavelet-based blind identification of the UCLA Factor building using ambient and earthquake responses*, Smart Materials and Structures, IOP Publishing. 19(2), 025005.

[64] Pakrashi, V., and O'Connor, A., and Basu, B. (2007) *A study on the effects of damage models and wavelet bases for damage identification and calibration in beams*, Computer-Aided Civil and Infrastructure Engineering, Wiley Online Library, 22(8), pp: 555–569.

[65] Pakrashi, V., and Basu, B., and Ó Connor, A. (2007) *Structural damage detection and calibration using a wavelet–kurtosis technique*, Engineering Structures, Elsevier, 29(9), pp: 2097–2108.

[66] Yang, Y., and Nagarajaiah, S. (2014) *Blind identification of damage in time-varying systems using independent component analysis with wavelet transform*, mechanical systems and signal processing, Elsevier, 47(1–2), pp: 3–20.

[67] Li, H., and Deng, X., and Dai, H. (2007) *Structural damage detection using the combination method of EMD and wavelet analysis*, Mechanical Systems and Signal Processing, Elsevier, 21(1), pp: 298–306.

[68] Sadhu A and Hazra B. (2013) *A novel damage detection algorithm using time-series analysis-based blind source separation*, Shock and Vibration, IOS Press. 20(3), 423–438.

[69] Zang, C., and Friswell, MI., and Imregun, M. (2004) *Structural damage detection using independent component analysis*, Structural Health Monitoring, Sage Publications, 3(1), pp: 69–83.

[70] Antoni, J. 2005. *Blind separation of vibration components: Principles and demonstrations.* Mechanical Systems and Signal Processing, Elsevier. 19(6), 1166–1180.

[71] Belouchrani, A., Abed-Meriam, K., Cardoso, JF., and Moulines, E. (1997) *A blind source separation technique using second-order statistics*, IEEE Transactions on Signal Processing, IEEE, 45(2), pp: 434–444.

[72] Azam SE, Chatzi E and Papadimitriou C. (2015) *A dual Kalman filter approach for state estimation via output-only acceleration measurements*, Mechanical Systems and Signal Processing, Elsevier, vol: 60–61, pp. 866–886, issn: 0888-3270

[73] Yang, JN., Lin, S., Huang, H. and Zhou, L. (2006) *An adaptive extended Kalman filter for structural damage identification*, Structural Control and Health Monitoring, Wiley Online Library, 13(4), pp. 849–867.

[74] Chatzi, EN. and Smyth, AW. (2009) *The unscented Kalman filter and particle filter methods for nonlinear structural system identification with non-collocated heterogeneous sensing*, Structural control and health monitoring, Wiley Online Library, 16(1), pp. 99–123.

[75] Azam, SE., Chatzi E., Papadimitriou C., and Smyth, AW. (2017) *Experimental validation of the Kalman-type filters for online and real-time state and input estimation*, Journal of Vibration and Control, SAGE Publications, 23(15), pp. 2494–2519.

[76] Mattsson P, Zachariah D and Stoica P. 2016. *Recursive Identification Method for Piecewise ARX Models: A Sparse Estimation Approach.* IEEE Transactions on Signal Processing, IEEE. 64(19), pp.: 5082-5093.

[77] Yang, JN, Lei Y, Lin, S and Huang, N. 2004. *Hilbert-Huang based approach for structural damage detection* Journal of engineering mechanics, American Society of Civil Engineers. 130(1), pp.: 85–95.

[78] Xu, YL., and Chen, J. (2004) *Structural damage detection using empirical mode decomposition: experimental investigation*, Journal of engineering mechanics, American Society of Civil Engineers, 130(11), pp: 1279–1288.

[79] Huang NE, Shen Z, Long SR, Wu MC, Shih HH, Zheng Q, Yen NC, Tung CC and Liu HH. (1998, March.) *The empirical mode decomposition and the Hilbert spectrum for nonlinear and nonstationary time series analysis*, In Proceedings of the Royal Society of London A (Vol. 454, No. 1971, pp. 903-995).

[80] Kunwar A, Jha R, Whelan M and Janoyan K (2013) *Damage detection in an experimental bridge model using Hilbert–Huang transform of transient vibrations*, Structural Control and Health Monitoring, Wiley Online Library. 20(1), 1–15.

[81] Peng ZK, Tse PW and Chu FL. (2005) *An improved Hilbert-Huang transform and its application in vibration signal analysis*, Journal of Sound and Vibration, Elsevier, 286(1), pp. 187–205

[82] Ding F, and Chen T. 2005. *Identification of Hammerstein nonlinear ARMAX systems.* Automatica, Elsevier. 41(9), pp.: 1479–1489.

[83] Misra M, Yue HH, Qin SJ and Ling C. (2002) *Multivariate process monitoring and fault diagnosis by multi-scale PCA*, Computers & Chemical Engineering, Elsevier. 26(9), 1281–1293.

[84] Yan, AM., Kerschen, G., De Boe, P. and Golinval, JC. (2005) *Structural damage diagnosis under varying environmental conditions part II: local PCA for non-linear cases*, Mechanical Systems and Signal Processing, Elsevier, 19(4), pp: 865–880.

[85] De Oliveira, MA. and Inman, DJ. (2015) *PCA-based Method for Damage Detection Exploring Electromechanical Impedance in a Composite Beam*, Structural Health Monitoring, SAGE Publications, UK.

[86] Gharibnezhad F, Mujica LE and Rodellar J. 2015. *Applying robust variant of Principal Component Analysis as a damage detector in the presence of outliers.* Mechanical Systems and Signal Processing, Elsevier. 50, 467–479.

[87] Lee DS, Park JM and Vanrolleghem PA. 2005. *Adaptive multiscale principal component analysis for on-line monitoring of a sequencing batch reactor.* Mechanical Systems and Signal Processing, Elsevier. 116(2), pp.: 195–210.

[88] Li W, Yue HH, Valle-Cervantes S and Qin SJ. (2000) *Recursive PCA for adaptive process monitoring*, Journal of process control, Elsevier. 10(5), 471–486.

[89] Nguyen, VH. and Golinval JC., (2010) *Fault detection based on kernel principal component analysis*, Engineering Structures, Elsevier, 32(11), pp. 3683–3691, doi:https://doi.org/10.1016/j.engstruct.2010.08.012

[90] De Boe, P. and Golinval, JC. (1998) *Principal component analysis of a piezosensor array for damage localization*, Structural health monitoring, SAGE Publications, 2(2), pp. 137–144.

[91] Tipping, ME., and Bishop, CM. (1999) *Probabilistic principal component analysis*, Journal of the Royal Statistical Society: Series B (Statistical Methodology), Wiley Online Library, 61(3), pp: 611–622.

[92] Kerschen, G., and Golinval, JC., and Vakakis, AF., and Bergman, LA. (2005) *The method of proper orthogonal decomposition for dynamical characterization and order reduction of mechanical systems: an overview*, Nonlinear dynamics, Springer, 41(1–3), pp: 147–169.

[93] Jolliffe, IT. (1986) *Principal component analysis and factor analysis*, Springer, pp: 115–128.

[94] Hot A and Kerschen G and Foltête E and Cogan, S (2012) *Detection and quantification of non-linear structural behavior using principal component analysis*, Mechanical Systems and Signal Processing, Elsevier. 26, 104–116.

[95] Lovera, M., Gustafsson, T. and Verhaegen M. (2000) *Recursive subspace identification of linear and non-linear Wiener state-space models*, Automatica, Elsevier. 36(11), pp: 1639–1650.

[96] Koh, BH., and Dharap, P., and Nagarajaiah, S., and Phan, MQ. (2005) *Real-time structural damage monitoring by input error function*, AIAA journal, JSTOR, 43(8), pp: 1808–1814.

[97] Richman MB. (1986) *Rotation of principal components*, John Wiley & Sons, Ltd. 6(3), 293–335, issn: 1097-0088, doi: 10.1002/joc.3370060305

[98] Yan AM, Kerschen G, De Boe P and Golinval, JC (2005) *Structural damage diagnosis under varying environmental conditions–part I: a linear analysis*, Mechanical Systems and Signal Processing, Elsevier. 19(4), 847–864.

[99] Mujica, L., Ruiz, M., Pozo, M., Rodellar, J. and Gaemes, A. (2013) *A structural damage detection indicator based on principal component analysis and statistical hypothesis testing*, Smart Materials and Structures, IOP Science, 23(2), pp: 025014.

[100] Golyandina N and Zhigljavsky A. (2013) *Singular Spectrum Analysis for time series*, Springer Science & Business Media.

[101] Carniel R, Barazza F, Tárraga M and Ortiz R. (2006) *On the singular values decoupling in the Singular Spectrum Analysis of volcanic tremor at Stromboli*, Natural Hazards and Earth System Science. 6(6), pp.: 903–909.

[102] Hassani H (2010) *A brief introduction to singular spectrum analysis*, Optimal decisions in statistics and data analysis, UK.

[103] Elsner JB and Tsonis AA (2013) *Singular spectrum analysis: a new tool in time series analysis*, Springer Science & Business Media.

[104] Hassani H, Xu Z and Zhigljavsky A. (2013) *Singular spectrum analysis based on the perturbation theory*, Nonlinear Analysis: Real World Applications, Elsevier. 12(5), 2752–2766.

[105] Liu K, Law SS, Xia Y and Zhu, XQ. (2014) *Singular spectrum analysis for enhancing the sensitivity in structural damage detection*, Journal of Sound and Vibration, Elsevier. 333(2), 392–417.

[106] Chao SH and Loh CH. (2014) *Application of singular spectrum analysis to structural monitoring and damage diagnosis of bridges*, Structure and Infrastructure Engineering, Taylor & Francis. 10(6), 708–727.

[107] Lakshmi K, Rao A and Gopalakrishnan N. (2016) *Singular spectrum analysis combined with ARMAX model for structural damage detection*, Structural Control and Health Monitoring, Wiley Online Library. 24(9).

[108] Kilundu, B., Chiementin, X. and Dehombreux, P. (2011) *Singular spectrum analysis for bearing defect detection*, Journal of vibration and acoustics, American Society of Mechanical Engineers, 133(5), pp: 051007.

[109] Murotani, K. and Sugihara, K. (2014) *New spectral decomposition method for three-dimensional shape models and its applications*, Journal of computing and information science in engineering, American Society of Mechanical Engineers, 5(4), pp: 277–282.

[110] Groth, A. and Ghil, M. (2015) *Monte Carlo singular spectrum analysis (SSA) revisited: Detecting oscillator clusters in multivariate datasets*, Journal of Climate, 28(19), pp: 7873–7893.

[111] Feeny BF. (2002) *On the Proper Orthogonal Modes and Normal Modes of Continuous Vibration Systems*, Journal of Vibration and Acoustics, ASME, 124(1), pp. 157–160, doi:10.1115/1.1421352.

[112] Han, S., and Feeny, BF. (2003) *Application of proper orthogonal decomposition to structural vibration analysis*, Mechanical Systems and Signal Processing, Elsevier, 17(5), pp: 989–1001.

[113] Kappagantu, R., and Feeny, BF. (2000) *Part 1: Dynamical characterization of a frictionally excited beam*, Nonlinear Dynamics, Springer, 22(4), pp: 317–333.

[114] Kappagantu, R., and Feeny, BF. (2000) *Part 2: Proper orthogonal modal modeling of a frictionally excited beam*, Nonlinear Dynamics, Springer, 23(1), pp: 1–11.

[115] Narasimha, R. (2011) *Kosambi and proper orthogonal decomposition*, Resonance, Springer, 16(6), pp: 574–581.

[116] Kosambi, DD. (2016) *Statistics in function space*, Springer, pp: 115–123.

[117] Karhunen, K. (1946) *Zur spektraltheorie stochastischer prozesse*, Ann. Acad. Sci. Fennicae, AI, vol. 34.

[118] Thiene, M., Zaccariotto, M., and Galvanetto, U. (2013) *Application of proper orthogonal decomposition to damage detection in homogeneous plates and composite beams.* Journal of Engineering Mechanics, ASCE, 13(11): pp.: 1539–1550.

[119] Feeny BF and Liang Y (2003) *Interpreting proper orthogonal modes of randomly excited vibration systems*, Journal of Sound and Vibration, Elsevier, 265(5), pp. 953–966.

[120] Kerschen, G. and Golinval, JC. (2002) *Physical interpretation of the proper orthogonal modes using the singular value decomposition*, Journal of Sound and vibration, Elsevier, 249(5), pp: 849–865.

[121] Feeny B (2002) *On proper orthogonal co-ordinates as indicators of modal activity*, Journal of Sound and Vibration,Elsevier 255(5). 805–817.

[122] Feeny, BF., and Kappagantu, R. (1998) *On the physical interpretation of proper orthogonal modes in vibrations*, Journal of sound and vibration, Elsevier, 211(4), pp: 607–616.

[123] Oropeza, V. and Sacchi, M. (2011) *Simultaneous seismic data denoising and reconstruction via multichannel singular spectrum analysis*, Geophysics, Society of Exploration Geophysicists. 76(3), V25–V32.

[124] Hsieh, WW and Wu, A. (2012) *Nonlinear multichannel singular spectrum analysis of the tropical Pacific climate variability using a neural network approach*, Journal of Geophysical Research: Oceans, Wiley Online Library. 10(7), pp: 903–909.

[125] Huang, W., Wang, R., and Yuan, Y., Gan, S.,and Chen, Y. (2016) *Signal extraction using randomized-order multichannel singular spectrum analysis*, Geophysiscs, Society of Exploration Geophysicists. 82(2), V69–V84.

[126] Rangelova E., Sideris, MG. and Kim, JW. (2012) *On the capabilities of the multi-channel singular spectrum method for extracting the main periodic and non-periodic variability from weekly GRACE data*, Journal of Geodynamics, Elsevier. vol:54, pp: 64–78.

[127] Watkins DS. (1982) *Understanding the QR Algorithm*, SIAM Review, SIAM, 24(4), pp. 427–440, doi:10.1137/1024100.

[128] Byers R. (1986) *A Hamiltonian QR Algorithm*, SIAM Journal on Scientific and Statistical Computing, SIAM, 7(1), pp. 212–229, doi:10.1137/0907015.

[129] Braman K., Byers R. and Mathias R. (2002) *The Multishift QR Algorithm. Part I: Maintaining Well-Focused Shifts and Level 3 Performance*, SIAM Journal on Matrix Analysis and Applications, SIAM, 23(4), pp. 929–947, doi:10.1137/S0895479801384573.

[130] Cullum, JK and Willoughby, R. (2002) *Lanczos Algorithms for Large Symmetric Eigenvalue Computations: Vol. 1: Theory*, SIAM, vol:41.

[131] Paige, CC. (1980) *Accuracy and effectiveness of the Lanczos algorithm for the symmetric eigenproblem*, Linear algebra and its applications, vol:34, pp: 235–258

[132] Golub GH and Van Loan CF. (2012) *Matrix computations*, JHU Press. vol:3.

[133] Sibson, R. (1979) *Studies in the robustness of multidimensional scaling: Perturbational analysis of classical scaling*, Journal of the Royal Statistical Society. Series B (Methodological), JSTOR, pp: 217–229.

[134] Golub GH and Zha, H. (1994) *Perturbation analysis of the canonical correlations of matrix pairs*, Linear algebra and its applications., 210, pp. 3–28.

[135] Kato, T. (2013) *Perturbation theory for linear operators*, Springer Science & Business Media, Vol.(132).

[136] Ljung L and Söderström, T. 1983. *Theory and practice of recursive identification*. MIT press.

[137] Zang, C., Friswell MI., and Imregun, M. (2004) *Structural damage detection using independent component analysis*, Structural Health Monitoring, SAGE Publications, 3 (1), pp.: 69–83.

[138] Kerschen, G., Poncelet, F. and Golinval, JC. (2007) *Physical interpretation of independent component analysis in structural dynamics*, Mechanical Systems and Signal Processing, Elsevier, 21(4), pp: 1561–1575.

[139] Thompson, B., 2000. *Canonical correlation analysis.*

[140] Härdle, W. K., and Simar, L. (2015). *Canonical correlation analysis*. Applied Multi- variate Statistical Analysis. Springer, pp. 443–454.

[141] Fan, X., and Konold, TR. (2010). *Canonical correlation analysis*. Quantitative methods in the social and behavioral sciences: A guide for researchers and reviewers, pp. 29–34.

[142] Thorndike, RM., (2000). *Canonical correlation analysis*. Handbook of applied multi- variate statistics and mathematical modeling. Elsevier, pp. 237–263.

[143] Akaike, H. (1976). *Canonical correlation analysis of time series and the use of an information criterion*. Mathematics in Science and Engineering, Elsevier. Vol. 126. pp. 27–96.

[144] Thompson, B. (1984). *Canonical correlation analysis: Uses and interpretation*. No. 47. SAGE Publications.

[145] Statheropoulos, M., Vassiliadis, N., and Pappa, A., 1998. *Principal component and canonical correlation analysis for examining air pollution and meteorological data*. Atmospheric Environment, 32(6), pp. 1087–1095.

[146] Bajorski, P. *Canonical correlation analysis*. Statistics for Imaging, Optics, and Photonics, pp. 241–259.

[147] Vía, J., Santamaria, I., and Pérez, J. (2005). *A robust RLS algorithm for adaptive canonical correlation analysis*. In Acoustics, Speech, and Signal Processing, 2005. Proceedings.(ICASSP'05). IEEE International Conference on, IEEE, Vol. 4, pp. iv–365.

[148] Bach, FR., and Jordan, M. I. (2005). *A probabilistic interpretation of canonical correlation analysis.*

[149] Ouarda, TB., Girard, C., Cavadias, G. S., and Bobée, B. (2001). *Regional flood frequency estimation with canonical correlation analysis.* Journal of Hydrology, 254(1-4), pp. 157– 173.

[150] Russell, E. L., Chiang, L. H., and Braatz, R. D. (2000). *Fault detection in industrial processes using canonical variate analysis and dynamic principal component analysis.* Chemometrics and intelligent laboratory systems, 51(1), pp. 81–93.

[151] Schólkopf, B., Smola, A., and Múller, K.R. (1998). *Nonlinear component analysis as a kernel eigenvalue problem.* Neural computation, 10(5), pp. 1299–1319.

[152] Feng L, Yi X, Zhu D, Xie X and Wang Y. (2015). *Damage detection of metro tunnel structure through transmissibility function and cross correlation analysis using local excitation and measurement.* Mechanical Systems and Signal Processing, Elsevier. vol:60, 59–74.

[153] Pakrashi V., Fitzgerald, P., OLeary, M., Jaksic, V., Ryan, K., and Basu, B. (2018). *Assessment of structural nonlinearities employing extremes of dynamic responses.* Journal of Vibration and Control, SAGE Publications. 24(1), 137–152.

[154] Cichocki, A., and Amari, SI. (2002). *Adaptive blind signal and image processing: learning algorithms and applications* Vol. 1. John Wiley & Sons.

[155] Roy, D., and Rao, GV. (2017). *Stochastic dynamics, filtering and optimization.* Cambridge University Press.

[156] Krishnan M., Bhowmik B., Tiwari AK. and Hazra B. (2017) *Online damage detection using recursive principal component analysis and recursive condition indicators*, Smart Materials and Structures, IOP Publishing. 26(8), 085017.

[157] Krishnan M., Bhowmik B., Hazra B. and Pakrashi V. (2017) *Real time damage detection using recursive principal components and time varying auto-regressive modeling*, Mechanical Systems and Signal Processing, Elsevier. 101. pp: 549–574.

[158] Bhowmik B., Krishnan M., Hazra B. and Pakrashi V (2018) *Real time unified single and multi channel structural damage detection using recursive singular spectrum analysis*, Structural Health Monitoring, SAGE Publications, pp. 1475921718760483, doi = 10.1177/1475921718760483.

[159] Carrillo J. (2015). *Damage index based on stiffness degradation of lowrise RC walls*. Earthquake Engineering and Structural Dynamics, 44(6), 831-848.